

Dissipative State Engineering in Quantum Many-Body Systems

Dissertation
zur Erlangung des wissenschaftlichen Grades
Doctor rerum naturalium

vorgelegt von

Alexander Schnell
geboren am 5. Oktober 1989 in Plauen (Vogtl.)

Institut für Theoretische Physik
Fakultät Physik
Technische Universität Dresden

Max-Planck-Institut
für Physik komplexer Systeme
Dresden

2019



MAX-PLANCK-GESellschaft

Eingereicht am 19. März 2019

Verteidigt am 23. August 2019

Erster Gutachter: Prof. Dr. Roland Ketzmerick

Zweiter Gutachter: Prof. Dr. Michael Fleischhauer

Dritter Gutachter: PD Dr. André Eckardt

Abstract

Quantum systems that are in weak contact with a thermal heat bath will ultimately relax to an equilibrium state which is characterized by the temperature of the environment only. This state is independent of the specific properties of the bath and of how it is coupled to the system. This changes completely, when the system is additionally driven. Such a driven-dissipative situation can emerge, for example, due to an additional time-periodic modulation of the system, or when it is brought into contact with a second bath of different temperature. Then, the system will run into a well-defined nonequilibrium steady state. This state, however, will depend on the very details of the environment and its coupling to the system.

We study whether this freedom can be used to engineer interesting properties of quantum systems, which are not found in their equilibrium states, i.e. in the absence of a drive. We focus on bosonic quantum many-body systems. We investigate when far-from-equilibrium ideal gases feature Bose condensation in a group of single-particle states, as opposed to situations where Bose condensation is completely absent in the nonequilibrium steady state. We show that Bose condensation can be induced in a finite one-dimensional ideal gas by the competition of two heat baths whose temperatures both lie well above the equilibrium condensation temperature. This setup also allows to engineer condensation in excited single-particle states. We discuss first ideas to study similar setups in weakly interacting Bose gases. Describing the microscopic dynamics of interacting many-body systems coupled to thermal baths is extremely challenging, due to the fact that generally the full many-body spectrum is inaccessible. Using ideas from semiclassics, we develop an approximation to the dynamics that yields good results at high and intermediate bath temperatures.

We also investigate the transient dynamics of driven-dissipative quantum systems. Our studies are motivated by a result that is well known for isolated quantum systems: for a system whose dynamics is generated by a time-periodic Hamiltonian, the stroboscopic dynamics (observed at integer multiples of the driving period) can always be understood as if it would stem from a time-independent Hamiltonian, the Floquet Hamiltonian. For open quantum systems in contact with an environment, we ask if a similar mapping to an effective generator, the Floquet Lindbladian, is always possible. For a simple qubit model we show that there are two extended parameter regions, one in which the Floquet Lindbladian exists, and one in which it does not. We discuss problems of analytical expansions that can give rise to this Floquet Lindbladian and discuss how we can interpret the region where it does not exist. These results are important for dissipative Floquet engineering and open up new perspectives for the control of open quantum systems via time-periodic driving.

Zusammenfassung

Quantensysteme, die in schwacher Wechselwirkung mit einem thermischen Wärmebad stehen, relaxieren stets in einen Gleichgewichtszustand, welcher allein durch die Temperatur der Umgebung beschrieben ist. Dieser Zustand ist unabhängig von den spezifischen Eigenschaften des Bades, und davon wie dieses an das System gekoppelt ist. Dies ändert sich, wenn das System zusätzlich angetrieben wird. Ein solches getrieben-dissipatives Szenario kann beispielsweise durch einen zusätzlichen zeitperiodischen Antrieb entstehen, oder wenn das System mit einem zweiten Bad unterschiedlicher Temperatur in Kontakt gebracht wird. In diesem Fall läuft das System in einen wohldefinierten stationären Nichtgleichgewichtszustand. Dieser Zustand hängt jedoch von den Details der Umgebung, und davon wie diese an das System gekoppelt ist, ab.

Es wird untersucht ob diese Freiheit genutzt werden kann um interessante Eigenschaften von Quantensystemen zu konstruieren, die in deren Gleichgewichtszuständen, d.h. in Abwesenheit des Antriebs, nicht zu finden sind. Der Fokus der Arbeit liegt auf bosonischen Quantenvielteilchensystemen. Es wird ergründet unter welchen Bedingungen ideale Gase fernab des thermischen Gleichgewichts Bose Kondensation in einer Gruppe von Einteilchenzuständen aufweisen, im Gegensatz zu Szenarien in denen überhaupt keine Bose Kondensation im stationären Nichtgleichgewichtszustand auftritt. Weiterhin wird gezeigt, dass Bose Kondensation in einem eindimensionalen idealen Gas durch das Wechselspiel zweier Wärmebäder induziert werden kann. Die Temperatur beider Bäder liegt dabei weit über der Kondensationstemperatur des Gleichgewichts. Diese Anordnung erlaubt außerdem kontrollierte Kondensation in angeregten Einteilchenzuständen. Erste Ideen für das theoretische Studium ähnlicher Anordnungen für schwach wechselwirkende Bosegase werden diskutiert. Eine Beschreibung der mikroskopischen Dynamik wechselwirkender Vielteilchensysteme ist extrem anspruchsvoll, da typischerweise das volle Vielteilchenspektrum unzugänglich ist. Unter Zuhilfenahme semiklassischer Ideen wird eine Näherung der Dynamik entwickelt, welche eine gute Beschreibung für hohe und intermediäre Temperaturen liefert.

Weiterhin wird die transiente Dynamik getrieben-dissipativer Quantensysteme untersucht. Die Motivation bietet ein bekanntes Resultat für abgeschlossene Quantensysteme: Für ein System, dessen Dynamik durch einen zeitperiodischen Hamiltonoperator bestimmt ist, kann die stroboskopische Dynamik (unter Beobachtung zu Zeiten, die Vielfache der Antriebsperiode sind) immer so verstanden werden als würde sie von einem zeitunabhängigen Hamiltonoperator, dem Floquet Hamiltonian, induziert. Für offene Quantensysteme im Kontakt mit einer Umgebung wird untersucht ob eine ähnliche Abbildung auf einen effektiven Generator, den Floquet Lindbladian, existiert. Für ein einfaches Qubit Modell wird gezeigt, dass es zwei ausgedehnte Parameterregionen gibt, eine in welcher der Floquet Lindbladian existiert und eine weitere in der dieser nicht existiert. Es werden Probleme von analytischen Entwicklungen des Floquet Lindbladian diskutiert. Auch wird eine Interpretation der Region gegeben, in der dieser nicht existiert. Diese Resultate sind maßgeblich für dissipatives Floquetengineering und eröffnen neue Blickwinkel auf die zeitperiodische Kontrolle offener Quantensysteme.

Contents

1. Introduction	1
2. Master equation for open quantum systems	7
2.1. Introduction	7
2.2. Axiomatic approach: Lindblad master equation	9
2.2.1. Quantum dynamical semigroups	9
2.2.2. Complete positivity	10
2.2.3. Lindblad master equation	11
2.3. Microscopic approach: Born-Markov rate equation	14
2.3.1. Born approximation	14
2.3.2. Markov approximation	15
2.3.3. Rotating wave approximation	17
2.3.4. Rates for coupling to thermal phonon reservoir	20
2.4. Rate equation for the ideal Bose gas	23
3. Existence of the Floquet Lindbladian	27
3.1. The Floquet Lindbladian	27
3.2. Model system: Driven-dissipative two-level system	33
3.3. Construction of an effective evolution with time-homogeneous memory kernel	36
3.4. High-frequency expansions of the Floquet Lindbladian	39
3.4.1. Emergence of unphysical terms in the Magnus expansion	40
3.4.2. Effective Lindbladian in extended space and van-Vleck high-frequency expansion	43
3.4.3. Unphysical terms in the van-Vleck high-frequency expansion	47
3.4.4. Magnus expansion in the rotating frame	48
3.4.5. Van-Vleck high-frequency expansion in the rotating frame	54
3.4.6. Concluding remarks on the high-frequency expansions	60
4. Number of Bose-selected modes in driven-dissipative ideal Bose gases	61
4.1. Driven-dissipative ideal Bose gas and Bose selection	61
4.2. Rates with continuum limit	66
4.2.1. Different selection scenarios	68
4.2.2. Random-wave model	70
4.3. Rates without continuum limit	72
4.3.1. Uncorrelated random rates	72

4.3.2. Chaotic quantum kicked rotor	76
4.3.3. Modified random wave model for the rates in the quantum kicked rotor	77
4.4. Rates with product structure	79
5. High-temperature nonequilibrium Bose condensation induced by a hot needle	83
5.1. System and model	83
5.2. Finite-size equilibrium condensation	85
5.3. High-temperature nonequilibrium condensation	86
5.4. Estimating the condensation temperature	91
5.4.1. Condensation destroyed by long-wavelength modes	91
5.4.2. Condensation destroyed by modes with large quasimomentum	93
5.5. Temperature for switch to excited-state condensation	95
5.6. Quasiexact Monte-Carlo results for a small system	97
5.7. Continuous system	98
5.8. Experimental prospects and the “Floquet needle”	103
6. Weakly interacting Bose gases far from thermal equilibrium	107
6.1. Semiclassical description of bath action	107
6.2. Benchmark: Equilibrium states	114
6.3. Nonequilibrium steady states: Hot-needle condensation in presence of weak interactions	117
6.4. Dynamics: Bistability in presence of local particle losses	121
7. Summary and outlook	127
Appendix	133
A. Extracting Hamiltonian and Lindblad operators from a Lindbladian generator matrix .	133
B. Construction of an effective memory kernel	134
B.1. Characteristic decay function of exponential kernel	134
B.2. Numerically stable procedure to find eigenvalues of \mathcal{L}_K	135
C. Discrepancy to the Magnus expansions presented in the literature	136
D. Commutator of two general qubit Lindblad superoperators	138
E. Matrix representation of the most general qubit Lindbladian	139
F. Degenerate perturbation theory in extended space for the dissipative system	140
G. Fourier components of the superoperator generating the rotating frame transformation	143
H. Explicit calculation of the perturbative expansion in extended space for the driven-dissipative qubit	144
I. Effective rates for the wavelet method	146
List of figures	151

1. Introduction

The laws of thermodynamics are an incredible finding. First formulated in the 19th century, together with the study of waves, they constitute the first attempt to describe collective phenomena in physical systems. However, these laws do not originate from a microscopic, atomistic, description of the thermodynamic system, but solely rely on a formal definition of macroscopic physical quantities like temperature, heat, or work. Still, they predict extremely successfully the state of systems on the smallest scale, as in the liquid drop model for the atomic nucleus, up to the largest scale, like for the black body spectrum of the cosmic background radiation.

Statistical mechanics provides a microscopic concept that gives rise to these laws of thermodynamics. One possible way to motivate statistical mechanics is from information theory: the state of the system is given by the ensemble that has the highest information entropy and is compatible with our knowledge of the system (for example its temperature, volume, etc.). On the one hand this is a great enlightenment, because it allows to find universal properties of the thermal steady states. On the other hand it implies also a great constraint for the possible properties that these states can show. One example is the universality that connects scaling exponents at equilibrium phase transitions [1–3]. Another example is the Mermin-Wagner-Hohenberg theorem [4–6] which forbids long-range order at finite temperatures for isotropic systems with short-range interactions in less than three dimensions. This has a direct consequence for Bose condensation: since the presence of a condensate can be associated with a $U(1)$ order parameter, in equilibrium, Bose condensation cannot occur in one or two spatial dimensions [7].

In recent years, a lot of theoretical and experimental interest has gone into systems that are *driven*. Such systems are inherently out-of-equilibrium and can give rise to new physics. One big class are isolated systems that are time-periodically driven, so called *Floquet systems*. Time-periodic modulations have been used as a tool to engineer interesting states of ultracold quantum gases in optical lattices [8, 9], a technique that has been called *Floquet engineering*. Examples include the dynamical control of tunneling in optical lattices [10, 11], which provides a tool to investigate the transition between the bosonic superfluid and the Mott-insulator phase [12, 13], and the creation of artificial magnetic fields for charge-neutral atoms [14–17], which led to the realization of systems with topologically nontrivial band structures [18–20]. Also the recent discovery of Floquet time crystals [21–27] and the possible control of many-body localization [28, 29] via time-periodic forcing reflect the importance of a deeper understanding of the physics of time-periodically modulated systems. Exciting transient states have also been found in time-periodically driven solid state systems, including light-induced topological insulators [30–33] as well as light-induced superconductivity [34–36]. What underlies Flo-

1. Introduction

quet engineering in many cases is a high-frequency expansion of the effective dynamics, governed by a time-independent *Floquet Hamiltonian*. In the long-time limit, however, it is believed that generic isolated interacting Floquet systems will heat up to an infinite-temperature state [37, 38]. One possible way to interpret this heating problem is that the high-frequency expansion breaks down [39], because in the presence of interactions the system possesses excitations at arbitrarily high energies. Thus, the assumption that the driving is ‘fast’ when compared to all time scales of the system will be violated. First quantitative studies to describe this heating were performed for atoms in periodically driven one-dimensional [40–43] and two-dimensional optical lattices [44–46].

A possible idea to counter this problem is to bring the system in contact with a reservoir which absorbs the heat that is generated by the driving. Such systems are called *driven-dissipative*. They fall in the general class of *open quantum systems*. Driven-dissipative systems have gained a lot of interest lately. One reason is that in the long-time limit they will run into a *nonequilibrium steady state*. This state is characterized by the violation of detailed balance, which can lead to steady, but nonvanishing currents through the system. This may for example be a steady current of heat, particles or spin. These nonequilibrium steady states share the property of being an *attractor of the dynamics* with equilibrium states. It means that irrespective of the initial state, in the long-time limit the dynamics will always run into the same nonequilibrium steady state (if it is unique). These states, however, are not constrained by equilibrium statistical mechanics, and will in general depend specifically on all properties of the environment and how it is coupled to the system, so we can imagine to engineer states with novel properties.

Such steady states were realized in photonic systems [47], where experimentally Bose-Einstein condensation has been achieved for exciton-polaritons [48–52] as well as for bare photons in a dye-filled microcavity [53–55]. While in these experiments one goal was to find states with thermal properties, it was shown for the exciton-polariton systems that the dissipation that is present gives rise to a length scale above which the nonequilibrium nature of the system is revealed, and deviations from universality are expected [56, 57]. The experiments have also triggered a debate about how Bose condensation can be distinguished from lasing [51, 53, 58–62]. Other photonic experiments exploit the fact that optical microcavities offer great freedom for designing system and dissipative environment. This allows to engineer the coherent emission of multiple modes [63, 64], switching between emission of two (or more) different modes [61, 65–68], and the development of topological microlasers [69, 70].

A second class of systems where nonequilibrium steady states have been studied are open Floquet systems. It has been explored under which conditions the steady state of a Floquet system in weak contact with a heat bath is effectively described by a thermal state [71–76]. Nevertheless, the question whether immersing an interacting Floquet system in some thermal background could actually fight heating and lead to exciting many-body states is still open [77–80]. In some systems it was ruled out already that true criticality can be observed at high frequencies even though criticality is found in the undriven limit [81]. Also, far-from-equilibrium steady states of open Floquet systems have been studied. For the ideal gas, it was shown that Bose condensation may occur not only in one but in a group of single particle states [62, 82–85], a fact that extends not just to Floquet systems but to all

driven ideal Bose gases that are weakly coupled to the environment. (We will discuss some of these results in Chapter 4.) This phenomenon has been linked to evolutionary game theory [86–88].

Finally, also in cold atom experiments nonequilibrium steady states have been realized in moving optical lattices [89], as well as systems subject to engineered local [90, 91] and non-local particle losses [92]. Furthermore, using shaped optical potentials, steady currents between atom reservoirs with temperature-, particle number-, and spin imbalance have been realized [93, 94]. Here, one- and two dimensional quantum wires between the reservoirs can be shaped. Also steady states of Rydberg excitations in optically driven lattice gases have been investigated recently [95–98] where it was shown that long-range order can emerge in two dimensions as a consequence of the driven-dissipative nature of the system [99].

In this thesis, we will discuss four questions that arise naturally from these works. First, we want to turn to the dynamics of time-periodically driven systems which are subject to dissipation. While for the closed system the stroboscopic dynamics (observed at integer multiples of the driving period) can always be recast into an effective evolution with the time-independent Floquet Hamiltonian, we investigate if such a mapping to an effective time-homogeneous evolution is also possible for time-periodically driven open systems. We will specifically focus on systems in memoryless, or *Markovian*, environments. Such systems are generally described by an evolution that is governed by a Lindblad superoperator. We want to discuss if also in the case of a time-periodically modulated Lindbladian it is always possible to find an effective time-independent generator of the stroboscopic dynamics, a Floquet Lindbladian. The existence of this Floquet Lindbladian has been implicitly assumed in recent works [100–103]. As we will discuss for a simple qubit system, it is not guaranteed that such an operator exists. In the parameter regime where it does not exist, the stroboscopic dynamics can therefore not be reproduced by a time-independent Markovian evolution. However, for our model system we are always able to construct an effective nonmarkovian evolution with some time-homogeneous exponential memory kernel. Still, for the model system we find that the existence of a Floquet Lindbladian for sufficiently high frequencies is guaranteed. Despite this fact, the Magnus expansion, a standard high-frequency expansion, fails to produce a valid generator in the leading order. This problem has already been observed in the recent literature [100, 104]. For our model system, we show that a possible way to avoid the emergence of unphysical terms is by first transforming into the rotating frame and then performing the Magnus expansion. Still, there is no guarantee that this procedure is a general strategy to avoid the problems of the Magnus expansion, which manifests the need to develop a high-frequency expansion that is tailored to the Floquet Lindblad problem.

The second question is motivated by recent studies on Bose condensation in nonequilibrium steady states [82, 83]. It was shown that for driven ideal Bose gases that are weakly coupled to their environment and may exchange energy (but no particles) with it, generally the following happens: in the limit of large particle number, there is one group of single-particle states whose occupations scale linearly with the total particle number, while the occupations of all other states saturate. The former states are called *Bose selected* and they can be inferred from the single-particle rates in the corresponding Lindblad master equation. While a general rule was found for when there is condensation in one

1. Introduction

single-particle state (namely when the rates feature a state that is ground-state-like), the question of in which physical scenario we expect how many Bose-selected states has still been unanswered. Depending on this number also the physics in the ultra-degenerate regime is possibly entirely different: for an intensive number of Bose-selected states, i.e. not scaling with the total number of states, the steady state can be seen as hosting fragmented condensation, while for an extensive number of selected states the steady state is rather like a classical gas in a reduced state space of e.g. half of the single-particle states. We show that in three scenarios general statements hold: if the rates are continuous, for random rates, and for rates that have a product structure. Moreover, we show that, for our purposes, the rates in chaotic Floquet systems cannot be simply assumed as uncorrelated random numbers, even though this was suggested in the literature [73]. Our results might also be useful to characterize the number of lasing modes in complex media, where the rate equations obey a similar structure [62].

With the third question, we want to come back to our original motivation about the possibility to engineer properties of nonequilibrium steady states which counter our intuition from the laws of equilibrium statistical mechanics. In one spatial dimension, Bose condensation is absent in the thermodynamic limit. The reason for this is that low-lying excitations, namely long-wave fluctuations, have thermal populations which are too high for an ordered condensed phase to form. In a *finite* one-dimensional ideal Bose gas, however, there is a crossover to a condensed phase at some equilibrium condensation temperature, which depends on system size. At fixed particle density, this temperature is inversely proportional to the system size such that the condensed phase vanishes in the thermodynamic limit. We will show a surprising finding: if a finite one-dimensional ideal Bose gas is in contact with two heat baths of different temperature, the emerging nonequilibrium steady state can feature Bose condensation even though there is no condensation when the gas is only in contact with any of the baths individually! Here, one of the baths is a global bath, representing a thermal environment. The other bath is a local bath that is much hotter than the global bath, which is why we want to refer to it as “hot needle”. At large system sizes, the environmental temperature for this nonequilibrium condensation can be several orders of magnitude higher than in equilibrium. The reason is the emergence of highly nonthermal occupation statistics in which the long-wave fluctuations are suppressed. The condensate is formed such that it overlaps only weakly with the driving site and therefore avoids the strong inflow of heat that is coming from the hot needle. This can be used to engineer condensation in excited states. In the thermodynamic limit, however, the one-dimensional nature of the system is revealed and also in the nonequilibrium steady state a true long-range ordered phase is absent.

The last question is how to find similar interesting steady states for *interacting* Bose gases. Here, if we want to find a microscopic description we are facing a problem that does not occur in the ideal gas. In the weak system–bath coupling limit the heat reservoir induces jumps between different eigenstates of the system Hamiltonian. These jumps happen at a rate given by the energy difference of these eigenstates. While the full many-body spectrum and the many-body eigenstates for the noninteracting gas directly follow from diagonalizing the single-particle Hamiltonian, diagonalizing the interacting problem (also beyond an effective low-energy description in terms of approximately

free quasiparticles) is usually extremely challenging. This strongly restricts the achievable system sizes and particle numbers. To circumvent this problem, we develop a semiclassical description of the bath interaction which assumes that we may reduce its action to transitions between localized wavelets. In contrast to other semiclassical methods, an ab-initio knowledge of if the system is condensed, or how many condensates (and therefore how many order-parameter fields) there are, is not needed. We employ our method for sufficiently weak interactions, where a good description of the interaction effects is expected by performing a mean-field approximation, which gives rise to an effective single-particle problem in a mean-field potential that is induced by the interaction with the background of all other particles. We benchmark the method at equilibrium. Furthermore, we apply it to the “hot needle” setup with weak interactions. Also, motivated by a recent quantum gas experiment [91] we study the dynamics of a mean-field interacting Bose-Hubbard system that is coupled to an external heat bath and undergoes local particle losses. The hope is that the external heat bath could model incoherent thermalization processes that are not captured in a mean-field approximation.

We think that all of these results constitute prime examples for *dissipative state engineering in quantum many-body systems*, or at least will guide the way to new ideas for how dissipation might be used as an additional “knob” to control complex quantum systems.

This thesis is organized as follows: in Chapter 2, we introduce the fundamental framework of this thesis, which is the master equation for open quantum systems. We will review both the axiomatic approach to the Lindblad master equation (which is essential for our considerations in Chapter 3), and the microscopic derivation of the Lindblad master equation from the assumption of weak system–bath coupling (which lays the foundation of the remaining chapters). We shift an introduction to Floquet theory to Chapter 3, where the concepts are introduced as soon as needed.

In Chapter 3 we discuss the existence of the Floquet Lindbladian. We apply the Markovianity test that was developed for general quantum channels in Ref. [105] to a simple qubit model and find that there are extended parameter regimes where the Floquet Lindbladian exists and where it does not. In the regime where it does not exist, we describe a method to find an effective time-homogeneous memory kernel, and we discuss the challenges of the high-frequency expansion for our model system.

Chapter 4 treats the number of Bose-selected states in nonequilibrium steady states of an ideal Bose gas. We shortly review the results of Ref. [82, 83] on Bose selection, where criteria were found with which one may determine the selected states from the antisymmetric part of the rate matrix only. We apply these criteria to find predictions for the typical number of selected states for continuous rates, uncorrelated random rates, and for rates with a product structure.

In Chapter 5 we turn to the “hot needle” setup for the ideal Bose gas. As a reference, we will first discuss equilibrium condensation in a finite one-dimensional tight-binding chain. Then, we qualitatively describe the high-temperature nonequilibrium condensation that we find. Following this, we turn to a quantitative analysis that predicts the nonequilibrium condensation temperature and the parameters for which excited-state condensation is expected. We show that the “hot needle” effect can also be found for the particle in a box as well as when the hot bath is replaced with a noisy Floquet drive.

1. Introduction

Chapter 6 gives an introduction to the semiclassical method that we have developed to overcome the problem that for the interacting gas, even writing down the master equation for a system coupled to a heat reservoir is a difficult task. We test our method with equilibrium states. Then, we find nonequilibrium states for the hot needle setup with mean-field interactions, and study the dynamics of a model that is motivated by the observation of a dynamical bistability in a recent quantum gas experiment with engineered local particle losses.

Finally, in Chapter 7 we summarize our results and give an outlook on possible future research directions and open questions.

2. Master equation for open quantum systems

The fundamental starting point for this thesis is the master equation for open quantum systems. Here, based on Refs. [73, 106–111], we motivate and introduce this equation.

2.1. Introduction

The master equation of open quantum systems is motivated by a very simple, yet fundamental question: What equation governs the dynamics of a quantum system that is not isolated from its environment, as it is assumed in the Schrödinger equation? As we sketch in Fig. 2.1, on a formal level, we may treat this problem by discussing scenarios where there is a sensible partition of the total physical Hilbert space $\mathcal{H}_{\text{tot}} = \mathcal{H}_S \oplus \mathcal{H}_E$ into a ‘system’, with Hamiltonian H_S , whose dynamics we want to keep track of, and its ‘environment’, with Hamiltonian H_E and some interaction H_{int} between both. The total Hamiltonian therefore reads ($\mathbb{1}_\alpha$ is the identity operator on \mathcal{H}_α , $\alpha = S, E$)

$$H_{\text{tot}} = H_S \otimes \mathbb{1}_E + \mathbb{1}_S \otimes H_E + H_{\text{int}}. \quad (2.1)$$

Here we focus on autonomous systems, $\partial_t H_S = 0$, we will turn to time-periodically driven systems in Chapter 3. For simplicity we restrict ourselves to finite-dimensional Hilbert spaces. Let $\varrho_{\text{tot}}(t)$ be the evolution of the total density matrix given by the Liouville-von-Neumann equation

$$\partial_t \varrho_{\text{tot}}(t) = -\frac{i}{\hbar} [H_{\text{tot}}, \varrho_{\text{tot}}(t)], \quad (2.2)$$

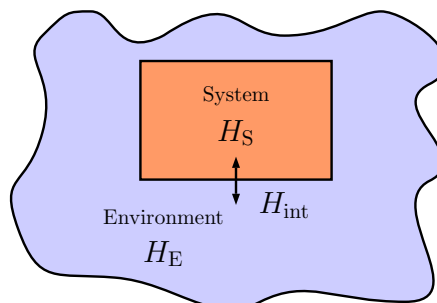


Figure 2.1.: Sketch of the general setup of interest in this thesis: there is a clear notion of a system and its environment.

2. Master equation for open quantum systems

which is solved formally by

$$\varrho_{\text{tot}}(t) = U(t)\varrho_{\text{tot}}(0)U^\dagger(t) \quad (2.3)$$

with unitary time-evolution operator $U(t) = \exp\left(-\frac{i}{\hbar}H_{\text{tot}}t\right)$. Let us consider the reduced density matrix of the system

$$\varrho_{\text{S}}(t) = \text{Tr}_{\text{E}}\varrho_{\text{tot}}(t), \quad (2.4)$$

where Tr_{E} is the partial trace over the environmental degrees of freedom. The question that we pose is which equation governs the time evolution of the reduced density matrix $\varrho_{\text{S}}(t)$. What we especially are looking for is an equation that depends on the reduced density matrix ϱ_{S} only, since in general it is hard to keep track of all (possibly infinitely many) environmental degrees of freedom.

Without interaction, $H_{\text{int}} = 0$, the dynamics factorizes $U(t) = U_{\text{S}}(t) \otimes U_{\text{E}}(t)$ with $U_{\text{S/E}}(t) = \exp\left(-\frac{i}{\hbar}H_{\text{S/E}}t\right)$. Then by using the Schmidt decomposition of $\varrho_{\text{tot}}(0) = \sum_i \alpha_i \otimes \beta_i$ we find that

$$\varrho_{\text{S}}(t) = \text{Tr}_{\text{E}}\varrho_{\text{tot}}(t) = \text{Tr}_{\text{E}} \left\{ U_{\text{S}}(t) \otimes U_{\text{E}}(t) \left(\sum_i \alpha_i \otimes \beta_i \right) U_{\text{S}}^\dagger(t) \otimes U_{\text{E}}^\dagger(t) \right\} \quad (2.5)$$

$$= U_{\text{S}}(t) \left[\sum_i \alpha_i \text{Tr} \left(U_{\text{E}}(t) \beta_i U_{\text{E}}^\dagger(t) \right) \right] U_{\text{S}}^\dagger(t) = U_{\text{S}}(t) \varrho_{\text{S}}(0) U_{\text{S}}^\dagger(t). \quad (2.6)$$

In the last step we have performed a cyclic permutation in the trace. As a result, we have

$$\partial_t \varrho_{\text{S}}(t) = -\frac{i}{\hbar} [H_{\text{S}}, \varrho_{\text{S}}(t)]. \quad (2.7)$$

Thus, without interaction we find the desired equation; the reduced density matrix undergoes independent coherent dynamics with Hamiltonian H_{S} . Under this coherent dynamics the eigenvalues (or populations) of $\varrho_{\text{S}}(t)$ remain constant and only the eigenstates are subject to a unitary rotation.

When the interaction is considered, $H_{\text{int}} \neq 0$, it is clear that in general the dynamics of ϱ_{S} cannot be unitary anymore. Think, e.g., of an atom in a cavity that is prepared in a mixed state $\varrho_{\text{S}}(0) = (|e\rangle\langle e| + |g\rangle\langle g|)/2$ of the ground state $|g\rangle$ and the excited state $|e\rangle$. At temperature $T = 0$ the atom will decay into the ground state, so asymptotically $\varrho_{\text{S}}(t \rightarrow \infty) = |g\rangle\langle g|$, which has different eigenvalues than the initial state. Thus, in the evolution of ϱ_{S} there must be an additional term that accounts for this population transfer, or more generally, for all noise and dissipation that are present in the effective description of subsystem ‘S’.

There are two possible approaches that one may take: The first one is *axiomatic* and motivated by the question ‘What is the ‘‘Schrödinger equation’’ of the open system?’, i.e. what is the most general (memoryless) equation of motion for ϱ_{S} which maps ‘physical’ density matrices onto ‘physical’ ones. This will lead us to master equations of Lindblad form. We will turn to this question in Section 2.2. Note that in order to provide some answer to this question one has to clarify what ‘physical’ should mean (which will lead us to the notion of completely positive quantum dynamical semigroups).

The second approach is *constructive* and finds a microscopic derivation of the master equation. As we discuss in Section 2.3, starting from the von-Neumann equation for the total system, Eq. (2.2), three approximations are needed to arrive at an equation of motion for the reduced density matrix that is of the form of a Lindblad master equation. All approximations are motivated by the assumption that the system–bath coupling is weak. First, it is assumed that no entanglement between system and bath is build up (Born approximation). Secondly, it is assumed that the bath has no memory (Markov approximation). Thirdly, we are looking at cases where the system–bath coupling is weak when compared to all energy splittings of H_S , such that the off-diagonal elements of ϱ_S decay asymptotically (rotating wave approximation). We will illustrate our discussion for a phononic heat bath.

2.2. Axiomatic approach: Lindblad master equation

Let us turn to the question ‘What is the most general equation that governs the evolution of a physical density matrix?’. Here we will restrict ourselves to memoryless (Markovian) evolutions. Then, ‘physical’ evolutions in the sense of ‘compatible with quantum mechanics’ are characterized by completely positive quantum dynamical semigroups. Their importance has first been recognized by Lindblad [112], Gorini, Kossakowski and Sudarshan [113].

2.2.1. Quantum dynamical semigroups

From now on, we focus on the dynamics of the reduced density matrix $\varrho \equiv \varrho_S$, so we will drop the index ‘S’. A *quantum dynamical semigroup* is a one-parameter family of superoperators $\mathcal{P}(t)$ on \mathcal{H} (that map operators in \mathcal{H} onto operators in \mathcal{H} ; more formally, let $L(\mathcal{H})$ be the space of linear operators on \mathcal{H} , then $\mathcal{P}(t) \in L(L(\mathcal{H}))$). The semigroup shall give rise to the time-evolution of the reduced density matrix,

$$\varrho(t) = \mathcal{P}(t)\varrho(0). \quad (2.8)$$

$\mathcal{P}(t)$ is also referred to as the *dynamical map*. Therefore it should fulfill the following requirements

- **Positivity:** For all positive operators $\sigma \in L(\mathcal{H})$, $\sigma \geq 0$, it holds that $\mathcal{P}(t)\sigma \geq 0$, such that we may interpret the eigenvalues as probabilities. Note that positivity also implies that $\mathcal{P}(t)$ preserves hermiticity, i.e. if $\sigma = \sigma^\dagger$ then $\mathcal{P}(t)\sigma = [\mathcal{P}(t)\sigma]^\dagger$.
- **Trace preservation:** For all operators $\sigma \in L(\mathcal{H})$ with $\text{Tr}(\sigma) = 1$ it holds that $\text{Tr}(\mathcal{P}(t)\sigma) = 1$, i.e. the (trace) norm of the physical states is conserved.
- **Semigroup property:** For all t, s it holds that $\mathcal{P}(s+t) = \mathcal{P}(s)\mathcal{P}(t)$. We will take this property as the definition of *time-homogeneous* (or *time-independent*) *Markovian dynamics*. It means, that at any point t in time we may stop the evolution, ‘reset’ it, and evolve the system for the remaining time s with the dynamical map again. Here, we already see an important implication: there cannot be any “memory” of the history of the system that is past time t . And since we may

2. Master equation for open quantum systems

perform this decomposition at any intermediate time t , it is clear that there is no memory of the history at all. So in an equation of motion $\partial_t \varrho(t) = \dots$, the right-hand side may also depend on $\varrho(t)$ only, similar to the von-Neumann equation.

- Continuity: For all operators $\sigma \in L(\mathcal{H})$ it holds that $\lim_{t \rightarrow 0^+} \mathcal{P}(t)\sigma = \sigma$, which is sensible, since the system should evolve continuously with parameter time.

2.2.2. Complete positivity

Although this list might look complete on first glance, there is an important point missing that is connected to the existence of entangled states in quantum mechanics,

$$\varrho_{\text{ent}} \in L(\mathcal{H} \otimes \mathcal{H}_A) \text{ with } \varrho_{\text{ent}} \neq \varrho \otimes \varrho_A, \quad (2.9)$$

where \mathcal{H}_A is the environment (or some part of it). It is easy to show [106, 114] that if $\mathcal{P}(t), \mathcal{P}_A(t)$ are quantum dynamical semigroups on \mathcal{H} and \mathcal{H}_A respectively, then $[\mathcal{P}(t) \otimes \mathcal{P}_A(t)]\varrho_{\text{ent}}$ need not be positive anymore.

To avoid this problem, we will expand the list by the requirement of

- Complete positivity: $\mathcal{P}(t)$ is n -positive for all $n \in \mathbb{N}$ and t , i.e. it holds that $\mathcal{P}_n(t) = \mathcal{P}(t) \otimes \mathbb{1}_n$ is positive, where $\mathbb{1}_n$ is the identity on an n -dimensional Hilbert space.

For simplicity, from now on we will use the term “quantum dynamical semigroup” for a quantum dynamical semigroup equipped with complete positivity. Disregarding the semigroup property, at given time t the resulting dynamical map $\mathcal{P}(t)$ is a *completely positive trace-preserving* (CPTP) map, or a *quantum channel*.

A characterization of completely positive maps is found by the Choi-Kraus theorem [110, 115]. It states that any linear map \mathcal{P} is completely positive iff it has the Kraus representation

$$\mathcal{P}\varrho = \sum_{i=1}^M V_i \varrho V_i^\dagger \text{ with linearly independent } V_i \in L(\mathcal{H}), \quad (2.10)$$

where $M \leq N^2$ and N is the dimension of \mathcal{H} . As a direct consequence it follows that \mathcal{P} is completely positive iff it is N -positive. Additionally, \mathcal{P} is trace-preserving iff additionally we have

$$\mathbb{1} = \sum_{i=1}^M V_i^\dagger V_i. \quad (2.11)$$

A handy tool to investigate a quantum channel \mathcal{P} is the *Choi(-Jamiołkowski) isomorphism*: it provides a mapping of the quantum channel $\mathcal{P} \in L(L(\mathcal{H}))$ onto a quantum state (i.e. density matrix) $\mathcal{P}^\Gamma \in L(\mathcal{H} \otimes \mathcal{H})$ in the Hilbert space extended with itself as an ancilla. Let us first define the maximally

entangled state

$$|\Phi\rangle = \frac{1}{\sqrt{N}} \sum_{i=1}^N |i\rangle \otimes |i\rangle \quad (2.12)$$

where $\{|i\rangle\}$ is the canonical basis of \mathcal{H} .

The Choi isomorphism is then given by

$$\mathcal{P}^\Gamma = N \cdot (\mathcal{P} \otimes \mathbb{1}_N)[|\Phi\rangle\langle\Phi|] = \sum_{i,j=1}^N \mathcal{P}(|i\rangle\langle j|) \otimes |i\rangle\langle j|. \quad (2.13)$$

It has the following properties [116]

- \mathcal{P} is hermiticity-reserving iff \mathcal{P}^Γ is a hermitian operator, $\mathcal{P}^\Gamma = \mathcal{P}^{\Gamma\dagger}$.
- \mathcal{P} is n -positive iff \mathcal{P}^Γ is an n -positive operator, i.e. $\langle\psi|\mathcal{P}^\Gamma|\psi\rangle \geq 0$ for all $|\psi\rangle \in \mathcal{H} \otimes \mathcal{H}$ with Schmidt rank n or less (the number of terms in the Schmidt decomposition).
- \mathcal{P} is completely positive iff \mathcal{P}^Γ is a positive operator, $\mathcal{P}^\Gamma \geq 0$.

As a result, in order to check if a map \mathcal{P} is completely positive (which is quite involved from its original definition) it suffices to compute the matrix \mathcal{P}^Γ , check if it is hermitian and whether its eigenvalues are nonnegative, which is straight-forward.

2.2.3. Lindblad master equation

Since the dynamical semigroup is a continuous semigroup, there exists a superoperator \mathcal{L} , the *generator* of the semigroup, such that

$$\mathcal{P}(t) = \exp(\mathcal{L}t). \quad (2.14)$$

Then, conversely, we may extract the generator \mathcal{L} , which we call the *Lindbladian*, from

$$\mathcal{L} = \lim_{t \rightarrow 0^+} \frac{\mathcal{P}(t) - \mathbb{1}}{t}. \quad (2.15)$$

On the level of the density matrix, one finds

$$\partial_t \varrho(t) = \mathcal{L}\varrho(t), \quad (2.16)$$

which is the master equation that we are aiming for. It is only left to find out how the other properties of the dynamical semigroup, trace preservation and complete positivity, restrict the shape of \mathcal{L} .

Using the Kraus representation, Eq. (2.10), of the dynamical semigroup we are able to find the desired master equation [117]. It is clear that for all t there exist Kraus operators $V_i(t)$ such that the

2. Master equation for open quantum systems

dynamical map can be represented as

$$\mathcal{P}(t)\varrho = \sum_{i=1}^M V_i(t)\varrho V_i^\dagger(t) \text{ with } \mathbb{1} = \sum_{i=1}^M V_i(t)^\dagger V_i(t). \quad (2.17)$$

Since $\mathcal{P}(t)$ is differentiable (because of Eq. (2.15)), for infinitesimal dt we may write

$$\mathcal{P}(0+dt)\varrho = \varrho + dt\mathcal{L}\varrho \equiv \sum_{i=1}^M V_i(0+dt)\varrho V_i(0+dt)^\dagger. \quad (2.18)$$

As a result, the Kraus operators have to obey the form

$$V_i(0+dt) = V_i^{(0)} + \sqrt{dt}V_i^{(1)} + dtV_i^{(2)} \quad (2.19)$$

where in order to have no term $\propto \sqrt{dt}$ in Eq. (2.18), it either holds that $V_i^{(0)} \neq 0$ and $V_i^{(1)} = 0$ or it holds $V_i^{(0)} = 0$ and then we may disregard the term $V_i^{(2)}$. Since $\mathcal{P}(0)$ is the identity channel, there can be only one Kraus operator with $V_i^{(0)} \neq 0$, namely

$$V_1(0+dt) = \mathbb{1} + (K - iH) \cdot dt \quad (2.20)$$

with $K = K^\dagger$, $H = H^\dagger$, where we have used that any operator can be written as the sum of its hermitian and its antihermitian part. We represent all other operators as

$$V_{i\neq 1}(0+dt) = L_{i-1}\sqrt{dt}. \quad (2.21)$$

Plugging this in Eq. (2.18) we find

$$\mathcal{L}\varrho = -i[H, \varrho] + (K\varrho + \varrho K) + \sum_{i=1}^{M-1} L_i\varrho L_i^\dagger. \quad (2.22)$$

From the Kraus sum normalization condition in Eq. (2.17), it follows

$$0 = i(H - H) + 2K + \sum_{i=1}^{M-1} L_i^\dagger L_i. \quad (2.23)$$

Solving for K we finally find the Lindblad master equation

$$\partial_t\varrho(t) = \mathcal{L}\varrho(t) = -i[H, \varrho(t)] + \sum_{i=1}^{M-1} \left(L_i\varrho(t)L_i^\dagger - \frac{1}{2}\{L_i^\dagger L_i, \varrho(t)\} \right), \quad (2.24)$$

where $\{\cdot, \cdot\}$ is the anticommutator. The first part gives rise to the reversible, coherent evolution. Nevertheless, H is not necessarily the system Hamiltonian H_S , but may also include contributions stemming from the system-bath interaction (we absorb \hbar into the Hamiltonian). The second part describes the irreversible, dissipative evolution. It is governed by the *Lindblad operators* (or *jump*

operators) L_i . The first term in the bracket describes how the interaction with the environment transfers populations in the reduced state ρ , while the second term is there to conserve the norm of ρ .

Note that we will always choose the Lindblad operators as traceless operators, $\text{Tr}(L_i) = 0$. This is because if we would choose operators with a finite trace, $\tilde{L}_i = c_i \mathbb{1} + L_i$, in Eq. (2.24) (with some complex number c_i) it is straight forward to prove that this only leads to a redefinition of the Hamiltonian $H \rightarrow H + i \sum_{i=1}^{M-1} (c_i^* L_i - c_i L_i^\dagger)$. The convention of traceless jump operators gets rid of this freedom.

Finally, let us reformulate the dissipative term in Eq. (2.24) in terms of an arbitrary traceless basis $\{A_i\}$ of the operator space $L(\mathcal{H})$. That means, we find a transformation T such that

$$L_i = \sum_{j=1}^{N^2-1} T_{ij} A_j. \quad (2.25)$$

Plugging this in Eq. (2.24), we obtain

$$\partial_t \rho(t) = -i [H, \rho(t)] + \sum_{i,j=1}^{N^2-1} d_{ij} \left(A_i \rho(t) A_j^\dagger - \frac{1}{2} \{A_j^\dagger A_i, \rho(t)\} \right), \quad (2.26)$$

with coefficient matrix

$$d_{ij} = \sum_{k=1}^{M-1} T_{ki} T_{kj}^*. \quad (2.27)$$

Then, we immediately see that d is hermitian, $d_{ij} = d_{ji}^*$, and for all vectors $x \in \mathbb{C}^{N^2-1}$ we have

$$x^\dagger dx \geq 0. \quad (2.28)$$

Thus, d is *positive semidefinite*.

Conversely, a general superoperator $\mathcal{L} \in L(L(\mathcal{H}))$ that is brought to the form of Eq. (2.26) is only a proper Lindbladian, if the matrix d is positive semidefinite. This requirement is the manifestation of complete positivity. Namely, only then we may diagonalize the matrix

$$d_{ij} = (U^\dagger D U)_{ij} = \sum_{k=1}^{N^2-1} U_{ki}^* \gamma_k U_{kj} \quad (2.29)$$

with nonnegative eigenvalues, or rates, $\gamma_k \geq 0$. With this we may bring Eq. (2.26) to the form of Eq. (2.24) by using

$$L_k = \sqrt{\gamma_k} \sum_{i=1}^{N^2-1} U_{ki}^* A_i. \quad (2.30)$$

To conclude, the Lindblad master equation is the result of our requirement of a physical evolution of the reduced density matrix, which we formalize in the postulates of the dynamical semigroup. The form of the Lindblad equation then follows by differentiating the Kraus representation that has to

hold for the dynamical map because of trace preservation and complete positivity.

2.3. Microscopic approach: Born–Markov rate equation

Our considerations in Sec. 2.2 are motivated from a more mathematical point of view, namely from the question what the most general equation of motion for a memoryless (Markovian) evolution of the reduced density matrix is. However, the question remains open what this equation will look like in a concrete physical system. Starting from the total Hamiltonian, Eq. (2.1), we will perform the Born, Markov and the rotating-wave approximation, which are basically motivated by a separation of time scales of the dynamics, to arrive at a rate equation which is of Lindblad form. We will illustrate our results for a phononic heat bath.

2.3.1. Born approximation

In this section we follow closely the argumentation in Ref. [109].

Let us start by transforming the von-Neumann equation (2.2) into the interaction picture. For any operator $A(t) \in L(\mathcal{H}_S \otimes \mathcal{H}_E)$, it is defined via

$$\tilde{A}(t) = [U_S^\dagger(t) \otimes U_E^\dagger(t)]A(t)[U_S(t) \otimes U_E(t)]. \quad (2.31)$$

Then, Eq. (2.2) takes the form

$$\partial_t \tilde{\varrho}_{\text{tot}}(t) = -\frac{i}{\hbar} [\tilde{H}_{\text{int}}(t), \tilde{\varrho}_{\text{tot}}(t)]. \quad (2.32)$$

We may formally integrate this equation to find

$$\tilde{\varrho}_{\text{tot}}(t) = \tilde{\varrho}_{\text{tot}}(0) - \frac{i}{\hbar} \int_0^t d\tau [\tilde{H}_{\text{int}}(\tau), \tilde{\varrho}_{\text{tot}}(\tau)]. \quad (2.33)$$

If we plug this back into the right hand side of Eq. (2.32) we obtain

$$\partial_t \tilde{\varrho}_{\text{tot}}(t) = -\frac{i}{\hbar} [\tilde{H}_{\text{int}}(t), \tilde{\varrho}_{\text{tot}}(0)] - \frac{1}{\hbar^2} \int_0^t d\tau [\tilde{H}_{\text{int}}(t), [\tilde{H}_{\text{int}}(\tau), \tilde{\varrho}_{\text{tot}}(\tau)]]. \quad (2.34)$$

This equation is equivalent to Eq. (2.32), however it includes the interaction Hamiltonian \tilde{H}_{int} on second order, which will be useful for the following considerations.

Throughout the whole derivation we want to assume that the system–environment coupling is ‘weak’ when compared to the energy scales of H_S and H_E . We will specify what we mean by ‘weak’ at multiple instances in the derivation. The first instance is now, when we want to discuss entanglement between the system and its environment. We require that at $t = 0$ there is no entanglement between the system and its environment. The Hamiltonian \tilde{H}_{int} shall be weak such that there is no significant

buildup of entanglement during the evolution, and we may approximate

$$\tilde{\varrho}_{\text{tot}}(t) \approx \tilde{\varrho}(t) \otimes \tilde{\varrho}_{\text{E}}. \quad (2.35)$$

Here, we have additionally assumed that the environment is ‘large’ in the sense that it has many degrees of freedom. We will call such an environment *reservoir* or *bath*. As a result, the state of the reservoir $\tilde{\varrho}_{\text{E}}$ is unaltered by the weak contact to the ‘smaller’ system. These approximations that lead to Eq. (2.35) are known as *Born approximation*.

Plugging Eq. (2.35) into Eq. (2.34) and performing the trace over the reservoir degrees of freedom we find

$$\partial_t \tilde{\varrho}(t) = -\frac{i}{\hbar} \left[\text{Tr}_{\text{E}}(\tilde{H}_{\text{int}}(t) \tilde{\varrho}_{\text{E}}), \tilde{\varrho}(0) \right] - \frac{1}{\hbar^2} \int_0^t d\tau \text{Tr}_{\text{E}} \left[\tilde{H}_{\text{int}}(t), [\tilde{H}_{\text{int}}(\tau), \tilde{\varrho}(\tau) \otimes \tilde{\varrho}_{\text{E}}] \right]. \quad (2.36)$$

Let us discuss the first term of the right hand side of this equation. Note that we may assume that $H_{\text{shift}} = \text{Tr}_{\text{E}}(H_{\text{int}} \varrho_{\text{E}}) = 0$. Because if it was nonzero, we simply may absorb its contribution in the system Hamiltonian, $H_{\text{int}} \rightarrow H_{\text{int}} - H_{\text{shift}} \otimes \mathbb{1}_{\text{E}}$ and $H_{\text{S}} \rightarrow H_{\text{S}} + H_{\text{shift}}$ in Eq. (2.1).

Thus, the first term in Eq. (2.36) drops out and we are left with the second term. Using a Schmidt decomposition of the interaction Hamiltonian we find

$$H_{\text{int}} = \sum_{\alpha} s_{\alpha} \otimes \Gamma_{\alpha}, \quad (2.37)$$

where we require that the system- and bath coupling operators are hermitian, $s_{\alpha} = s_{\alpha}^{\dagger}$, $\Gamma_{\alpha} = \Gamma_{\alpha}^{\dagger}$. Transforming this into the interaction picture, we may rewrite Eq. (2.36) as

$$\partial_t \tilde{\varrho}(t) = -\frac{1}{\hbar^2} \sum_{\alpha, \beta} \int_0^t d\tau \left([\tilde{s}_{\alpha}(t) \tilde{s}_{\beta}(\tau) \tilde{\varrho}(\tau) - \tilde{s}_{\beta}(\tau) \tilde{\varrho}(\tau) \tilde{s}_{\alpha}(t)] \langle \tilde{\Gamma}_{\alpha}(t) \tilde{\Gamma}_{\beta}(\tau) \rangle_{\text{E}} + \text{h.c.} \right). \quad (2.38)$$

with $\langle \cdot \rangle_{\text{E}} = \text{Tr}_{\text{E}}(\varrho_{\text{E}} \cdot)$. This is the master equation in Born approximation. Note that the right-hand side still depends on $\tilde{\varrho}(\tau)$, i.e. the evolution is non-Markovian as it will, in general, depend on the history of the reduced state.

2.3.2. Markov approximation

In many physical situations, one can get rid of this cumbersome dependence on the history of the state. This will lead us to a discussion of the time scales of the dynamics.

Let us investigate the bath correlation functions $C_{\alpha\beta}(t, \tau) = \langle \tilde{\Gamma}_{\alpha}(t) \tilde{\Gamma}_{\beta}(\tau) \rangle_{\text{E}}$. Since the state of the bath is stationary, it is clear that they may only depend on the temporal distance $t - \tau$, i.e.

$$C_{\alpha\beta}(t, \tau) \equiv C_{\alpha\beta}(t - \tau) = \langle \tilde{\Gamma}_{\alpha}(t - \tau) \tilde{\Gamma}_{\beta}(0) \rangle_{\text{E}}. \quad (2.39)$$

In most physical reservoirs, these correlation functions will decay on a time scale τ_{B} . Since the reservoir is large, typically, the information gets scrambled on time scales τ_{B} that are much faster than the time

2. Master equation for open quantum systems

scale τ_R of the relaxation dynamics of the system, $\tau_B \ll \tau_R$. Note that this is especially compatible with our requirement of ‘weak’ system–bath coupling H_{int} , because the time scale τ_R is inversely proportional to the small energy scale of H_{int} (to be precise, τ_R is scaling as $\tau_R \propto \hbar^2 \gamma^{-2}$ if $H_{\text{int}} \propto \gamma$). Therefore, on the relevant time scales of the integral in Eq. (2.38), the reduced density matrix is approximately constant. Consequently, we may perform the first step of the *Markov approximation* and replace $\tilde{\varrho}(\tau)$ with $\tilde{\varrho}(t)$ to obtain

$$\partial_t \tilde{\varrho}(t) = -\frac{1}{\hbar^2} \sum_{\alpha, \beta} \int_0^t d\tau \left([\tilde{s}_\alpha(t), \tilde{s}_\beta(\tau) \tilde{\varrho}(t)] C_{\alpha\beta}(t-\tau) + \text{h.c.} \right). \quad (2.40)$$

This is the *Redfield master equation*.

Now it is convenient to replace the integration variable $\tau \rightarrow t - \tau$, such that in the integral it occurs the factor $C_{\alpha\beta}(\tau)$. Then, since $C_{\alpha\beta}(\tau)$ decays rapidly, we may extend the upper bound of the integral to infinity, which is the second part of the Markov approximation,

$$\partial_t \tilde{\varrho}(t) = -\frac{1}{\hbar^2} \sum_{\alpha, \beta} \int_0^\infty d\tau \left([\tilde{s}_\alpha(t), \tilde{s}_\beta(t-\tau) \tilde{\varrho}(t)] C_{\alpha\beta}(\tau) + \text{h.c.} \right). \quad (2.41)$$

This is, in principle, the Born-Markov master equation.

We may arrive at a form that is more convenient by introducing the eigenstates of the system Hamiltonian,

$$H_S |n\rangle = E_n |n\rangle. \quad (2.42)$$

Then, we may rewrite

$$\langle n | \tilde{s}_\alpha(t) | m \rangle = e^{\frac{i}{\hbar}(E_n - E_m)t} s_{nm}^\alpha, \quad \text{and} \quad \langle n | \tilde{\varrho}(t) | m \rangle = e^{\frac{i}{\hbar}(E_n - E_m)t} \varrho_{nm}(t), \quad (2.43)$$

with matrix elements $s_{nm}^\alpha = \langle n | s_\alpha | m \rangle$ as well as $\varrho_{nm}(t) = \langle n | \varrho(t) | m \rangle$.

Taking the matrix elements of Eq. (2.41) and inserting the completeness relation $\mathbb{1}_S = \sum_k |k\rangle \langle k|$ between the operators, we find

$$\begin{aligned} \partial_t \varrho_{nm}(t) = & -\frac{i}{\hbar} (E_n - E_m) \varrho_{nm}(t) \\ & + \frac{1}{2} \sum_{k,l} \left[R_{ml,nk} \varrho_{kl}(t) - R_{kn,kl} \varrho_{lm}(t) + R_{nk,ml}^* \varrho_{kl}(t) - R_{lm,lk}^* \varrho_{nk}(t) \right]. \end{aligned} \quad (2.44)$$

where and we have defined the rates

$$R_{nm,kl} = \frac{2\pi}{\hbar} \sum_{\alpha, \beta} s_{mn}^\alpha s_{kl}^\beta W_{\alpha\beta}(E_k - E_l), \quad (2.45)$$

and the (imaginary) Laplace transform of the bath-correlation function

$$W_{\alpha\beta}(E) = \frac{1}{\pi\hbar} \int_0^\infty d\tau e^{-\frac{i}{\hbar}E\tau} C_{\alpha\beta}(\tau). \quad (2.46)$$

Equation (2.44) is what we want to call the *Born-Markov master equation*. Note that Eq. (2.44) is generally not of Lindblad form, which we would wish to hold such that a physical evolution of the density matrix is guaranteed. For example, by using the Lindblad operators $L_{nm} = |n\rangle\langle m|$, $n \neq m$, one may bring it to a form that is pseudo Lindblad, in the sense that it looks like Eq. (2.26) but with a coefficient matrix d that is *not* positive semidefinite. Hence, complete positivity (or even positivity) may be violated during the evolution with the Born-Markov master equation. However, it will be violated only on short time scales. The physical reason is that on these time scales the error that we made in Eq. (2.41) by replacing t in the integral with infinity is severe [118].

2.3.3. Rotating wave approximation

In the long time limit, however, complete positivity is guaranteed. This is because in this limit we may perform the rotating wave approximation (or secular approximation) to find a master equation that is of Lindblad form.

This approximation is again justified from a discussion of time scales of the dynamics. Here, we assume that the time scale of relaxation τ_R is slow when compared to a typical time scale of the system dynamics τ_S . Therefore, the dynamics may be thought of obeying the form

$$\varrho_{nm}(t) \approx e^{-\frac{i}{\hbar}(E_n - E_m)t} \varrho_{nm}(0) + \mathcal{O}(\gamma^2 t / \hbar^2), \quad (2.47)$$

with fast coherent oscillations on time scale $\tau_S = \max_{n \neq m} \hbar / (E_n - E_m)$ and slow dissipative dynamics on time scale $\tau_R \propto \hbar^2 / \gamma^2$ where γ is the order of magnitude of the system–bath coupling, $H_{\text{int}} \sim \gamma$. If $\tau_S \ll \tau_R$ the first term will dephase much faster than the time scale τ_R where contributions of the second term start to play a role, so in the dissipative dynamics we may assume that $\varrho_{nm}(t)$ is asymptotically diagonal.

More formally, this can be seen from transforming (2.44) back into the interaction picture

$$\varrho_{nm}(t) = e^{-\frac{i}{\hbar}\Delta_{nm}t} \tilde{\varrho}_{nm}(t), \quad (2.48)$$

with $\Delta_{nm} = E_n - E_m$. We find

$$\partial_t \tilde{\varrho}_{nm}(t) = \frac{1}{2} \sum_{k,l} \left[e^{\frac{i}{\hbar}(\Delta_{nm} - \Delta_{kl})t} (R_{ml,nk} + R_{nk,ml}^*) \tilde{\varrho}_{kl}(t) - e^{\frac{i}{\hbar}\Delta_{nl}t} R_{kn,kl} \tilde{\varrho}_{lm}(t) - e^{\frac{i}{\hbar}\Delta_{km}t} R_{lm,lk}^* \tilde{\varrho}_{nk}(t) \right]. \quad (2.49)$$

Now let us perform the *rotating wave approximation*: Since the dynamics of $\tilde{\varrho}$ is much slower, we average over the fast oscillating exponential functions. Assuming that there are no degeneracies in the

2. Master equation for open quantum systems

spectrum of H_S , i.e. $\Delta_{nm} \neq 0$ for $n \neq m$, this averaging yields

$$\begin{aligned} \partial_t \tilde{\varrho}_{nm}(t) = & \frac{1}{2} (R_{mm,nn} + R_{nn,mm}^*) \tilde{\varrho}_{nm}(t) + \\ & \frac{1}{2} \delta_{nm} \sum_{k \neq n} (R_{nk,nk} + R_{nk,nk}^*) \tilde{\varrho}_{kk}(t) - \frac{1}{2} \sum_k (R_{kn,kn} + R_{km,km}^*) \tilde{\varrho}_{nm}(t). \end{aligned} \quad (2.50)$$

Note that here we also assumed that there are no accidental degeneracies in the energy splittings, i.e. $\Delta_{nm} \neq \Delta_{kq}$ for $n \neq k$ and $m \neq q$.

As a result, in rotating wave approximation the probabilities $p_n(t) = \varrho_{nn}(t)$ relax independently from the coherences $\varrho_{nm}(t)$, $n \neq m$, namely as

$$\partial_t p_n(t) = \sum_m (R_{nm} p_m(t) - R_{mn} p_n(t)). \quad (2.51)$$

This is the *Pauli master equation*. Herein, we have defined the real-valued Pauli rates

$$R_{nm} = \frac{1}{2} (R_{nm, nm} + R_{nm, nm}^*). \quad (2.52)$$

These rates are nonnegative. The Pauli master equation is classical in the sense that the probability flow between states n is described by a classical Markov chain with rates R_{nm} . The quantum properties of the system manifest themselves in the existence of quantized states n and in the properties of the rates R_{nm} .

For the coherences one finds

$$\partial_t \varrho_{nm}(t) = \left[-\frac{i}{\hbar} (E_n - E_m) + \frac{1}{2} (R_{mm,nn} + R_{nn,mm}^*) - \frac{1}{2} \sum_k (R_{kn,kn} + R_{km,km}^*) \right] \varrho_{nm}(t). \quad (2.53)$$

Note that we may rewrite

$$R_{kn,kn} = R_{kn} + iQ_{kn} \quad (2.54)$$

with real matrix Q . Then, we may redefine the system energies

$$E'_n = E_n + \frac{\hbar}{2} \sum_k Q_{kn}. \quad (2.55)$$

This energy correction is known as *Lamb shift*. It is obvious that the correction scales as $\propto \gamma^2$, where γ is the overall strength of the system–bath coupling. Since, throughout this work, we are focusing on the limit $\gamma \rightarrow 0$, this correction will vanish for all of our purposes.

Finally, in rotating wave approximation we may reformulate the dynamics in a Lindblad master

equation

$$\begin{aligned} \partial_t \varrho(t) = & -\frac{i}{\hbar} [H', \varrho(t)] + \sum_{n \neq m} R_{nm} \left(L_{nm} \varrho(t) L_{nm}^\dagger - \frac{1}{2} \{L_{nm}^\dagger L_{nm}, \varrho(t)\} \right) \\ & + \sum_{n \neq m} D_{nm} \left(L_{nn} \varrho(t) L_{mm}^\dagger - \frac{1}{2} \{L_{mm}^\dagger L_{nn}, \varrho(t)\} \right). \end{aligned} \quad (2.56)$$

with Hamiltonian $H' = \sum_n E'_n |n\rangle\langle n|$, jump operators $L_{nm} = |n\rangle\langle m|$ and dephasing matrix

$$D_{nm} = \frac{1}{2} (R_{mm,nn} + R_{nn,mm}^*) = D_{mn}^*, \quad (2.57)$$

which can be rewritten as

$$D_{nm} = \frac{1}{2} \sum_{\alpha, \beta} s_{mm}^\alpha s_{nn}^\beta (W_{\alpha\beta}(0) + W_{\beta\alpha}^*(0)). \quad (2.58)$$

For the case where there are no cross-correlations, $W_{\alpha\beta}(E) = \delta_{\alpha\beta} W_\alpha(E)$, we directly see that this matrix is positive semidefinite and Eq. (2.56) is a proper Lindblad master equation. (Note that the Lindblad operators L_{nm} still have to be made traceless, which gives another Lamb-shift contribution that we want to ignore.)

Note that we have the scaling $R_{nm}, D_{nm} \propto \gamma^2$. Therefore, in the strict weak-coupling limit, $\gamma \rightarrow 0$, the corresponding terms vanish and we observe that the steady state, $\partial_t \varrho_{\text{st}} = 0$, has to commute with the Hamiltonian

$$0 = \partial_t \varrho_{\text{st}} = -\frac{i}{\hbar} [H_S, \varrho_{\text{st}}], \quad \text{for } \gamma \rightarrow 0. \quad (2.59)$$

More systematically, we may expand the steady state density matrix

$$\varrho_{\text{st}} = \sum_n p_n^{(0)} |n\rangle\langle n| + \gamma^2 \sum_{nm} \varrho_{nm}^{(2)} |n\rangle\langle m| + \mathcal{O}(\gamma^4). \quad (2.60)$$

Since the off-diagonal elements are suppressed in this limit, in the asymptotic dynamics the dephasing terms in the Lindblad equation are effectively suppressed with an additional factor γ^2 . So if we are only interested in the dominating order of the asymptotic late-time dynamics it suffices to study the Lindblad equation

$$\partial_t \varrho(t) = -\frac{i}{\hbar} [H_S, \varrho(t)] + \sum_{n \neq m} R_{nm} \left(L_{nm} \varrho(t) L_{nm}^\dagger - \frac{1}{2} \{L_{nm}^\dagger L_{nm}, \varrho(t)\} \right). \quad (2.61)$$

Intuitively, the bath transfers particles from state m to n with rate R_{nm} .

The dominating order of the steady state is diagonal in the eigenbasis of H_S with occupations $p_n^{(0)}$ that are obtained from the steady state of the Pauli equation (2.51).

2. Master equation for open quantum systems

2.3.4. Rates for coupling to thermal phonon reservoir

We want to find the Born-Markov rates for a typical heat bath. Let us specify the environmental degrees of freedom and the system–environment coupling in Eq. (2.1). A common choice for a bath environment is a collection of harmonic oscillators

$$H_E = \sum_{\alpha} \hbar\omega_{\alpha} b_{\alpha}^{\dagger} b_{\alpha} \quad (2.62)$$

It describes the quantized oscillatory (phononic) degrees of freedom in a heat bath, with bosonic annihilation operator b_{α} and frequency ω_{α} . We want to focus on the *diffusive regime*, where the system couples to the displacement $x_{\alpha} \propto (b_{\alpha}^{\dagger} + b_{\alpha})$ of the oscillators.

Let us assume that all oscillators couple to the same system coupling operator v . Then, the system–bath coupling takes the form

$$H_{\text{int}} = \gamma v \otimes \sum_{\alpha} c_{\alpha} (b_{\alpha}^{\dagger} + b_{\alpha}), \quad (2.63)$$

with (real) coupling coefficients c_{α} to each mode α . We have extracted the overall strength γ of the interaction, while v and c_{α} are assumed on the order of unity. Note that the Hamiltonian H_{int} already has the form of a direct product. Thus, its Schmidt rank is one and we have only one bath coupling operator $\Gamma = \sum_{\alpha} c_{\alpha} (b_{\alpha}^{\dagger} + b_{\alpha})$. A generalization to an interaction Hamiltonian H_{int} with multiple terms of this form is straight-forward.

Finally, let us fix the state ϱ_E of the reservoir. We want to assume that it is in a thermal state with temperature T (phonons have chemical potential $\mu = 0$),

$$\varrho_E = \frac{1}{\text{Tr}(e^{-H_E/k_B T})} e^{-H_E/k_B T} = \prod_{\alpha} \left(1 - e^{-\hbar\omega_{\alpha}/k_B T}\right) e^{-\hbar\omega_{\alpha} b_{\alpha}^{\dagger} b_{\alpha}/k_B T}. \quad (2.64)$$

Note that indeed we have $\text{Tr}_E(H_{\text{int}}\varrho_E) = 0$.

Let us compute the bath-correlation function

$$C(t) = \langle \tilde{\Gamma}(t) \tilde{\Gamma}(0) \rangle_E. \quad (2.65)$$

First, we transform the bath-coupling operator to the interaction picture,

$$\tilde{\Gamma}(t) = \sum_{\alpha} c_{\alpha} \left(e^{i\omega_{\alpha} t} b_{\alpha}^{\dagger} + e^{-i\omega_{\alpha} t} b_{\alpha} \right). \quad (2.66)$$

This yields

$$C(t) = \sum_{\alpha} c_{\alpha}^2 \left[e^{i\omega_{\alpha} t} n(\hbar\omega_{\alpha}) + e^{-i\omega_{\alpha} t} (n(\hbar\omega_{\alpha}) + 1) \right], \quad (2.67)$$

where we have defined the Planck occupation function $n(E) = (\exp(E/k_B T) - 1)^{-1}$.

Let us define the spectral density of the bath,

$$\bar{J}(E) = \sum_{\alpha} c_{\alpha}^2 \delta(E - \hbar\omega_{\alpha}), \quad (2.68)$$

which counts how many bath modes there are at energy E and how strong the system is coupled to them. Typically, Markovian baths have a continuum of modes α such that $\bar{J}(E)$ is a continuous function. A very prominent choice is $\bar{J}(E) = E$, the *ohmic bath*. This is because in the classical limit of the kinetic Hamiltonian $H = p^2/2m + V(q)$, this choice (together with system coupling operator $v = -q$ and $\gamma = \sqrt{\eta}$) gives rise to a Langevin equation with a linear friction term $-\eta\dot{q}$ [73, 119]. Other common choices are $\bar{J}(E) = E^d$, where for $d > 1$ the bath is called *superohmic*, and for $d < 1$ *subohmic*.

Also, to avoid divergences it is often needed to add a cutoff scale to $\bar{J}(E)$, for example by using an exponential cutoff at energy E_c [111]. However, throughout this work, we are mainly investigating systems with a bounded energy spectrum. In that case we do not run into such problems.

With this choice, we write

$$W(E) = \frac{1}{\pi\hbar} \int_{-\infty}^{\infty} dE' \int_0^{\infty} d\tau e^{-\frac{i}{\hbar}E\tau} \bar{J}(E') \left[e^{\frac{i}{\hbar}E'\tau} n(E') + e^{-\frac{i}{\hbar}E'\tau} (n(E') + 1) \right], \quad (2.69)$$

where we have set $\bar{J}(E) = 0$ for $E < 0$ and exchanged the two integrals. First, let us split the complex function W into its real and imaginary part

$$W(E) = g(E) + iw(E). \quad (2.70)$$

Then, using the Sokhotski–Plemelj formula (\mathcal{P} is the Cauchy principle value),

$$\lim_{\varepsilon \rightarrow 0^+} \int_{-\infty}^{\infty} dE \int_0^{\infty} d\tau e^{-iE\tau - \varepsilon\tau} f(E) = \pi f(0) - i\mathcal{P} \int_{-\infty}^{\infty} dE \frac{f(E)}{E}, \quad (2.71)$$

we directly obtain the real part of the bath-correlation function

$$g(E) = \begin{cases} \bar{J}(E)n(E) & \text{for } E > 0, \\ \bar{J}(-E)(n(-E) + 1) & \text{for } E < 0. \end{cases} \quad (2.72)$$

Note that for the Planck distribution it holds that $n(-E) + 1 = -n(E)$ such that it is convenient to define the antisymmetrized spectral density

$$J(E) = \bar{J}(E) - \bar{J}(-E), \quad (2.73)$$

which allows for a compact form which is valid for all E ,

$$g(E) = \frac{J(E)}{e^{E/k_{\text{B}}T} - 1}. \quad (2.74)$$

2. Master equation for open quantum systems

From this we find the Pauli rates for the phonon bath

$$R_{nm} = \frac{2\pi\gamma^2}{\hbar} |\langle n|v|m\rangle|^2 g(E_n - E_m). \quad (2.75)$$

This is the main result of this section. This rate is of Fermi's golden rule type as it depends on the matrix element of the coupling operator squared multiplied by some function which counts the density of states in the bath. However, it differs from Fermi's golden rule because we additionally have to take into account the thermal occupation of the bath at the given energy difference that occurs in the process.

Note that since the state ρ_E of the bath is thermal, it holds that

$$g(-E) = e^{E/k_B T} g(E). \quad (2.76)$$

As a result, the rates R_{nm} fulfill the following condition: there exist probabilities p_n such that

$$R_{nm}p_m = R_{mn}p_n \quad \text{for all } n, m. \quad (2.77)$$

It means that in the Pauli rate equation (2.51) all terms in the sum vanish *individually*. This condition is known as *detailed balance*, because there is no net probability flow between state n and m . This condition is only fulfilled in *thermal equilibrium*. In our case, it immediately follows that the probabilities p_n are given by the Boltzmann factors $p_n \propto \exp(-E_n/k_B T)$. As soon as we choose rates R_{nm} that do not fulfill a detailed balance condition, the system will relax to a *nonequilibrium steady state*. Possibly the easiest way of breaking detailed balance is by coupling the system to two heat baths of different temperature T_1 and T_2 . Then the total rates R_{nm} will be the sum of the individual rates of when the system is coupled to one of the baths only.

Let us shortly discuss the imaginary part w which is essential for the rates in the Born-Markov rate equation (2.44). Using Eq. (2.71) on Eq. (2.69), we obtain

$$w(E) = \frac{1}{\pi} \mathcal{P} \int_{-\infty}^{\infty} dE' \left(\frac{\bar{J}(E - E')n(E - E')}{E - E'} - \frac{\bar{J}(E' - E)(1 + n(E' - E))}{E' - E} \right). \quad (2.78)$$

For ohmic spectral density we find

$$w(E) = \frac{1}{\pi} \mathcal{P} \int_{-\infty}^{\infty} dE' n(E - E') \quad (2.79)$$

In the integral we may shift the variable $E' \rightarrow E - E'$ to find that the integral is independent on E . Thus, we have $w(E) = w_0 = \text{const.}$ (note that, strictly speaking, the integral diverges at the boundary infinity, but as we discussed earlier, we may cut it off at some energy E_c). If we think about what a redefinition $W(E) \rightarrow W(E) + iw_0$ means in the Born-Markov rate equation (2.44), we see that it may

be interpreted as a modification of the Hamiltonian

$$H_S \rightarrow H_S + \pi w_0 \sum_{k,n,m} \sum_{\alpha,\beta} s_{nk}^\alpha s_{km}^\beta |n\rangle\langle m| = H_S + \pi w_0 \sum_{\alpha,\beta} s_\alpha s_\beta, \quad (2.80)$$

which is a contribution that again vanishes in the weak-coupling limit $\gamma \rightarrow 0$.

As a result, for an ohmic bath we may absorb the imaginary part of the bath-correlation function in the Hamiltonian, giving rise to the Born-Markov rates

$$R_{nm,kl} = \frac{2\pi\gamma^2}{\hbar} \langle m|v|n\rangle\langle k|v|l\rangle g(E_n - E_m). \quad (2.81)$$

2.4. Rate equation for the ideal Bose gas

The mere requirement that the eigenenergies E_n and the eigenstates $|n\rangle$ of the system Hamiltonian H_S are known is extremely challenging for a quantum many-body system, since e.g. for distinguishable particles the Hilbert space grows exponentially with the number N of particles in the system. Therefore, for interacting quantum many-body systems, already writing down a Born-Markov rate equation in the form of Eq. (2.44) is an extremely challenging task.

An interesting exception are many-body localized systems [120–124]. There, the existence of localized integrals of motion (or l-bits) provides a convenient basis in which the full, interacting Hamiltonian is diagonal. We have discussed this in detail in Ref. [125], but these considerations will not be part of this thesis.

Noninteracting many-body systems, however, are readily treated if the diagonal form of the single-particle Hamiltonian is at hand. Let us discuss this fact for bosons, since throughout this work we will only discuss Bose gases. Similar considerations hold for noninteracting fermions [83]. Let us assume that we have diagonalized the single-particle Hamiltonian

$$H_S^{\text{SP}} = \sum_{k=1}^M \varepsilon_k |k\rangle\langle k|. \quad (2.82)$$

Note that we assume that the system is finite with M being the total number of single-particle states. Then, the many-particle Hamiltonian for the ideal gas of N bosons takes the form

$$H_S = \sum_k \varepsilon_k c_k^\dagger c_k, \quad (2.83)$$

where c_k is the bosonic annihilation operator for state k . This Hamiltonian is diagonal in the Fock basis $|\mathbf{n}\rangle = |n_1, n_2, \dots, n_M\rangle$ with occupation numbers $n_k \in \mathbb{N}_0$ of the single-particle states k , namely

$$H_S|\mathbf{n}\rangle = E_{\mathbf{n}}|\mathbf{n}\rangle = \sum_k \varepsilon_k n_k |\mathbf{n}\rangle. \quad (2.84)$$

2. Master equation for open quantum systems

Let us assume that the system's coupling operator v is a single-particle operator

$$v = \sum_{nm} v_{nm} c_n^\dagger c_m. \quad (2.85)$$

with $v_{mn} = v_{nm}^*$. Note that since the eigenstates and the spectrum of the system are known, we may find a Born-Markov rate equation (2.44) or a Pauli rate equation (2.51) for the Fock space matrix elements $\varrho_{\mathbf{m}\mathbf{m}'}$ of the density matrix. Such ideas are e.g. discussed in Refs. [83, 125].

Here we want to take a different approach that starts from the basis-free representation of the Born-Markov equation, Eq. (2.41). First, we note that

$$\tilde{v}(t - \tau) = \sum_{nm} e^{-\frac{i}{\hbar}(\varepsilon_n - \varepsilon_m)\tau} v_{nm} \tilde{c}_n^\dagger(t) \tilde{c}_m(t). \quad (2.86)$$

Plugging this in Eq. (2.41) [remember that here we use $s_\alpha = \gamma v$] we find

$$\partial_t \tilde{\varrho}(t) = -\frac{\pi\gamma^2}{\hbar} \sum_{nmkl} \left(\left[v_{mn} \tilde{c}_m^\dagger(t) \tilde{c}_n(t), v_{kl} \tilde{c}_k^\dagger(t) \tilde{c}_l(t) \tilde{\varrho}(t) \right] g(\varepsilon_k - \varepsilon_l) + \text{h.c.} \right). \quad (2.87)$$

Here, again, we have identified the Laplace transform $g(E)$ of the bath correlation function (let us focus on ohmic baths and ignore the renormalization of the system Hamiltonian). Now we may use the single-particle rates

$$R_{nm,kl} = \frac{2\pi\gamma^2}{\hbar} v_{mn} v_{kl} g(\varepsilon_k - \varepsilon_l), \quad (2.88)$$

and transform the equation back to the Schrödinger picture to find

$$\partial_t \varrho(t) = -\frac{i}{\hbar} [H_S, \varrho(t)] + \frac{1}{2} \sum_{nmkl} R_{nm,kl} \left(\left[c_k^\dagger c_l \varrho(t), c_m^\dagger c_n \right] + \text{h.c.} \right). \quad (2.89)$$

This is the second-quantized version of the Born-Markov rate equation for the ideal Bose gas. It is the starting point for our considerations in Chapter 6.

In the weak-coupling limit, $\gamma \rightarrow 0$, we may perform the rotating wave approximation to find the second-quantized version of the Lindblad equation (2.61) that governs the asymptotic dynamics. We find that it has the same form as Eq. (2.61), but with Lindblad operators $L_{nm} = c_n^\dagger c_m$, i.e.

$$\partial_t \varrho(t) = -\frac{i}{\hbar} [H_S, \varrho(t)] + \sum_{n \neq m} R_{nm} \left(c_n^\dagger c_m \varrho(t) c_m^\dagger c_n - \frac{1}{2} \{ c_m^\dagger c_n c_n^\dagger c_m, \varrho(t) \} \right). \quad (2.90)$$

Note that we can perform the rotating wave approximation only if the energies $E_{\mathbf{n}}$ of the states *connected* by v are nondegenerate. Since v is a single-particle operator, here it suffices that there are no degeneracies in the single-particle spectrum ε_k .

From this equation, we find the asymptotic dynamics of the expectation value of the occupation

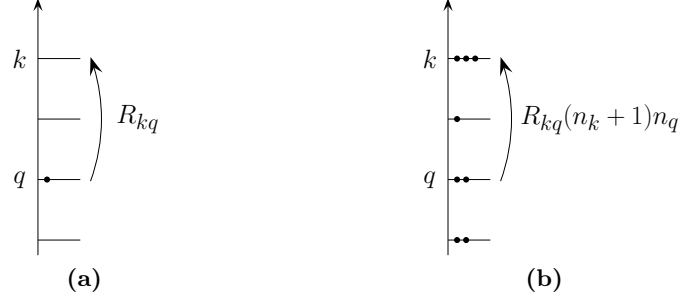


Figure 2.2.: Sketch of the dynamics of the occupations in an ideal Bose gas in weak coupling to its environment. (a) For a single particle, the environment induces jumps from level q to k which happen at rate R_{kq} . (b) Also in the ideal gas, single particles are transferred. The single particle rate for this process is amplified with the occupation n_q of the departure state and the bosonic enhancement factor $n_k + 1$.

numbers $n_k = c_k^\dagger c_k$,

$$\begin{aligned} \partial_t \langle n_k \rangle &= \text{Tr}(\partial_t \varrho(t) n_k) = -\frac{i}{\hbar} \langle [n_k, H_S] \rangle \\ &+ \frac{1}{2} \sum_{n \neq m} R_{nm} \left(\langle [c_m^\dagger c_n, n_k] c_n^\dagger c_m \rangle + \langle c_m^\dagger c_n [n_k, c_n^\dagger c_m] \rangle \right). \end{aligned} \quad (2.91)$$

Note that here we have suppressed the time dependence of all expectation values $\langle \cdot \rangle \equiv \langle \cdot \rangle(t)$. Now we use $[n_k, H_S] = 0$ as well as

$$[c_m^\dagger c_n, n_k] = c_m^\dagger [c_n, n_k] + [c_m^\dagger, n_k] c_n = (\delta_{nk} - \delta_{mk}) c_m^\dagger c_n. \quad (2.92)$$

Finally we use that for $n \neq m$ it holds that $c_m^\dagger c_n c_n^\dagger c_m = (n_n + 1)n_m$, giving

$$\partial_t \langle n_k \rangle = \sum_q \left[R_{kq} \langle (n_k + 1)n_q \rangle - R_{qk} \langle (n_q + 1)n_k \rangle \right]. \quad (2.93)$$

This is the many-particle rate equation for the occupations in an ideal Bose gas. It is the starting point for our analysis in Chapter 4 and 5. Its dynamics is sketched in Fig. 2.2. For the single-particle problem, Fig. 2.2(a), the environment induces quantum jumps of one particle from level q to level k . However, for the ideal Bose gas, Fig. 2.2(b), the rate for this process is the single-particle (Pauli) rate R_{kq} multiplied with two factors: the first factor is the occupation n_q of the departure state. This factor also occurs for classical, i.e. distinguishable, particles. The second factor $1 + n_k$ depends on the occupation of the target state and is the manifestation of quantum statistics. Bosons favor to occupy the same state, thus the rate is increasing with the occupation of the target state. This factor is known as bosonic enhancement- or bunching factor.

Note that Eq. (2.93) depends on higher-order correlators $\langle n_k n_q \rangle$. This is a result of the fact that, even though the system Hamiltonian is noninteracting, the full problem is interacting. This can be seen on two levels: The Lindblad operators L_{nm} are quadratic and therefore the dissipator is quartic.

2. Master equation for open quantum systems

This, again, is a consequence of the fact that the system–bath interaction H_{int} is cubic. For quadratic H_{int} , Eq. (2.93) becomes linear.

Remember that in the weak-coupling limit, $\gamma \rightarrow 0$, asymptotically the state will be diagonal in the eigenstates of the system, the Fock states,

$$\varrho(t) \xrightarrow{t \rightarrow \infty} \sum_{\mathbf{n}} p_{\mathbf{n}} |\mathbf{n}\rangle \langle \mathbf{n}|. \quad (2.94)$$

As a result, the steady state is fully characterized by the knowledge of all the moments of the occupations n_k , i.e. $\langle n_k \rangle$, $\langle n_k n_q \rangle$, $\langle n_k n_q n_l \rangle$, and so on. As was noted by Vorberg *et. al.* [82–84] and will be shortly discussed in Chapter 4, in many physical systems we may assume that the steady state factorizes, i.e. $p_{\mathbf{n}} \approx p_{n_1} p_{n_2} \cdots p_{n_M}$. Under this assumption, the state is fully characterized by knowledge of the mean occupations $\langle n_k \rangle$ only, and we may decompose the correlator $\langle n_k n_q \rangle \approx \langle n_k \rangle \langle n_q \rangle$, for $k \neq q$, in Eq. (2.93) to find a *mean field-* or *kinetic equation*. Then, by setting $\partial_t \langle n_k \rangle = 0$, we find a nonlinear equation from which we may extract these mean occupations in the steady state.

3. Existence of the Floquet Lindbladian

The stroboscopic evolution of a time-periodically driven isolated quantum system can always be described by an effective time-independent Hamiltonian. Whether this concept can be generalized to open Floquet systems, described by a Markovian master equation with time-periodic Lindbladian generator, remains an open question. By using a two level system as a model, we find two different phases. In one phase the stroboscopic evolution can be described by an effective Markovian master equation with a time-independent Floquet Lindbladian. In the other phase it cannot; but here the one-cycle evolution operator can be reproduced with an effective time-homogeneous master equation that is nonmarkovian. Interestingly, we find that the boundary between the phases depends on when during the period the evolution is monitored stroboscopically. This reveals the non-trivial role played by the micromotion in the dynamics of open Floquet systems. We discuss how the Floquet Lindbladian can be extracted from a high-frequency expansion and gain thereby some understanding of the role of the micromotion. These results shed light on opportunities and challenges for dissipative Floquet engineering.

The results of Sec. 3.1-3.3 have been published in Ref. [126]. Major parts of these sections are directly adapted from the publication and are expanded in order to provide for a more detailed discussion of the concept of the Floquet Lindbladian. The results of Sec. 3.4 on the high-frequency expansions are unpublished.

3.1. The Floquet Lindbladian

When the coherent evolution of an isolated quantum Floquet system, described by the time-periodic Hamiltonian $H(t) = H(t + T)$, is monitored stroboscopically in steps of the driving period T , this dynamics is described by repeatedly applying the one-cycle time-evolution operator

$$U(T) = \mathcal{T} \exp \left[-\frac{i}{\hbar} \int_0^T dt' H(t') \right] \quad (3.1)$$

(with time ordering \mathcal{T}) [127, 128]. It can always be expressed in terms of an effective time-independent Hamiltonian H_F , called Floquet Hamiltonian, $U(T) \equiv \exp(-iH_F T/\hbar)$. While the Floquet Hamiltonian is not unique due to the multi-branch structure of the operator logarithm $\log U(T)$, the unitarity of $U(T)$ implies that every branch is Hermitian like a proper Hamiltonian. The concept of the Floquet Hamiltonian suggests a form of quantum engineering, where a suitable time-periodic driving protocol is designed in order to effectively realize a system described by a Floquet Hamiltonian with desired novel properties. This type of Floquet engineering was successfully employed with ultracold atoms [8],

3. Existence of the Floquet Lindbladian

e.g. to realize artificial magnetic fields and topological band structures for charge neutral particles [14, 18–20, 129, 130].

However, systems like atomic quantum gases, which are very well isolated from their environment, should rather be viewed as an exception. Many quantum systems that are currently studied in the laboratory and used for technological applications are based on electronic or photonic degrees of freedom that couple to their environment. It is, therefore, desirable to extend the concept of Floquet engineering also to open Floquet systems. In this context, a number of papers investigating properties of the nonequilibrium steady states approached by these driven dissipative systems in the long-time limit have been published [71, 72, 74, 75, 77–80, 82, 83, 85, 89, 98], and we will cover some of the properties of steady states in bosonic quantum many body systems in the following chapters. In this chapter, in turn, we are interested in the (transient) dynamics of open Floquet systems and address the question as to whether it is possible to describe their stroboscopic evolution with time-independent generators, like it is the case for isolated systems.

We can distinguish three different possible scenarios for a given time-periodic Lindbladian $\mathcal{L}(t)$: (a) the action of the dynamical map $\mathcal{P}(T)$ can be reproduced with an effective Markovian master equation described by a time-independent Floquet Lindbladian \mathcal{L}_F , $\mathcal{P}(T) = \exp(T\mathcal{L}_F)$; (b) the action of $\mathcal{P}(T)$ is reproduced with an effective nonmarkovian master equation characterized by a time-homogeneous memory kernel; (c) the action of $\mathcal{P}(T)$ cannot be reproduced with any time-homogeneous master equation. Scenario (a) is implicitly assumed in recent papers [100–102], where a high-frequency Floquet-Magnus expansion [131] (routinely used for isolated Floquet systems [9, 39, 132]) is employed in order to construct an approximate Floquet Lindbladian. It requires that one branch of the operator logarithm $\log \mathcal{P}(T)$ has to be of Lindblad form so that it can be associated with $T\mathcal{L}_F$. However, differently from the case of isolated systems, for which any logarithm branch of the unitary evolution operator is guaranteed to be Hermitian, it is not obvious whether there is at least one valid branch for a given open Floquet system, since general CPTP maps do not always possess a logarithm of Lindblad type [105]. Below we demonstrate that scenario (a) is indeed not always realized even in the case of a simple two-level model. Instead, we find that the parameter space is shared by two phases corresponding to scenario (a) and (b), respectively.

We consider a time-dependent Markovian master equation [133]

$$\dot{\rho} = \mathcal{L}(t)\rho = -\frac{i}{\hbar}[H(t), \rho] + \mathcal{D}(t)\rho, \quad (3.2)$$

for the system's density operator ρ , described by a time-periodic generator $\mathcal{L}(t) = \mathcal{L}(t + T)$. It is characterized by a Hermitian time-periodic Hamiltonian $H(t)$ and a dissipator

$$\mathcal{D}(t)\rho = \sum_i \gamma_i(t) \left[L_i(t)\rho L_i^\dagger(t) - \frac{1}{2} \{ L_i^\dagger(t)L_i(t), \rho \} \right], \quad (3.3)$$

with traceless jump operators $L_i(t)$ and non-negative rates $\gamma_i(t)$, which both are time periodic. Note that the time-dependent variation of $\mathcal{L}(t)$ may either be due to a time-periodic modulation of the coherent evolution, governed by the Hamiltonian $H(t)$, or due to a time-periodic modulation of

the dissipative channels, represented by the rates $\gamma_i(t)$ and Lindblad operators $L_i(t)$. This is the most general time-local form guaranteeing an evolution described by a completely positive and trace preserving (CPTP) map consistent with quantum mechanics [133]. Such an evolution may also be called *time-dependent Markovian*.

Let us quickly revisit the Lindblad master equation. A quantum dynamical semigroup is an evolution $\mathcal{P}(t, t_0) \in L(L(\mathcal{H}))$ of the density matrix $\varrho \in L(\mathcal{H})$ in a Hilbert space \mathcal{H} ,

$$\varrho(t) = \mathcal{P}(t, t_0)\varrho(t_0), \quad \text{and we denote } \mathcal{P}(t) = \mathcal{P}(t, 0), \quad (3.4)$$

that is motivated by the constraints that a ‘physical’ evolution of the density matrix should obey: It is continuous, $\lim_{t \rightarrow 0^+} \mathcal{P}(t)\varrho = \varrho$, trace preserving, $\text{Tr}(\mathcal{P}(t)\varrho) = \text{Tr}(\varrho)$, has the semigroup property, $\mathcal{P}(t+s) = \mathcal{P}(t)\mathcal{P}(s)$, i.e. the evolution has no memory of its history, it is time-local or Markovian, and is completely positive, $\mathcal{P}(t) \otimes \mathbb{1} \geq 0$, where $\mathbb{1}$ is the identity on the operator space $L(\mathcal{H})$ over the Hilbert space \mathcal{H} .

As it was shown by Lindblad, Gorini, Kossakowski and Sudarshan [112], the superoperator \mathcal{L} that generates this evolution, i.e.

$$\partial_t \rho(t) = \mathcal{L}\rho(t), \quad \text{or equally } \mathcal{P}(t) = \exp(\mathcal{L}t), \quad (3.5)$$

has to obey the Lindblad form, Eq. (2.26), where H is a Hermitian operator, the Hamiltonian, $\{A_i\}$ is a traceless operator basis of $L(\mathcal{H})$ ($\dim(\mathcal{H}) = N$) and $d \geq 0$ is a Hermitian positive semidefinite coefficient matrix. The Lindblad operators L_i and the corresponding nonnegative rates γ_i can then be found by diagonalizing the coefficient matrix d .

Now, let us turn to the evolution $\mathcal{P}(t)$ that is generated by a time-dependent Lindbladian $\mathcal{L}(t)$, as in Eq. (3.2), which formally yields

$$\mathcal{P}(t) = \mathcal{T} \exp\left(\int_0^t dt \mathcal{L}(t)\right). \quad (3.6)$$

By definition, this gives rise to an evolution $\mathcal{P}(t)$ that is continuous, trace preserving and completely positive.

Since the evolution is time periodic, it is intriguing to study the stroboscopic dynamics, given by the one-cycle evolution superoperator [134, 135]

$$\mathcal{P}(T) = \mathcal{T} \exp\left[\int_0^T dt \mathcal{L}(t)\right], \quad (3.7)$$

which is CPTP, i.e. it is a quantum channel. The repeated application of it describes the stroboscopic evolution of the system, i.e. for all $\rho(0)$ one has

$$\rho(nT) = \mathcal{P}(T)^n \rho(0). \quad (3.8)$$

Let us first address the question of the existence of a Floquet Lindbladian. In the time-periodically

3. Existence of the Floquet Lindbladian

modulated isolated system, i.e. in our notation Eq. (3.2) with $\gamma_i(t) = 0$ for all i , it is well known that there always exists an effective time-independent Hamiltonian H_F , the Floquet Hamiltonian, such that

$$\mathcal{P}(T) = \exp\left(-\frac{i}{\hbar} [H_F, \cdot] T\right). \quad (3.9)$$

This Floquet Hamiltonian is subject to many theoretical studies, mainly due to the fact that it can be used as an experimental tool to create interesting dynamics that would not be present in the autonomous system. This technique has been coined Floquet engineering. Apart from that, the notion of a Floquet-Hamiltonian is also a very powerful tool in nuclear magnetic resonance spectroscopy [136]. How can one see that such a Floquet Hamiltonian H_F exists? For the coherent dynamics, the evolution operator reduces to a unitary rotation of the density matrix

$$\mathcal{P}(T) = U(T) \cdot U(T)^\dagger. \quad (3.10)$$

The unitary one-cycle evolution operator $U(T)$ is divisible (any root of it is a unitary operator) and yields a countably infinite set of Hermitian generators, $H_{U,\{x_1,\dots,x_N\}}$, $x_a \in \mathbb{Z}$, $U(T) = e^{-iH_U T/\hbar}$, parametrized by a choice of a branch of the logarithm $\log U(T)$. This can be seen most easily by representing the evolution operator $U(T)$, Eq. (3.1), in its spectral decomposition. Since it is unitary we may represent it as

$$U(T) = \sum_{a=1}^N e^{-i\varepsilon_a T/\hbar} P_a \quad (3.11)$$

with real numbers ε_a and (Hermitian) orthogonal projectors P_a onto the eigenspace a . Now it becomes apparent that, when computing the logarithm of $U(T)$, for every subspace a there is a freedom to pick a branch of the complex logarithm giving a whole set

$$\log [U(T)]_{\{x_1,\dots,x_N\}} = -i \sum_{a=1}^N (\varepsilon_a T/\hbar + 2\pi x_a) P_a. \quad (3.12)$$

parameterized by N integer numbers $x_a \in \mathbb{Z}$. For the corresponding Hermitian generator,

$$H_{U,\{x_1,\dots,x_N\}} = \sum_{a=1}^N (\varepsilon_a + \hbar\omega x_a) P_a, \quad (3.13)$$

this change of branch corresponds to a redefinition of the ‘energy’ $\varepsilon_a \rightarrow \varepsilon_a + \hbar\omega x_a$, where $\omega = 2\pi/T$ is the driving frequency. That means, the ‘energies’ ε_a are only defined up to integer multiples of $\hbar\omega$, which is why they are typically referred to as *quasi-energies*. Note that in the case of the coherent dynamics, any of these generators can be chosen as Floquet Hamiltonian H_F , since all of the generators $H_{U,\{x_1,\dots,x_N\}}$ qualify as physically sensible Hamiltonians. This choice can be made, e.g. by using the principal branch, $\forall x_s \equiv 0$, or the branch closest to the time-averaged Hamiltonian $\overline{H}(t)$.

In analogy to the closed system, a Floquet Lindbladian is a time-independent Lindblad superoper-

ator \mathcal{L}_F for which

$$\mathcal{P}(T) = \exp(\mathcal{L}_F T). \quad (3.14)$$

The aim is to find a time-independent Markovian evolution, generated by the Floquet Lindbladian \mathcal{L}_F , that coincides with $\mathcal{P}(t)$ at stroboscopic instances of time. As it was discussed in Ref. [105, 126], it is not necessary that such a Lindblad operator exists. Although, by using the complex matrix logarithm one is always able to find a general superoperator \mathcal{K} such that

$$\mathcal{P}(T) = \exp(\mathcal{K}T), \text{ i.e. } \mathcal{K} = \log(\mathcal{P}(T))/T, \quad (3.15)$$

this superoperator \mathcal{K} is not necessarily of Lindblad form, i.e. the corresponding evolution $\exp(\mathcal{K}t)$ is not necessarily a quantum dynamical semigroup anymore.

Since $\mathcal{P}(T)$ is a hermiticity-preserving map, its spectrum is invariant under complex conjugation. Thus, its N^2 eigenvalues are either real or appear by complex conjugated pairs (we denote the number of these pairs n_c). The Jordan normal form of the map $\mathcal{P}(T)$ can thus be represented as

$$\mathcal{P}(T) = \sum_{r=1}^{n_r} \lambda_r P_r + \sum_{c=1}^{n_c} (\lambda_c P_c + \lambda_c^* P_{c*}), \quad (3.16)$$

where λ_r are the real eigenvalues, λ_c, λ_c^* the pairs of complex eigenvalues, and P_x the corresponding (not necessarily Hermitian) orthogonal projectors on the corresponding subspaces.

Again, due to the nature of the complex logarithm, the operator \mathcal{K} in Eq. (3.15) is not uniquely defined, but for every branch of the logarithm we get a different operator. A straight-forward procedure to test whether a given candidate \mathcal{K} is a valid Lindblad generator is the Markovianity test proposed by Wolf *et al.* in Refs. [105, 137]: (i) Check if the operator \mathcal{K} is preserving Hermiticity, i.e. $\mathcal{K}\sigma = \mathcal{K}\sigma^\dagger$ for all $\sigma \in L(\mathcal{H})$ that are Hermitian, $\sigma = \sigma^\dagger$. (ii) For the second test, let us first define the maximally entangled state $|\Phi\rangle = \sum_{i=1}^N (|i\rangle \otimes |i\rangle) / \sqrt{N}$ where $\{|i\rangle\}$ is the canonical basis of \mathcal{H} . We need to check that the operator \mathcal{K} is conditionally completely positive, i.e. it has to hold

$$\Phi_\perp \mathcal{K}^\Gamma \Phi_\perp \geq 0, \quad (3.17)$$

where $\Phi_\perp = \mathbb{1} - |\Phi\rangle\langle\Phi|$ is the projector on the orthogonal complement of the maximally entangled state and $\mathcal{K}^\Gamma = N(\mathcal{K} \otimes \mathbb{1})[|\Phi\rangle\langle\Phi|] \in L(\mathcal{H}^2)$ is the Choi matrix of \mathcal{K} . Then the corresponding branch can be nominated for an effective Lindblad generator \mathcal{L}_F . Already here the contrast with the unitary case becomes apparent: it is not guaranteed that such branch exists.

Condition (i) simply demands that the spectrum of the candidate \mathcal{K} has to be invariant under complex conjugation. This means, in turn, that the spectrum of the map $\mathcal{P}(T)$ should not contain negative real eigenvalues $\lambda_r = -|\lambda_r|$ (strictly speaking, there must be no negative eigenvalues of odd degeneracy). That is, because if one would set the logarithm of such an occasion e.g. to $\log(\lambda_r) = i\pi + \log(|\lambda_r|)$, the spectrum is not invariant under conjugation anymore. In this case there is no Floquet

3. Existence of the Floquet Lindbladian

Lindbladian.

If $\mathcal{P}(T)$ has no negative real eigenvalues, we find that we may represent the family of all candidates $\mathcal{K}_{\{x_1, \dots, x_{n_c}\}}$ as

$$\mathcal{K}_{\{x_1, \dots, x_{n_c}\}} = \mathcal{K}_0 + i\omega \sum_{c=1}^{n_c} x_c (P_c - P_{c*}), \quad (3.18)$$

where \mathcal{K}_0 is the generator that follows from the principle branch of the logarithm of $\mathcal{P}(T)$. We have the freedom to pick integer numbers $\{x_c\} \in \mathbb{Z}^{n_c}$ that determine the branch of the logarithm for every pair of complex eigenvalues. Note that for the isolated system all eigenvalues of $\mathcal{P}(T)$ lie on the unit circle, therefore all eigenvalues of \mathcal{K} are purely imaginary (or zero). In the isolated system, with the freedom in Eq. (3.18) we recover that the eigenvalues of the Floquet Hamiltonian H_F , the quasi-energies, are only defined up to multiples of the driving frequency ω , so all branches lead to a physical evolution. For the open system, typically only a few, sometimes even none of the branches lead to a generator that is physical in the sense that it is of Lindblad form.

For that, we need to check condition (ii), which is more complicated and involves properties of the eigenelements of the Floquet map. As coined in Refs. [105, 137], by plugging the candidates, Eq. (3.18), into the test for conditional complete positivity, Eq. (3.17), it comes in handy to define a set of $n_c + 1$ Hermitian matrices

$$V_0 = \Phi_{\perp} \mathcal{K}_0^{\Gamma} \Phi_{\perp}, \quad V_c = i\omega \Phi_{\perp} (P_c - P_{c*})^{\Gamma} \Phi_{\perp}, \quad c = 1, \dots, n_c. \quad (3.19)$$

The condition is fulfilled, if there is a set of n_c integers, $\{\mathbf{x}\} \in \mathbb{Z}^{n_c}$, such that

$$V_{\Sigma} = V_0 + \sum_{c=1}^{n_c} x_c V_c \geq 0. \quad (3.20)$$

At a first glance, to test this condition, we have to inspect all branches, i.e., a countably infinite number of combinations of n_c integers. Fortunately, the situation is not that hopeless because finding the solution for this equation is related to two known programming problems [138, 139]. When $\{\mathbf{x}\}$ ranges over \mathbb{R}^{n_c} , the condition $V_{\Sigma} = 0$ outshapes either zero or a finite volume in which V_{Σ} is positive semidefinite. In the former case there is evidently no Floquet Lindbladian. In the latter case, the volume is enclosed by a convex body called spectrahedron [140]. To check whether the spectrahedron contains an integer point is a problem of polynomial complexity with respect to $\max\{|x_1^0|, \dots, |x_{n_c}^0|\}$, where $\{\mathbf{x}^0\} \subset \mathbb{R}^{n_c}$ is the solution set of $V_{\Sigma} = 0$. Finally, when the test is successful for one branch, the Floquet Lindbladian \mathcal{L}_F is found, and we can extract from it the corresponding time-independent Hamiltonian and jump operators. This decomposition of a Lindbladian into Hamiltonian and dissipative parts is not unique. However, it becomes so if we assume that all operators are traceless. The procedure is given in Appendix A.

Note that, given that one has extracted the operator \mathcal{K} via the matrix logarithm, one is always able to bring it into a form that is pseudo Lindblad, meaning that it has the form of Eq. (2.26) but

with some operator H and some coefficient matrix d . Then, condition (i) is equivalent to testing for Hermiticity of H and d and condition (ii) is equivalent to testing for d to be positive semi-definite, $d \geq 0$. This is how we will apply these conditions when performing the high-frequency expansions in Section 3.4.

If there is no set of integers such that Eq. (3.20) is fulfilled, no Floquet Lindbladian exists. Then it is instructive to quantify the distance from Markovianity for the non-Lindbladian generator $\mathcal{K}_{\{\mathbf{x}\}}$, by picking the branch giving the minimal distance. For this purpose, we compute two different measures for nonmarkovianity proposed by Wolf *et al.* [105] and Rivas *et al.* [141], respectively. The first measure is based on adding a noise term $\mu\mathcal{N}$ of strength μ to the generator and noting the minimal strength required to make at least one of the candidate channels Lindbladian, i.e.

$$\mu_{\min} = \min_{\{\mathbf{x}\}} \min \left\{ \mu \geq 0 \mid \mathcal{K}_{\{\mathbf{x}\}} + \mu\mathcal{N} \text{ is a valid Lindblad generator} \right\}. \quad (3.21)$$

Here, \mathcal{N} is the generator of the depolarizing channel $\exp(T\mu\mathcal{N})\rho = e^{-\mu T}\rho + [1 - e^{-\mu T}]\frac{\mathbb{1}}{N}$.

The second measure quantifies the violation of positivity of the Choi image [115, 142, 143] of the generated map [141]. It is based on the fact that a given map \mathcal{P} is completely positive iff its Choi representation is positive, $\mathcal{P}^\Gamma \geq 0$ [115, 142]. Together with the fact that the map is trace-preserving, $\text{Tr}\mathcal{P}^\Gamma = 1$, one finds that $\|\mathcal{P}^\Gamma\|_1 = 1$ iff \mathcal{P} is Markovian and $\|\mathcal{P}^\Gamma\|_1 > 1$ if it is not (here $\|\varrho\|_1 = \text{Tr}\sqrt{\varrho^\dagger\varrho}$ is the trace norm). On the level of the generator \mathcal{K} , $\mathcal{P}(t) = \exp(\mathcal{K}t)$, the derivative of this norm $\|\mathcal{P}(t)^\Gamma\|_1$ at $t = 0$ can be used to define a distance measure [141]

$$d_{\text{RHP}} = \lim_{\varepsilon \rightarrow 0} \frac{\|(\mathbb{1} + \varepsilon\mathcal{K})^\Gamma\|_1 - 1}{\varepsilon}. \quad (3.22)$$

Interestingly, we find that for our model system, that we introduce in Sec. 3.2, both measures agree: within the numerical accuracy, the second measure is always found to be equal to $\mu_{\min}/2$. For small distances $d_{\text{RHP}} < 10^{-7}$ the distance measure d_{RHP} is hard to obtain numerically, therefore we will use the measure μ_{\min} , which is better in this respect.

3.2. Model system: Driven-dissipative two-level system

To illustrate the problem, let us consider a driven two level system in a lossy channel,

$$\mathcal{L}(t) = -\frac{i}{\hbar}[H(t), \cdot] + \gamma \left(\sigma_- \cdot \sigma_+ - \frac{1}{2}\{\sigma_+ \sigma_-, \cdot\} \right), \quad (3.23)$$

with

$$H(t) = \frac{\Delta}{2}\sigma_z + E \cos(\omega t - \varphi)\sigma_x. \quad (3.24)$$

Here σ_x , σ_z and σ_- are standard Pauli and lowering operators. Using the level splitting Δ and \hbar/Δ as units for energy and time (so that henceforth in this chapter $\Delta = \hbar = 1$), the model is characterized by four dimensionless real parameters: the driving strength E , frequency ω , and phase φ , as well as

3. Existence of the Floquet Lindbladian

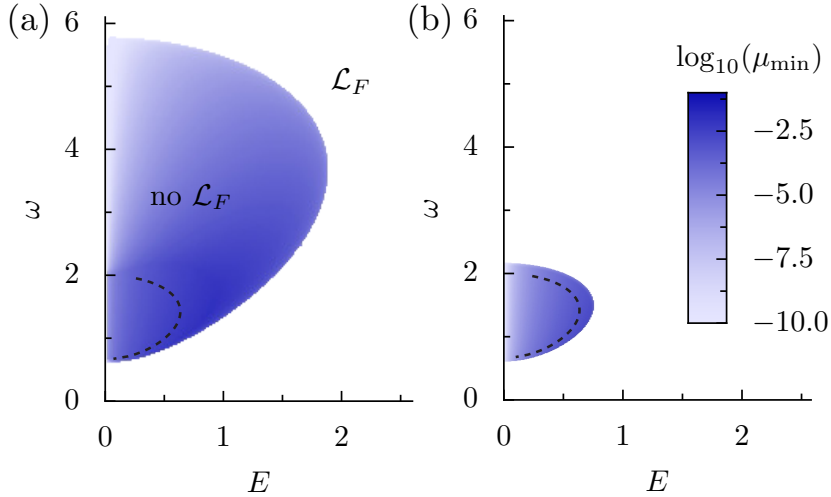


Figure 3.1.: Distance to Markovianity μ_{\min} of the effective generator \mathcal{K} of the one-cycle evolution superoperator as a function of driving strength E and frequency ω , for weak dissipation $\gamma = 0.01$ and two driving phases (a) $\varphi = 0$ and (b) $\varphi = \pi/2$. In the white region, where $\mu_{\min} = 0$, a Floquet Lindbladian \mathcal{L}_F exists. On the dashed line the Floquet map $\mathcal{P}(T)$ possesses two negative real eigenvalues.

the dissipation strength γ .

In Fig. 3.1 we follow the procedure that we have outlaid above and calculate the candidates \mathcal{K} from the logarithm of $\mathcal{P}(T)$, and then check whether for any given branch condition (i) and (ii) is fulfilled. Note that for the qubit, one has at most one pair of complex eigenvalues, therefore one only has to check a single number x labeling the branches. If we find a branch x_0 with a valid generator, then this is the Floquet-Lindbladian $\mathcal{L}_F = \mathcal{K}_{x_0}$. In Fig. 3.1(a), we fill the region where there is such a branch and the Floquet-Lindbladian exists with white color in the parameter space (E, ω) . In the region where no such branch exists we plot the distance from Markovianity μ_{\min} for the closest branch of the effective generator of the one-cycle evolution superoperator. We choose weak dissipation $\gamma = 0.01$ and $\varphi = 0$. This extended non-Lindbladian phase is surrounded by a Lindbladian phase (white region) where $\mu_{\min} = 0$ so that \mathcal{L}_F can be constructed [scenario (a)]. It contains also the ω axis, corresponding to the trivial undriven limit $E = 0$. Note that only for a fine-tuned set of parameters, lying on the dashed line in Fig. 3.1(a), $\mathcal{P}(T)$ possesses negative eigenvalues. However, they come in a degenerate pair, such that the construction of a Floquet Lindbladian is not hindered by condition (i). Both the high- and the low frequency limit are surrounded by finite frequency intervals, where the Floquet Lindbladian exists. This suggests that a (Floquet-)Magnus-type expansion for the Floquet-Lindbladian [100–102] can indeed describe the high-frequency regime. We will turn to this question in Sec. 3.4. Somewhat counter-intuitively, we find that the Floquet Lindbladian also exists in a finite region of driving strengths E around the strongly-driven limit, so that for large E the low and the high-frequency Lindbladian phases are connected. In turn, for intermediate frequencies, the Lindbladian phase does not stretch over a finite interval of driving strengths E around the undriven limit $E = 0$. This can also be seen from Fig. 3.2(a) and (b), where we plot μ_{\min} along horizontal cuts

through the phase diagram of Fig. 3.1(a), using a logarithmic and a linear scale, respectively.

Figure 3.1(b) shows the phase diagram for a different driving phase, $\varphi = \pi/2$. Remarkably, compared to $\varphi = 0$, Fig. 3.1(a), the non-Lindbladian phase covers now a much smaller area in parameter space. The phase boundaries depend on the driving phase or, in other words, on when during the driving period we monitor the stroboscopic evolution of the system. In the coherent limit, we can decompose the time evolution operator of a Floquet system from time t_0 to time t like

$$U(t, t_0) = U_F(t) \exp[-i(t - t_0)H_{\text{eff}}]U_F^\dagger(t_0), \quad (3.25)$$

where $U_F(t) = U(t+T)$ is a unitary operator describing the time-periodic micromotion of the Floquet states of the system and H_{eff} is a time-independent effective Hamiltonian. The Floquet Hamiltonian $H_{t_0}^F$, defined via $U(t_0 + T, t_0) = \exp(-iT H_{t_0}^F)$ so that it describes the stroboscopic evolution of the system at times $t_0, t_0 + T, \dots$, is for general t_0 then given by $H_{t_0}^F = U_F(t_0)H_{\text{eff}}U_F^\dagger(t_0)$ [39]. Note that above we use the lighter notation $H_F = H_0^F$ for $t_0 = 0$. The operator $H_{t_0}^F$ depends on the micromotion via a t_0 -dependent unitary rotation. However, in the dissipative system the micromotion will no longer be captured by a unitary operator. This explains, why the effective time-independent generator of the stroboscopic evolution can change its character as a function of t_0 (or, equivalently, the driving phase φ) in a nontrivial fashion, e.g. from Lindbladian to non-Lindbladian. A quantitative discussion of this is found in Sec. 3.4, where we aim to extract the micromotion operator for the dissipative system.

In Fig. 3.2(c), the dependence of the phase diagram on the dissipation strength γ is investigated. We find that the extent of the non-Lindbladian phase both in frequency, $\Delta\omega$, and driving strength, ΔE ,

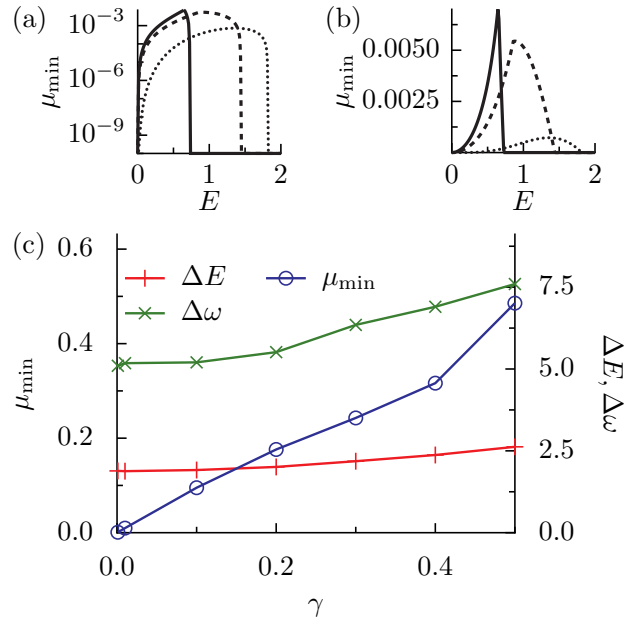


Figure 3.2.: Distance to Markovianity μ_{\min} along horizontal cuts through the phase diagram in Fig. 4.1(a) for $\omega = 1, 2, 3$ (solid, dashed, dotted line), in (a) logarithmic and (b) linear plots. (c) Maximum extent of the non-Lindbladian phase with respect to frequency, $\Delta\omega$, and driving strength, ΔE , and maximum non-Markovianity $\mu_{\min} = \max_{\omega, E}[\mu_{\min}(\omega, E)]$ versus dissipation strength γ .

3. Existence of the Floquet Lindbladian

does not vanish in the limit $\gamma \rightarrow 0$. Thus, even for arbitrary weak dissipation the Floquet Lindbladian does not exist in a substantial region of parameter space. It is noteworthy that the maximum distance from Markovianity μ_{\min} goes to zero linearly with γ , i.e., the nonmarkovianity is a first-order effect with respect to the dissipation strength.

Note that in Fig. 3.1(a) there is only a finite ‘ear-shaped’ region where there is no Floquet Lindbladian. Especially, in the limits $\omega \rightarrow \infty$, $\omega \rightarrow 0$, $E \rightarrow \infty$ there always exists a finite bound, e.g. for $\omega \gtrsim 5.8$, above which the Floquet-Lindbladian is guaranteed to exist. It is puzzling that, despite this fact, in the literature it was found that one of the most conventional high-frequency expansions, the Magnus expansion, does not produce a valid Lindblad generator on the lowest order [100, 104]. Just to make this point clear, in the high-frequency limit, by direct calculation of the logarithm one finds that there exists a valid Floquet Lindbladian that is physical, however the dominating term in the high-frequency approximation to the Floquet Lindbladian is not physical, because it violates our condition (ii), i.e. it is not conditionally completely positive [even though conditional complete positivity is only violated in higher orders of $1/\omega$ than the expansion was performed]. To illustrate this, in Section 3.4.1, we will perform the Magnus expansion for our example system, Eq. (3.23).

In Section 3.4.4 we show that this problem can be circumvented by performing the Magnus expansion in the rotating frame. Then, already the lowest order gives rise to a nontrivial approximation that is physical for all parameter values. The lowest-order approximation in the rotating frame already contains terms on all orders of $1/\omega$, which cures the problems of the high-frequency expansion in the direct frame.

While in the (white) parameter region where there is a Floquet Lindbladian \mathcal{L}_F , we are able to reconstruct the stroboscopic evolution with a time-local evolution

$$\partial_t \tilde{\varrho}(t) = \mathcal{L}_F \tilde{\varrho}(t), \quad (3.26)$$

with a time-homogeneous generator \mathcal{L}_F , we may ask whether in the other (blue) region we may always find a time-nonlocal evolution but with a time-homogeneous memory kernel. As we show in the following section, this is always possible for the qubit model.

3.3. Construction of an effective evolution with time-homogeneous memory kernel

While in the non-Lindbladian phase, we are not able to find a Markovian time-homogeneous master equation reproducing the one-cycle evolution operator $\mathcal{P}(T)$, one might still be able to construct a time-homogeneous non-Markovian master equation, which is nonlocal in time and described by a memory kernel. In order to construct such an equation, we make the following ansatz [144–146]

$$\partial_t \tilde{\varrho}(t) = \int_0^t d\tau e^{(\tau-t)/\tau_{\text{mem}}} \mathcal{L}_K \tilde{\varrho}(\tau), \quad \text{for } t \in [0, T], \quad (3.27)$$

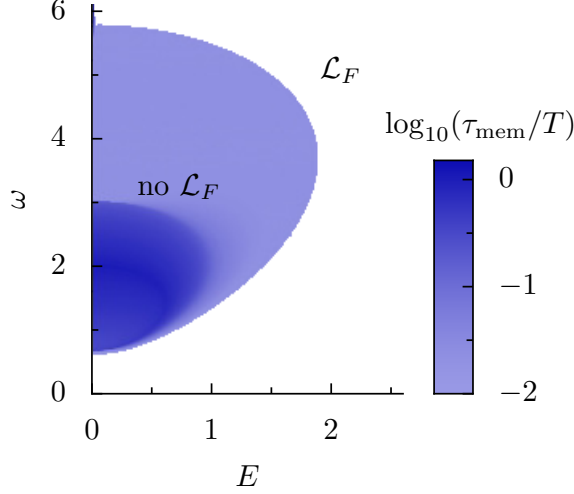


Figure 3.3.: Shortest memory time τ_{mem} for the exponential kernel of the effective nonmarkovian generator in Eq. (3.27). $\tau_{\text{mem}} = 0$ (white) indicates the Lindbladian phase. Due to limited numerical accuracy, we cannot resolve values of $\tau_{\text{mem}} \leq 10^{-2}T$. This leads to a spurious plateau at small τ_{mem} . Other parameters as in Fig. 3.1(a).

where τ_{mem} is the memory time and \mathcal{L}_K is the kernel superoperator. The kernel on the right-hand side is not of arbitrary form. In order to find an effective evolution that is CPTP, the choice of possible kernel superoperators \mathcal{L}_K needs to be restricted. In the Markovian limit, $\tau_{\text{mem}} \rightarrow 0$, it suffices to guarantee that \mathcal{L}_K is a valid Lindbladian. For finite τ_{mem} , however, an ‘easy’ criterion that characterizes all admissible \mathcal{L}_K is yet unknown. For the exponential kernel a sufficient (but not necessary) criterion is that $\mathcal{E} = \mathbb{1} + \mathcal{L}_K$ is a CPTP map [144]. It is useful to introduce a map $\tilde{\mathcal{P}}$ describing the evolution resulting from the effective master equation (3.27), $\tilde{\varrho}(t) = \tilde{\mathcal{P}}(t)\varrho(0)$. It solves the equation

$$\partial_t \tilde{\mathcal{P}}(t) = \int_0^t d\tau e^{(\tau-t)/\tau_{\text{mem}}} \mathcal{L}_K \tilde{\mathcal{P}}(\tau) \quad (3.28)$$

with $\tilde{\mathcal{P}}(0) = \mathbb{1}$. We now have to construct a superoperator \mathcal{L}_K , so that $\tilde{\mathcal{P}}(T) = \mathcal{P}(T)$. For that purpose, we represent the one-cycle evolution in its Jordan normal form, Eq. (3.16). A natural ansatz is then $\mathcal{L}_K = \sum_a \lambda_a^K P_a$, with P_a being the projectors in Eq. (3.16). For this ansatz we find an evolution operator of the form $\tilde{\mathcal{P}}(t) = \sum_a h_a(t) P_a$, with characteristic decay functions $h_a(t)$ obeying $h_a(0) = 1$. Plugging everything into the equation of motion, Eq. (3.28), the problem reduces to solving a set of scalar equations

$$\partial_t h_a(t) = \int_0^t d\tau e^{(\tau-t)/\tau_{\text{mem}}} \lambda_a^K h_a(\tau). \quad (3.29)$$

They possess solutions (cf. Appendix B.1)

$$h_a(t) = e^{-t/2\tau_{\text{mem}}} [\cosh(\Gamma_a t) + \sinh(\Gamma_a t)/(2\Gamma_a \tau_{\text{mem}})], \quad (3.30)$$

3. Existence of the Floquet Lindbladian

with $\Gamma_a = [\tau_{\text{mem}}^{-2}/4 + \lambda_a^K]^{1/2}$. Requiring $\tilde{\mathcal{P}}(T) = \mathcal{P}(T)$ implies $h_a(T) = \lambda_a$, where λ_a are the eigenvalues of $\mathcal{P}(T)$, Eq. (3.16). Solving this equation, we obtain the eigenvalues λ_a^K as a function of the memory time τ_{mem} (for details on the numerical implementation see Appendix B.2). It is then left to check, whether the corresponding \mathcal{L}_K , which depends on the memory time τ_{mem} , is an admissible superoperator such that the evolution $\tilde{\mathcal{P}}(t)$ is CPTP. We have checked that for all memory times τ_{mem} the superoperator $\mathcal{E} = \mathbb{1} + \mathcal{L}_K$ violates complete positivity, therefore we cannot simply apply the criterion of Ref. [144]. In lack of a simple criterion, one way is to guarantee that $\tilde{\mathcal{P}}(t)$ complete positivity numerically: We find that there is always a memory time τ_{mem} such that a physical evolution is guaranteed by testing $\tilde{\mathcal{P}}(t)^\Gamma \geq 0$ for all t on a numerical grid $t_n \in [0, T]$ (data not shown).

Here we present a different approach that is motivated by the fact that complete positivity is often broken for short times only, as we observe e.g. in Fig. 3.4(b). For short times $t \ll \tau_{\text{mem}}$, we find $h_a(t) \approx 1 + t^2 \lambda_a^K / 2 \approx \exp(t^2 \lambda_a^K / 2)$. As a result, for short times the evolution $\tilde{\mathcal{P}}(t)$ is approximated by $\tilde{\mathcal{P}}(t) \approx \exp(t^2 \mathcal{L}_K / 2)$, which is a semigroup with rescaled time t . As a result, we can guarantee complete positivity for short times by requiring that \mathcal{L}_K is of Lindblad form by performing the test for condition (ii). In the phase where the Floquet Lindbladian \mathcal{L}_F exists, we find a Lindbladian \mathcal{L}_K for arbitrarily short memory times τ_{mem} . However, in the non-Lindbladian phase the memory time τ_{mem} cannot be chosen smaller than a minimal value. In Fig. 3.3 we plot this minimal memory time versus driving strength and frequency. It shows good qualitative agreement with the distance to Markovianity μ_{min} shown in Fig. 3.1(a) (note that the apparent plateau for small values of τ_{min} is an artifact related to the fact that our numerics cannot resolve memory times below $10^{-2}T$). Note that the minimal memory time τ_{mem} in principle also qualifies as a measure for the distance from Markovianity. The fact that there is still some different behavior visible when comparing it to μ_{min} might be due to the restricted choice of the kernel Lindbladian \mathcal{L}_K that we make.

The fact that for the used model we can always construct a time-homogeneous memory kernel shows that for our qubit model the non-Lindbladian phase corresponds to scenario (b). It is an intriguing open question whether this holds only for our model or if such a construction is always possible. One should be aware, however, that a time-homogeneous master equation with memory kernel like Eq. (3.27) cannot reproduce the full stroboscopic evolution, since $\tilde{\mathcal{P}}(2T)$, $\tilde{\mathcal{P}}(3T)$, etc., will depend on the history of the previous periods. The stroboscopic evolution can only be obtained by erasing the memory after each period, which corresponds to a modification of the integrand of Eq. (3.27),

$$\partial_t \tilde{\rho}(t) = \int_0^t d\tau e^{(\tau-t)/\tau_{\text{mem}}} \Theta(\tau - \lfloor t/T \rfloor T) \mathcal{L}_K \tilde{\rho}(\tau), \text{ for all } t, \quad (3.31)$$

where Θ denotes the Heaviside step function and $\lfloor \cdot \rfloor$ is the floor function.

In Fig. 3.4 we show two examples of the driven-dissipative two-level system. It is instructive to analyze the eigenvalues λ^Γ of the Choi image $\mathcal{P}(t)^\Gamma$ of the dynamical map $\mathcal{P}(t)$. The evolution is CPTP only if all these eigenvalues are nonnegative. The parameters in Fig. 3.4(a) lie in the region where a Floquet Lindbladian exists, therefore there is a semigroup evolution (dashed lines) that coincides with $\mathcal{P}(nT)$, $n \in \mathbb{N}_0$, and is CPTP for all times. For the parameters in Fig. 3.4(b) such a semigroup evolution does not exist. We show the semigroup evolution that is closest to a CPTP

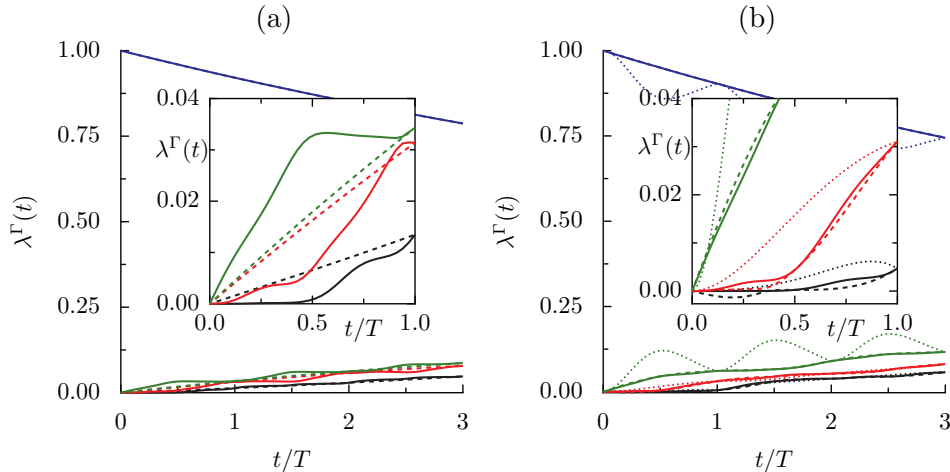


Figure 3.4.: Instantaneous eigenvalues $\lambda^\Gamma(t)$ of the Choi matrix of the full evolution $\mathcal{P}(t)$ (solid lines) and of the effective semigroup $\exp(t\mathcal{K})$ (dashed lines) for the two-level model with $\gamma = 0.01$, $\varphi = 0$ and (a) $\omega = 1.5$, $E = 1.5$ as well as (b) $\omega = 1.2$, $E = 0.75$. $\mathcal{K} = \log(\mathcal{P}(T))/T$ is chosen from the branch that is closest to Markovianity. By definition, both evolutions coincide at integer multiples of the period, $t = nT$. The inset shows a zoom into the three smallest eigenvalues and the first period. The evolution is CPTP, only if all eigenvalues of the Choi matrix are nonnegative for all times. By construction $\mathcal{P}(t)$ is CPTP. The semigroup evolution in (a) is CPTP, thus \mathcal{L}_F exists, but in (b) it is not CPTP, thus no \mathcal{L}_F exists. The dotted lines stem from the evolution with the designed exponential kernel. Even though there is no time-local effective evolution with a time-independent generator \mathcal{L}_F , the time-homogeneous time-nonlocal evolution with the designed kernel is CPTP at all times and coincides with \mathcal{P} at the full period T .

evolution (in the sense of the distance measure μ_{\min}). However, there exists an evolution with a time-homogeneous exponential kernel in the sense of Eq. (3.31) (dotted lines) [using that we erase the memory at stroboscopic times with the Heaviside function], which coincides with $\mathcal{P}(nT)$, $n \in \mathbb{N}_0$, and is CPTP for all times.

3.4. High-frequency expansions of the Floquet Lindbladian

A standard tool to extract the Floquet Hamiltonian for high frequencies is the Magnus expansion [131]. It has originally been developed as a general tool to find the fundamental solutions of an ordinary linear differential equation with time-dependent coefficients. As such, we will apply it to our dissipative qubit model to extract the Floquet Lindbladian. Even though the existence of the Floquet Lindbladian is guaranteed in the high-frequency limit (as we have seen in Section 3.2), as we show in Sec. 3.4.1, the Magnus expansion does not yield a physical generator (i.e. it is not a proper Lindbladian) on the dominating order of the high-frequency expansion.

A second high-frequency expansion that we want to consider is a van-Vleck-type perturbation theory in the extended Hilbert space. For the coherent case it has been developed in Ref. [39]. It has the advantage that it yields an effective generator that is independent of the driving phase and a unitary rotation that accounts for the micromotion. In Sec. 3.4.2 we introduce this van-Vleck high-frequency expansion and generalize it to open quantum systems. As we show in Sec. 3.4.3, the problem of an

3. Existence of the Floquet Lindbladian

unphysical leading order is shared by this expansion.

In Sec. 3.4.4 we show that this problem of an unphysical leading order can be cured by transforming into the (generalized) rotating frame, where the driving term is integrated out. In this frame, not the driving, but the static part of the Lindbladian enters on a perturbative level both in the Magnus as well as in the van-Vleck high-frequency expansion. As we discuss in Sec. 3.4.4, for our model system, performing the Magnus expansion in the rotating frame instead of the direct frame leads to a generator that is much closer to the generator that we obtain numerically from the logarithm. Additionally, on the dominating order of the expansion we obtain a generator that is physical for all parameters.

In Sec. 3.4.5 we turn to the van-Vleck high-frequency expansion in the rotating frame. It yields a valid effective Lindbladian on the first two orders of the expansion. As a result, for our model system and on these orders of the expansion, the origin of the non-Lindbladian phase can be traced back to the (non-unitary) micromotion that transforms the effective Lindbladian in a generator that is not of Lindblad form anymore.

3.4.1. Emergence of unphysical terms in the Magnus expansion

The Magnus expansion is a high-frequency expansion of the dynamics that is commonly used for systems with coherent dynamics governed by a time-periodic Hamiltonian $H(t)$. Despite this success, for open quantum systems, however, it was observed in the literature that the Magnus expansion typically produces unphysical terms in low orders [100, 104]. These terms are unphysical as the corresponding superoperator cannot be brought into Lindblad form.

In order to illustrate this problem, let us discuss the first and second order of the Magnus expansion of the driven-dissipative qubit model, Eq. (3.23). Because the Lindblad superoperator is time-periodic, we may represent it in a Fourier expansion,

$$\mathcal{L}(t) = \sum_{n \in \mathbb{Z}} e^{i\omega n t} \mathcal{L}_n. \quad (3.32)$$

The Magnus expansion [131] is a general high-frequency expansion for linear differential equations with time-dependent coefficients. Therefore it can be directly applied to our problem. It gives rise to one candidate \mathcal{K} for \mathcal{L}_F . Let us denote this expansion of the generator by

$$\mathcal{K}_{\text{Mag}} = \sum_{n \in \mathbb{N}_0} \frac{1}{\omega^n} \mathcal{K}^{(n)}. \quad (3.33)$$

Then, it holds that

$$\mathcal{K}^{(0)} = \frac{1}{T} \int_0^T dt \mathcal{L}(t) = \mathcal{L}_0 \quad (3.34)$$

$$\mathcal{K}^{(1)} = \frac{\omega}{2T} \int_0^T dt \int_0^t dt' [\mathcal{L}(t), \mathcal{L}(t')] = i \sum_{n=1}^{\infty} \frac{[\mathcal{L}_n, \mathcal{L}_{-n}] + [\mathcal{L}_0, \mathcal{L}_n - \mathcal{L}_{-n}]}{n}, \quad (3.35)$$

$$\mathcal{K}^{(2)} = \frac{\omega^2}{6T} \int_0^T dt \int_0^t dt' \int_0^{t'} dt'' ([\mathcal{L}(t), [\mathcal{L}(t'), \mathcal{L}(t'')]] + [\mathcal{L}(t''), [\mathcal{L}(t'), \mathcal{L}(t)]]). \quad (3.36)$$

Note that for the second order Magnus expansion, Eq. (3.36), we do not present an explicit expression in terms of the Fourier components of $\mathcal{L}(t)$. This is due to the fact that such an explicit expression is tedious to obtain analytically. As we discuss in Appendix C we have found explicit expressions for $\Omega^{(2)}$ in the literature [100, 136], however some of them have to be questioned since for our example system they do not produce the correct result.

For our example system, Eq. (3.23), the driven qubit with driving phase $\varphi = 0$, one has

$$\mathcal{L}_0 = -i \left[\frac{\sigma_z}{2}, \cdot \right] + \gamma \left(\sigma_- \cdot \sigma_+ - \frac{1}{2} \{ \sigma_+ \sigma_-, \cdot \} \right) \text{ and } \mathcal{L}_1 = \mathcal{L}_{-1} = -i \frac{E}{2} [\sigma_x, \cdot]. \quad (3.37)$$

Therefore the first order $1/\omega$ drops out, $\mathcal{K}^{(1)} = 0$ (as all odd orders will). Using Eq. (3.36) we find up to the second order

$$\mathcal{K}_{\text{Mag}} = \mathcal{L}_0 + \frac{2}{\omega^2} [\mathcal{L}_0, [\mathcal{L}_0, \mathcal{L}_1]] - \frac{1}{\omega^2} [\mathcal{L}_1, [\mathcal{L}_0, \mathcal{L}_1]] + \mathcal{O}(1/\omega^4). \quad (3.38)$$

Let us in the following denote the general qubit Lindblad form by

$$\mathcal{L}(H, d) = -i[H, \cdot] + \sum_{nm} d_{nm} \left(\sigma_n \cdot \sigma_m - \frac{1}{2} \{ \sigma_m \sigma_n, \cdot \} \right), \quad (3.39)$$

with Hamiltonian H governing the coherent evolution and coefficient matrix d governing the dissipative part. Recall that for the evolution to be physical, i.e. completely positive and trace-preserving, this matrix must be positive semi-definite $d \geq 0$.

By using the general expressions for the commutator of two general qubit Lindblad superoperators

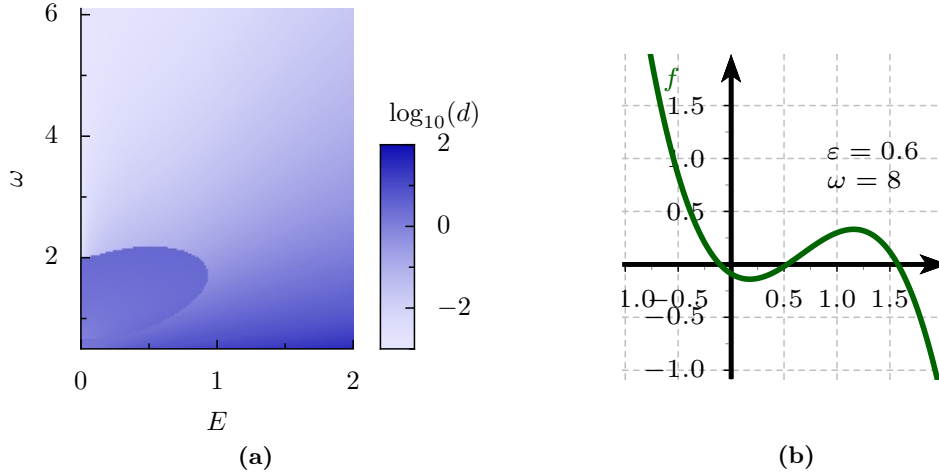


Figure 3.5.: (a) Matrix distance $d = \|\mathcal{K}_{\text{Mag}} - \mathcal{K}_{x_0}\|_F$ (using the Frobenius norm $\|\cdot\|_F$) of the generator \mathcal{K}_{Mag} obtained by second order Magnus expansion in the direct frame to the exact candidate $\mathcal{K}_{x_0} \in \log(\mathcal{P}(T))/T$ for the Floquet Lindbladian \mathcal{L}_F of branch x_0 , which is closest to a physical generator. (b) Typical graph $f(\lambda)$ of the characteristic polynomial of the coefficient matrix d/γ of the second order Magnus expansion \mathcal{K}_{Mag} of the Floquet Lindbladian. The matrix d therefore has one negative eigenvalue.

3. Existence of the Floquet Lindbladian

that we present in Appendix D, we compute

$$[\mathcal{L}_0, \mathcal{L}_1] = \mathcal{L}(H, d), \text{ with } H = \frac{E}{2}\sigma_y, \text{ and } d = \gamma E \begin{pmatrix} 0 & 0 & -i \\ 0 & 0 & -1 \\ i & -1 & 0 \end{pmatrix}. \quad (3.40)$$

Similarly, we find

$$[\mathcal{L}_0, [\mathcal{L}_0, \mathcal{L}_1]] = \mathcal{L}(H, d), \text{ with } H = -\frac{E}{2}\sigma_x, \text{ and } d = 2\gamma E \begin{pmatrix} 0 & 0 & 1 \\ 0 & 0 & -i \\ 1 & i & 0 \end{pmatrix}, \quad (3.41)$$

as well as

$$[\mathcal{L}_1, [\mathcal{L}_0, \mathcal{L}_1]] = \mathcal{L}(H, d), \text{ with } H = \frac{E^2}{2}\sigma_z + \mathcal{O}(\gamma^2), \text{ and } d = \gamma E^2 \begin{pmatrix} 0 & i & 0 \\ -i & 2 & 0 \\ 0 & 0 & -2 \end{pmatrix} + \mathcal{O}(\gamma^2). \quad (3.42)$$

Altogether, we find that up to second order in $1/\omega$ and first order in γ

$$\mathcal{K}_{\text{Mag}} = \mathcal{L}(H, d), \text{ with } H = -\frac{\varepsilon}{\omega}\sigma_x + \frac{1}{2}(1 - \varepsilon^2)\sigma_z, \text{ and } d = \gamma \begin{pmatrix} 1 & i(1 - \varepsilon^2) & 4\varepsilon/\omega \\ -i(1 - \varepsilon^2) & 1 - 2\varepsilon^2 & -4i\varepsilon/\omega \\ 4\varepsilon/\omega & 4i\varepsilon/\omega & 2\varepsilon^2 \end{pmatrix}. \quad (3.43)$$

where $\varepsilon = E/\omega$. The matrix distance of the matrix representation of the superoperator \mathcal{K}_{Mag} to matrix representation of the exact candidate \mathcal{K} for the Floquet Lindbladian is shown in Fig. 3.5(a). Note that although for high frequencies, $\omega \rightarrow \infty$, this distance approaches zero, the generator \mathcal{K}_{Mag} is not a physical generator in the whole region of the parameters. This can be seen from the characteristic polynomial of its dissipator matrix d (let us extract the common prefactor γ from the eigenvalues λ)

$$f(\lambda) = \det(d/\gamma - \lambda\mathbb{1}) = -\lambda^3 + 2\lambda^2 - \lambda \left(4\varepsilon^2 - 5\varepsilon^4 - \frac{32\varepsilon^2}{\omega^2} \right) - 2\varepsilon^6. \quad (3.44)$$

As illustrated in Fig. 3.5(b), for $\lambda \rightarrow -\infty$ we have $f(\lambda) \rightarrow \infty$, but at the same time one finds $f(0) = -2\varepsilon^6 < 0$. Therefore there will always be a negative eigenvalue λ and the dissipator matrix d is not positive semi-definite. As a result, the dominating order \mathcal{K}_{Mag} of the Magnus expansion is not a valid Lindblad generator and cannot serve as a good approximation for the Floquet-Lindbladian \mathcal{L}_F . Note again, that this is unsatisfactory because from direct calculation of the logarithm it is known that in the high-frequency limit, $\omega \rightarrow \infty$, the Floquet-Lindbladian \mathcal{L}_F exists, so one would like to have an approximation to it which is a physical generator.

As was already pointed out in the literature [100], the negative eigenvalue emerges due to the fact that the characteristic polynomial has terms that are of higher order than $1/\omega^2$ up to which the

Magnus expansion was performed. It is indeed expected, that the characteristic polynomial is correct only up to this order,

$$f(\lambda) = -\lambda^3 + 2\lambda^2 - 4\varepsilon^2\lambda, \quad (3.45)$$

and that the next higher order will only be revealed after evaluating the Magnus expansion up to fourth order and so on. Note that if we only take into account the terms up to order $1/\omega^2$, Eq. (3.45), indeed, the characteristic polynomial only has positive eigenvalues, so one could argue that complete positivity is only violated in orders higher than $1/\omega^2$. However, if one would want to find a generator that is physical in this order $1/\omega^2$, there is no well-defined procedure on how to modify the terms in the dissipator matrix d , such that its characteristic polynomial is exactly the one in Eq. (3.45).

Note that the problem of an unphysical generator \mathcal{K}_{Mag} is not originating from a faulty choice of branch for \mathcal{K}_{Mag} . We have also checked the other branches of \mathcal{K}_{Mag} numerically and they also do not yield a physical generator. In the high-frequency limit $\omega \rightarrow \infty$, we generally expect that it suffices to investigate the principle branch. This is because for a high-frequency expansion $\mathcal{K}_{\text{Mag}}(\omega)$ it holds that

$$\mathcal{K}_{\text{Mag},\{\mathbf{x}\}}(\omega) = \mathcal{K}_{\text{Mag}}(\omega) + i\omega \sum_{c=1}^{n_c} x_c (P_c(\omega) - P_{c^*}(\omega)). \quad (3.46)$$

In the high-frequency limit, the principle branch $\mathcal{K}_{\text{Mag}}(\omega)$ converges to the diabatic (or rotating-wave) Lindbladian $\mathcal{K}_{\text{Mag}}(\omega) \rightarrow \mathcal{L}_0$, therefore all the projectors will also converge, $P_c(\omega) \rightarrow P_c(\infty)$. As long as it holds that

$$\Phi_{\perp} (P_c(\infty) - P_{c^*}(\infty))^{\Gamma} \Phi_{\perp} \neq 0 \quad (3.47)$$

the matrices V_c in the Markovianity test, Eq. (3.20), will scale linearly with ω in that limit. Therefore, for $\omega \rightarrow \infty$ all matrices $V_{\Sigma}(\omega)$ for branches different from $\mathbf{x} = 0$ will diverge, leaving only the principle branch as a candidate.

In Section 3.4.4 we show that for our model system this problem of an unphysical leading order does not occur, when we first transform into a co-rotating frame, and then perform the Magnus expansion.

3.4.2. Effective Lindbladian in extended space and van-Vleck high-frequency expansion

Instead of performing time integration, the stroboscopic map $\mathcal{P}(T)$ and therefore also the candidate \mathcal{K} for the Floquet Lindbladian can be obtained by solving an eigenvalue equation in the extended Hilbert space (extended by the space of time-periodic functions), much like in the case of the coherent evolution.

If this diagonalization is only performed perturbatively up to a given order in inverse frequency, we find a high-frequency expansion that we want to call van-Vleck high-frequency expansion [147]. We will see that the problem of an unphysical leading order that we found for the Magnus expansion is also present in this approach.

3. Existence of the Floquet Lindbladian

Extended Hilbert space

Since $\mathcal{L}(t)$ is periodic we may apply Floquet's theorem to Eq. (3.2) to find that the fundamental solutions of Eq. (3.2) take the form

$$\varrho_a(t) = e^{-i\Omega_a t} \Phi_a(t) \quad (3.48)$$

where the index a runs over all N^2 fundamental solutions (the Hilbert space \mathcal{H} has dimension N), and where Ω_a and $\Phi_a(t) = \Phi_a(t+T)$ denote complex numbers and time-periodic matrices, respectively. We may expand the time-periodic \mathcal{L} and Φ_a in the Fourier series

$$\mathcal{L}(t) = \sum_{n \in \mathbb{Z}} e^{i\omega n t} \mathcal{L}_n, \quad (3.49)$$

$$\Phi_a(t) = \sum_{n \in \mathbb{Z}} e^{i\omega n t} \Phi_{a,n}. \quad (3.50)$$

Note that all \mathcal{L}_n are superoperators acting on the $\Phi_{a,n}$ which are linear operators on \mathcal{H} , $\Phi_{a,n} \in L(\mathcal{H})$. Plugging everything into Eq. (3.2), we find

$$\sum_n (-i\Omega_a + i\omega n) \Phi_{a,n} e^{i\omega n t} = \sum_{k,m} \mathcal{L}_k \Phi_{a,m} e^{i\omega(k+m)t}. \quad (3.51)$$

By comparing the prefactors, we find an eigenvalue equation in the ‘‘extended’’ Hilbert space $L(\mathcal{H}) \otimes \mathcal{F}$, with \mathcal{F} being the space of periodic functions with period T . It reads

$$\Omega_a \Phi_{a,n} = \sum_m (i\mathcal{L}_{n-m} + \delta_{n,m} m\omega \mathbb{1}) \Phi_{a,m} = \sum_m \bar{\mathcal{Q}}_{nm} \Phi_{a,m}, \quad (3.52)$$

where $\bar{\mathcal{Q}}$ is the extended-space representation of the ‘‘quasi-energy’’ superoperator,

$$Q(t) = i\mathcal{L}(t) - i\partial_t, \quad (3.53)$$

the generalization of the quasi-energy operator [39] to the open system.

Very similar to the isolated system, Eq. (3.52) obeys the structure

$$\Omega_a \begin{pmatrix} \dots \\ \Phi_{a,-1} \\ \Phi_{a,0} \\ \Phi_{a,1} \\ \dots \end{pmatrix} = \begin{pmatrix} \dots & & & & & & \\ & i\mathcal{L}_1 & i\mathcal{L}_0 - \omega \mathbb{1} & i\mathcal{L}_{-1} & i\mathcal{L}_{-2} & i\mathcal{L}_{-3} & \\ & i\mathcal{L}_2 & i\mathcal{L}_1 & i\mathcal{L}_0 & i\mathcal{L}_{-1} & i\mathcal{L}_{-2} & \\ & i\mathcal{L}_3 & i\mathcal{L}_2 & i\mathcal{L}_1 & i\mathcal{L}_0 + \omega \mathbb{1} & i\mathcal{L}_{-1} & \\ & & & & & & \dots \end{pmatrix} \begin{pmatrix} \dots \\ \Phi_{a,-1} \\ \Phi_{a,0} \\ \Phi_{a,1} \\ \dots \end{pmatrix}, \quad (3.54)$$

however the entries in the vectors are operators and the entries in the matrix are nonhermitian (but Hermiticity-preserving) superoperators.

Van-Vleck high-frequency expansion

The aim of the van-Vleck high-frequency expansion is to find a rotation $\bar{\mathcal{D}}$ that does not necessarily diagonalize, but block diagonalizes the problem in the extended space,

$$\bar{\mathcal{Q}}' = \bar{\mathcal{D}}^{-1} \bar{\mathcal{Q}} \bar{\mathcal{D}}, \quad (3.55)$$

such that

$$\bar{\mathcal{Q}}'_{nm} = \delta_{nm} (i\mathcal{L}_{\text{eff}} + m\omega \mathbb{1}). \quad (3.56)$$

However, in contrast to the closed system, $\bar{\mathcal{Q}}$ is not necessarily Hermitian, so the rotation \mathcal{D} is in general not a unitary transformation. Still, the spectrum Ω_a is of course invariant under this transformation.

In analogy to the closed system [39], it suffices to take into account time-periodic transformations $\mathcal{D}(t) = \sum_n e^{i\omega n t} \mathcal{D}_n$, therefore in extended space the operator $\bar{\mathcal{D}}_{nm}$ may only depend on the difference of the phonon indices $\bar{\mathcal{D}}_{nm} = \mathcal{D}_{n-m}$. First of all, we observe that for two time-local time-periodic superoperators,

$$\mathcal{A}(t) = \sum_{n \in \mathbb{Z}} e^{i\omega n t} \mathcal{A}_n \quad \text{and} \quad \mathcal{B}(t) = \sum_{n \in \mathbb{Z}} e^{i\omega n t} \mathcal{B}_n, \quad (3.57)$$

the product of both operators in the time domain

$$\mathcal{C}(t) = \mathcal{A}(t)\mathcal{B}(t) = \sum_{n, m \in \mathbb{Z}} e^{i\omega(n+m)t} \mathcal{A}_n \mathcal{B}_m = \sum_{n, m \in \mathbb{Z}} e^{i\omega n t} \mathcal{A}_{n-m} \mathcal{B}_m, \quad (3.58)$$

leads in extend space to

$$\bar{\mathcal{C}}_{nm} = \mathcal{C}_{n-m} = \sum_{k \in \mathbb{Z}} \mathcal{A}_{n-m-k} \mathcal{B}_k = \sum_{k \in \mathbb{Z}} \mathcal{A}_{n-k} \mathcal{B}_{k-m} = (\bar{\mathcal{A}}\bar{\mathcal{B}})_{nm}. \quad (3.59)$$

Therefore, products in the time domain directly translate into products in the extended space and vice versa. As a result, the inverse transformation $\bar{\mathcal{D}}^{-1}$ in extended space is indeed just the representation of the inverse transformation in time,

$$\mathcal{D}^{-1}(t) = \sum_n e^{i\omega n t} (\mathcal{D}^{-1})_n \quad \text{with} \quad \mathcal{D}^{-1}(t)\mathcal{D}(t) = 1, \quad (3.60)$$

i.e. we have $(\bar{\mathcal{D}}^{-1})_{nm} = (\mathcal{D}^{-1})_{n-m}$.

Thus, it holds that

$$\Phi'_a(t) = \mathcal{D}^{-1}(t)\Phi_a(t), \quad \rightarrow \quad \varrho'(t) = \mathcal{D}^{-1}(t)\varrho(t). \quad (3.61)$$

3. Existence of the Floquet Lindbladian

The equation of motion in the transformed frame reads

$$\partial_t \varrho'(t) = (\partial_t \mathcal{D}^{-1}(t))\varrho(t) + \mathcal{D}^{-1}(t)\partial_t \varrho(t) \equiv \mathcal{L}'(t)\varrho'(t) \quad (3.62)$$

Thus, much like in the coherent case, this transformation is equivalent to a generalized gauge transformation

$$\mathcal{L}'(t)[\cdot] = (\partial_t \mathcal{D}^{-1}(t))\mathcal{D}(t) \cdot + \mathcal{D}^{-1}(t)\mathcal{L}(t)[\mathcal{D}(t)\cdot], \quad (3.63)$$

resembling a gauge transformation for unitary rotations.

As it was put forward recently in the literature [103], in analogy to the closed system, Eq. (3.25), the effective Lindbladian \mathcal{L}_{eff} is the time-independent operator that fulfills

$$\mathcal{P}(t, t_0) = \mathcal{D}(t) \exp[(t - t_0)\mathcal{L}_{\text{eff}}]\mathcal{D}^{-1}(t_0), \quad (3.64)$$

but since the system is dissipative, the time-periodic “micromotion” operator $\mathcal{D}(t)$ is not necessarily unitary anymore. It follows directly that the Floquet Lindbladian can be represented as

$$\mathcal{L}_{t_0}^F = \mathcal{D}(T + t_0)\mathcal{L}_{\text{eff}}\mathcal{D}^{-1}(t_0), \quad (3.65)$$

where here we use the more general notion of the Floquet Lindbladian $\mathcal{L}_{t_0}^F$,

$$\mathcal{P}(t_0 + T, t_0) = \exp(\mathcal{L}_{t_0}^F T), \quad (3.66)$$

in which we allow for any initial time t_0 , and in our notation we denote $\mathcal{L}_F = \mathcal{L}_0^F$. From Eq. (3.65) we see that even if \mathcal{L}_{eff} is a physical generator, due to the fact that \mathcal{D} is in general non-unitary, it is possible that \mathcal{D} changes the character of the generator such that $\mathcal{L}_{t_0}^F$ is not a physical generator anymore.

It is an intriguing question whether, also in the dissipative system it is possible to find a high-frequency expansion for the effective Lindbladian \mathcal{L}_{eff} and the micromotion superoperator \mathcal{D} . Such an expansion has been found in a recent work by Dai et al. [103]. However, to establish a connection to van-Vleck perturbation theory also for the dissipative system, we want to derive this expansion from a perturbative expansion in the extended space, much like it is done in Ref. [39] for the coherent system. We closely follow the reasoning of Ref. [39] and decompose

$$\bar{\mathcal{Q}} = \bar{\mathcal{Q}}_0 + \lambda \bar{\mathcal{V}} \quad (3.67)$$

with $(\bar{\mathcal{Q}}_0)_{nm} = \delta_{nm} m\omega \mathbb{1}$ taking the role of the unperturbed quasienergy operator. As we present in Appendix F, where we perform a nonhermitian van-Vleck-type perturbation theory on this problem, it becomes apparent that it is sufficient to replace all Hamiltonians H_n in the resulting expressions for the coherent system with the corresponding term $i\mathcal{L}_n$. In this way we obtain a high-frequency

expansion, $\mathcal{K}_{\text{eff}} = \sum_{n=0}^{\infty} \mathcal{K}_{\text{eff}}^{(n)} / \omega^n$, with [39, 103]

$$\mathcal{K}_{\text{eff}}^{(0)} = \mathcal{L}_0, \quad (3.68)$$

$$\mathcal{K}_{\text{eff}}^{(1)} = i \sum_{n=1}^{\infty} \frac{[\mathcal{L}_n, \mathcal{L}_{-n}]}{n}, \quad (3.69)$$

$$\mathcal{K}_{\text{eff}}^{(2)} = - \sum_{n \neq 0} \left(\frac{[\mathcal{L}_n, [\mathcal{L}_0, \mathcal{L}_{-n}]]}{2n^2} + \sum_{m \neq 0, m \neq n} \frac{[\mathcal{L}_m, [\mathcal{L}_{n-m}, \mathcal{L}_{-n}]]}{3nm} \right). \quad (3.70)$$

By $n \neq 0$ we denote the sum over $n \in \mathbb{Z} \setminus \{0\}$. Again, we find a candidate superoperator \mathcal{K}_{eff} for the effective Lindbladian \mathcal{L}_{eff} and we have to decide whether it is a proper Lindbladian. We may also perform an expansion for the micromotion superoperator

$$\mathcal{D}(t) = \exp(G(t)) \quad \text{with} \quad G(t) = \sum_{n=1}^{\infty} G^{(n)}(t) / \omega^n, \quad (3.71)$$

where

$$G^{(1)}(t) = -i \sum_{n \neq 0} e^{in\omega t} \frac{\mathcal{L}_n}{n}, \quad (3.72)$$

$$G^{(2)}(t) = - \sum_{n \neq 0} e^{in\omega t} \left(\frac{[\mathcal{L}_0, \mathcal{L}_n]}{n^2} + \sum_{m \neq 0, m \neq n} \frac{[\mathcal{L}_{n-m}, \mathcal{L}_m]}{2mn} \right). \quad (3.73)$$

3.4.3. Unphysical terms in the van-Vleck high-frequency expansion

It is an intriguing question whether the candidate \mathcal{K}_{eff} for the effective Lindbladian \mathcal{L}_{eff} , that one finds in a van-Vleck high-frequency expansion, shares the problem of a leading order that is unphysical. We show that for our model system this is indeed the case.

We may now calculate the candidate for the effective Lindbladian for our model system,

$$\mathcal{K}_{\text{eff}} = \mathcal{L}_0 - \frac{1}{\omega^2} [\mathcal{L}_1, [\mathcal{L}_0, \mathcal{L}_1]] + \mathcal{O}(1/\omega^4). \quad (3.74)$$

Using Eq. (3.42), we find that up to second order in $1/\omega$ and first order in γ it holds that

$$\mathcal{K}_{\text{eff}} = \mathcal{L}(H, d), \quad \text{with} \quad H = \frac{1}{2} (1 - \varepsilon^2) \sigma_z, \quad \text{and} \quad d = \gamma \begin{pmatrix} 1 & i(1 - \varepsilon^2) & 0 \\ -i(1 - \varepsilon^2) & 1 - 2\varepsilon^2 & 0 \\ 0 & 0 & 2\varepsilon^2 \end{pmatrix}. \quad (3.75)$$

Here we may directly read off one eigenvalue of d/γ

$$\lambda_3 = 2\varepsilon^2. \quad (3.76)$$

3. Existence of the Floquet Lindbladian

The other eigenvalues follow from solving

$$0 = \tilde{f}(\lambda) = \lambda^2 - 2(1 - \varepsilon^2)\lambda - \varepsilon^4. \quad (3.77)$$

Again, $\tilde{f}(0) = -\varepsilon^4 < 0$ while asymptotically \tilde{f} is positive, therefore there must be one negative eigenvalue, and also the candidate for the effective Lindbladian is unphysical. Thus, the van-Vleck high-frequency expansion shares the problems of the Magnus expansion in the rest frame.

3.4.4. Magnus expansion in the rotating frame

We present an alternative high-frequency expansion for the driven qubit that is performed in a rotating frame of reference obtained by integrating out the driving term. For the isolated system, this transformation is known to yield better results for strong driving. The reason that this transformation allows to treat also higher driving strengths $E \propto \omega$ is that it is equivalent to a summation of an infinite number of terms in a perturbative series in E/ω . As a result, when performing the Magnus expansion in the rotating frame instead of the direct frame, the result is not a perturbative expansion in E/ω anymore. For our model system, surprisingly, by performing the Magnus expansion of the generator in the rotating frame, we find a generator that is physical already in the lowest order of the high-frequency expansion, which solves the problem that we encountered in Section 3.4.1. Whether and how this procedure can be generalized to more complex systems and for systems where the dissipative part of the generator is driven remains an open question.

Transformation to the rotating frame

Note that, in general, we may assume a decomposition of the Lindbladian in its time-constant part plus a driving term

$$\mathcal{L}(t) = \mathcal{L}_d(t) + \mathcal{L}_0 \text{ with } \mathcal{L}_d(t) = \sum_{n \neq 0} e^{in\omega t} \mathcal{L}_n. \quad (3.78)$$

Let us, for the sake of simplicity assume that $\mathcal{L}_d(t)$ commutes with itself at different times,

$$[\mathcal{L}_d(t), \mathcal{L}_d(t')] = 0, \quad \forall t, t', \quad (3.79)$$

which is equivalent to $[\mathcal{L}_n, \mathcal{L}_m] = 0, \forall n, m \neq 0$. In analogy to the coherent system one may define a transformation to a generalized rotating frame in which the driving term is integrated out,

$$\tilde{\varrho}(t) = \Lambda^{-1}(t)\varrho(t), \text{ with } \Lambda^{-1}(t) = \exp\left(-\int_0^t dt' \mathcal{L}_d(t')\right). \quad (3.80)$$

We denote operators in the rotating frame with a tilde. This definition is sensible because in case that only the coherent part of the Lindbladian is driven, $\mathcal{L}_d(t) = -i[H_d(t), \cdot]$, it reduces to a standard

definition of a rotating frame

$$\tilde{\varrho}(t) = U(t)^\dagger \varrho(t) U(t), \text{ with } U(t) = \exp\left(-i \int_0^t dt' H_d(t')\right). \quad (3.81)$$

The equation of motion in the rotating frame reads

$$\partial_t \tilde{\varrho}(t) = (\partial_t \Lambda^{-1}(t)) \varrho(t) + \Lambda^{-1}(t) \partial_t \varrho(t) \equiv \tilde{\mathcal{L}}(t) \tilde{\varrho}(t) \quad (3.82)$$

with gauge-transformed Lindbladian

$$\tilde{\mathcal{L}}(t)[\cdot] = (\partial_t \Lambda^{-1}(t)) \Lambda(t) \cdot + \Lambda^{-1}(t) \mathcal{L}(t) [\Lambda(t) \cdot]. \quad (3.83)$$

Now because $\mathcal{L}_d(t)$ commutes with itself at different times, also $\Lambda(t)$ commutes with $\mathcal{L}_d(t)$, therefore we find

$$\tilde{\mathcal{L}}(t)[\cdot] = -\mathcal{L}_d(t) \cdot + \Lambda^{-1}(t) \mathcal{L}_d(t) [\Lambda(t) \cdot] + \Lambda^{-1}(t) \mathcal{L}_0 [\Lambda(t) \cdot] \quad (3.84)$$

$$= \Lambda^{-1}(t) \mathcal{L}_0 [\Lambda(t) \cdot]. \quad (3.85)$$

As a result, we have eliminated the driving term, but it comes at the expense of a (possibly nonunitary) “rotation” of the part of the dissipator that was static before.

Note that we aim for a high-frequency expansion in the rotating frame, similar to the one that we performed in Section 3.4.1. This yields an effective time-independent generator $\tilde{\mathcal{K}}$, such that, in analogy to Eq. (3.15), we have

$$\tilde{\mathcal{P}}(T) = \exp(\tilde{\mathcal{K}}T) \quad (3.86)$$

in the rotating frame. However, since for our choice of $\mathcal{L}_d(t)$, where $\int_0^{nT} dt \mathcal{L}_d(t) = 0$, $n \in \mathbb{N}_0$, we find that

$$\tilde{\varrho}(nT) = \varrho(nT), \quad (3.87)$$

i.e. the rest frame and the rotating frame coincide at stroboscopic times. Therefore $\tilde{\mathcal{P}}(T) = \mathcal{P}(T)$, and thus $\tilde{\mathcal{K}}$ is also a candidate for the Floquet Lindbladian \mathcal{L}_F in the rest frame. Note that this does for a general choice of $\mathcal{L}_d(t)$, e.g. if $\mathcal{L}_d(t)$ does not commute with itself at different times.

Explicit transformation for model system

Let us, for our model system, transform the generator $\mathcal{L}(t)$ into the rotating frame and calculate the Fourier components of the transformed generator. For our model, Eq. (3.23), we find the unitary transformation

$$\tilde{\varrho}(t) = U(t) \varrho(t) U(t)^\dagger, \text{ with } U(t) = \exp(i\chi(t)\sigma_x), \quad (3.88)$$

3. Existence of the Floquet Lindbladian

where $\chi(t) = \frac{E}{\omega} \sin(\omega t)$ and

$$\tilde{\mathcal{L}}(t)[\cdot] = -i \left[\frac{1}{2} \tilde{\sigma}_z(t), \cdot \right] + \gamma \left(\tilde{\sigma}_-(t) \cdot \tilde{\sigma}_+(t) - \frac{1}{2} \{ \tilde{\sigma}_+(t) \tilde{\sigma}_-(t), \cdot \} \right). \quad (3.89)$$

We have introduced Pauli operators in the rotating frame,

$$\tilde{\sigma}_z(t) = U(t) \sigma_z U(t)^\dagger = \cos(2\chi(t)) \sigma_z + \sin(2\chi(t)) \sigma_y, \quad (3.90)$$

$$\tilde{\sigma}_\pm(t) = U(t) \sigma_\pm U(t)^\dagger = \sigma_x \pm i [\cos(2\chi(t)) \sigma_y - \sin(2\chi(t)) \sigma_z]. \quad (3.91)$$

In order to perform the high-frequency expansions in the rotating frame, let us first determine the Fourier components of the gauge-transformed Lindbladian $\tilde{\mathcal{L}}(t)$, Eq. (3.89). Using the definition $z = 2E/\omega$, we may rewrite the Fourier transform

$$\mathcal{F}_n[\cos(2\chi(t))] \equiv \frac{1}{T} \int_0^T \cos(2\chi(t)) e^{-in\omega t} dt = \frac{1}{T} \int_0^T \frac{1}{2} \left(e^{iz \sin(\omega t)} + e^{-iz \sin(\omega t)} \right) e^{-in\omega t} dt \quad (3.92)$$

$$= \frac{1}{2} [J_n(z) + J_{-n}(z)] = e_n J_n(z). \quad (3.93)$$

Here $J_n(z)$ is the n -th Bessel function of first kind, we have used $J_{-n}(z) = (-1)^n J_n(z)$ and we set

$$e_n = \begin{cases} 1, & n \text{ even,} \\ 0, & n \text{ odd,} \end{cases} \quad \text{and } o_n = \begin{cases} 0, & n \text{ even,} \\ 1, & n \text{ odd.} \end{cases} \quad (3.94)$$

Similarly, we find

$$\mathcal{F}_n[\sin(2\chi(t))] = -i o_n J_n(z), \quad (3.95)$$

$$\mathcal{F}_n[\sin(2\chi(t)) \cos(2\chi(t))] = -i \frac{o_n}{2} J_n(2z), \quad (3.96)$$

$$\mathcal{F}_n[\cos(2\chi(t))^2] = \frac{1}{2} [\delta_{n0} + e_n J_n(2z)], \quad (3.97)$$

$$\mathcal{F}_n[\sin(2\chi(t))^2] = \frac{1}{2} [\delta_{n0} - e_n J_n(2z)]. \quad (3.98)$$

As a result, the Fourier components read

$$\tilde{\mathcal{L}}_n = \mathcal{L}(H_n, d_n), \quad \text{with } H_n = \frac{J_n(z)}{2} (e_n \sigma_z - i o_n \sigma_y) \quad (3.99)$$

$$\text{and } d_n = \gamma \begin{pmatrix} \delta_{n0} & i e_n J_n(z) & -o_n J_n(z) \\ -i e_n J_n(z) & \frac{1}{2} (\delta_{n0} + e_n J_n(2z)) & \frac{i}{2} o_n J_n(2z) \\ o_n J_n(z) & \frac{i}{2} o_n J_n(2z) & \frac{1}{2} (\delta_{n0} - e_n J_n(2z)) \end{pmatrix} \quad (3.100)$$

where for odd n only $i\tilde{\mathcal{L}}_n$ is of Lindblad form (for $n \neq 0$ the operators \mathcal{L}_n in the Fourier series can actually be any complex number times some Lindblad operator).

Zeroth order Magnus expansion in the rotating frame

The lowest order of the Magnus expansion in the rotating frame reads

$$\tilde{\mathcal{K}}_{\text{Mag},0} = \tilde{\mathcal{L}}_0 = \mathcal{L}(H, d), \quad (3.101)$$

$$\text{with } H = \frac{J_0(z)}{2}\sigma_z \text{ and } d = \gamma \begin{pmatrix} 1 & iJ_0(z) & 0 \\ -iJ_0(z) & \frac{1}{2}[1 + J_0(2z)] & 0 \\ 0 & 0 & \frac{1}{2}[1 - J_0(2z)] \end{pmatrix}, \quad (3.102)$$

where, again, $z = 2E/\omega$. Note that for $z \rightarrow 0$, i.e. for $E \rightarrow 0$ or $\omega \rightarrow \infty$, such that $J_0(z) \rightarrow 1$ and, as expected, we recover the static Hamiltonian and dissipator. In Fig. 3.6(a) we plot the distance of the matrix representation of the superoperator of this approximation $\tilde{\mathcal{K}}$ to the exact candidate for the Floquet Lindbladian and see a much better agreement than in Fig. 3.5(a), especially for smaller values of ω . This is expected because the transformation to the rotating frame integrates out the driving term which corresponds to a summation of infinite terms in E/ω , here entering in the function J_0 . In the direct frame, however, the leading order correction in the Magnus expansion only captures terms up to order $(E/\omega)^2$.

The eigenvalues of the coefficient matrix d read

$$\lambda_{1/2} = \gamma \left[\mu(z) \pm \sqrt{\mu(z)^2 + J_0(z)^2 - \frac{1}{2}[1 + J_0(2z)]} \right], \quad (3.103)$$

$$\lambda_3 = \frac{\gamma}{2}[1 - J_0(2z)], \quad (3.104)$$

with $\mu(z) = [3 + J_0(2z)]/4$. The corresponding generator is a valid physical generator only if all three eigenvalues are non-negative. This is generally the case since

$$J_0(z)^2 - \frac{1}{2}[1 + J_0(2z)] = J_0(z)^2 - \frac{1}{2} \sum_{k \in \mathbb{Z}} J_k(z) J_{-k}(z) - \frac{1}{2} \quad (3.105)$$

$$= J_0(z)^2 - \frac{1}{2} \sum_{k \in \mathbb{Z}} J_{2k}(z)^2 + \frac{1}{2} \sum_{k \in \mathbb{Z}} J_{2k+1}(z)^2 - \frac{1}{2} \quad (3.106)$$

$$= J_0(z)^2 - \sum_{k \in \mathbb{Z}} J_{2k}(z)^2 = - \sum_{k \neq 0} J_{2k}(z)^2 \leq 0, \quad (3.107)$$

In the first step we have used the identity $J_n(y+z) = \sum_{k \in \mathbb{Z}} J_k(y) J_{n-k}(z)$ and in the third step we have used that $1 = \sum_{k \in \mathbb{Z}} J_k(z)^2$.

This shows that the values that the square root in Eq. (3.103) takes will be smaller than $\mu(z)$. Therefore, the zeroth order expansion in the rotating frame produces a nontrivial term that is physical, i.e. $\tilde{\mathcal{K}}_{\text{Mag},0}$ is a valid Lindblad generator for all parameter values. Note again that this first order term already has terms of all orders in $\varepsilon = E/\omega$, which is probably the reason for why high-frequency expansions (or weak-driving expansions which we have performed but do not present here) in the direct frame have a very slow convergence only. In fact, by comparing the result that we obtain in the rotating frame, Eq. (3.102), to the one that we obtain when directly performing the Magnus expansion,

3. Existence of the Floquet Lindbladian

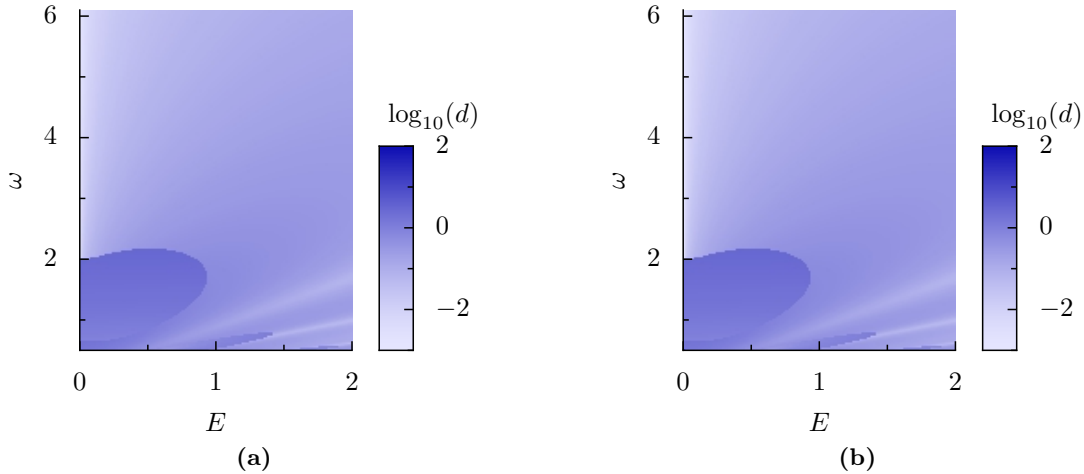


Figure 3.6.: Matrix distance $d = \|\tilde{\mathcal{K}} - \mathcal{K}_{x_0}\|_F$ of the generator $\tilde{\mathcal{K}}$ obtained by (a) zeroth order Magnus expansion $\tilde{\mathcal{K}}_{\text{Mag},0}$ and (b) first order Magnus expansion $\tilde{\mathcal{K}}_{\text{Mag},1}$ in the rotating frame, to the exact candidate $\mathcal{K}_{x_0} \in \log(\mathcal{P}(T))/T$ for the Floquet-Lindbladian \mathcal{L}_F of branch x_0 , which is closest to a physical generator.

Eq. (3.43), we find that by expanding the Bessel function to second order, $J_0(z) \approx 1 - z^2/4$, by using $z = 2\varepsilon$ we recover the terms $\propto \varepsilon^2$ in Eq. (3.43), while the terms $\propto \varepsilon/\omega$ do not occur (we will find them after performing the next order of the Magnus expansion in the rotating frame). However, if one eliminates the terms $\propto \varepsilon/\omega$ in Eq. (3.43), only keeping the terms $\propto \varepsilon^2$, still, the resulting generator is not physical. Thus, to find a physical generator one needs to know the higher order terms in $1/\omega$, but those are hard to extract in the direct frame because orders higher than two in the Magnus expansion are cumbersome to compute.

Note that from comparing Eq. (3.34) to Eq. (3.68) we learn that on this zeroth order in $1/\omega$, the van-Vleck high-frequency expansion of the effective Lindbladian $\tilde{\mathcal{K}}_{\text{eff}}$ and the Magnus expansion $\tilde{\mathcal{K}}_{\text{Mag}}$ coincide, $\tilde{\mathcal{K}}_{\text{eff},0} = \tilde{\mathcal{K}}_{\text{Mag},0}$, therefore on this order also the effective Lindbladian exists for all parameter values. We will have a more detailed discussion of the van-Vleck high-frequency expansion in the rotating frame in Sec. 3.4.5.

First order Magnus expansion in the rotating frame

The order $1/\omega$ of the Magnus expansion in the rotating frame reads

$$\tilde{\mathcal{K}}^{(1)} = i \sum_{n>0} \frac{[\tilde{\mathcal{L}}_n, \tilde{\mathcal{L}}_{-n}] + [\tilde{\mathcal{L}}_0, \tilde{\mathcal{L}}_n - \tilde{\mathcal{L}}_{-n}]}{n} = \sum_{n>0} 2o_n \frac{[\tilde{\mathcal{L}}_0, i\tilde{\mathcal{L}}_n]}{n}, \quad (3.108)$$

where in the second step we have used that for the Fourier components in Eq. (3.100) we have $\tilde{\mathcal{L}}_{-n} = (-1)^n \tilde{\mathcal{L}}_n$.

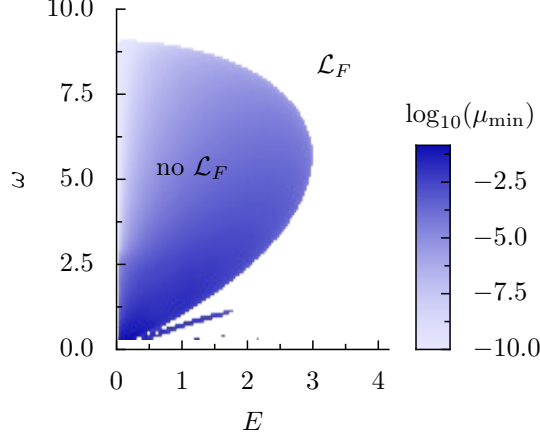


Figure 3.7.: Distance to Markovianity μ_{\min} of the candidate $\tilde{\mathcal{K}}_{\text{Mag},1}$ for the Floquet-Lindbladian obtained from a first order Magnus expansion in the rotating frame for the same model and parameter $\gamma = 0.01$ as in Fig. 3.1. The candidate $\tilde{\mathcal{K}}_{\text{Mag},0}$ that we obtain in zeroth order of the expansion is physical for all parameters (E, ω) . Note that we only calculate distances for $\omega \geq 0.3$, values below this are drawn in white.

It is straight-forward to compute that for odd n

$$[\tilde{\mathcal{L}}_0, i\tilde{\mathcal{L}}_n] = \mathcal{L}(H_n, d_n), \quad (3.109)$$

$$\text{with } H_n = -\frac{J_0(z)J_n(z)}{2}\sigma_x \text{ and } d_n = \frac{\gamma}{2} \begin{pmatrix} 0 & 0 & f_n(z) \\ 0 & 0 & -4iJ_0(z)J_n(z) \\ f_n(z) & 4iJ_0(z)J_n(z) & 0 \end{pmatrix}, \quad (3.110)$$

with $f_n(z) = J_n(z)[1 + J_0(2z)] + J_n(2z)J_0(z)$ and we ignore terms of higher order in γ . Thus, up to first order in $1/\omega$, the Magnus expansion in the rotating frame reads

$$\tilde{\mathcal{K}}_{\text{Mag},1} = \mathcal{L}(H, d), \text{ with } H = J_0(z) \left[\frac{1}{2}\sigma_z - \frac{\nu(z)}{\omega}\sigma_x \right], \text{ and} \\ d = \gamma \begin{pmatrix} 1 & iJ_0(z) & \frac{1}{\omega}[\nu(z)(1 + J_0(2z)) + J_0(z)\nu(2z)] \\ -iJ_0(z) & \frac{1}{2}[1 + J_0(2z)] & -\frac{4i}{\omega}J_0(z)\nu(z) \\ \frac{1}{\omega}[\nu(z)(1 + J_0(2z)) + J_0(z)\nu(2z)] & \frac{4i}{\omega}J_0(z)\nu(z) & \frac{1}{2}[1 - J_0(2z)] \end{pmatrix}, \quad (3.111)$$

where we have introduced $\nu(z) = \sum_{n>0} [o_n J_n(z)/n]$. Note that in lowest order $\nu(z) \approx z/2$ and therefore we also recover the terms $\propto \varepsilon/\omega$ in Eq. (3.43). In Fig. 3.6(b) we show the distance of the matrix representation of the superoperator of this approximation $\tilde{\mathcal{K}}$ to the exact candidate for the Floquet Lindbladian and see only a minor improvement over the zeroth order result in Fig. 3.6(a).

In contrast to the lowest order of the expansion, in this order the candidate for the Floquet-Lindbladian is not a physical generator for all parameters E, ω . Similar to Section 3.2, we check whether the Floquet Lindbladian is a valid generator by testing for conditional complete positivity and in case that this fails we compute the distance μ_{\min} to Markovianity. We show this distance in

3. Existence of the Floquet Lindbladian

Fig. 3.7 and in this order it resembles already very much the structure that one obtains by directly computing the logarithm of the map $\mathcal{P}(T)$. Nevertheless, the ear-shaped structure extends to larger values of E and ω than it does for the exact generator.

Interestingly, since $\tilde{\mathcal{L}}_{-n} = (-1)^n \tilde{\mathcal{L}}_n$ we have $[\tilde{\mathcal{L}}_n, \tilde{\mathcal{L}}_{-n}] = 0$, therefore in first order, the van-Vleck high-frequency expansion of the effective Lindbladian in the rotating frame has no contribution. Thus, we have $\tilde{\mathcal{K}}_{\text{eff},1} = \tilde{\mathcal{K}}_{\text{eff},0}$, and also in this order the effective Lindbladian is physical for all parameters. It is an intriguing question whether the effective Lindbladian is also a physical operator in the next order $\tilde{\mathcal{K}}_{\text{eff},2}$. Unfortunately, the next order involves quite a number of commutators, so it is complicated to obtain analytically. In the next section, we will thus evaluate the van-Vleck high-frequency expansion numerically.

3.4.5. Van-Vleck high-frequency expansion in the rotating frame

In our example system we observe that the Magnus expansion produces better results in the co-rotating frame where the driving term has been integrated out. Compared to an expansion in the direct frame, the results are better in two ways: First, the distance from the exact result is much smaller, and secondly the expansion yields a proper Lindbladian in the high-frequency and strong-driving limit. Here, we discuss that also the van-Vleck high-frequency expansion yields better results in the rotating frame. Other than in the previous section where we found analytical expressions for the Magnus expansion, here calculations get quite involved, so we treat this expansion only numerically. To this end, it is instructive to discuss the action of the generalized rotating-frame transformation $\Lambda(t)$ in the extended Hilbert space first, because it yields expressions that are easy to treat numerically, when superoperators are mapped to matrices.

As we have seen in Section 3.4.2, the aim of the van-Vleck high-frequency expansion is to find a transformation $\mathcal{D}(t)$ that “removes” the micromotion leaving an evolution with the time-independent effective Lindbladian \mathcal{L}_{eff} . This transformation \mathcal{D} can be regarded as a generalized gauge transformation much like the generalized rotating-frame transformation Λ . It is therefore instructive to represent Λ in the extended Hilbert space. By doing so, we obtain a more systematic approach to the high-frequency expansion in the rotating frame.

Formalism

Both the rotating-frame transformation $\Lambda(t)$ and the micromotion $\mathcal{D}(t)$ are generalized gauge transformations. Instead of finding $\mathcal{D}(t)$ directly, however, we may first perform a transformation to the rotating frame, $\tilde{\varrho}(t) = \Lambda^{-1}(t)\varrho(t)$, and then find the micromotion transformation there. Since $\Lambda(t)$ is periodic, we have

$$\Lambda(t) = \sum_n e^{in\omega t} \Lambda_n, \quad (3.112)$$

so we also may represent it in extended space $\bar{\Lambda}_{nm} = \Lambda_{n-m}$. Note that this representation is only possible due to the fact that we assume that the driving term $\mathcal{L}_d(t)$ commutes with itself at different

times, so in its definition we do not have to introduce a time-ordering operator and $\Lambda(t)$ is effectively a time-local superoperator.

As a result, the quasi-energy operator in the rotating frame reads

$$\bar{\bar{Q}} = \bar{\Lambda}^{-1} \bar{Q} \bar{\Lambda}. \quad (3.113)$$

Like in the direct frame, the goal is to find a transformation \tilde{D} such that

$$\bar{Q}' = \tilde{D}^{-1} \bar{\bar{Q}} \tilde{D} \quad (3.114)$$

where \bar{Q}' is block diagonal. We directly observe that

$$\mathcal{D}(t) = \Lambda(t) \tilde{D}(t). \quad (3.115)$$

Here we again see why in the limit of high frequency and strong driving the high-frequency expansion in the direct frame will at least have a slow convergence only. The transformation Λ involves a summation of infinitely many terms in E/ω . However, a high-frequency expansion in the direct frame tries to capture the dynamics of $\tilde{D}(t)$ and $\Lambda(t)$ on an equal footing from which problems are arising.

Note that on the other hand for the quasienergy operator in the rotating frame we have

$$\tilde{Q} = i\tilde{\mathcal{L}} - i\partial_t \quad (3.116)$$

with $\tilde{\mathcal{L}}$ according to Eq. (3.85), which in the extended space reads

$$\bar{\bar{\mathcal{L}}} = \bar{\Lambda}^{-1} \bar{\mathcal{L}}_0 \bar{\Lambda} \quad \text{i.e.} \quad \bar{\bar{\mathcal{L}}}_{nm} = \tilde{\mathcal{L}}_{n-m} = \sum_k \Lambda_{n-k}^{-1} \mathcal{L}_0 \Lambda_{k-m}. \quad (3.117)$$

This equation allows for a very efficient calculation of the Fourier components $\tilde{\mathcal{L}}_n$ of the Lindbladian in the rotating frame $\tilde{\mathcal{L}}$. To this end let us determine the coefficients Λ_n . In Appendix G we show that for driving terms of the form

$$\mathcal{L}_d(t) = \phi(t) \mathcal{L}'_d, \quad \text{with scalar function} \quad \phi(t) = \sum_{m \neq 0} e^{im\omega t} \phi_m, \quad (3.118)$$

one finds an explicit expression in extended space

$$\bar{\Lambda} = \prod_{m \neq 0} \bar{f}^{(m)} \left(\frac{\phi_m \mathcal{L}'_d}{im\omega} \right) \bar{g}^{(m)} \left(\frac{\phi_m \mathcal{L}'_d}{im\omega} \right). \quad (3.119)$$

3. Existence of the Floquet Lindbladian

Here we denote $\bar{f}_{nl}^{(m)} = f_{n-l}^{(m)}$, $\bar{g}_{nl}^{(m)} = g_{n-l}^{(m)}$ and

$$f_n^{(m)}(x) = \begin{cases} J_k(x) & \text{if } n = km, k \in \mathbb{Z}, \\ 0 & \text{else.} \end{cases}, \quad g_n^{(m)}(x) = \begin{cases} e^{-x} I_k(x) & \text{if } n = km, k \in \mathbb{Z}, \\ 0 & \text{else.} \end{cases} \quad (3.120)$$

We use the Bessel functions of first kind J_k , and modified Bessel functions of first kind I_k , taken at some matrix argument (which may be evaluated most easily by performing a spectral decomposition of \mathcal{L}'_d). Since $\Lambda^{-1}(t)$ is directly obtained from $\Lambda(t)$ by setting $\phi(t) \rightarrow -\phi(t)$, we find $\bar{\Lambda}^{-1}$ from Eq. (3.119) by setting $\phi_m \rightarrow -\phi_m$.

First order van-Vleck high-frequency expansion in the rotating frame

For our example system we have

$$\phi(t) = 2 \cos(\omega t), \quad \mathcal{L}'_d = \mathcal{L}_1 = \mathcal{L}_{-1} = -i \left[\frac{E}{2} \sigma_x, \cdot \right] \quad (3.121)$$

From Eq. (3.119) (or an explicit calculation) we find

$$\Lambda_n = J_n \left(\frac{2\mathcal{L}_1}{i\omega} \right), \quad (3.122)$$

which finally yields

$$\tilde{\mathcal{L}}_n = \sum_k J_{n-k} \left(-\frac{2\mathcal{L}_1}{i\omega} \right) \mathcal{L}_0 J_k \left(\frac{2\mathcal{L}_1}{i\omega} \right). \quad (3.123)$$

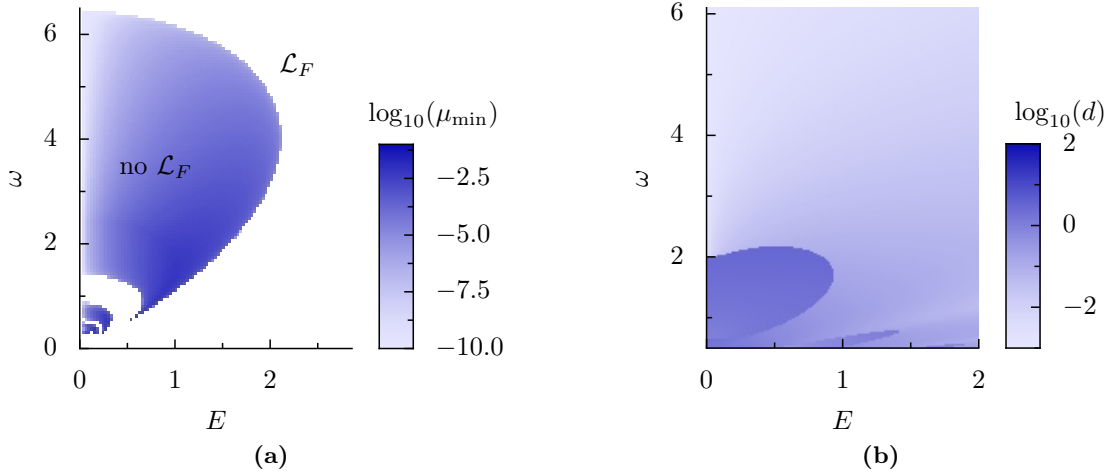


Figure 3.8.: (a) Distance to Markovianity μ_{\min} of the candidate for the Floquet Lindbladian \mathcal{K} obtained from a first order van-Vleck high-frequency expansion $\tilde{\mathcal{K}}_{vV,1}$ in the rotating frame, where we do not expand the exponential in $\tilde{\mathcal{D}}(t) = \exp(\tilde{\mathcal{G}}(t))$. We present the same model and parameter $\gamma = 0.01$ as in Fig. 3.1(a). Note that we only calculate for $\omega \geq 0.3$, values below this are drawn in white. (b) Matrix distance d of the candidate $\tilde{\mathcal{K}}_{vV,1}$ to the exact candidate \mathcal{K} obtained by the logarithm of $\mathcal{P}(T)$.

By translating superoperators into $N^2 \times N^2$ -dimensional matrices as shown in Appendix E, we therefore have an alternative procedure to the one we obtained in Section 3.4.4 to calculate the operators $\tilde{\mathcal{L}}_n$ and from this the van-Vleck high-frequency expansion. An explicit calculation using this matrix representation is presented in Appendix H and on zeroth order of the Magnus expansion we recover the result $\tilde{\mathcal{K}}_{\text{Mag},0}$ of Section 3.4.4.

Equation (3.123) is a good starting point for numerical investigations, because it is easy to evaluate numerically after we have translated the superoperators $\mathcal{L}_0, \mathcal{L}_1$ into $N^2 \times N^2$ -dimensional matrices. We then may use the expressions in Section 3.4.2 to perform the van-Vleck high-frequency expansion in the rotating frame. By this procedure we find candidates for the effective Lindbladian $\tilde{\mathcal{K}}_{\text{eff},n} = \sum_{k=0}^n \tilde{\mathcal{K}}_{\text{eff}}^{(k)} / \omega^k$ and for the Floquet Lindbladian

$$\tilde{\mathcal{K}}_{\text{vV},n} = \tilde{\mathcal{D}}_n(0) \tilde{\mathcal{K}}_{\text{eff},n} \tilde{\mathcal{D}}_n^{-1}(0). \quad (3.124)$$

Here we cut off the expansion in the exponent of $\tilde{\mathcal{D}}_n(t) = \exp(\sum_{k=1}^n G_k(t)/\omega^k)$ and do *not* perform an expansion of the exponential function. Only after doing so, we would recover the candidate from the Magnus expansion $\tilde{\mathcal{K}}_{\text{Mag},n}$ in the rotating frame [39].

On zeroth order we find that the candidate for the Floquet Lindbladian is given by the effective Lindbladian, $\tilde{\mathcal{K}}_{\text{vV},0} = \tilde{\mathcal{K}}_{\text{eff},0}$. Furthermore, as we discussed in Section 3.4.4 already, on zeroth order one also finds that the effective Lindbladian coincides with the corresponding order of the Magnus expansion, $\tilde{\mathcal{K}}_{\text{eff},0} = \tilde{\mathcal{K}}_{\text{Mag},0}$. As a result, also here, the zeroth order expansion of the Floquet Lindbladian yields a generator is physical for all parameters (E, ω) .

The first order where this expansion produces a different result is therefore $n = 1$. As mentioned in Section 3.4.4, one finds that there is no contribution to the effective Lindbladian, $\tilde{\mathcal{K}}_{\text{eff},1} = \tilde{\mathcal{K}}_{\text{eff},0}$ which is, thus, also a valid Lindblad generator for all (E, ω) . On this order, the only contribution to the Floquet Lindbladian $\tilde{\mathcal{K}}_{\text{vV},1}$ is therefore stemming from the rotation $\tilde{\mathcal{D}}_1(0)$. As we observe impressively in Fig. 3.8(a), this rotation gives rise to a large ear-shaped region, where $\tilde{\mathcal{K}}_{\text{vV},1}$ is not a valid Lindbladian. The shape and dimensions of this region are very similar to the exact values in

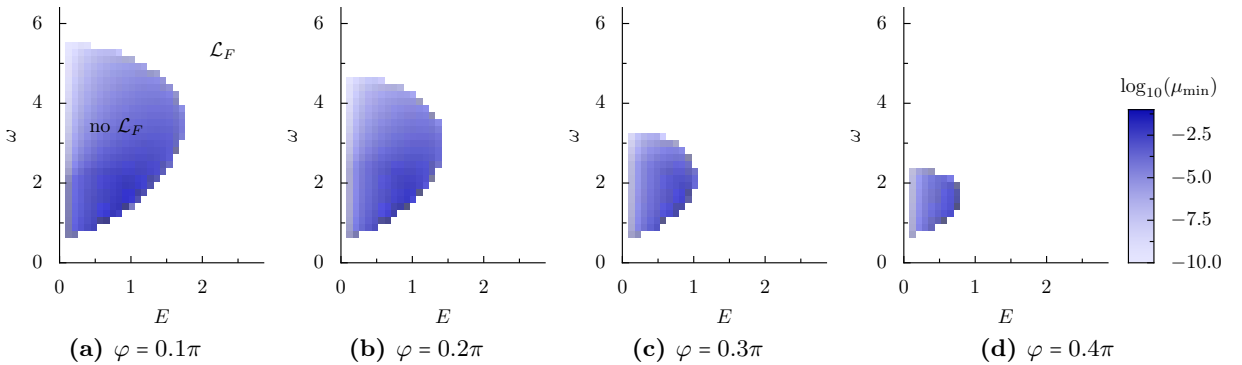


Figure 3.9.: Distance to Markovianity μ_{\min} of the exact effective generator \mathcal{K} as in Fig. 3.1 for some intermediate values of the driving phase φ .

3. Existence of the Floquet Lindbladian

Fig. 3.1(a), therefore we expect that $\tilde{\mathcal{K}}_{\text{vV},1}$ is a very good approximation for the exact candidate \mathcal{K} already. This is also confirmed in Fig. 3.8(b) where we observe even smaller distance values than for the Magnus expansion on this order, cf. Fig 3.6(b).

At this point, we gain a little of understanding for why the region where there is no Floquet Lindbladian shrinks so much for a different driving phase φ , as in Fig. 3.1(b): In the rotating frame, in leading order of the van-Vleck high-frequency expansion, the effective Lindbladian $\tilde{\mathcal{L}}_{\text{eff}}$ is a physical generator for all parameter values (E, ω) , while the non-unitary micromotion superoperator $\tilde{\mathcal{D}}(t_0)$ (with $t_0 = T\varphi/2\pi$ being the initial time which relates to the initial phase φ) may ‘rotate’ the generator such that the resulting generator is not physical for some parameter values. Note that in the direct frame for $t_0 \neq 0$ the candidate for the Floquet Lindbladian \mathcal{K} is given after the rotation $\mathcal{D}(t_0) = \Lambda(t_0)\tilde{\mathcal{D}}(t_0)$. However, for our model system $\Lambda(t_0)$ is a unitary transformation and thus does not change whether the generator is physical or not. As a result, the closer $\tilde{\mathcal{D}}(t_0)$ is to the identity (or to a unitary transformation) the smaller the region of unphysical generators in the (E, ω) will be. This confirms on the formal level of a high-frequency expansion our previous discussion of the non-trivial role of the micromotion, Sec. 3.2.

That this is a valid picture is confirmed also by Fig. 3.9 which shows, similar as in Fig. 3.1, the region where the *exact* effective generator \mathcal{K} is unphysical, but for four intermediate values of the driving phase φ . We see how this region continuously shrinks from the $\varphi = 0$ to the $\varphi = \pi/2$ behavior, which is expected since $\tilde{\mathcal{D}}(t_0)$ is a continuous function. That the region is smallest for driving phase $\varphi = \pi/2$ can be understood from the dominating order of the rotation already,

$$\tilde{\mathcal{D}}_1(t_0) = \exp\left(-i \sum_{n \neq 0} e^{in\omega t_0} \frac{\tilde{\mathcal{L}}_n}{n\omega}\right) = \exp\left(-i \sum_{n=1}^{\infty} 2 \cos(n\omega t_0) \frac{\tilde{\mathcal{L}}_n}{n\omega}\right), \quad (3.125)$$

where in the second step we have used that for our model we find $\tilde{\mathcal{L}}_{-n} = (-1)^n \tilde{\mathcal{L}}_n$. The biggest contribution to the sum in Eq. (3.125) stems from the $n = 1$ term. This term vanishes for a value of t_0 that corresponds to the driving phase $\varphi = \pi/2$. Therefore for $\varphi = \pi/2$ we expect the rotation $\tilde{\mathcal{D}}_1(t_0)$ to be closest to the identity.

In conclusion, on a first-order van-Vleck high-frequency expansion in the rotating frame it becomes apparent that for our model indeed there exists a phase-independent generator, the effective Lindbladian $\tilde{\mathcal{L}}_{\text{eff}}$, which is a valid Lindblad generator for all parameters. In this order we can directly trace back the non-Lindbladian phase of the candidate for the Floquet Lindbladian to the micromotion which yields a nonunitary rotation for the dynamics of open quantum systems. It is an interesting open question, if this picture is also valid in higher orders of the high-frequency expansion and for more complex model systems. Here, we want to conclude our calculations by discussing the next order of the expansion of the effective Lindbladian $\tilde{\mathcal{L}}_{\text{eff}}$.

Second order van-Vleck high-frequency expansion in the rotating frame

As we have seen in the previous section, the effective Lindbladian \mathcal{L}_{eff} is a physical generator in the dominating order $\tilde{\mathcal{K}}_{\text{eff},1}$ of the van-Vleck high-frequency expansion. In the last section of our

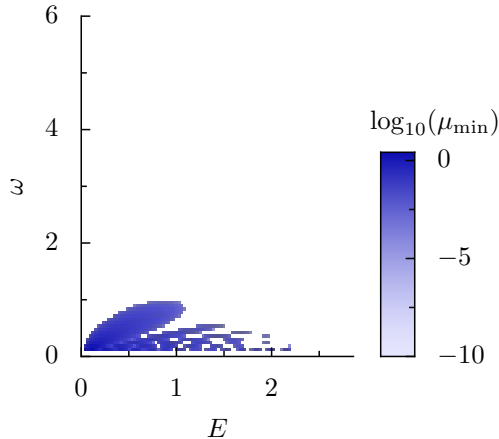


Figure 3.10.: Distance to Markovianity μ_{\min} of the candidate $\tilde{\mathcal{K}}_{\text{eff},2}$ for the effective Lindbladian obtained from a second order van-Vleck high-frequency expansion in the rotating frame for the same model and parameter $\gamma = 0.01$ as in Fig. 3.1. We only calculate for $\omega \geq 0.1$, values below this are drawn in white.

discussion of this high-frequency expansion we aim to shed some light on an intriguing hypothesis that one can make based on our observations: Even though it is generally not guaranteed that the Floquet Lindbladian \mathcal{L}_F exists, maybe the effective Lindbladian \mathcal{L}_{eff} is always a valid generator?

To this end, we calculate numerically the candidate for the effective Lindbladian $\tilde{\mathcal{K}}_{\text{eff},2}$ from a second order van-Vleck high-frequency expansion in the rotating frame. In Figure 3.10 we show the result of a markovianity test for the resulting operator. At first glance, we observe that at low frequencies there is some region where the candidate for the effective Lindbladian is unphysical, so our hypothesis could be wrong. However, we have to keep in mind that the Magnus expansion is expected to converge only in the high-frequency regime where [131, 148]

$$\int_0^T \|\mathcal{L}(t)\|_2 dt < \pi. \quad (3.126)$$

Here, $\|A\|_2 = \max_{\|x\|_2=1} \|Ax\|_2$ is the induced 2-norm. We can gain a very rough estimate for the region of convergence by discussing the undriven limit of $E = 0$ and $\gamma = 0$. As shown in Appendix H, the matrix representation of the generator then reads $\mathcal{L}|_{E=0,\gamma=0} = \text{diag}(0, -i, i, 0)$, therefore $\|(\mathcal{L}|_{E=0,\gamma=0})\|_2 = 1$. Thus, for $E = 0$ and $\gamma = 0$ we find that the Magnus expansion is only expected to converge for $\omega > 2$. For finite values of the driving strength E the norm of $\mathcal{L}(t)$ will increase and thus the radius of convergence will decrease even further.

As a result, Figure 3.10 shows that within the region of convergence of the Magnus expansion, $\tilde{\mathcal{K}}_{\text{eff},2}$ is a valid Lindbladian. Our hypothesis, that the effective Lindbladian could exist for all parameters, is therefore also not violated on the second order of the van-Vleck high-frequency expansion in the rotating frame.

3.4.6. Concluding remarks on the high-frequency expansions

Our results shed new light on the problems of the Magnus expansion that were already observed in Ref. [100, 104]. Namely, even though for our model system it is guaranteed that the Floquet Lindbladian exists in the high-frequency limit, the Magnus expansion, a standard high-frequency expansion, does not yield a physical Lindblad generator in the leading order of the expansion. The reason is that physicality follows from the eigenvalues of the dissipator matrix d . The characteristic polynomial that yields these eigenvalues, however, is a nonlinear function of the matrix d . It thus generally has terms that are of a higher order than the order in which the Magnus expansion was performed. These higher order terms can lead to a violation of physicality, as in our case where they give rise to one negative eigenvalue of the dissipator matrix d .

As a result, we can conclude that the Magnus expansion is generally not an effective tool to extract the Floquet Lindbladian. In the future, the hope is that these problems could be cured by developing an alternative expansion which is a systematic expansion of the eigenvalues and eigenvectors of dissipator matrix d in powers of inverse frequency.

Here, however, we observe that some of these problems can be cured by transforming into a (generalized) rotating frame where the driving term has been integrated out. Why this transformation is so successful can be observed for example by investigating the characteristic polynomial of the Magnus expansion in the direct frame in Eq. (3.44). We observe that the problems of an unphysical generator arise from terms that are a function of E/ω where E is the driving strength. By transforming into the rotating frame, the driving is integrated out which corresponds to a summation of infinitely many terms in E/ω . As a result, the expansion in the rotating frame is not perturbative in E/ω anymore, which cures the problems of the direct frame. It is an intriguing open question, if also for general time-periodically driven Lindbladians one can always identify problematic terms in the characteristic polynomial and cure these terms by integrating out the corresponding quantity.

Finally, by performing a van-Vleck high-frequency expansion in the rotating frame, we are able to show that for our model system, in first order of the expansion, indeed there is a driving-phase independent effective Lindbladian $\tilde{\mathcal{L}}_{\text{eff}}$ that is a valid physical generator for all parameters of the driving. However, the Floquet Lindbladian \mathcal{L}_F , giving rise to the stroboscopic dynamics, only follows after a nonunitary rotation that is due to the micromotion. In that way the micromotion can be accounted for the emergence of the non-Lindbladian phase. Whether or not this picture also holds on higher orders of the expansion and for more general time-periodically driven Lindbladians is an intriguing open question.

4. Number of Bose-selected modes in driven-dissipative ideal Bose gases

In an ideal Bose gas that is driven into a steady state far from thermal equilibrium, a generalized form of Bose condensation can occur. Namely, the single-particle states unambiguously separate into two groups: the group of Bose-selected states, whose occupations increase linearly with the total particle number, and the group of all other states whose occupations saturate [82]. However, so far very little is known about how the number of Bose-selected states depends on the properties of the system and its coupling to the environment. The answer to this question is crucial since systems hosting a single, a few, or an extensive number of Bose-selected states will show rather different behavior. While in the former two scenarios each selected mode acquires a macroscopic occupation, corresponding to (fragmented) Bose condensation, the latter case rather bears resemblance to a high-temperature state of matter. In this chapter, we systematically investigate the number of Bose-selected states, considering different classes of the rate matrices that characterize the driven-dissipative ideal Bose gases in the limit of weak system–bath coupling. These include rate matrices with continuum limit, rate matrices of chaotic driven systems, random rate matrices, and rate matrices resulting from thermal baths that couple to a few observables only.

This chapter has been published in Ref. [85]. Only minimal changes have been made in order to match the general frame of this thesis. Also, some results of this chapter, presented in Sec. 4.2 and Sec. 4.3.1, have already been discussed in the author’s master’s thesis [149].

4.1. Driven-dissipative ideal Bose gas and Bose selection

In this chapter, we are focusing on driven-dissipative ideal gases of N noninteracting bosons that exchange energy with the environment but no particles. They can be driven out of equilibrium, e.g. by periodic driving in combination with the coupling to a heat bath or by coupling the system to two heat baths of different temperature. In such setups the ideal gas will relax to a nonequilibrium steady state (NESS) which is characterized by a finite heat current through the system. It is an interesting question, whether (and if yes when and in which form) a system can show Bose condensation (or other forms of ordering) under such nonequilibrium conditions. Since this NESS does not follow from thermodynamic principles it is not obvious whether such a state will feature Bose condensation or not. It was observed in Ref. [82] that in the quantum degenerate limit of large densities the single-particle states split into two groups; the *Bose-selected states*, whose occupations increase linearly with the total particle number, much like for the ground state in thermal equilibrium, while the occupations

4. Number of Bose-selected modes in driven-dissipative ideal Bose gases

of all other states saturate.

However, so far very little is known about the factors that determine the number of Bose-selected states. The answer to this question is crucial since systems hosting a single, a few, or an extensive number of Bose-selected states will show rather different behavior. While in the former two scenarios each selected mode acquires a macroscopic occupation, corresponding to (fragmented) Bose condensation, the latter case rather bears resemblance to a high-temperature state of matter. Moreover, inducing transitions between several condensate modes can be a very efficient mechanism to exchange energy with the environment, which is not present in systems hosting a single condensate only [82].

In the limit of weak system–bath coupling, the system will approach a nonequilibrium steady state ρ_S that is diagonal in the eigenstates i of the Hamiltonian for an autonomous (i.e. non-driven) system or in the Floquet states i for a time-periodically driven system [83, 108, 150]. The mean occupations of these states obey the equation of motion Eq. (2.93) [82]. The rate for a boson to jump from single-particle level j to i is given by the single-particle rate R_{ij} multiplied by the bosonic enhancement factor $(n_i + 1)$ which manifests that bosons favor to “jump” into states that already have large occupation.

It was pointed out in Refs. [82, 83] that a generalization of Bose condensation is also observed in the NESS, called Bose selection. Here, a whole group of an odd number of single-particle states, the Bose-selected states, can acquire large occupation. As we briefly recapitulate in this section, these selected states are only determined by the rate asymmetry matrix

$$A_{ij} = R_{ij} - R_{ji}. \quad (4.1)$$

We assume that the gas may exchange heat with an environment of one or more thermal phonon baths. As we discuss in Sec. 2.3.4, a single bath is described as a collection of harmonic oscillators $H_B = \sum_{\alpha} \hbar\omega_{\alpha} b_{\alpha}^{\dagger} b_{\alpha}$ which are in thermal equilibrium. The corresponding system–bath coupling operator reads $H_{SB} = \gamma v \sum_{\alpha} c_{\alpha} (b_{\alpha}^{\dagger} + b_{\alpha})$ with dimensionless system coupling operator v , coefficients c_{α} and coupling strength γ . We assume that the baths are Markovian. Thus, the single-particle rate R_{ij} for the autonomous system, Eq. (2.75), is of golden rule type. Here enter the energy ε_i of single-particle eigenstate $|i\rangle$ and the bath-correlation function $g(\varepsilon)$, Eq. (2.74), where T is the temperature (measured in units of energy, $k_B = 1$) of the bath and J is its spectral function $J(\varepsilon) = \sum_{\alpha} c_{\alpha}^2 [\delta(\varepsilon - \hbar\omega_{\alpha}) - \delta(\varepsilon + \hbar\omega_{\alpha})]$. In the following we will consider ohmic baths with a continuum of modes α and spectral function $J(\varepsilon) = \varepsilon$.

A nonequilibrium situation is found when e.g. the system is coupled to multiple baths at different temperatures, where the total rate is given by the sum of the rates $R_{ij}^{(b)}$ corresponding to the individual bath b ,

$$R_{ij} = \sum_b R_{ij}^{(b)}. \quad (4.2)$$

Another possible scenario are time-periodically driven systems coupled to a heat bath. In this case

the rates read [73, 151]

$$R_{ij} = \frac{2\pi\gamma^2}{\hbar} \sum_{m=-\infty}^{\infty} |v_{ij}(m)|^2 g(\varepsilon_i - \varepsilon_j - m\hbar\omega) \quad (4.3)$$

with $v_{ij}(m) = \frac{\omega}{2\pi} \int_0^{2\pi/\omega} e^{im\omega t} \langle i(t)|v|j(t)\rangle dt$, driving frequency ω , Floquet states $|i(t)\rangle$, and corresponding quasienergies ε_i .

The equation of motion (2.93) for the mean occupations depends also on the two-particle density-density correlations, the equations of which depend in turn on three-particle correlations and so on. In this way it establishes a hierarchy, which in the following will be truncated already at the single-particle level by employing the mean-field decomposition $\langle n_i n_j \rangle \approx \langle n_i \rangle \langle n_j \rangle$, $i \neq j$. As a result, the steady state occupations, $\partial_t \langle n_i \rangle = 0$, follow from the nonlinear equations of motion

$$0 = \sum_j A_{ij} \langle n_j \rangle \langle n_j \rangle + R_{ij} \langle n_j \rangle - R_{ji} \langle n_i \rangle. \quad (4.4)$$

Here we have used the rate asymmetries A_{ij} , which for the rates of a single bath read

$$A_{ij}^{(b)} = \frac{2\pi\gamma^2}{\hbar} |\langle i|v|j\rangle|^2 J(\varepsilon_j - \varepsilon_i), \quad (4.5)$$

so that they are independent of temperature. Note that it has been shown by comparison to quasi-exact Monte-Carlo simulations [83] that the mean-field (or kinetic) equation (4.4) yields excellent predictions for the mean occupations $\langle n_i \rangle$ for a broad range of models. A possible reason for this good agreement has been pointed out recently [152, 153]; a driven system with a set of observables $\{A_i\}$ which are approximately conserved quantities will relax towards a steady state that is well described by a generalized Gibbs ensemble $\varrho_{\text{GGE}} = Z_{\text{GGE}}^{-1} \exp(-\sum_i \lambda_i A_i)$. Due to the weak-coupling limit that we assume, the occupations n_i of the system's single-particle states i are almost conserved, so in our context this set is given by $\{n_i\}$. For a state $\varrho_{\text{GGE}} \propto \exp(-\sum_i \lambda_i n_i)$, the mean-field decomposition is exact, $\langle n_i n_j \rangle = \langle n_i \rangle \langle n_j \rangle$, $i \neq j$.

The solid lines in Fig. 4.1 show the steady-state solutions of Eq. (4.4) as a function of the total particle number $N = \sum_i \langle n_i \rangle$ for three different scenarios: Fig. 4.1(a) shows occupations for a tight-binding chain of $M = 20$ sites, coupled to one heat bath only; therefore, the steady state is thermal. Figure 4.1(b) shows occupations for the same chain, but additionally in contact also with a second, population inverted heat bath described by a negative temperature $T_2 < 0$. Note that negative temperatures have been realized, e.g., in atomic quantum gases by preparing a state at the upper edge of a Bloch band [154]. Figure 4.1(c) shows occupations for a time-periodically driven quantum kicked rotor with $M = 20$ Floquet states coupled to a single bath. The system is in a regime, where the corresponding classical system, the Chirikov standard map [155], is known to be chaotic.

For small total particle number N , the bosons behave classically and the occupations $\langle n_i \rangle$ are given by the single-particle probabilities p_i^{SP} to occupy the state i scaled linearly with particle number N , $\langle n_i \rangle \simeq p_i^{\text{SP}} N$. However, at large total particle numbers the bosonic quantum statistics makes itself

4. Number of Bose-selected modes in driven-dissipative ideal Bose gases

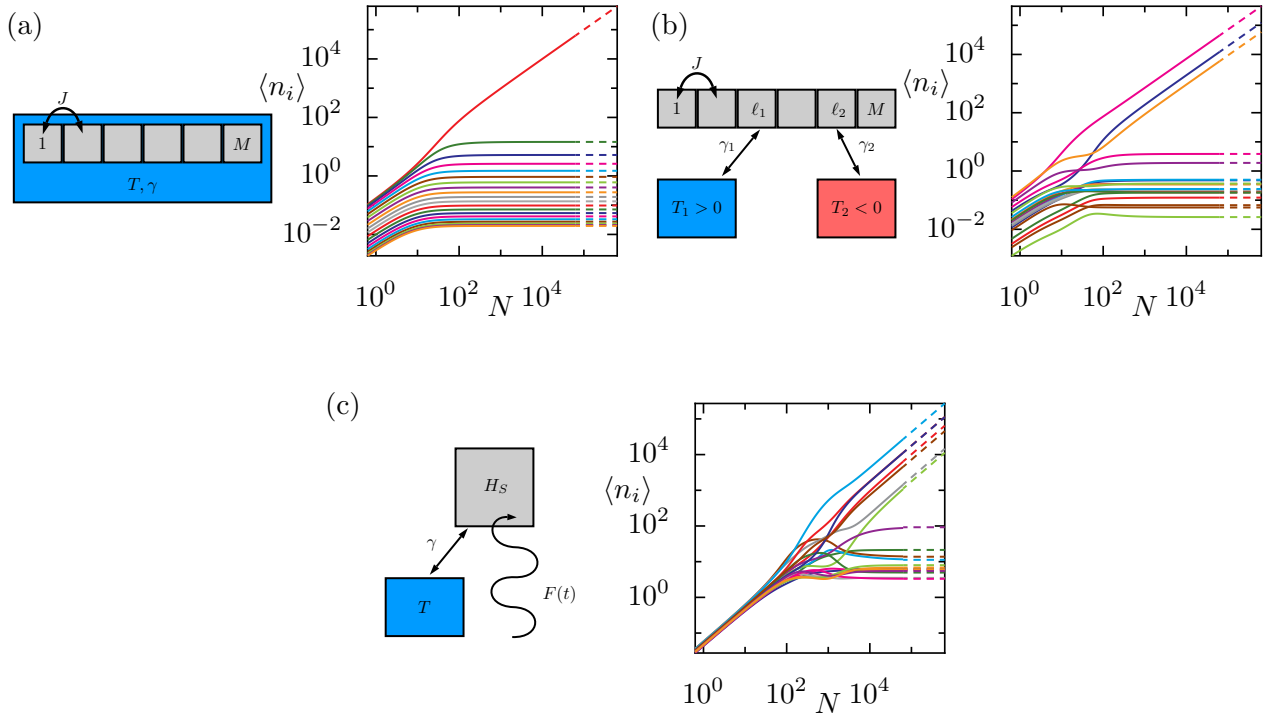


Figure 4.1.: Mean occupations $\langle n_i \rangle$ of the single-particle eigenstates i as a function of the total particle number N for the nonequilibrium steady state of an ideal Bose gas. Solid lines are from mean field theory, Eq. (4.4), dashed lines from the asymptotic theory. (a,b) The system is a tight-binding chain with $M = 20$ sites, tunneling parameter J , that is (a) in thermal equilibrium, coupled to a bath at temperature $T = J$ and (b) in a nonequilibrium steady state, coupled to a bath at temperature $T_1 = J$ to the occupation number operator at site $\ell_1 = 3$ and a second bath with temperature $T_2 = -0.2J$ at site $\ell_2 = 5$ with equal coupling strength $\gamma_1 = \gamma_2$. (c) Nonequilibrium steady state of a fully chaotic Floquet system (frequency ω) with $M = 20$ modes, the quantum kicked rotor with kicking strength $K = 10$, coupled to a single bath at temperature $T = \hbar\omega$.

felt. As a result, we observe Bose selection [82]: the occupations of some of the states saturate, while all additional particles gather in a set S of selected states whose occupations grow linearly with N . In equilibrium, Fig. 4.1(a), this corresponds to Bose condensation in the ground state. Away from equilibrium several states can be Bose selected.

From Figs. 4.1(a)-4.1(c) we already observe that the number $M_S = |S|$ of selected states can range from only few up to an extensive number, while the former case corresponds to fragmented Bose condensation, since each of the selected state acquires a macroscopic occupation in the limit $N \rightarrow \infty$, the latter case does not correspond to Bose condensation, since none of the selected states will acquire a macroscopic occupation. To be more precise, in the thermodynamic limit, $N, M \rightarrow \infty$, $N/M = \text{const.}$, there can only be (fragmented) condensation if the number M_S of Bose-selected states is intensive, i.e. asymptotically independent of M . However, if there is an extensive number of selected states, $M_S \propto M$, the system will behave effectively classically also in the ultra degenerate limit. So far, however, very little is known about how M_S depends on the properties of the system and in particular on the form of rates. The main goal of this chapter is to obtain a better understanding of how the number of selected states is determined by the properties of the rate matrix.

Before we begin with our analysis, let us briefly review the equations that determine the set of selected states and what so far has been known about their number. It has been shown that generally the number M_S of these selected states is odd. The starting point for determining the set of selected states is an asymptotic expansion (dashed lines in Fig. 4.1) of the mean occupations in the limit of large occupation, $N \gg 1$. For the selected states, $i \in S$, Eq. (4.4) yields in this limit [82, 83]

$$0 = \sum_{j \in S} A_{ij} \eta_j, \forall i \in S, \quad (4.6)$$

where η_i are the leading order occupations $\langle n_i \rangle = \eta_i N + \mathcal{O}(N^0)$. Note that for the nonselected states, these contributions vanish, so it must hold $\eta_i = 0, i \notin S$. The vector $\eta_i, i \in S$, is thus a nontrivial vector in the kernel of the skew-symmetric matrix $A_S = \{A_{ij} | i, j \in S\}$. The leading order of the occupations of the nonselected states, $i \notin S$, is then given by

$$\langle n_i \rangle = - \frac{\sum_{j \in S} R_{ij} \eta_j}{\sum_{j \in S} A_{ij} \eta_j} + \mathcal{O}(N^{-1}). \quad (4.7)$$

The physical condition of having positive occupations, $\langle n_i \rangle > 0$ for both the selected and the nonselected states, has been shown to uniquely determine the set of the selected states [83]. Using equations (4.6) and (4.7) this condition can be cast into the simple form

$$\mu = A\eta \text{ with } \begin{cases} \mu_i = 0, \eta_i > 0, & \text{for } i \in S \\ \mu_i < 0, \eta_i = 0, & \text{for } i \notin S. \end{cases} \quad (4.8)$$

From this condition a few simple statements about the number of selected states have been drawn already. First, we know that M_S is generically odd, since without fine tuning the skew-symmetric A_S possesses a nontrivial kernel for an odd number of selected states only. Second, in case the system possesses a ground-state like state k defined by

$$R_{ki} > R_{ik}, \forall i \neq k, \quad (4.9)$$

one can immediately see that the problem (4.8) is solved by $S = \{k\}$, i.e. a single selected state is found. Finally, for uncorrelated random rates it has been observed numerically that the number of selected states follows a binomial distribution. Thus, an extensive number of states (on average half of the states) are selected.

However, a general estimate for M_S is not straight forward. In the following, we will discuss different scenarios in which such estimates can be found; First we will study rates which possess a well-defined continuum limit for $M \rightarrow \infty$. Second we will consider rates that do not have such a continuum limit, discussing the two important cases where rates are truly random, and rates that stem from a chaotic kicked system. Finally, we will discuss rates that are given by a sum of direct products, as they are relevant for autonomous systems that couple to the environment via a few observables only.

4.2. Rates with continuum limit

In this section we discuss systems described by rate matrices that have a smooth continuum limit and which are, thus, strongly correlated. We assume that the quantum numbers $i \in \{0, \dots, M-1\}$ can be labeled by a variable

$$k_i = \alpha \frac{i}{M}, \text{ with constant } \alpha \in \mathbb{R}, \quad (4.10)$$

that becomes continuous in the limit $M \rightarrow \infty$. Moreover, we focus on one-dimensional systems whose rate matrices shall become smooth in that limit, i.e. that there exists a function $R(k, q)$, such that

$$R_{ij} = R(k_i, k_j) \Delta^2 \quad (4.11)$$

with $\Delta = \alpha/M$. The generalization to higher-dimensional systems described by several continuous quantum numbers is straight forward.

An example for this situation are the rates for a single bath coupled to site ℓ of the tight-binding chain described by the Hamiltonian [see Fig. 4.1(b)]

$$H_S = -J \sum_{i=1}^{M-2} (a_{i+1}^\dagger a_i + a_i^\dagger a_{i+1}), \quad (4.12)$$

where J is the tunneling constant and a_i is the bosonic annihilation operator at site i . In this case we find [156]

$$R(k, q) = \frac{2\gamma^2}{\pi\hbar} g(\varepsilon(k) - \varepsilon(q)) \sin(k\ell)^2 \sin(q\ell)^2 \quad (4.13)$$

with dispersion $\varepsilon(k) = -2J \cos(k)$ and k -space sampling with $i = 1, \dots, M-1$, and $\alpha = \pi$.

We make the ansatz that there is a discrete set of Bose-selected states $S = \{k_s\}$, such that in the asymptotic limit for large densities $n \rightarrow \infty$ the mean occupation density reads

$$\langle n(k) \rangle = \langle n_n(k) \rangle + \bar{n}_s \delta(k - k_s), \quad (4.14)$$

where we have introduced the normalization condition

$$n = N\Delta = \sum_i \langle n_i \rangle \Delta \Rightarrow n = \int_0^\alpha \langle n(k) \rangle dk. \quad (4.15)$$

Eq. (4.6) then translates to

$$a(k_s) = 0, \quad \forall k_s \in S, \quad (4.16)$$

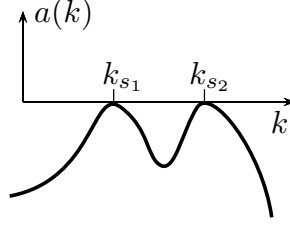


Figure 4.2.: Sketch of the typical behavior of the function $a(k)$ defined in Eq. (4.17). The function is globally negative with zeros at the Bose-selected states k_s .

where we have defined the function

$$a(k) = \sum_{s \in S} A(k, k_s) \bar{n}_s, \quad (4.17)$$

with rate asymmetry function $A(k, q) = R(k, q) - R(q, k)$. Note that for smooth rates, the function $a(k)$ will be smooth as well. The starting point for our reasoning is the analog of Eq. (4.7), which predicts that in the continuum limit the asymptotic occupations of all modes $k \notin S$ read

$$\langle n_n(k) \rangle = - \frac{\sum_{s \in S} R(k, k_s) \bar{n}_s}{a(k)}. \quad (4.18)$$

Since here the numerator is strictly nonnegative, the denominator has to be strictly negative

$$a(k) < 0, \quad \forall k \notin S. \quad (4.19)$$

In the following, we assume that R is two-fold differentiable. By discussing the rate function in the vicinity of the selected states, we will then be able to restrict the possible selected states to a few candidates only. From Eqs. (4.16) and (4.19) it follows that $a(k)$ is negative almost everywhere, however at local maxima it assumes the value zero, whenever $k = k_s$, see sketch in Fig. 4.2. This implies both

$$0 = a'(k_s) = \sum_{p \in S} A'(k_s, k_p) \bar{n}_p, \quad (4.20)$$

and

$$0 > a''(k_s) = \sum_{p \in S} A''(k_s, k_p) \bar{n}_p, \quad (4.21)$$

where we have defined $A'(k, q) = \partial_k A(k, q)$ and $A''(k, q) = \partial_k^2 A(k, q)$. Note that these local criteria are necessary, but not sufficient for Bose selection in state k_s . Note also that state space k may have a boundary or not. For example for the tight-binding chain in Fig. 4.1(b), we do not impose periodic boundary conditions in real space, then k takes values in the interval $[0, \pi]$. Thus the dispersion $\varepsilon(k)$ is not a periodic function of k and our state space possesses boundaries at 0 and π . At such boundaries

4. Number of Bose-selected modes in driven-dissipative ideal Bose gases

the criteria (4.20) and (4.21) do not have to apply, because here the maxima of $a(k)$ are no longer characterized by derivatives.

As we will see, the criteria (4.20) and (4.21) strongly constrain the set of selected states. To illustrate this fact, we will discuss different scenarios in the following subsection.

4.2.1. Different selection scenarios

If only one state k_0 is selected and does not lie at the boundary of the state space, it follows that

$$0 = \partial_k A(k, q)|_{(k_0, k_0)} \quad \text{and} \quad 0 > \partial_k^2 A(k, q)|_{(k_0, k_0)}. \quad (4.22)$$

Since A is skew-symmetric,

$$A(k, q) = -A(q, k), \quad \forall k, q, \quad (4.23)$$

we also find

$$0 = \partial_q A(k, q)|_{(k_0, k_0)} \quad \text{and} \quad 0 < \partial_q^2 A(k, q)|_{(k_0, k_0)}. \quad (4.24)$$

Since also the gradient of A vanishes at (k_0, k_0) , this point must be an extreme point of the asymmetry function A . Moreover, we find that the mixed derivative at this point must vanish

$$\begin{aligned} \partial_k \partial_q A(k, q)|_{(k_0, k_0)} &= \partial_q \partial_k A(k, q)|_{(k_0, k_0)} \\ &= -\partial_q \partial_k A(q, k)|_{(k_0, k_0)} = -\partial_k \partial_q A(k, q)|_{(k_0, k_0)} = 0. \end{aligned} \quad (4.25)$$

Here we first used Schwarz' theorem and in the third step renamed the variables. Thus k_0 either corresponds to a saddle point on the diagonal of the rate asymmetry matrix or it lies at the boundary of state space (if there is one), where both local criteria do not have to apply.

An example is given by the rate-asymmetry function A shown in Fig. 4.3(a). Here we mark the position of the selected state by black arrows on the side and the relevant matrix element $A(k_0, k_0)$ by a red arrow. It lies at a saddle point (having the correct curvature) on the diagonal. Clearly, also the rest of function $a(k) \propto A(k, k_0)$ must remain below the blue $A = 0$ plane.

For $M_S > 1$ the vector of the occupations $\{\bar{n}_s\}_{s \in S}$ is a homogeneous solution of Eq. (4.16) and at the same time of Eq. (4.20). This provides a strong restriction, since both equations generally will not have a common set of solutions. Therefore, selected states will generically occur in two special scenarios.

The first scenario is the following. Since the rate asymmetry A is continuous we will naturally find zero lines $A(k, q) = 0$ also away from the diagonal $A(k, k) = 0$. If the selected states lie at these zero lines, i.e. $A(k_s, k_p) = 0$, the occupations $\{\bar{n}_s\}_{s \in S}$ are only determined by Eq. (4.20).

Note that since the coefficient matrix $(A'(k_s, k_p))_{s,p}$ is not necessarily skew-symmetric, in this case also an even number of selected states k_s may occur in the continuum limit. In the discrete case, an even number M_S of selected states requires fine-tuning in the rate matrix [83] such that for example

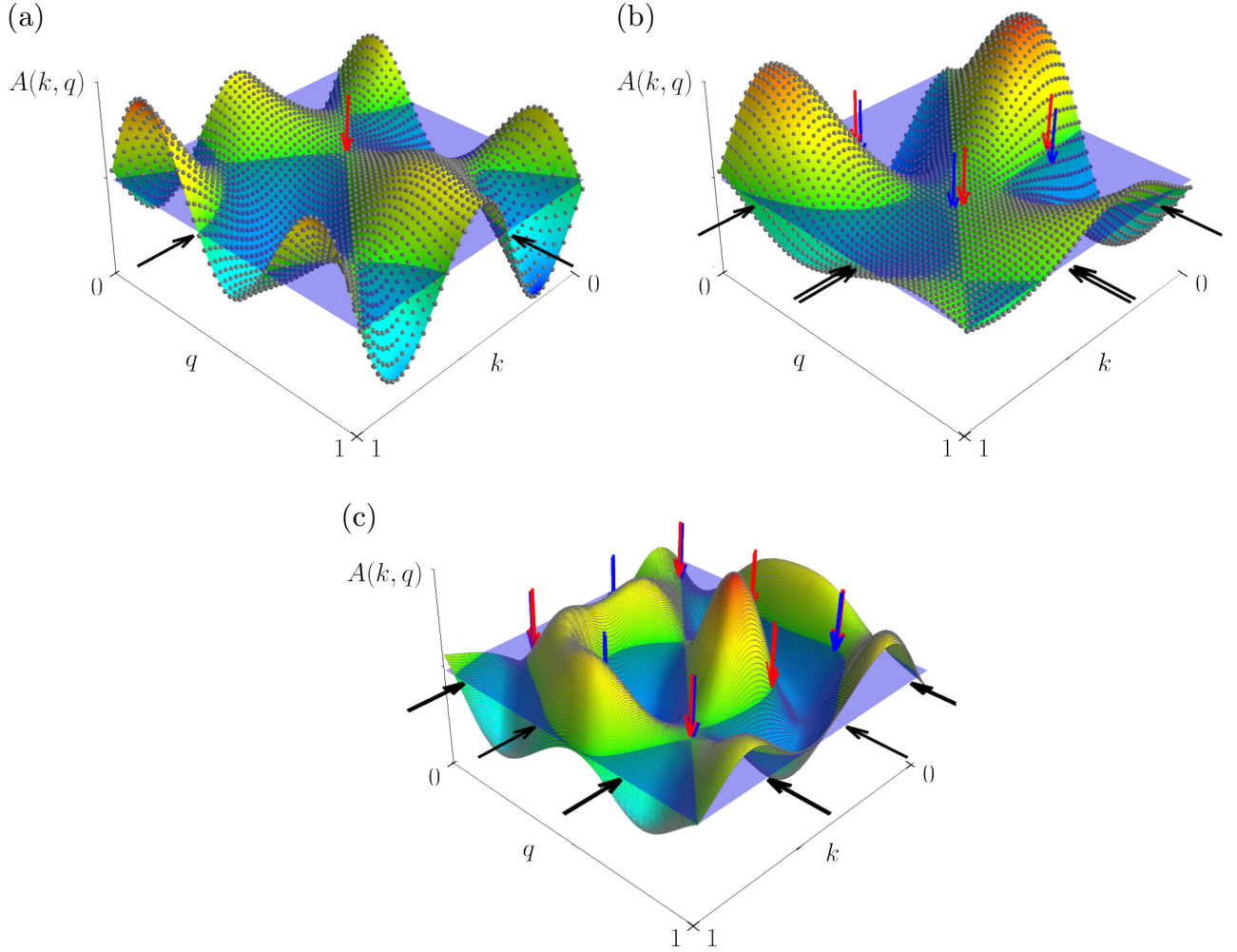


Figure 4.3.: Gallery of selected states in the random wave model, Eq. (4.26), for a superposition of $L = 80$ plane waves with wavenumber $\kappa = 3\pi$ (a, b) and $\kappa = 5\pi$ (c). We discretize k -space such that $M = 50$ (a, b) and $M = 200$ (c) states exist. The smooth rate-asymmetry function $A(k, q)$ is sampled at the grey points. The blue plane represents $A = 0$. Selected states are marked by black arrows at the k - and q -axis. We indicate the contributing matrix elements $A(k_s, k_p)$ by red (for $A \geq 0$) and blue (for $A < 0$) arrows. For clarity we do not mark diagonal elements $A(k_s, k_s)$ if $M_S > 1$.

some of the A_{ij} vanish. However, for continuous rate asymmetry functions it is natural to have zero lines, i.e. $A(k_s, k_p) = 0$ for $k_s \neq k_p$, such that in the continuous case no fine-tuning is needed to observe an even number M_S . However, if an even number of selected states k_s occurs in the continuous model, a corresponding discrete system will still feature an odd number of selected states. We then typically find pairs of neighboring selected states around at least one¹ of the selected states k_s of the continuous model [as in the example in Fig. 4.3(b)]. To avoid confusion, we refer to the number of selected states in the continuous system as *continuum number of selected states* $M_S = 1, 2, 3, 4, \dots$

In Fig. 4.3(b) we observe Bose selection at zero lines where the continuum selection of $M_S = 2$ states

¹Around which of the states k_s pairs form is, however, not universal and depends on the discrete grid. If one plots the selected states as a function of discretization parameter M for example, one can observe how such pairs jump from one k_s to the other quite irregularly (not shown).

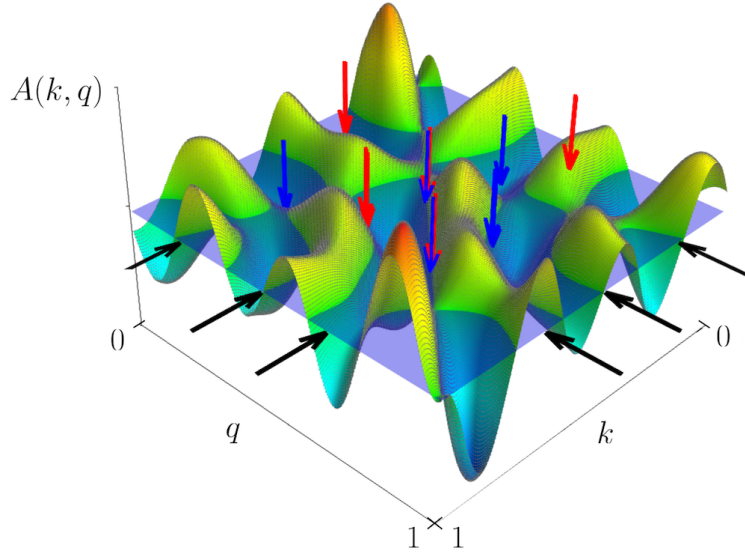


Figure 4.4.: Typical example for Bose selection in a more complex rate matrix. Parameters are like in Fig. 4.3, but $M = 300$ and $\kappa = 7\pi$.

occurs. The asymptotic states k_1, k_2 lie at a zero line of A . Since in the discrete system the number of selected modes M_S is always odd, we find $M_S = 3$ in the discrete system with a pair of neighboring states in the vicinity of state $k_2 > k_1$.

Another possible scenario is that the selected states are found such that at (k_s, k_p) the rate asymmetry function possesses saddle points. Then $A'(k_s, k_p) = 0$ such that the occupations $\{\bar{n}_s\}_{s \in S}$ are solely determined by Eq. (4.16). In this case the corresponding continuum M_S will be odd.

However typically neither of the cases – selection at only zero lines or only saddle points – occurs in a “pure” form. This can be seen in the example in Fig. 4.3(c), where we observe the selection at both zero lines and saddle points with a continuum selection of $M_S = 3$ states. In this case, some of the relevant points (k_s, k_p) lie on the zero lines of A , and others have saddle points in the vicinity of the point (k_s, k_p) . Here, $M_S = 5$ states are selected in the discrete system, with pairs at two continuum wave numbers k .

But it is only in continuous rate matrices with few oscillations (like in the examples chosen in Fig. 4.3) that we find selected states defined by one of the different mechanisms stated above. If we consider systems with more variation in the rate matrix, like in Fig. 4.4, the points (k_s, k_p) are not clearly relatable to either zero lines nor saddle points anymore. Nevertheless, these points are often still found in the vicinity of zero lines and saddle points.

4.2.2. Random-wave model

The rate functions shown in Fig. 4.3 and 4.4 are motivated by a random wave model for chaotic eigenfunctions [157]. They are defined by

$$R(k, q) = \sum_{l=1}^L \operatorname{Re}\{c_l \exp[i(\kappa_{k,l}k + \kappa_{q,l}q)]\} + C. \quad (4.26)$$

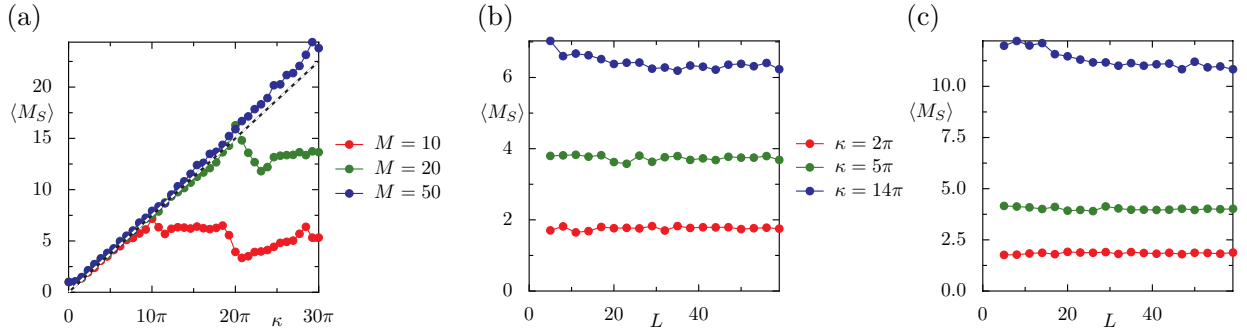


Figure 4.5.: Mean number $\langle M_S \rangle$ of selected states in the random wave model (4.26) for (a) a superposition of $L = 50$ plane waves as a function of the wave-number κ . The rates $R(k, q)$ are sampled at $M = 10, 20$ and 50 discrete states. We average over 500 realizations of the random rates. We see a linear increase with $\langle M_S \rangle \approx 0.75\kappa/\pi$ (dashed line, guide to the eye) before it saturates at a value where more than half of the single particle states are Bose selected. (b, c) Mean number of selected states as a function of the number L of components for (b) $M = 10$ and (c) $M = 20$ discretization steps and 250 realizations. We see only a weak dependence on L .

It is a superposition of L independent plane waves with $\kappa_{k,l} = \kappa \sin(\varphi_l)$, $\kappa_{q,l} = \kappa \cos(\varphi_l)$, fixed absolute value of the wavenumber κ and uniformly distributed angles $\varphi_l \in [0, 2\pi)$. Amplitudes $|c_l|$ are drawn from a normal distribution and phases $\arg(c_l)$ are distributed uniformly. The global constant C is chosen such that all rates are nonnegative. Its specific value is irrelevant for the set of the Bose-selected states, which are solely determined by the rate-asymmetry function $A(k, q)$ in which C will drop out.

This model produces rate functions that are smooth and show oscillations on the length scale $2\pi/\kappa$ in state space, see e.g. Fig. 4.3. It allows us to investigate the typical behavior of smooth rates that show variations on such a scale. We discretize state space via Eq. (4.10) where, to unravel the continuum physics, we choose the discretization length Δ to be small with respect to the oscillation length of the model, $\Delta = 1/M \ll 2\pi/\kappa$.

As we increase the wavenumber κ of the model the structure of R will become more and more complex, leading to more and more zero-lines and saddle points in the rate asymmetry function. Thus, we expect that with the characteristic wavenumber κ , which determines the typical oscillation length $2\pi/\kappa$ of the smooth rate function R , also the average number of selected modes $\langle M_S \rangle$ will increase. This is confirmed by the numerical results shown in Fig. 4.5(a). The mean number of selected states increases as soon as κ exceeds the threshold $\kappa \approx \pi$, where the wavelength $2\pi/\kappa$ of the plane waves is about double the system size. Afterwards, we see a linear increase with $\langle M_S \rangle \approx 0.75\kappa/\pi$ as marked by the black and white dashed line. The linear scaling is explained by the above reasoning, since e.g. the number of extrema (and also the number of zeros) of $\sin(\kappa k)$ on the interval $k \in [0, 1]$ is of the order of κ/π . However the origin of the prefactor of about 0.75 remains open.

Note that the mean number $\langle M_S \rangle$ only depends weakly on the number of components L that we use in the random wave model as shown in Fig. 4.5(b) for $M = 10$ discrete states and (c) $M = 20$ and three different values of κ .

The behavior seen in Fig. 4.5(a) clearly suggests that for smooth rates, the number of selected states

4. Number of Bose-selected modes in driven-dissipative ideal Bose gases

is typically on the order of the number of oscillations in the rate asymmetry function A . Therefore, for fixed smooth A , even if the number of discrete states M is large, $M \rightarrow \infty$, as observed in Fig. 4.5, the number M_S will remain intensive as it is solely the property of the smooth function A .

We expect a breakdown of the theory for continuous rates as soon as the oscillation length of the rate function becomes comparable to the discretization length. For the random rates this breakdown occurs for $\kappa \approx M\pi$ as visible in Fig. 4.5(a). Interestingly, the mean number of selected states $\langle M_S \rangle$ for the random wave model does not saturate at $\langle M_S \rangle = M/2$ as one would expect for truly random rates (see Sec. 4.3.1). We observe a first saturation at values that are slightly above $M/2$: for $M = 20$ discrete states we find saturation at about $\langle M_S \rangle = 13$, or for $M = 10$ we find $\langle M_S \rangle \approx 6$.²

4.3. Rates without continuum limit

4.3.1. Uncorrelated random rates

The single particle rates R_{ij} that one observes typically for a fully chaotic quantum rotor have been shown to roughly follow an exponential distribution [73]. If we suppose that there are no additional correlations between the rates R_{ij} , we may draw typical rates from a random realization of the exponential distribution, where $p(R_{ij}) = \exp(-\lambda R_{ij})/\lambda$. Note that the choice of the parameter λ is irrelevant, since it only determines the time scale on which the system relaxes but not the steady state.

Figure 4.6(a) shows the distribution of the number M_S of Bose-selected states for random rates connecting $M = 40$ single particle states. The odd number of Bose-selected states is given by a binomial distribution,

$$p(M_S) = \begin{cases} 0 & \text{for } M_S \text{ even} \\ \frac{1}{2^{M-1}} \binom{M}{M_S} & \text{for } M_S \text{ odd} \end{cases} \quad (4.27)$$

centered around $\langle M_S \rangle = M/2$ [cf. Fig. 4.6(c)]. Such a behavior was observed in the literature for random rates, mostly in the context of population dynamics, where similar equations, the Lotka-Volterra equations, appear [82, 158–161]. Usually this result is motivated by arguing that for the random rates all states are equal, so that every state has the same probability to be Bose selected or not. Taking into account the additional constraint that the total M_S must be odd, one can in this way motivate the distribution (4.27) by just counting the number of possible choices of M_S states among the total M states.

However, the argument that every state has the same probability to be Bose selected or not must also follow rigorously from the steady state equations, and thus also from Eq. (4.8). To fill this gap, we will compute the distribution of selected states. To this end, we will first construct transformations

²Note that after this first saturated regime, for the red line $M = 10$, the number drops again at around $\kappa = 2\pi M$. This is related to the effect of aliasing occurring when the wavelength $2\pi/\kappa$ of the random wave model is smaller than the discretization length $\Delta = 1/M$.

of the rate-asymmetry matrix $A = (A_{ij})$ under which the number of Bose-selected states M_S remains invariant, i.e. the solutions of the problem (4.8) have the same M_S .

Reordering transformations

Since the indexing of the states is arbitrary, M_S will remain invariant when reordering the states. The matrix $T_{k,l}$ describes the transpositions that exchange state k and l . Since $T_{k,l}^{-1} = T_{k,l}$ the corresponding transformation takes the form

$$A \rightarrow T_{k,l} A T_{k,l}. \quad (4.28)$$

Under this transformation, the matrix remains skew-symmetric, and also the number of Bose-selected states remains invariant.

So for discussing the properties of a general A with a given number M_S of Bose-selected states, we can thus assume solutions of the form

$$\eta = (\eta_1, \dots, \eta_{M_S}, 0, \dots, 0)^T. \quad (4.29)$$

Rescaling transformations

We are only interested in the number of selected states and not in their occupation. Therefore, let us consider a rescaling of the coefficients η_i and μ_i . This is accomplished by a transformation induced by the matrix

$$D_\lambda = \text{diag}(\lambda_1, \dots, \lambda_M), \quad \text{with positive } \lambda_k > 0. \quad (4.30)$$

As we want to apply this matrix to both the vectors η and μ , it is important that only positive rescaling $\lambda_k > 0$ is allowed. Otherwise we would transform a solution of problem (4.8) into vectors that do not solve a problem of this type. Since the inverse of this matrix is again diagonal, $D_\lambda^{-1} = D_{(1/\lambda_1, \dots)}$ we find that the rescaling transformation

$$\eta \rightarrow D_\lambda \eta, \quad \mu \rightarrow D_\lambda^{-1} \mu, \quad A \rightarrow D_\lambda^{-1} A D_\lambda^{-1} \quad (4.31)$$

preserves skew-symmetry of the matrix A . Note that we multiply A with the inverse from the left and the right. The rescaled quantities $\tilde{\mu}, \tilde{\eta}, \tilde{A}$ with $\tilde{S} = S$ fulfil again Eq. (4.8), since

$$\tilde{\mu} = D_\lambda^{-1} \mu = D_\lambda^{-1} A D_\lambda^{-1} D_\lambda \eta = \tilde{A} \tilde{\eta}. \quad (4.32)$$

M_S -dimensional skew-symmetric matrix $A_{M_S}^S$ restricted by the existence of the homogeneous solution

$$A_{M_S}^S \begin{pmatrix} 1 \\ \vdots \\ 1 \end{pmatrix} = 0. \quad (4.35)$$

Consequence for random rates

For a random rate matrix, all entries $(A_{ij})_{j>i}$ of the rate asymmetry are random and statistically independent. We aim to find the probability to randomly choose a matrix that is from the class generated by the A_{M_S} -matrix (under the transformations (4.28) and (4.31)). To this end, we first count the number d of degrees of freedom in determining a general matrix A_{M_S} . In a second step we then discuss the influence of the transformations.

Let us begin with the block $A_{M_S}^S$. To construct such a matrix, we start from an arbitrary M_S -dimensional skew-symmetric matrix which has $d_S = \frac{1}{2}(M_S - 1)M_S$ degrees of freedom. We have to distinguish two different cases: For odd M_S this matrix has always a homogeneous solution, for even M_S we have to fine tune one parameter for a homogeneous solution to exist, which reduces the number of degrees of freedom by one. Furthermore we have to subtract $M_S - 1$ degrees because the homogeneous solution is pinned to $(1, \dots, 1)^T$. Thus the number of degrees of freedom in the subspace of the selected modes is

$$d_S^o = \frac{1}{2}(M_S - 1)(M_S - 2), \quad (4.36)$$

$$d_S^e = d_S^o - 1 \quad (4.37)$$

for an odd or even number of selected modes, respectively.

Then, there are $M - M_S$ rows, each of which has $M_S - 1$ free variables $x^{(i)}$ to choose. This contributes

$$d_f = (M - M_S)(M_S - 1) \quad (4.38)$$

degrees of freedom.

Also there is still an arbitrary $(M - M_S)$ -dimensional skew-symmetric matrix free to choose, which adds another

$$d_{\text{arb}} = \frac{1}{2}(M - M_S)(M - M_S - 1) \quad (4.39)$$

degrees of freedom.

4. Number of Bose-selected modes in driven-dissipative ideal Bose gases

This sums up to

$$d^o = d_S^o + d_f + d_{\text{arb}} = \frac{1}{2}(M-1)(M-2) \quad (4.40)$$

$$d^e = d^o - 1 \quad (4.41)$$

for odd and for even M_S respectively. Interestingly for every M_S the number of free parameters of the generating matrix A_{M_S} depends on the parity of M_S only. Matrices with an even M_S have one degree of freedom less.

If we now choose a rate-asymmetry matrix randomly, the probability to hit a matrix with a specific number of selected states is proportional to its size in parameter space. The diagonal transformations (4.31) do not favour any number of selected states, as they always contribute M degrees of freedom. For an even number of selected states there is one free parameter less than for an odd number M_S , such that their generating matrices form a set of probability measure zero in parameter space. Therefore all generators A_{M_S} of odd selection numbers have equal size in probability space and the even numbers are suppressed.

It is left to discuss the influence of the reordering transformations (4.28). They allow to distribute the M_S selected states over the M states. The number of possible configurations for this is given by the binomial factor

$$\binom{M}{M_S}. \quad (4.42)$$

After normalization, we infer the distribution (4.27).

4.3.2. Chaotic quantum kicked rotor

We want to compare these results for uncorrelated random rates to chaotic systems.

A paradigm for quantum chaos is the quantum kicked rotor, a one-dimensional rotor governed by the Hamiltonian

$$H(\varphi, p, t) = \frac{p^2}{2} + K \cos(\varphi) \sum_{n \in \mathbb{Z}} \delta(t - n) \quad (4.43)$$

with time-periodic kicks of strength K , period $\tau = 1$ and $[\varphi, p] = i\hbar_{\text{eff}}$. For $\hbar_{\text{eff}} = \frac{2\pi}{M}$, $M \in \mathbb{N}$, we can restrict the system to a torus with periodic coordinate $\varphi \in [0, 2\pi)$ and periodic momentum $p \in [-\pi, \pi)$. Note that since the available phase space volume on the torus is $V = (2\pi)^2$, there exist $V/(2\pi\hbar_{\text{eff}}) = M$ Floquet states on the torus.

These Floquet states $|i(t)\rangle$ are eigenstates of the one-cycle evolution operator

$$U(1, 0) = e^{-\frac{i}{\hbar_{\text{eff}}} K \cos(\varphi)} e^{-\frac{i}{\hbar_{\text{eff}}} \frac{p^2}{2}} \quad (4.44)$$

fulfilling $U(1, 0)|i(0)\rangle = \exp(-i\varepsilon_i/\hbar_{\text{eff}})|i(0)\rangle$ with corresponding quasienergies ε_i .

This kicked rotor is coupled to a bath with temperature T . We consider the coupling operator

$$v = \sin(\varphi) + \cos(\varphi), \quad (4.45)$$

which respects the periodicity of φ and breaks the parity (such that also even and odd Floquet states are coupled to each other).

In Fig. 4.6(b) we show the distribution for the number of selected states M_S that we obtain when randomly choosing the kicking strength K within the interval $[9.5, 10.5]$ (where the classical counterpart of the quantum kicked rotor is essentially fully chaotic) for a rotor with $M = 40$ Floquet states. From Fig. 4.6(b) and (c) it is clear that the random rate model fails to predict the number of selected states for a typical realization of the chaotic quantum kicked rotor. The distribution is centered around a much larger value than $M_S = M/2$ expected for random rates [Fig. 4.6(a)]. It also seems that the distribution may not be fitted with a binomial distribution, which for example for $p = 0.62$ (black crosses) is much broader than the one that is observed. This trend also manifests itself in Fig. 4.6(c) where the triangles show the mean number $\langle M_S \rangle$ of Bose-selected states for the quantum kicked rotor. This number lies well above $M/2$, for systems of size $M \gtrsim 150$ about 80% of the states are Bose selected. Consequently, we come to the intriguing conclusion that there must be additional correlations among the rates R_{ij} that are responsible for the fact that significantly more states are selected for the chaotic quantum kicked rotor than in the random-rate model. In the following section, we describe a model with correlated random rates that shows a similar distribution of selected states as the quantum kicked rotor model. However, the origin of the large number of selected states for our quantum kicked rotor model remains an interesting open question.

4.3.3. Modified random wave model for the rates in the quantum kicked rotor

The deviations from the random rate model indicate that the rates of the chaotic quantum kicked rotor contain correlations that lead to the Bose selection of more states than in the uncorrelated case. In this section we construct a random rate matrix that has correlations that lead to similar behavior.

Correlations of the rates associated with the quantum-kicked-rotor model in contact with a heat bath that we considered were discussed in Ref. [73] (where the single-particle problem was studied). The rate R_{ij} and the backwards rate were proposed to obey

$$R_{ji} = (1 + \xi_{ij})R_{ij}, \text{ for } i > j, \quad (4.46)$$

with both R_{ij} and ξ_{ij} stemming from individual exponential distributions with scale parameters λ and λ_ξ , where λ_ξ decreases with system size as $\lambda_\xi \propto M^{-1.2}$. However, the rate model (4.46) leads to steady states with even less than half of the states being Bose selected (data not shown).

Note that in Sec. 4.2.2 we have encountered a model, which also features that typically more than half of the states are Bose selected. It is the random wave model, Eq. (4.26), with parameter $\kappa \approx 1.9\pi M$ [cf. also Fig. 4.5]. A suggestive point of view for why the random wave model might be suitable to approximate rates of a chaotic map, is that random waves have been used successfully to model

4. Number of Bose-selected modes in driven-dissipative ideal Bose gases

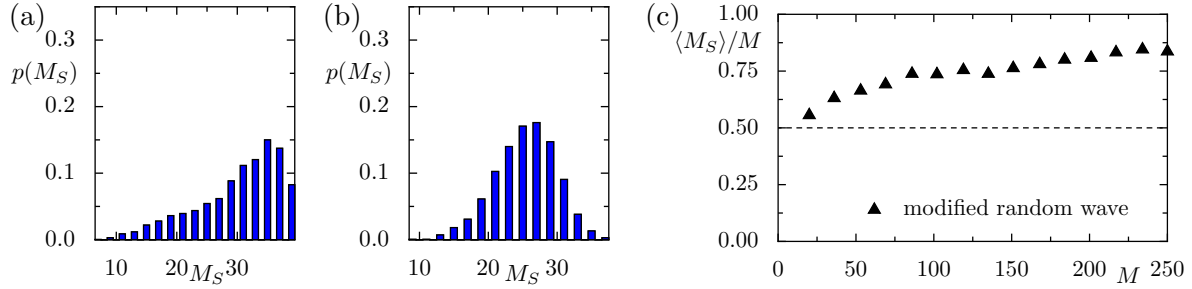


Figure 4.7.: (a) Distribution of the number M_S of Bose-selected states for 5000 realizations of rates R_{ij} stemming from the random wave model, Eq. (4.26), with $\kappa = 1.9\pi M$, $L = 80$ and $M = 40$ states. (b) Same as in (a) but for 5000 realizations of the modified random wave model, Eq. (4.47), with $M = 40$ states, $\kappa = 1.9\pi M$, $L = 80$ and $\lambda = 10$. (c) Mean number $\langle M_S \rangle$ of Bose-selected states divided by system size M as a function M for the modified random wave model (triangles) for 50 realizations of the system. We use $L = 2M$ components. The dashed line is at $M_S = M/2$.

typical chaotic eigenstates [157, 162, 163]. Note, however, that this vague reasoning is not based on a microscopic picture for the derivation of the rates.

We can see in Fig. 4.7(a) that the distribution for the random wave model with $M = 40$ is much broader than the one we observe for the quantum kicked rotor in Fig. 4.6(b). Also the rates R_{ij} that result from a random wave model, Eq. (4.26), do not follow an exponential distribution. Their distribution $p(R_{ij})$ is rather peaked at some finite value. To correct for this, we introduce a modified random wave model for the rates

$$R(k, q) = \sum_{l=1}^L |c_l| \text{Re} \left\{ 1 + e^{i(\kappa_{k,l}k + \kappa_{q,l}q + \alpha_l)} \right\} e^{-\lambda|k-q|}, \quad (4.47)$$

where we constrain the waves to positive values and localize them on a length λ^{-1} by introducing an exponential factor. In this model we choose $\kappa_{k,l} = \kappa \sin(\varphi_l)$, $\kappa_{q,l} = \kappa \cos(\varphi_l)$ similar to the random wave model with fixed absolute value of the wavenumber κ , uniformly distributed angles $\varphi_l, \alpha_l \in [0, 2\pi]$ and c_l from a normal distribution.

We observe that the modified random-wave model has rates that are distributed exponentially and the distribution of the M_S shows relatively good agreement with the data from the quantum kicked rotor for $\kappa = 1.9\pi M$ and localization parameter $\lambda = 400/M$. This can be seen for example by comparing the distribution for $M = 40$ discrete states in Fig. 4.7(b) to the distribution of the quantum kicked rotor in Fig. 4.6(b), although the mean values coincide, the distribution of our model is, however, a bit broader than the one obtained for the quantum kicked rotor. Also as a function of system size, Fig. 4.7(c), the model seems to reproduce the mean value of selected states in Fig. 4.6(c) quite nicely.

However, despite the fact that the modified random wave model (4.47) gives rise to a similar distribution of the number of selected states as the one obtained for the quantum kicked rotor, we have no evidence that the modified random-wave model mimics the physics of the quantum kicked rotor coupled to a heat bath [see Sec. 4.3.2].

4.4. Rates with product structure

Consider an arbitrary time-independent system with Hamiltonian H_S which is coupled to a positive temperature bath (B_1) and a population-inverted bath (B_2) described by a negative temperature through coupling operators which obey the form of a projector on a single quantum state,

$$v^{(B_1)} = |f\rangle\langle f|, \quad v^{(B_2)} = |g\rangle\langle g|. \quad (4.48)$$

Note that the states $|f\rangle$ and $|g\rangle$ can also be coherent superpositions of the single-particle eigenstates i . In this section we show that the number of selected states remains always lesser than or equal three, $M_S \leq 3$, for all system sizes M . Note that in case of this specific system-bath coupling even a system with chaotic single-particle dynamics features only a maximum number of three condensates. An example of a system with such a system bath coupling is the one depicted in Fig. 4.1(b). Here the states f and g correspond to the local Wannier orbitals at lattice sites ℓ_1 and ℓ_2 , respectively.

For coupling operators of the form (4.48), we find the rate asymmetry matrix

$$A_{ij} = \frac{2\pi}{\hbar} J(\varepsilon_j - \varepsilon_i) (f_i f_j - g_i g_j) \quad (4.49)$$

from Eq. (4.5), where $f_i = |\langle i|f\rangle|^2$, and $g_i = |\langle i|g\rangle|^2$. Here we assume that $J_{B_2}(\varepsilon) = -J_{B_1}(\varepsilon) = -J(\varepsilon)$, giving rise to rates $R_{ij} \geq 0$. Moreover, let us first consider ohmic baths with spectral density $J(\varepsilon) \propto \varepsilon$. We find a rate asymmetry matrix having the product structure

$$A_{ij} \propto f_i f_j \varepsilon_j - f_i f_j \varepsilon_i - g_i g_j \varepsilon_j + g_i g_j \varepsilon_i. \quad (4.50)$$

Now let η_i be the solution of Eq. (4.8). It then follows that in the subspace of selected states one has

$$0 = \mathbf{A}\boldsymbol{\eta} = \begin{pmatrix} f_{i_1} \\ f_{i_2} \\ \dots \\ f_{i_{M_S}} \end{pmatrix} c_1 - \begin{pmatrix} f_{i_1} \varepsilon_{i_1} \\ f_{i_2} \varepsilon_{i_2} \\ \dots \\ f_{i_{M_S}} \varepsilon_{i_{M_S}} \end{pmatrix} c_2 - \begin{pmatrix} g_{i_1} \\ g_{i_2} \\ \dots \\ g_{i_{M_S}} \end{pmatrix} c_3 + \begin{pmatrix} g_{i_1} \varepsilon_{i_1} \\ g_{i_2} \varepsilon_{i_2} \\ \dots \\ g_{i_{M_S}} \varepsilon_{i_{M_S}} \end{pmatrix} c_4 \quad (4.51)$$

with

$$\begin{aligned} c_1 &= \sum_{i \in S} \varepsilon_i f_i \eta_i, & c_2 &= \sum_{i \in S} f_i \eta_i, \\ c_3 &= \sum_{i \in S} \varepsilon_i g_i \eta_i, & c_4 &= \sum_{i \in S} g_i \eta_i. \end{aligned} \quad (4.52)$$

Since $f_i > 0$, $g_i > 0$ and $\varepsilon_i > 0$ (otherwise we can always shift all ε_i by some constant), these coefficients are positive,

$$c_i > 0. \quad (4.53)$$

4. Number of Bose-selected modes in driven-dissipative ideal Bose gases

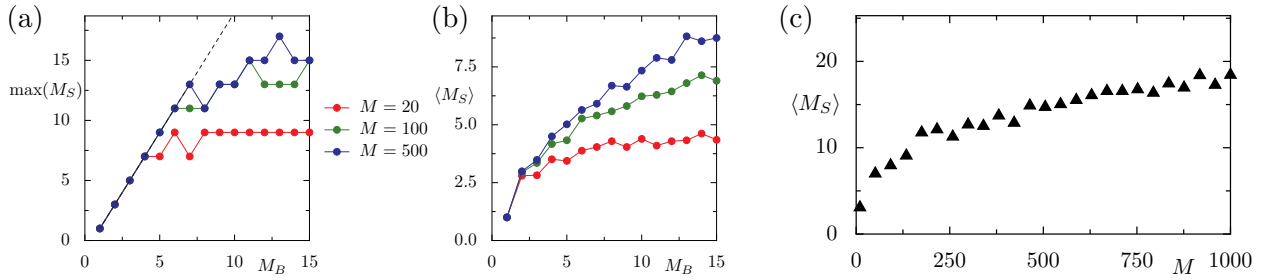


Figure 4.8.: (a) Maximum number and (b) mean number M_S of Bose-selected states observed for 200 realizations of a random chaotic system $H_S \in \text{GOE}(M)$ as a function of the number of baths M_B coupled to the system. We place M_B ohmic baths at some random index i (coupling operator $v = |i\rangle\langle i|$). We choose half of the baths with positive, the other half with negative temperature (for odd M_B we randomly decide). The dashed line in (a) is the predicted upper bound $2M_B - 1$. (c) mean number M_S of selected states in this model (here only 50 realizations are used) but as a function of system size M . We choose $M_B = M/2$, i.e. we are in the regime of so many baths that the number M_S is saturated.

Now if $M_S = 1$ or $M_S = 3$ then the four vectors in Equation (4.51) will be linearly dependent, thus the c_i can be positive as they should. However, if M_S was greater than three, then generally the four vectors will be linearly independent, so that $c_i = 0$ must hold, in contradiction to the assumption $c_i > 0$.

Therefore we have shown that for two ohmic baths with product coupling to the system, the number of Bose-selected states is restricted to a maximum of three.

There is a straight-forward generalization of this simple algebraic argument to the case where M_B ohmic baths are coupled to an autonomous system via coupling operators of the product form, Eq. (4.48). In this case, we find an analog to Eq. (4.51), but with a linear combination of $2M_B$ vectors. By similar reasoning the number of selected states is then restricted to $M_S \leq 2M_B - 1$.

We expect that there is a generalization of the above argument also to non-ohmic systems described by arbitrary spectral densities. We have checked functions of the form (remember that J must be odd)

$$J(\varepsilon) \propto |\varepsilon|^d \text{sgn}(\varepsilon) \quad (4.54)$$

with some power d (not necessarily integer) and similarly observe $M_S \leq 2M_B - 1$.

Fig. 4.8(a) confirms the result for ohmic spectral densities $J(\varepsilon) \propto \varepsilon$. It shows the maximum number M_S of selected states for 200 systems that are randomly drawn from the Gaussian orthogonal ensemble, $\text{GOE}(M)$, the ensemble of orthogonal $M \times M$ matrices, where the probability to find a matrix H is given by $p(H) \propto \exp(-\frac{M}{4} \text{tr}(H^2))$. In random matrix theory these Hamiltonians serve as a model for a fully chaotic system with time-reversal symmetry. We choose random Hamiltonians to make sure that the number of Bose-selected states is not additionally restricted by the system dynamics. We couple these systems to M_B ohmic baths, where we randomly choose an index $i \in \{1, \dots, M\}$ to which the bath is coupled with operator $v = |i\rangle\langle i|$. For half of the baths we choose positive temperature, for

the other half negative temperature (the selected states are only determined by the rate asymmetry matrix A and thus independent of the absolute values of these temperatures).

In Fig. 4.8(a) we plot the maximum number of selected states found for an ensemble of 200 realizations of this model. For sufficiently small M_B it equals the predicted upper bound for M_S . However, we observe that for larger values of M_B , the observed maximum number of selected states saturates very quickly at values that are of the order of \sqrt{M} where M is the system size. This bounds the mean number of selected states as shown in Fig. 4.8(b).

We would like to stress that the behavior of the autonomous GOE is very different from that of the time-periodically driven rotor, although both systems exhibit chaotic single particle dynamics. First, in the limit of large system size, $M \rightarrow \infty$, the number of selected states can be intensive, as long as the number of baths M_B is not scaled with system size, so that we may find fragmented condensation in the thermodynamic limit. However, even if we scale M_B with system size, as shown in Fig. 4.8(c) for $M_B = M/2$, the mean number of selected states seems to scale strongly sublinear with at maximum $\langle M_S \rangle \propto \sqrt{M}$, rather than the drastically different extensive $\langle M_S \rangle \propto M$ scaling that is observed for time-periodically driven systems, cf. Sec. 4.3.

5. High-temperature nonequilibrium Bose condensation induced by a hot needle

We investigate theoretically a one-dimensional ideal Bose gas that is driven into a steady state far from equilibrium via the coupling to two heat baths: a global bath of temperature T and a “hot needle”, a bath of temperature $T_h \gg T$ with localized coupling to the system. Remarkably, this system features a crossover to finite-size Bose condensation at temperatures T that are orders of magnitude larger than the equilibrium condensation temperature. This counterintuitive effect is explained by a suppression of long-wavelength excitations resulting from the competition between both baths. Moreover, for sufficiently large needle temperatures ground-state condensation is superseded by condensation into an excited state, which is favored by its weaker coupling to the hot needle. Our results suggest a general strategy for the preparation of quantum degenerate nonequilibrium steady states with unconventional properties and at large temperatures.

This chapter has been published in Ref. [156]. Most of this chapter is directly adapted from the publication, only a few additions have been made. The results on the “Floquet needle” in Sec. 5.8, however, are yet unpublished.

5.1. System and model

In this chapter we investigate the nonequilibrium steady state of a quantum gas in contact with two heat baths of different temperature. In particular, we consider a one-dimensional (1D) ideal Bose gas that is coupled globally to an environment of temperature T and driven into a steady state far from equilibrium via the additional coupling to a “hot needle”, a local bath of temperature $T_h \gg T$, as sketched in Fig. 5.2(a). We find the surprising effect that a crossover to Bose condensation can occur when both temperatures T and T_h are orders of magnitude larger than the temperature where (finite-size) condensation occurs in equilibrium. We explain this behavior by a suppression of long-wavelength excitations resulting from the competition between both baths. Moreover, we observe that for sufficiently large needle temperatures Bose condensation occurs in an excited state of the system, which provides a better decoupling from the hot needle. This intriguing phenomenon bears resemblance to the quantum Zeno effect.

Let us consider a one-dimensional system of N noninteracting bosons that tunnel between adjacent

5. High-temperature nonequilibrium Bose condensation induced by a hot needle

sites of a tight-binding chain of length M . The Hamiltonian reads

$$H = -J \sum_{i=1}^{M-1} (a_{i+1}^\dagger a_i + a_i^\dagger a_{i+1}) = \sum_k \varepsilon_k n_k. \quad (5.1)$$

Here J is the tunneling parameter and a_i the bosonic annihilation operator at lattice site i . The dimensionless wave numbers $k = \pi\nu/(M+1)$ with $\nu = 1, \dots, M$ characterize the single-particle energy eigenmodes with energy $\varepsilon_k = -2J \cos(k)$, wave function $\langle i|k \rangle = \sqrt{2/(M+1)} \sin(ki)$ (describing a superposition of states with quasimomenta k and $-k$), and number operator $n_k = c_k^\dagger c_k$ with $c_k = \sum_i \langle k|i \rangle a_i$. The eigenstates of the Hamiltonian are Fock states $|\mathbf{n}\rangle$ labeled by the vector \mathbf{n} of occupation numbers n_k .

A heat bath b is modeled as a collection of harmonic oscillators in thermal equilibrium with temperature T_b that couple to a single-particle system operator $v^{(b)} \equiv \sum_{qk} v_{qk}^{(b)} c_q^\dagger c_k$. In the limit of weak system–bath coupling (small compared to $\min_{k \neq q} \{|\Delta_{qk}|\} \approx 1.5J/M^2$, with $\Delta_{qk} \equiv \varepsilon_q - \varepsilon_k$), the bath induces quantum jumps between the energy eigenstates $|\mathbf{n}\rangle$ of the system, Eq. (2.93), where a boson is transferred from mode k to mode q with rate $(n_q + 1)n_k R_{qk}^{(b)}$. Here the dependence on the occupation n_q reflects the bosonic quantum statistics. The single-particle rate $R_{qk}^{(b)}$ is obtained within the rotating-wave Born-Markov approximation and is given by the golden-rule-type expression in Eq. (2.75) [108]. We choose ohmic baths with spectral density $J_b(\varepsilon) = \varepsilon$ (though the precise form of the spectral density should not be essential). Setting $\hbar = k_B = 1$ from now on, the rates take the form

$$R_{qk}^{(b)} = \gamma_b^2 f_{qk}^{(b)} \frac{\Delta_{qk}}{e^{\Delta_{qk}/T_b} - 1} \quad (5.2)$$

with the coupling strength γ_b (in which we absorb the factor $\sqrt{2\pi}$) and factor $f_{qk}^{(b)} = |v_{qk}^{(b)}|^2$. We also define the rate asymmetry

$$A_{qk}^{(b)} = R_{qk}^{(b)} - R_{kq}^{(b)} = -f_{qk}^{(b)} \gamma_b^2 \Delta_{qk}. \quad (5.3)$$

We will consider two baths, $R_{qk} = R_{qk}^{(g)} + R_{qk}^{(h)}$, a global bath g of temperature T and coupling strength γ as well as a hot local bath h at site ℓ (the hot needle) of temperature T_h and coupling strength γ_h , cf. Fig. 5.2(a). The hot needle couples to the operator $v^{(h)} = a_\ell^\dagger a_\ell$ so that $f_{qk}^{(h)} = 4 \sin^2(\ell q) \sin^2(\ell k)$, whereas the global bath is modeled by a collection of local baths of temperature $T_g = T$, each coupling to the occupation $a_i^\dagger a_i$ of one site with strength γ/\sqrt{M} , so that $R_{qk}^{(g)} = \sum_i R_{qk}^{(g_i)}$ gives $f_{qk}^{(g)} = \sum_i 4 \sin^2(iq) \sin^2(ik)/M \simeq 1$.

In order to treat large systems and as a starting point for analytical approximations, we employ the meanfield approximation $\langle n_q n_k \rangle \approx \langle n_q \rangle \langle n_k \rangle$. It gives rise to a closed set of nonlinear kinetic equations for the mean occupations $\langle n_k \rangle$ from which we obtain the steady state,

$$\partial_t \langle n_k \rangle = \sum_q [A_{kq} \langle n_q \rangle \langle n_k \rangle + R_{kq} \langle n_q \rangle - R_{qk} \langle n_k \rangle] = 0. \quad (5.4)$$

In Section 5.6 we compare mean field with exact Monte-Carlo results for $M = 50$ and find excellent agreement (see also Ref. [83] for a detailed description of both methods). Note that for a fixed ratio γ_h/γ , the steady state does not depend on γ . After having defined the system, we are now in the position to compute the steady-state mean occupations $\langle n_k \rangle$ from Eq. (5.4).

5.2. Finite-size equilibrium condensation

Let us first recapitulate the equilibrium case, where the system is coupled to a single bath of temperature T only, as sketched in Fig. 5.1(a). Here, i.e. for $\gamma_h = 0$ in the kinetic Equation (5.4), one recovers the familiar grand-canonical mean occupations

$$\langle n_k \rangle = \frac{1}{e^{(\varepsilon_k - \mu)/T} - 1}, \quad (5.5)$$

which are independent of all properties of the bath but its temperature T . Here the chemical potential μ has to be adjusted so that $\sum_k \langle n_k \rangle = N$ and k runs over the discrete wave numbers $k = \pi\nu/(M + 1)$ with $\nu = 1, 2, 3, \dots$

In the thermodynamic limit, $M \rightarrow \infty$ at constant density $n = N/M$, thermal fluctuations prevent the formation of a Bose condensate in a one-dimensional system at finite temperature. However, for a finite system size M , a crossover into a Bose condensed regime with a relative occupation of order one in the ground state $k_c = \pi/(M + 1)$ occurs when T reaches the condensation temperature T_c^{eq} . This is illustrated in Fig. 5.1(b) where we plot this relative ground-state occupation $\langle n_{k_c} \rangle/N$ (which may also be referred to as the condensate fraction) of the tight binding chain with density $n = 3$ particles per site as a function of system size M . We observe that in this one-dimensional system at a given finite system size M there is indeed a temperature T_c^{eq} below which almost all particles occupy the ground state. Nonetheless, at fixed density this temperature scales like $T_c^{\text{eq}} \propto 1/M$ and therefore there will be no condensation in the thermodynamic limit.

We define this condensation temperature T_c^{eq} as the temperature at which half of the particles occupy the single-particle ground state. In the following, we find an analytic approximation to this temperature that gives rise to the dotted line in Fig. 5.1(b): When (finite-size) Bose condensation sets in, μ approaches ε_{k_0} from below, so that the occupations of the low-energy modes with $k \ll 1$ can be approximated by

$$\langle n_k \rangle \simeq \frac{T}{\varepsilon_k - \mu} \simeq \frac{T}{Jk^2 - 2J - \mu}, \quad (5.6)$$

where we have used $\varepsilon_k = -2J \cos(k) \simeq -2J + Jk^2$. Using this expression, the chemical potential can be expressed in terms of the occupation $N_c = \langle n_{k_c} \rangle$ of the ground state,

$$\mu = -2J + Jk_c^2 - T/N_c. \quad (5.7)$$

For low temperatures, the number N' of particles occupying excited states, with $k = \pi\nu/(M + 1) \simeq$

5. High-temperature nonequilibrium Bose condensation induced by a hot needle

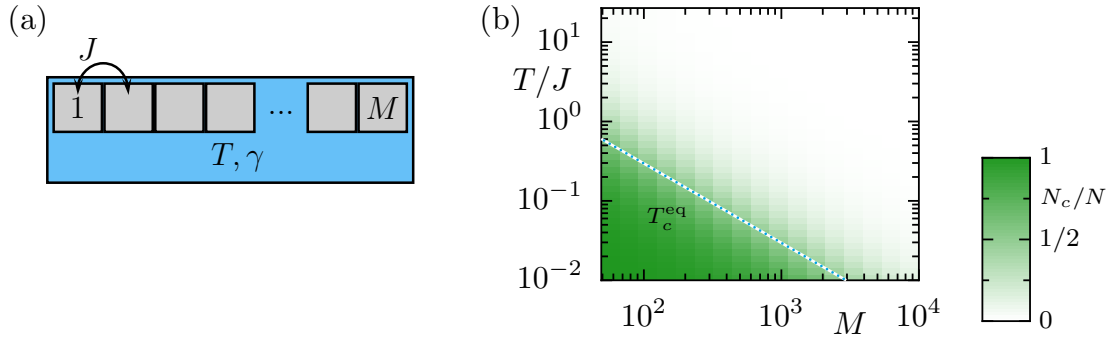


Figure 5.1.: (a) Sketch of the equilibrium situation: A finite tight-binding chain with M sites and tunneling constant J is coupled with strength γ to a heat bath of temperature T . (b) Condensate fraction N_c/N at temperature T (green shading) as function of system size M . The blue-white dotted line gives the analytical estimate for the condensation temperature, where half of the particles occupy the single-particle ground state.

$\pi\nu/M$, is dominated by the long-wavelength modes $k \ll 1$. Therefore we may approximate

$$N' = \sum_{k' \neq k_0} \langle n_k \rangle \simeq \sum_{\nu=2}^{\infty} \frac{1}{\frac{J\pi^2}{TM^2}(\nu^2 - 1) + \frac{1}{N_c}}. \quad (5.8)$$

For a finite system, we define the characteristic temperature T_c^{eq} , where Bose condensation sets in, as the temperature for which half of the particles occupy the single-particle ground state, $N' = N_c = N/2$. Thus, at this temperature we find

$$\frac{N}{2} = \frac{T_c^{\text{eq}} M^2}{J\pi^2} \sum_{\nu=2}^{\infty} \frac{1}{(\nu^2 - 1) + \frac{2T_c^{\text{eq}} M^2}{N J \pi^2}}. \quad (5.9)$$

Consequently, the condensation temperature is approximately given by

$$T_c^{\text{eq}} \simeq \frac{a\pi^2 nJ}{2M} \approx 8.3 \frac{nJ}{M}, \quad (5.10)$$

where $a \approx 1.68$ solves $1 = a \sum_{\nu=2}^{\infty} 1/(\nu^2 + a - 1)$. We plot this as the dotted line in Fig. 5.1(b). The inverse dependence of T_c^{eq} on the system size M reflects the well-known result that in one spatial dimension, in the thermodynamic limit Bose-Einstein condensation is suppressed by thermal long-wavelength fluctuations.

5.3. High-temperature nonequilibrium condensation

Turning to the nonequilibrium situation with both the global bath and the hot needle present, we have to compute the steady state by solving Eq. (5.4) numerically. Figure 5.2(b) shows the condensate fraction N_c/N , with occupation N_c of the most populated mode k_c , versus both temperatures T and T_h for a system of $M = 500$ sites with $n = 3$, $\ell = 5$, and $\gamma_h/\gamma = 0.5$. For low needle temperatures, $T_h \lesssim T$, we find a crossover into a Bose-condensed regime, roughly when the global temperature T falls below

the equilibrium value T_c^{eq} (blue-white dotted line). However, when the needle temperature is *increased* further, a surprising effect occurs: The global temperature at which condensation occurs *increases* by almost two orders of magnitude until it reaches a saturation value. Thus, for an environment well above the equilibrium condensation temperature T_c^{eq} , coupling the system to a second, even hotter local bath (the hot needle) can induce Bose condensation. When the needle temperature is increased even further, we can observe another intriguing effect: the condensate is suddenly formed in an excited state, $k_c \approx \pi/\ell$, as indicated by the color code. Only for very large needle temperatures, condensation eventually breaks down completely.

In Fig. 5.2(c) the condensate fraction is plotted versus global temperature T and system size M . One sees that up to large system sizes of about 10^3 sites, condensation occurs at a large condensation temperature T_c^{ne} that is practically independent of the system size. This behavior is reminiscent of the physics of Bose condensation in a three-dimensional (3D) system. Only at even larger system sizes, the condensation temperature decreases with M resembling the equilibrium behavior in one dimension. In the limit of small M ($\lesssim 100$), again excited-state condensation in the mode $k_c \approx \pi/\ell$ is found.

In order to obtain a better understanding of the intriguing behavior observed in Figs. 5.2(b) and (c), let us have a look at the full momentum distribution $\langle n_k \rangle$. It is plotted in Fig. 5.3(a) for the parameters indicated by the black dot in Fig. 5.2(b). The occupation of the condensate formed in the ground state is indicated by a red cross and the occupation of all other modes by a red line. We find an unconventional nonmonotonous behavior of $\langle n_k \rangle$ with equidistant peaks or dips. They are located around those wave numbers $\kappa_\alpha = \pi\alpha/\ell$ with $\alpha = 0, 1, \dots, \ell$ that decouple from the hot needle, $f_{q\kappa_\alpha}^{(h)} = f_{\kappa_\alpha q}^{(h)} = 0$. For momenta $k \approx \kappa_\alpha$ the distribution $\langle n_k \rangle$ approximately follows a thermal distribution with temperature T (dashed gray line). Between the momenta κ_α , the distribution roughly follows the thermal distribution associated with the hot temperature T_h of the needle (dashed black line), which

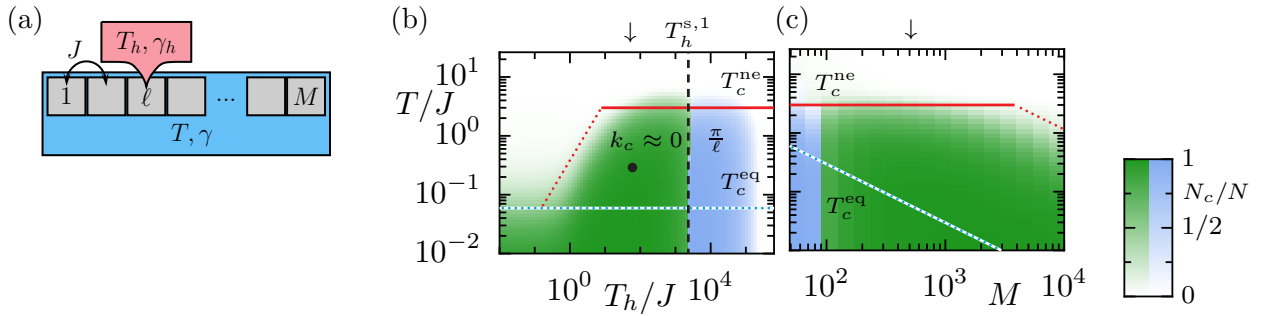


Figure 5.2.: (a) Tight-binding chain with $N = nM$ bosons on M sites and tunneling parameter J , coupled with strengths γ and γ_h to a global bath of temperature T and to a “hot needle” of temperature T_h at site ℓ , respectively. (b,c) Condensate fraction N_c/N indicated by green (blue) shading for ground-state (excited-state) condensation in the mode $k_c \approx 0$ ($k_c \approx \pi/\ell$) versus T and T_h or M ; for $\ell = 5$, $\gamma_h = 0.5\gamma$, $n = 3$ and (b) $M = 500$ or (c) $T_h = 60J$. Estimated temperature T_c^{ne} for 1D-like (3D-like) Bose condensation plotted as red dotted (solid) lines. Blue-white dotted lines give equilibrium condensation temperature T_c^{eq} (for $\gamma_h = 0$). Black dashed line gives estimated needle temperature $T_h^{s,1}$, where excited-state condensation sets in. Black arrows indicate the parameters where (b) and (c) coincide.

5. High-temperature nonequilibrium Bose condensation induced by a hot needle

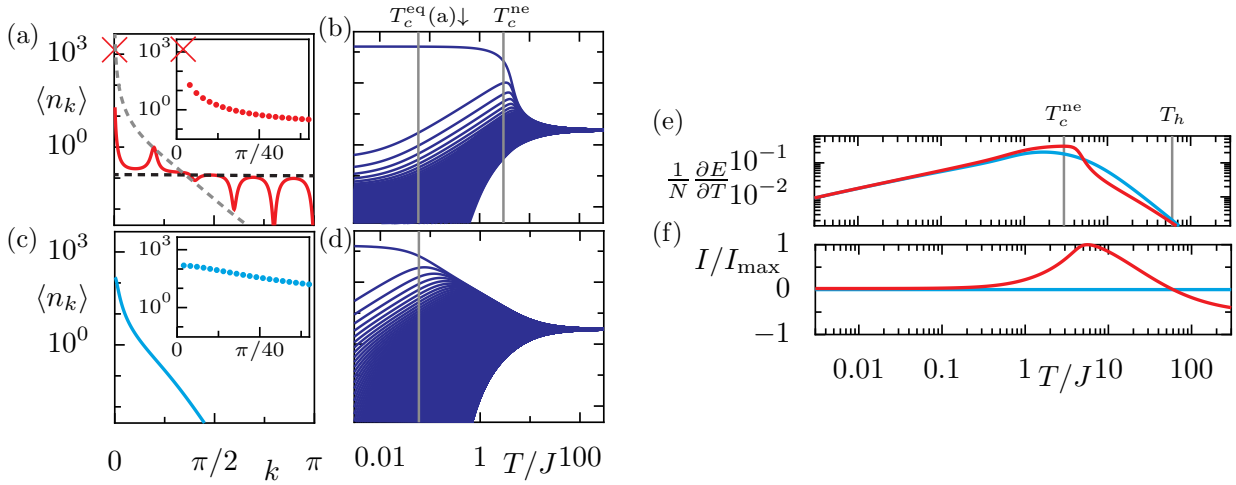


Figure 5.3.: (a,b) Mean occupations $\langle n_k \rangle$ for the parameters of Fig. 5.2 with $T_h = 60J$ and $M = 500$, (a) versus k [for $T = 0.29J$, black dot in Fig. 5.2(b)] and (b) versus T . In (a) the crosses indicate the condensate occupation, the gray (black) dashed line in the main panel shows thermal distributions for the temperature T (T_h); the inset shows $\langle n_k \rangle$ for small k . (c,d) Like (a,b), but for the equilibrium situation with $\gamma_h/\gamma = 0$. Occupations obey the Bose-Einstein distribution. (e) Specific heat per particle in equilibrium [blue line] versus the analogous quantity in the nonequilibrium steady state [red line, parameters like in (b)]. (f) Heat current I from the needle through the system into the global bath versus T for the nonequilibrium steady state [red line, parameters like in (b)], the blue line shows the trivial equilibrium value $I = 0$.

is rather flat. This behavior can be explained by noting that for high bath temperatures, $T_b \gg |\Delta_{qk}|$, (or equally for small energy differences) the rates (5.2) become proportional to the bath temperature,

$$R_{qk}^{(b)} = \gamma_b^2 f_{qk}^{(b)} \frac{\Delta_{qk}}{e^{\Delta_{qk}/T_b} - 1} \xrightarrow{T_b \gg |\Delta_{qk}|} f_{qk}^{(b)} \gamma_b^2 T_b, \quad (5.11)$$

so that the occupations $\langle n_k \rangle$ are dominated by the hot bath with $T_h \gg T$, except for momenta near κ_α that almost decouple from the needle.

This discussion gives us already an idea of the mechanism behind the high-temperature condensation induced by the needle. Due to the fact that we place the needle relatively close to the boundary of the system $\ell \ll M$, the ground state, which vanishes at the boundaries, and many of the long-wave modes, have a small coupling to the needle only. Therefore, the width of the peak of $\langle n_k \rangle$ around $k = 0$ is now determined by the competition between the global bath and the hot needle. An estimate w for the peak width can be obtained from requiring that within the width of the peak, the rates induced by the hot needle are suppressed, i.e.

$$\frac{R_{qk}^{(h)}}{R_{qk}^{(g)}} \approx \frac{\gamma_h^2 T_h f_{qk}^{(h)}}{\gamma^2 T} \lesssim 1 \quad (5.12)$$

for $k < w$ and all q . Using $f_{qk}^{(h)} \lesssim \ell^2 k^2$ for small k , this yields

$$w = \frac{\gamma}{\ell \gamma_h} \sqrt{\frac{T}{T_h}}. \quad (5.13)$$

This width can be small compared to the width of the thermal distribution at temperature T , see Fig. 5.3(c). Indeed, in Section 5.4.1 we derive an analytical estimate, Eq. (5.21), for the occupations for small k and recover this width w . In this way, long-wavelength excitations, which destroy Bose condensation in one-dimensional equilibrium systems for temperatures above T_c^{eq} , are reduced. The effect of Bose condensation and the dramatic increase of the condensation temperature T_c induced by the hot needle can clearly be observed in Figs. 5.3(b) and (d), showing the T -dependence of the occupations $\langle n_k \rangle$ for a system with and without coupling to the needle, respectively.

To summarize the discussion, the effect of high-temperature condensation relies on the presence of highly nonthermal occupation statistics that are present in the nonequilibrium steady state. These nonthermal occupations may roughly be divided into two groups: Those modes k that have a large amplitude at the needle site ℓ thermalize with the needle temperature T_h , therefore their distribution is rather flat. Then there are modes, as the ground mode, that have a node close to the coupling site, so they decouple from the needle and thermalize with environmental temperature T . Occupations of the long-wave modes are suppressed due to the interplay of the hot and the cold bath, which leads to a pole that can be much narrower than in equilibrium at temperature T . Thus, to find condensation in the nonequilibrium steady state two conditions have to hold: First, this pole has to be narrow enough to suppress long-wave excitations at given system size M , which is true at environmental temperatures $T \lesssim T_c^{\text{ne1}}$, the dotted red lines in Fig. 5.2(b) and (c). This is discussed in detail in Section 5.4.1. Second, also the occupations of the “flat” distribution of the modes that thermalize with T_h must be small enough, which is true at environmental temperatures $T \lesssim T_c^{\text{ne2}}$, the solid red lines in Fig. 5.2(b) and (c). A detailed consideration of this can be found in Section 5.4.2. For condensation to occur, the temperature T must lie below both of these temperatures which allows us to define the nonequilibrium condensation temperature as $T_c^{\text{ne}} = \min(T_c^{\text{ne1}}, T_c^{\text{ne2}})$.

Figure 5.4(d) shows how the occupations depend on the needle temperature T_h for a system with $\gamma_h/\gamma = 1$, $M = 500$, $\ell = 7$, and $T = 2J$. Since the global temperature T lies well above the equilibrium condensation temperature $T_c^{\text{eq}} \approx 0.05J$, no Bose condensate is found at $T_h = T$, where the system is in equilibrium. However, when T_h is increased, soon ground-state Bose condensation sets in. When the needle temperature is increased further, remarkably a Bose condensate in the excited mode $k \approx \pi/\ell$ supersedes the ground-state condensate at a switch temperature $T_h^{\text{s},1}$. The condensate mode switches once more to $k \approx 2\pi/\ell$ at $T_h^{\text{s},2}$, before eventually at very large needle temperatures $T_h \gtrsim 10^4 J$ condensation breaks down again. The panels (a), (b), and (c) depict the momentum distribution for the three different needle temperatures marked in (d) and clearly show condensation in three different modes. Details on how we obtain an estimate for the switch temperature $T_h^{\text{s},\alpha}$, the dashed lines in Fig. 5.2 and Fig. 5.4, are presented in Section 5.5.

An intuitive interpretation of the high-temperature and excited-state Bose condensation observed

5. High-temperature nonequilibrium Bose condensation induced by a hot needle

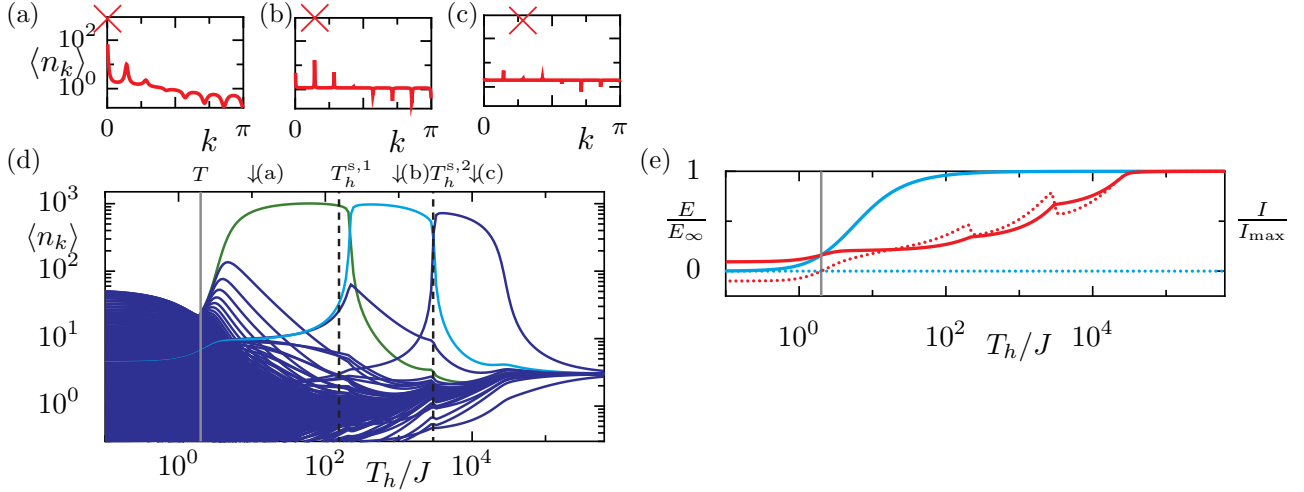


Figure 5.4.: Mode occupations (d) versus needle temperature T_h for $T = 2J$, $\ell = 7$, $M = 500$, $n = 3$, and $\gamma_h/\gamma = 1$. With increasing T_h the system passes from a state without Bose condensate through a sequence of states with a condensate in the states $k_0 \approx 0$ (green line), $k_1 \approx \pi/\ell$ (light blue line), and $k_2 \approx 2\pi/\ell$ (violet line), before condensation breaks eventually down again. (a-c) Momentum distribution for states with condensates in three different modes. (e) Total inner energy (solid lines) and heat current (dotted lines) for the parameters of (d) (red) compared to equilibrium at temperature T_h (blue).

here is that the nonequilibrium condensation can also be viewed as a mechanism that suppresses the heat influx I_h from the hot bath, with

$$I_b = \sum_{qk} \Delta_{qk} R_{qk}^{(b)} (\langle n_q \rangle + 1) \langle n_k \rangle. \quad (5.14)$$

Namely, keeping the distribution $\langle n_k \rangle$ fixed, I_h would increase linearly with T_h (according to Eq. (5.2)), while it still has to be balanced by the outflux I_g into the colder global bath (since $I_h = -I_g$ for a steady state). This increase is prevented by forming of a condensate in a mode that almost decouples from the hot needle. This interpretation is supported by Fig. 5.3(f) showing that the heat current $I = I_h = -I_g$ through the system plotted versus T shows a maximum near the condensation temperature and, thus, a negative differential heat conductivity, $\partial I/\partial(T_h - T) < 0$, in the condensed regime. This counterintuitive effect is explained by noting that the number of particles contributing to the heat transport is reduced by condensing into the ground state k_0 , which hardly couples to the hot needle. The onset, first of ground-state condensation and later also of excited-state condensation observed when the needle temperature T_h is increased as we observe in Fig. 5.4(d), can therefore be understood as a strategy of the system to minimize its coupling to the hot needle, and with that the current I , further and further. This can be observed in the drops in the dotted line in Fig. 5.4(e). Namely, typically the allowed wave numbers $k = \nu\pi/(M + 1)$ that comply with the boundary conditions, do not assume those values κ_α that would perfectly decouple from the hot needle. We denote by k_α the allowed wavenumber that minimizes the distance $\delta_\alpha = |k - \kappa_\alpha|$, which quantifies the coupling, $f_{qk_\alpha}^{(h)} \simeq 4 \sin^2(\ell q) \ell^2 \delta_\alpha^2$. With increasing T_h we generally find a sequence of condensate modes $k_0, k_{\alpha_1}, k_{\alpha_2} \dots$, where α_{j+1} is the

smallest value of α with $\alpha > \alpha_j$ and $\delta_\alpha < \delta_{\alpha_j}$. The sequence ends, when the coupling cannot be lowered anymore by a larger α . Since one has $\delta_0 = k_0$ for the ground state k_0 and fluctuating values $\delta_\alpha \leq \delta_0/2$ (depending on M and ℓ) for $\alpha \geq 1$, one always finds at least one switch of the condensate mode and $\alpha_1 = 1$. While for the parameters of Fig. 5.2(b) the sequence ends already with k_1 , it ends with k_2 for the parameters of Fig. 5.4 (for $\ell = 21$ and $M = 200$, we observe the sequence $\alpha = 0, 1, 2, 7$, not shown).

Note that these intriguing effects do not rely on the discrete nature of the tight-binding chain considered here and, therefore, occur equally in a continuous system, as we discuss in Section 5.7.

5.4. Estimating the condensation temperature

Based on our qualitative discussion, we can estimate the nonequilibrium condensation temperature T_c^{ne} . In the hot-needle setup a Bose condensate in the ground state $k_0 = \pi/(M+1)$ can be destroyed either by a large occupation of long-wavelength modes or by large occupations of excited states at all energies. While the former case resembles condensation in a one-dimensional system in equilibrium and leads to a system-size dependent condensation temperature T_c^{ne1} , the latter case bears similarity to equilibrium condensation in three dimensions and happens at a condensation temperature T_c^{ne2} , which is independent of the system size. In this section, we give an estimate to both temperatures. The generalization to excited-state condensation is straightforward and not presented here.

5.4.1. Condensation destroyed by long-wavelength modes

Deep in the condensate regime, where a large fraction N_c/N of the particles occupy the ground-state mode $k_0 = \pi/(M+1)$, the occupation of excited modes $k \ll 1$ in the vicinity of k_0 is approximately given by a second order pole. We obtain this as follows: We assume that all particles occupy long-wavelengths modes $k \ll 1$ (which is a valid approximation for $T \ll T_c^{\text{ne2}}$, see next section) and neglect the coupling of the hot bath to the condensate mode k_0 , but not to other long-wavelength modes. The condensation temperature T_c^{ne1} , defined by the point where $N_c = N/2$, is then estimated. To arrive at an analytical estimate for T_c^{ne1} , there are a number of approximations needed. For the sake of clarity, we list all these approximations in Table 5.1.

For our analysis, we start with the meanfield equation for the steady state, Eq. (5.4), where we split

	Limit of	where
Approx. 1	large system size	$M \gg 1/w$
Approx. 2	global temperature below 3D transition	$T \ll T_c^{\text{ne2}}$
Approx. 3	high needle temperature	$T, J \ll T_h$
we consider	long-wave modes (consequence of Approx. 2)	$k \ll 1$

Table 5.1.: Approximations that are used to derive T_c^{ne1} .

5. High-temperature nonequilibrium Bose condensation induced by a hot needle

the ground state k_0 from some of the sums

$$0 = [A_{kk_0}\langle n_k \rangle \langle n_{k_0} \rangle + R_{kk_0}\langle n_{k_0} \rangle] + \sum_{q \neq k_0} [A_{kq}\langle n_q \rangle \langle n_k \rangle + R_{kq}\langle n_q \rangle] - \sum_q R_{qk}\langle n_k \rangle. \quad (5.15)$$

Let us suppose that the system is in the condensed regime, where a large fraction N_c/N of the particles occupy the ground-state mode and the modes at large quasimomenta are approximately unoccupied (which requires Approx. 2, $T \ll T_c^{\text{ne}2}$, see next section). The mean occupations $\langle n_k \rangle$ of the long-wavelength modes k with $k_0 < k \ll 1$ in the vicinity of k_0 are then obtained from

$$0 \approx A_{kk_0}^{(g)}\langle n_k \rangle N_c + R_{kk_0}^{(g)}N_c + \sum_{q \neq k_0} A_{kq}\langle n_k \rangle \langle n_q \rangle + \sum_{q \neq k_0} R_{kq}\langle n_q \rangle - \sum_q R_{qk}\langle n_k \rangle, \quad (5.16)$$

which was derived from Eq. (5.15) by neglecting the weak residual coupling of the ground-state mode to the hot needle, $R_{kk_0}^{(h)} \approx 0 \approx A_{kk_0}^{(h)}$. One may neglect those contributions as a consequence of the small- $|\Delta_{kq}|/T$ expression, Eq. (5.11), and Approx. 1 and 3, since using these we have

$$R_{kk_0}^{(h)} \ll R_{kk_0}^{(g)} \stackrel{\text{Approx. 3}}{\Leftrightarrow} \gamma^2 T_h f_{kk_0}^{(h)} \ll \gamma^2 T \quad \Leftrightarrow \quad \gamma_h^2 T_h \sin(k_0 \ell)^2 \ll \gamma^2 T \quad \Leftrightarrow \quad \frac{1}{w} \ll M \quad (5.17)$$

and similar considerations lead to $A_{kk_0}^{(h)} \ll A_{kk_0}^{(g)}$.

We can now use the assumption of a large needle temperature $T_h \gg T$, Approx. 3. Employing the scaling $\langle n_k \rangle \propto T/T_h$ (which will be shown to be self-consistent below), we find on leading order

$$0 = R_{kk_0}^{(g)}N_c + \sum_{q \neq k_0} R_{kq}^{(h)}\langle n_q \rangle - \sum_q R_{qk}^{(h)}\langle n_k \rangle + \mathcal{O}(T/T_h), \quad (5.18)$$

where we assumed the temperature-dependent scaling $R_{kq}^{(b)} \propto T_b$ and $A_{kq}^{(b)} \propto \text{const.}$ from Eqs. (5.11) and (5.3). The rates $R_{kq}^{(h)}$ scale like k^2 for small k . So for k going to zero, we may omit the second term, but not the third one since $\langle n_k \rangle$ is peaked around zero, which will keep the third term finite. This yields

$$0 \approx R_{kk_0}^{(g)}N_c - \sum_q R_{qk}^{(h)}\langle n_k \rangle \stackrel{\text{Approx. 3}}{\approx} \gamma^2 T N_c - 2\gamma_h^2 \ell^2 k^2 M T_h \langle n_k \rangle. \quad (5.19)$$

For the second approximation we used the small- $|\Delta_{kq}|/T$ expression, Eq. (5.11), for the rates $R_{kk_0}^{(g)}$ and

$$\sum_q R_{qk}^{(h)} \stackrel{\text{Approx. 3}}{\approx} 4\gamma_h^2 T_h \sin(\ell k)^2 \sum_q \sin^2(\ell q) \stackrel{k \ll 1}{\approx} 2\gamma_h^2 T_h \ell^2 k^2 M. \quad (5.20)$$

Thus, for large T_h we have

$$\langle n_k \rangle = \frac{N_c \gamma^2 T}{2M \gamma_h^2 \ell^2 T_h k^2} = \frac{N_c}{2M} \frac{w^2}{k^2}, \quad (5.21)$$

with the pole width w as defined in Eq. (5.13). We have tested this prediction against numerical calculations of the distribution $\langle n_k \rangle$ in the non-equilibrium steady state and see generally a good agreement. The occupations scale like T/T_h as required by self consistence. Even though expression (5.21) is derived for modes k with $k_0 < k \ll 1$, we can use it for all $k \neq k_0$ since it vanishes rapidly with increasing k . With that, the condensate depletion due to the long wave modes $N' = \sum_{k \neq k_0} \langle n_k \rangle$ is approximately given by

$$N' \approx N_c w^2 \frac{M}{2\pi^2} \sum_{\nu=2}^{\infty} \frac{1}{\nu^2} = N_c w^2 \frac{M}{2\pi^2} \left(\frac{\pi^2}{6} - 1 \right). \quad (5.22)$$

Using the definition that at the condensation temperature $N_c = N' = N/2$, we can estimate

$$T_c^{\text{ne1}} \approx 30.6 \frac{\ell^2 \gamma_h^2 T_h}{\gamma^2} \frac{1}{M}. \quad (5.23)$$

This estimate is plotted as red dotted line in Figs. 5.2(b) and (c) and agrees well with the observed behavior. Like in equilibrium in one dimension, also the nonequilibrium condensation relies on the infrared cutoff given by the inverse system size.

5.4.2. Condensation destroyed by modes with large quasimomentum

In contrast to equilibrium, in the nonequilibrium steady state Bose condensation can also be destroyed by increasing the occupation of modes with large momenta q , which couple to the condensate via the rates induced by the global bath. This effect can be estimated by considering the regime $T \ll T_c^{\text{ne1}}$, where the total occupation of excited long-wavelength modes is suppressed by the finite system size M , so that we can approximate the occupation of excited states by the flat distribution $\langle n_k \rangle \approx N'/M$ induced by the dominant hot-needle bath (dashed black line in Fig. 5.3(a)). Considering the coupling of the so-occupied excited states to the condensate via the global bath, we find the condensation temperature $T_c^{\text{ne2}} \approx nJ$. The fact that it does not depend on the system size, has some similarity to the break-down of Bose condensation in a three-dimensional system in equilibrium, which is not driven by long-wavelength modes either. Again, we list all the approximations that we make to find the expression for T_c^{ne2} in Table 5.2.

Let us suppose that the system is in the condensed regime with a large fraction N_c/N of particles occupying the ground-state mode. But now, we assume that $T \ll T_c^{\text{ne1}}$, Approx. 4, so that the long-wavelength modes are hardly occupied. Furthermore, we assume that the occupations of most of the

	Limit of	where
Approx. 1	large system size	$M \gg 1/w$
Approx. 3	high needle temperature	$T, J \ll T_h$
Approx. 4	global temperature below 1D transition	$T \ll T_c^{\text{ne1}}$
Explicit term is found for	intermediate densities	$n \gtrsim 1$

Table 5.2.: Approximations that are used to derive T_c^{ne2} .

5. High-temperature nonequilibrium Bose condensation induced by a hot needle

excited modes $k \neq k_0$ are close to a flat distribution corresponding to the hot temperature $T_h \gg J$, Approx. 3, so that we can approximate $\langle n_k \rangle \approx N'/M$ for $k \neq k_0$. Plugging this ansatz into the mean-field equation, Eq. (5.4), we find for $k = k_0$

$$0 \approx \frac{N'}{M} N_c \sum_q A_{k_0 q}^{(g)} + \frac{N'}{M} \sum_{q \neq k_0} R_{k_0 q}^{(g)} - N_c \sum_{q \neq k_0} R_{q k_0}^{(g)}. \quad (5.24)$$

Analogous to Eq. (5.16), here we assumed that the ground state k_0 almost from the needle, which is true for sufficiently large systems, Approx. 1. Note that by combining Approx. 1 and 4 we see

$$\frac{1}{w} \stackrel{\text{Approx. 1}}{\ll} M \stackrel{\text{Approx. 4}}{\ll} \frac{1}{w^2}, \quad (5.25)$$

where typically $w \ll 1$ holds because $T_h \gg T$, so the assumptions in this section are only valid in an intermediate system-size regime, which also becomes apparent in Fig. 5.2(c).

In the condensed regime we find $N_c \gg T/J$, and $N_c \gg N'/M$ and therefore the first and the last term in Eq. (5.24) dominate over the second one. Using $\sum_q A_{k_0 q}^{(g)} = \gamma^2 \sum_q \Delta_{q k_0} \approx \gamma^2 2JM$ this leads to

$$0 \approx \gamma^2 N_c \left[2JN' - T s(T) \right], \quad (5.26)$$

where we have defined the sum

$$s(T) = \sum_{q \neq k_0} \frac{\Delta_{q k_0}/T}{e^{\Delta_{q k_0}/T} - 1}. \quad (5.27)$$

So we find the total depletion to be given by

$$N' = \frac{T s(T)}{2J}. \quad (5.28)$$

Solving this equation for $N_c = N' = nM/2$, we may obtain T_c^{ne2} numerically from solving

$$JnM = T_c^{\text{ne2}} s(T_c^{\text{ne2}}). \quad (5.29)$$

However, with the limiting value of

$$s(T_c^{\text{ne2}}) \xrightarrow{T_c^{\text{ne2}} \gg J} M - 1. \quad (5.30)$$

the condensation temperature reads

$$T_c^{\text{ne2}} \approx nJ, \quad (5.31)$$

which is consistent with the assumption $T_c^{\text{ne2}} \gg J$ as long as densities are intermediate $n \gtrsim 1$. For densities that are below this value of unity, T_c^{ne2} needs to be evaluated numerically.

This temperature $T_c^{\text{ne}2} = nJ$ is plotted as red solid line in Fig. 5.2(b) and (c). Also from combining Eq. (5.28) and (5.30) it follows that $N' \approx TM/2J$ and from our assumption of a flat distribution we find the occupations $\langle n_k \rangle \approx N'/M \approx T/2J$ which we plot as the dashed black line in Fig. 5.3(a) which describes the order of magnitude of the flat part of the distribution very well. Note that $T_c^{\text{ne}2}$ does not depend on the system size. This behavior is similar to the break-down of Bose condensation in a three-dimensional system in equilibrium, which is not driven by long-wavelength modes either.

Another reminiscent of the three-dimensional phase transition can be seen in Fig. 5.3(e) where we plot the quantity

$$\frac{1}{N} \left(\frac{\partial E}{\partial T} \right)_{M,N,T_h} \quad \text{with total inner energy } E = \sum_k \langle n_k \rangle \varepsilon_k, \quad (5.32)$$

which is, without the coupling to the needle, the thermodynamic specific heat per particle C_V/N (blue line in Fig. 5.3(e)): As we expect for an ideal one-dimensional Bose gas it scales like $T^{1/2}$ for low temperatures T . For high temperatures T , in the continuous one-dimensional system one recovers the classical value of $1/2$ (remember that we set $k_B = 1$). Nevertheless, here we see that for high temperatures the specific heat decreases again. This is expected for the considered tight binding system with only a single energy band, where the total inner energy E is bounded from above. If we look at the same quantity in presence of the needle (red line in Fig. 5.3(e)), we see that the curve has a cusp in the vicinity of the condensation temperature T_c^{ne} , which is very similar to the famous Lambda-shape of the specific heat with a kink at the critical temperature of the second order phase transition in an ideal three-dimensional Bose gas.

5.5. Temperature for switch to excited-state condensation

Here we estimate the switch temperature $T_h^{\text{s},\alpha}$, above which a condensate in mode k_α forms, which gives rise to the dashed lines in Fig. 5.4(d). We find this temperature by noting that there is a point, below which, i.e. for $T_h < T_h^{\text{s},\alpha}$, a condensate in the k_α cannot be supported, because it would give rise to occupations that are unphysical for some of the other modes. The point $T_h^{\text{s},\alpha}$ above which all occupations are physical, coincides with the point where the switching of the condensate occurs, as long as by this switching of modes, the system can reduce the coupling of the condensate to the needle.

Let us discuss, under which conditions we can expect condensation in an excited state, $k_c = k_\alpha \approx \frac{\alpha\pi}{\ell}$, in the finite system. The mean field equation (5.4) must hold for all k , which we may solve formally

	Limit of	where
Approx. 3	high needle temperature	$T, J \ll T_h$
Approx. 2 & 4	global temperature below 1D and 3D transition	$T \ll T_c^{\text{ne}1}, T_c^{\text{ne}2}$
Approx. 5	intermediate system size	$M \gg \frac{1}{w} \sqrt{\frac{T}{T_h}} = \frac{\gamma \hbar}{\gamma} \ell$

Table 5.3.: Approximations that are used to derive $T_h^{\text{s},\alpha}$.

5. High-temperature nonequilibrium Bose condensation induced by a hot needle

like

$$\langle n_k \rangle = \frac{\sum_q R_{kq} \langle n_q \rangle}{\sum_q (A_{qk} \langle n_q \rangle + R_{qk})}. \quad (5.33)$$

We will use the fact that all occupations must be non-negative, $\langle n_k \rangle \geq 0$, to find the regime where excited state condensation may occur.

Since the numerator of Eq. (5.33) is strictly positive, the denominator has to be positive, too. Deep in the condensed regime, i.e. under Approx. 2 and 4, we may neglect the depletion, $N_c \approx N$, which yields

$$A_{k_c k} N + \sum_q R_{qk} > 0. \quad (5.34)$$

Under Approx. 5 the condensate decouples sufficiently from the hot bath, and the rate imbalance $A_{k_c k}$ is dominated by the global bath and we can approximate $A_{k_c k} \approx A_{k_c k}^{(g)} = \gamma^2 \Delta_{k k_c}$. Note that, since only the rate imbalance $A_{k_c k}^{(h)}$ has to be small when compared to $A_{k_c k}^{(g)}$, this only relies on a weaker approximation of intermediate system size M , Approx. 5, rather than the large the system size limit, Approx. 1, that is needed for $R_{k_c k}^{(h)} \ll R_{k_c k}^{(g)}$.

Additionally $T_h \gg T$, Approx. 3, holds, such that $\sum_q R_{qk} \approx \sum_q R_{qk}^{(h)} \approx \gamma_h^2 T_h 2M \sin(k\ell)^2$. In total, we have to satisfy

$$\gamma^2 \Delta_{k k_c} N + \gamma_h^2 T_h 2M \sin(k\ell)^2 > 0 \quad (5.35)$$

for all k . For ground-state condensation $k_c = k_0 = \pi/(M+1)$ both terms are positive, such that for all parameter values the ground state condensate ansatz does not violate the physical requirement

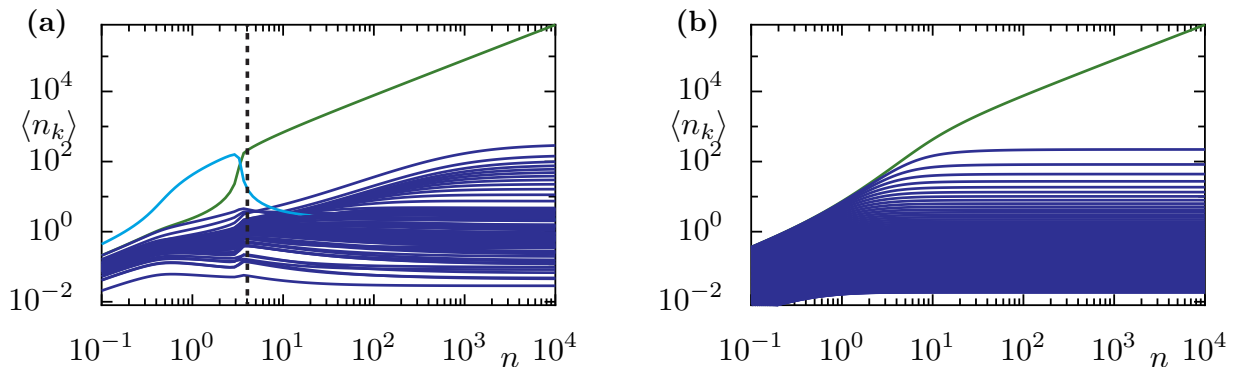


Figure 5.5.: (a) Mean occupations $\langle n_k \rangle$ of the single-particle eigenstates as function of particle density n for system with $M = 80, l = 5, \gamma = 2\gamma_h, T = J, T_h = 80J$. At intermediate densities n there is a condensate in the excited state with $k_c \approx \pi/l$ (light blue), while in the limit of $N \rightarrow \infty$ ground state (green line) condensation is found. The switch is estimated by the dashed line which is found by solving Eq. (5.36) for the density n where this switching occurs, $n^{s,1}$. (b) Occupations in equilibrium, $\gamma_h = 0$, for comparison.

of positive occupations. For $k_\alpha \approx \kappa_\alpha = \frac{\alpha\pi}{\ell}$ with $\alpha \geq 1$ however, the first term is negative for all $k < k_\alpha$ and must be compensated by the second term. Since the second term is minimal at one of the decoupling wavenumbers $k_{\alpha'}$, $\alpha' < \alpha$, it suffices to check for positivity at these wave numbers. From this requirement, we find that for

$$T_h > T_h^{s,\alpha} = \frac{n\gamma^2}{2(\ell\gamma_h)^2} \max_{\alpha' < \alpha} \left(\frac{\Delta_{k_\alpha k_{\alpha'}}}{\delta_{\alpha'}^2} \right) \quad (5.36)$$

condensation in the excited state k_α may occur. We have plotted this temperature as the dashed lines in Fig. 5.2 and Fig. 5.4 and observe a good agreement with the transitions that we find in the numerical data. This is remarkable, since our estimations only predict the temperature where this switching of the condensate mode *could* occur. However, from the numerics we observe that, if the coupling to the needle can be reduced by such a transition, it also *will* occur at this temperature.

The linear dependence of $T_h^{s,\alpha}$ on n indicates that excited-state condensation is suppressed (shifted to $T_h = \infty$) in the limit of high densities, where ground-state condensation is expected for a system coupled to two thermal baths (of positive temperature, cf. the discussion on Bose selection in Sec.) [82, 83]. This can also be observed in Fig. 5.5(a) where we plot the mean occupations as a function of particle density n . Excited state condensation is found at intermediate densities only. We may solve Eq. (5.36) also for the density n where a switching to ground state condensation occurs. This gives rise to the dashed line that nicely predicts the switching in Fig. 5.5(a). The comparison to equilibrium, Fig. 5.5(b), reveals that over a wide range of the density n excitations are strongly suppressed in the nonequilibrium steady state.

While we have presented examples for $\ell \ll M$, with the needle placed near the edge of the sample, and assumed this limit also in our analytical estimates, simulations show that the enhancement of the condensation temperature equally occurs for any needle position. However, placing the needle away from the edge we typically observe excited-state condensation, as it is indicated also by the ℓ^{-2} behavior of the estimated shift temperature $T_h^{s,\alpha}$.

5.6. Quasiexact Monte-Carlo results for a small system

The mean-field approximation $\langle n_q n_k \rangle \approx \langle n_q \rangle \langle n_k \rangle$, which gives rise to the closed set of kinetic equations (5.4) for the mean occupations, allows us to treat large systems of up to $M = 10^4$ lattice sites and to find analytical estimates for the parameters where condensation sets in. In order to justify this approximation, we have also simulated the full many-body rate equation for the probability distribution $p_{\mathbf{n}}$ for finding the system in the eigenstate $|\mathbf{n}\rangle$. It directly follows from writing down the Pauli master equation, Eq. (2.51), in Fock space giving [83]

$$\dot{p}_{\mathbf{n}} = \sum_{kq} (1 + n_q) n_k (R_{kq} p_{\mathbf{n}_{q \leftarrow k}} - R_{qk} p_{\mathbf{n}}), \quad (5.37)$$

5. High-temperature nonequilibrium Bose condensation induced by a hot needle

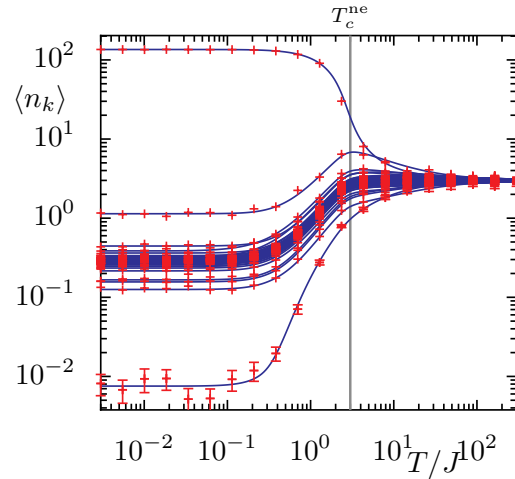


Figure 5.6.: Mean occupations $\langle n_k \rangle$ for a system with $M = 50$, $n = 3$, $l = 3$, $\gamma = \gamma_h$, $T_h = 120J$. Crosses represent the Monte-Carlo results. We show error bars for the least occupied state only, because for the other states they are too small to be visible. The data is well approximated by the solid lines which result from the meanfield approximation.

where $\mathbf{n}_{q \leftarrow k}$ denotes the vector of occupation numbers obtained from \mathbf{n} by transferring a particle from mode k to mode q .

An efficient way of solving this equation is given by quantum-jump Monte-Carlo simulations (see, e.g., [164]). For that purpose we generate a random walk in the classical space of Fock states \mathbf{n} (which is exponentially large with respect to the system size, but much smaller than the Fock space, which contains also the coherent superpositions of the Fock states). Namely, according to the sum and the relative weight of the many-body rates $R_{qk}(n_q + 1)n_k$ leading away from the current state \mathbf{n} , we draw both the time after which a quantum jump happens and the new state $\mathbf{n}_{q \leftarrow k}$, respectively. Expectation values like the mean occupations $\langle n_k \rangle$ are computed by averaging over a random path. This method gives quasixact results, in the sense that the accuracy is controlled by the length of the random path. A detailed description of the method is given in Ref. [83].

In Fig. 5.6 we plot the mean occupations $\langle n_k \rangle$ of a system of $M = 50$ sites and $n = 3$, $l = 3$, $\gamma_h/\gamma = 1$, and $T_h = 120J$. The Monte-Carlo data (red crosses) are reproduced almost perfectly by the mean-field solution (solid lines). Already in this rather small system, we can see a relatively sharp crossover, to a Bose condensed regime at T_c^{ne} .

5.7. Continuous system

In Section 5.3, we treat a one-dimensional system of noninteracting bosons in a tight-binding lattice. However, the effects discussed in Section 5.3 do not depend on the discrete nature of the tight-binding lattice. They occur in a similar form also in a continuous one-dimensional system in a setup that is sketched in Fig. 5.7(a). Here, the system consists of noninteracting bosons trapped in a box potential,

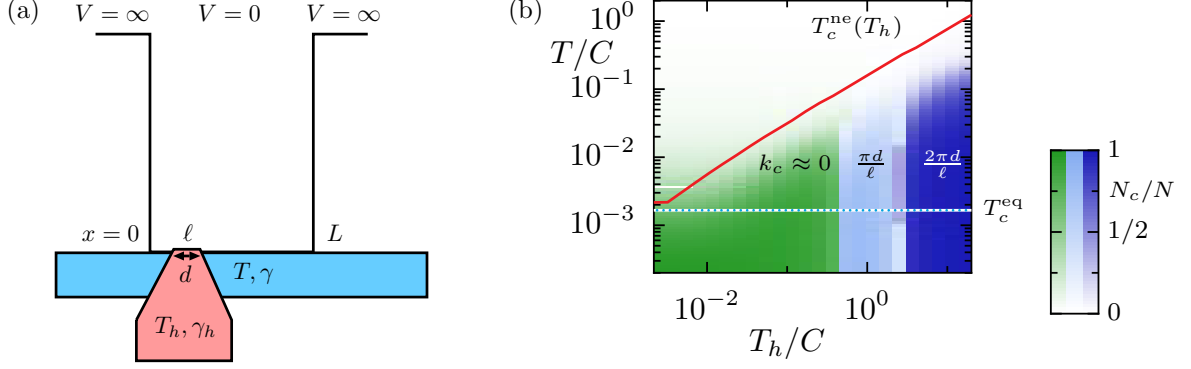


Figure 5.7.: (a) Sketch of the system. Bosons, mass m , are trapped in a box potential of length L . With strength γ the full system is in contact with a global heat bath at temperature T as well as with a local bath, strength γ_h , temperature T_h , that is located at $x = \ell$ and has a spatial width d . (b) Condensate fraction N_c/N for the continuous 1D system of length $L = 500d$ and density of $n = 0.1/d$ versus the temperatures T and T_h of the global bath and the hot needle, respectively. The hot needle is placed at distance $\ell = 40d$ from the edge. The relative coupling between both baths is $\gamma_h/\gamma = 1/4$. Green (light blue) shading indicates the relative number of particles in the mode $k_0 \approx 0$ ($k_1 \approx \pi d/\ell$). The blue-white dotted line corresponds to the condensation temperature in equilibrium.

which is described by the Hamiltonian

$$H = \int_0^L dx \psi^\dagger(x) \left(-\frac{\hbar^2}{2m_\circ} \frac{d^2}{dx^2} \right) \psi(x) = \sum_k \varepsilon_k n_k, \quad (5.38)$$

where m_\circ denotes the mass of the particles and $\psi(x)$ is the field operator annihilating a boson at position x . In the following we will again use $\hbar = 1$. The dimensionless wavenumbers $k = \nu\pi d/L$ with $\nu = 1, 2, \dots$ and some length scale d (which we take to be the extent of the hot needle defined below) characterize the single-particle eigenstates with energy

$$\varepsilon_k = \frac{k^2}{2m_\circ d^2} \equiv Ck^2, \quad (5.39)$$

and wave functions $\langle x|k\rangle = \sqrt{2/L} \sin(kx/d)$. The corresponding number operator reads $n_k = c_k^\dagger c_k$ with $c_k = \int_0^L dx \langle k|x\rangle \psi(x)$. The energy eigenstates of the system are Fock states $|\mathbf{n}\rangle$ labeled by the vector of occupation numbers n_k . In a similar calculation as presented in Section 5.2 one finds that for the particles in the box the equilibrium condensation temperature reads

$$T_c^{\text{eq}} = \frac{a\pi^2 n}{4m_\circ} \frac{1}{L} \approx 8.3C \frac{nd^2}{L}, \quad (5.40)$$

where, again, $a \approx 1.68$ solves $1 = a \sum_{\nu=2}^{\infty} 1/(\nu^2 + a - 1)$ and $n = N/L$ is the density of the particles.

In such a continuous system, a hot local bath at position $x = \ell$ of spatial extent d , can be described

5. High-temperature nonequilibrium Bose condensation induced by a hot needle

by the coupling operator

$$v_h = \frac{L}{d} \int_{\ell-\frac{d}{2}}^{\ell+\frac{d}{2}} dx \psi^\dagger(x) \psi(x). \quad (5.41)$$

The corresponding single-particle rates are of the form of Eq. (5.2), with $f_{kq}^{(h)} = [\cos(k\frac{\ell}{d}) \text{sinc}(k/2) - \cos(q\frac{\ell}{d}) \text{sinc}(q/2)]^2$ approaching $f_{kq}^{(h)} \simeq 4 \sin^2(k\ell/d) \sin^2(q\ell/d)$ in the limit $d \rightarrow 0$. A global heat bath is still described by Eq. (5.2) with $f_{kq}^{(g)} = 1$.

From these rates we compute the corresponding mean occupations for a system of $N = 0.1L/d$ particles, length $L = 500d$, and needle position $\ell = 20d$. In Fig. 5.7(b) we plot the condensate fraction, i.e. the fraction of particles occupying the most occupied mode whose wave number is indicated by the color of the shading (green for $k_0 \approx 0$, light blue for $k_1 \approx \pi d/\ell$, blue for $k_2 \approx 2\pi d/\ell$). Note that for computational reasons, we cut off the unbounded spectrum at $M = 300$ states, however we make sure that the occupations of the states at this cut-off value are sufficiently low for all parameters. As for the tight-binding chain, we can clearly see that the temperature T of the global bath at which the system condenses increases with needle temperature T_h . As a result, Bose condensation is found for the nonequilibrium steady state in a system coupled to two baths both having temperatures well above the equilibrium condensation temperature T_c^{eq} (which is indicated as blue-white dotted line). Moreover, when the needle temperature is increased further, ground-state condensation in mode $k_0 \approx 0$ is superseded by the formation of a condensate in the excited mode $k_1 \approx \pi d/\ell$, which provides a better

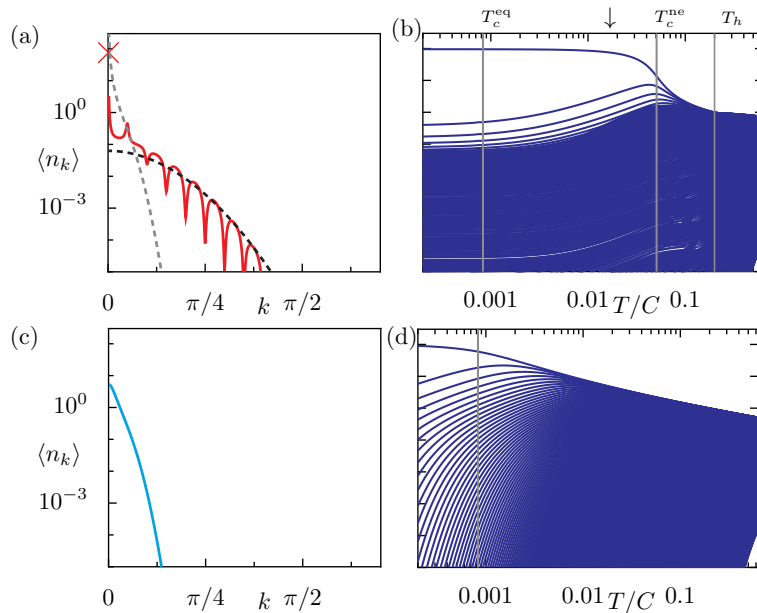


Figure 5.8.: Analogous plots to Fig. 5.3(a)-(d), but for ideal bosons in a box with $L = 1000d$, $\ell = 20d$, $\gamma_h/\gamma = 1$, $n = 0.1/d$ and T_h as indicated in Figure (b) and the temperature T used in Figures (a) and (c) is given by the arrow in Figure (b). We cut off the spectrum above the first $M = 700$ states, because their occupations are small, only at very high temperatures $T \approx 0.5C$ we observe that their occupations would be on the order 10^{-4} .

decoupling from the hot needle.

Following our reasoning in Section 5.3, we analogously find a decomposition into modes that thermalize with environmental and needle temperature. In the limit $d \rightarrow 0$ the rates take the same form as in the tight-binding system and approximations of the 1D-like condensation temperature $T_c^{\text{ne},1}$ and of the switching temperature $T_h^{\text{s},\alpha}$ can be found by similar type of arguments as in the case of the tight-binding chain.

However for the 3D-like condensation temperature $T_c^{\text{ne},2}$ a slight modification of the arguments is needed, since in the continuous system the single-particle spectrum is not bounded, therefore the occupations of the modes that thermalize with T_h cannot assumed to be flat, which e.g. becomes apparent in Fig. 5.8(a). Rather than this, let us assume that all particles are either in the ground-state condensate $\langle n_{k_0} \rangle = N_c$ or in the depletion, which, for sufficiently low $T \ll T_c^{\text{ne},1}$ has no contributions from the long-wave modes. For this reason, we can assume that the depletion follows a Bose-Einstein distribution,

$$\langle n_{k \neq k_0} \rangle = \frac{1}{z_h^{-1} e^{\varepsilon_k/T_h} - 1}, \quad (5.42)$$

with temperature T_h and fugacity of the depletion $z_h = \exp(\mu_h/T_h)$ which is connected to the total number of particles in the depletion via

$$N' = \sum_{k \neq k_0} \langle n_k \rangle. \quad (5.43)$$

We plug this ansatz into the mean field equation, Eq. (4.4), for $k = k_0$, and approximate that the condensate decouples from the needle, similar as in Eq. (5.24), to find

$$0 \approx N_c \sum_{q \neq k_0} A_{k_0 q}^{(g)} \langle n_q \rangle + \sum_{q \neq k_0} R_{k_0 q}^{(g)} \langle n_q \rangle - N_c \sum_{q \neq k_0} R_{q k_0}^{(g)}. \quad (5.44)$$

This is, again, dominated by the first and last term so that it has to hold

$$0 \approx \sum_{q \neq k_0} A_{k_0 q}^{(g)} \langle n_q \rangle - \sum_{q \neq k_0} R_{q k_0}^{(g)} \approx \gamma^2 \sum_{q \neq k_0} \left(\frac{\varepsilon_q}{z_h^{-1} e^{\varepsilon_q/T_h} - 1} - \frac{\varepsilon_q}{e^{\varepsilon_q/T} - 1} \right) \quad (5.45)$$

where we have employed $\varepsilon_{k_0} \approx 0$, which is true in the limit of large system size. Here we already observe why the 3D-like behavior is expected: The fugacity z_h is determined by a sum in which the IR-divergence is suppressed by an additional $\varepsilon_q \propto q^2$ in the numerator. Therefore Eq. (5.45) will give rise to an z_h -behaviour which is independent of the cutoff.

We may now use the geometric series to find

$$0 \approx \gamma^2 \sum_{q \neq k_0} \varepsilon_q \left(\frac{z_h e^{-\varepsilon_q/T_h}}{1 - z_h e^{-\varepsilon_q/T_h}} - \frac{e^{-\varepsilon_q/T}}{1 - e^{-\varepsilon_q/T}} \right) = \gamma^2 \sum_{q \neq k_0} \varepsilon_q \sum_{m=1}^{\infty} \left(z_h^m e^{-m\varepsilon_q/T_h} - e^{-m\varepsilon_q/T} \right) \quad (5.46)$$

5. High-temperature nonequilibrium Bose condensation induced by a hot needle

Dividing by γ^2 and exchanging the sums, this may further be simplified to read

$$0 \approx \sum_{m=1}^{\infty} \sum_{q \neq k_0} \left(-z_h^m \frac{\partial}{\partial(m/T_h)} e^{-m\varepsilon_q/T_h} + \frac{\partial}{\partial(m/T)} e^{-m\varepsilon_q/T} \right) \quad (5.47)$$

In the large system-size limit we may approximate the sum over the momentum q by the integral

$$\sum_q = \frac{L}{\pi d} \sum_q \frac{\pi d}{L} \approx \frac{L}{\pi d} \int dq \quad (5.48)$$

This yields

$$0 \approx \sum_{m=1}^{\infty} \left[-z_h^m \frac{\partial}{\partial(m/T_h)} \int_0^{\infty} e^{-mCq^2/T_h} dq + \frac{\partial}{\partial(m/T)} \int_0^{\infty} e^{-mCq^2/T} dq \right] \quad (5.49)$$

$$= \sum_{m=1}^{\infty} \left[-z_h^m \frac{\partial}{\partial(m/T_h)} \sqrt{\frac{\pi T_h}{2mC}} + \frac{\partial}{\partial(m/T)} \sqrt{\frac{\pi T}{2mC}} \right] \quad (5.50)$$

and after performing the derivatives we find

$$0 = \sqrt{\frac{\pi}{2C}} \sum_{m=1}^{\infty} \left[-z_h^m \left(\frac{T_h}{m} \right)^{3/2} + \left(\frac{T}{m} \right)^{3/2} \right] = \sqrt{\frac{\pi}{2C}} \left[-T_h^{3/2} \text{Li}_{3/2}(z_h) + T^{3/2} \zeta\left(\frac{3}{2}\right) \right]. \quad (5.51)$$

Here $\text{Li}_s(z)$ is the polylogarithm function and $\zeta(s) = \text{Li}_s(1)$ is the Riemann zeta function. This can be solved for the fugacity,

$$z_h(T, T_h) = \text{Li}_{3/2}^{-1} \left(\left(\frac{T}{T_h} \right)^{3/2} \zeta\left(\frac{3}{2}\right) \right), \quad (5.52)$$

which indeed is independent of the system size. Note that for $T < T_h$ the equation has a solution $z_h \in [0, 1)$, but for the ansatz to be valid, we have to satisfy that the corresponding number of particles $N' = \sum_k (z_h^{-1} \exp(\varepsilon_k/T_h) - 1)^{-1}$ is smaller than the total number of particles in the system. This prediction for $z_h(T, T_h)$ gives rise to the Bose-Einstein distribution, Eq. (5.42), that is shown as a black dashed line in Fig. 5.8(a) and we see an excellent agreement with the distribution of the high-energy modes that couple to the needle.

Since z_h depends directly on T_h , the critical temperature T_c^{ne2} , where condensation is destroyed by the high-energy modes, is not T_h -independent like for the chain. For given T_h , the critical temperature T_c^{ne2} follows implicitly from

$$\frac{N'}{L} = \frac{n}{2} = \left(\frac{m_o T_h}{2\pi} \right)^{1/2} \text{Li}_{1/2}(z_h(T_c^{\text{ne2}}, T_h)), \quad (5.53)$$

which is also found by performing the continuum approximation, Eq. (5.48). This equation can be solved numerically for T_c^{ne2} and gives the prediction that is shown as a red line in Fig. 5.7(b).

5.8. Experimental prospects and the “Floquet needle”

The effects that we find in presence of both a global environmental bath and a hot local bath are intriguing and suggest that via bath engineering one is able to induce and control condensation in a one-dimensional system. However, if one would like to find such effects in an experiment, one needs experimental setups in which there is a high level of control over a quantum many-body system. A prime example of such setups are ultracold atom experiments. But while they offer a high level of controllability – e.g. the strength of the interactions between the atoms can be tuned via Feshbach resonances [165]– and the possibility to access the timescales of their dynamics experimentally, typically ultracold atom experiments are well isolated from their environment. So in order to observe such interesting nonequilibrium steady states in ultracold quantum gases one would have to artificially introduce an environmental bath as well as the local hot bath. It should be feasible to model the presence of an environmental bath in a mixture of two species of atoms: There is one species of noninteracting bosons, the system, that is immersed in and interacts weakly with a big number of atoms of another species, the bath, that is thermalized. Such mixtures have already been used widely in experiments, mostly for sympathetic cooling [166, 167], but in recent experiments also the dynamics of one [168, 169] or a few [170] impurity atoms in weak contact to a Bose condensed cloud have been addressed. Other experiments have used two different hyperfine states of a single species of atoms where the atoms in one hyperfine state act as a bath to the atoms in another hyperfine state [171].

While the prospects of engineering a global bath are good, it is unclear whether and how it is possible to create a second bath which only couples locally to the system. A very successful tool to control ultracold quantum gases is by time-periodic forcing, which has been coined Floquet engineering [8]. In this section, we investigate very similar nonequilibrium steady states as in the hot needle setup that are found if one keeps the ideal Bose gas in weak contact with a global environment but replaces the hot local bath with a driving field that couples locally to the system. It is expected that a local Floquet drive can act as a heat source, since in general isolated quantum systems are expected to heat up to an infinite temperature state under periodic driving. Also, studies of nonequilibrium steady states that emerge when a time-periodically driven system is coupled to a bath show that there is a heat current from the driven system into the bath [83].

We find that for a tight-binding system

$$H(t) = -J \sum_{i=1}^{M-1} \left(a_{i+1}^\dagger a_i + a_i^\dagger a_{i+1} \right) + \gamma_\ell f(t) n_\ell \quad (5.54)$$

where at site ℓ the local density $n_\ell = a_\ell^\dagger a_\ell$ is coupled to a time-periodic field $f(t) = f(t + \mathcal{T})$ with strength γ_ℓ . Such a local driving field could e.g. be imprinted experimentally by a spatial light modulator [172].

If this time-periodically driven system is coupled weakly to a bath, asymptotically, its density matrix will be diagonal in the Floquet states $|a(t)\rangle = |a(t + \mathcal{T})\rangle$ (respectively in the corresponding Floquet-Fock states for the ideal gas) [73]. Again, via operator $a_i^\dagger a_i$, we couple each site i with strength γ/\sqrt{M}

5. High-temperature nonequilibrium Bose condensation induced by a hot needle

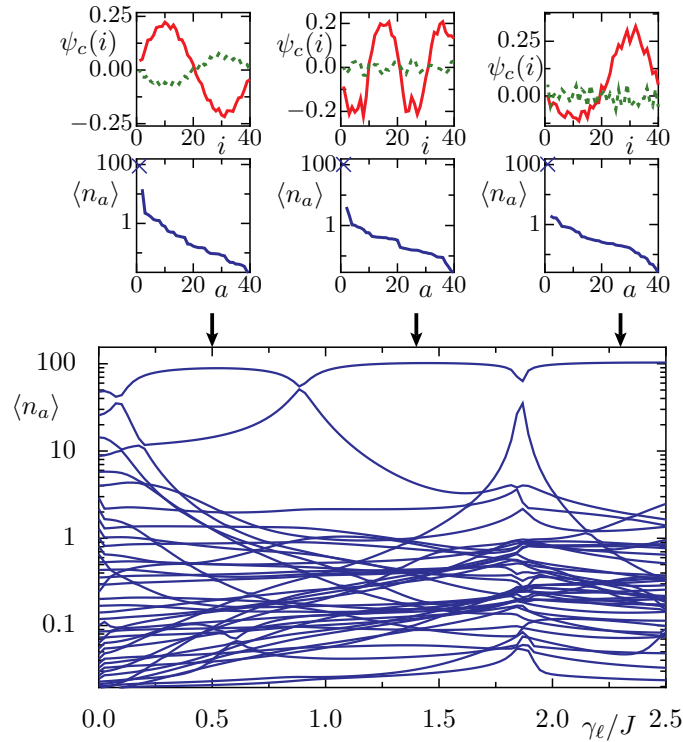


Figure 5.9.: Main figure: Mean occupations $\langle n_a \rangle$ of the Floquet modes a for a system of $M = 40$ sites and $n = 3$ particles per site and environmental bath temperature $T = J$ as a function of the driving amplitude γ_ℓ of the time-periodic drive with the noisy function $f(t)$. We choose driving frequency $\omega = 0.7J$ and use $M_f = 5$ higher harmonics. The driving site is $\ell = 20$. Insets: Arrows indicate the value of γ_ℓ at which we show the occupation statistics (we sort the levels a according to their population) as well as the real (solid red) and imaginary part (dashed green line) of the condensate Floquet mode ψ_c (snapshot at $t = 0$).

to a bath at temperature T leading to the single-particle rates

$$R_{ab} = 2\pi \frac{\gamma^2}{M} \sum_{i=1}^M \sum_{m=-\infty}^{\infty} |v_{ab}^{(i)}(m)|^2 g(\varepsilon_a - \varepsilon_b - m\hbar\omega), \quad (5.55)$$

where $\omega = 2\pi/\mathcal{T}$ is the frequency of the drive, $v_{ab}^{(i)}(m) = \frac{1}{\mathcal{T}} \int_0^{\mathcal{T}} e^{im\omega t} \langle a(t) | a_i^\dagger a_i | b(t) \rangle dt$, and ε_a is the quasienergy of Floquet state a .

It turns out that, similar to the case with a localized hot bath (the hot needle) one can find interesting nonequilibrium steady states which feature a higher condensate fraction than the thermal state without the drive. To this end it is important that there is actually a significant amount of heat transferred into the system. This can be achieved by choosing a drive $f(t)$ with a relatively low frequency $0 < \omega \lesssim J$ and additionally adding M_f higher harmonic components

$$f(t) = \frac{1}{\sqrt{M_f}} \sum_{m=1}^{M_f} \cos(m\omega t + \varphi_m) \quad (5.56)$$

to make the drive sufficiently noisy. Note that we have to add random phases φ_m because otherwise $f(t)$ will be largely peaked around $t = 0$. To make our results reproducible, rather than random phases we choose quasiperiodic phases

$$\varphi_m = \cos(2\pi m\alpha) \quad (5.57)$$

where $\alpha = (1 + \sqrt{5})/2$ is the golden ratio. We would like to refer to this setup as the ‘Floquet needle’.

By solving the corresponding mean-field equations we find the mean occupation $\langle n_a \rangle$ of the Floquet states a in the ideal gas. In Figure 5.9 we show the steady state occupations $\langle n_a \rangle$ of the Floquet modes a for fixed environmental temperature $T = J$ as a function of the driving amplitude. Remarkably, already for a relatively small system size $M = 40$, we see a very similar behavior as for the static hot needle scenario in Fig. 5.4. By driving the system locally at site ℓ (here it is in the middle of the system), the condensate fraction increases significantly over its equilibrium value at $\gamma_\ell = 0$, where the Floquet states are simply the eigenstates of the autonomous Hamiltonian H . In the insets we show, for given value of γ_ℓ , both the occupation statistics $\langle n_a \rangle$ (sorted in descending order) as well as a snapshot of the condensed Floquet mode ψ_c at time $t = 0$. With increasing γ_ℓ we first observe the emergence of a condensate in a mode whose profile resembles very much the one of a π/ℓ -mode that has a node at the coupling site. This node is an indicator that should be clearly visible in the steady state density profile $\langle n_i \rangle$ of the gas in a possible experimental realization. Much like in the case of the hot needle, after a transition into a second phase there is even a condensate in a ‘higher excited’ $2\pi/\ell$ -like mode emerging. After this phase, at very large γ_ℓ there is another phase which is more different from the ones that we observe in the hot needle scenario. In this phase the condensate localizes dominantly on one side of the driven site, as the barrier that is due to the relatively large driving amplitude γ_ℓ is beginning to make itself felt.

By going to higher system sizes M , and reducing the basic driving frequency ω while at the same

5. High-temperature nonequilibrium Bose condensation induced by a hot needle

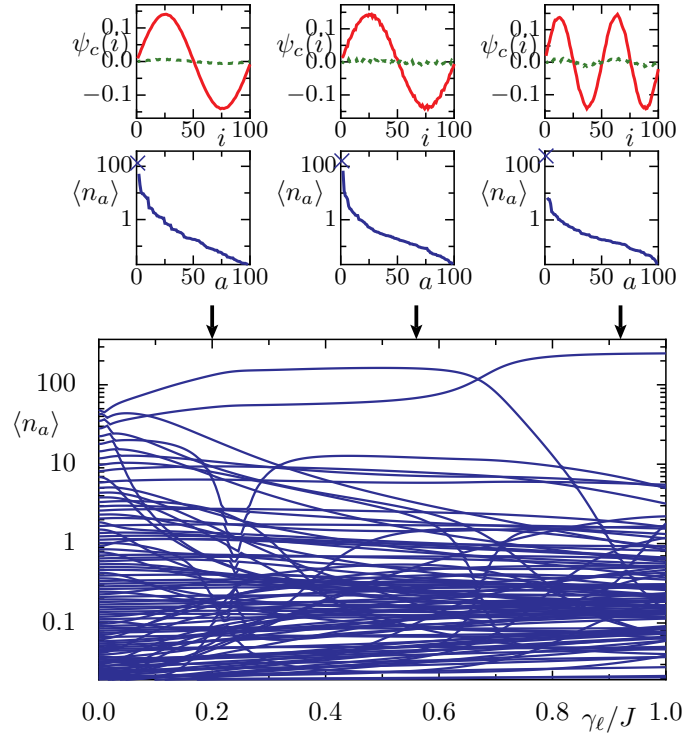


Figure 5.10.: Same as in Fig. 5.9, but for system size $M = 100$, $\omega = 0.3J$ and $M_f = 12$.

time adding more higher harmonics M_f , one can make the effects more clear, as shown in Fig. 5.10. With these parameters, the increase in the condensate fraction is even more pronounced, and the observed condensed Floquet modes resemble the ones of the hot needle even better.

In conclusion, we observe similar physics if the hot needle is replaced by a noisy Floquet drive. It can equally provide a strong in-flow of heat, which induces condensation in a state that decouples from the drive. Quite different to existing experiments in Floquet engineering, here, interesting physics arises from an incoherent drive. We expect that a similar condensation phenomenon occurs even when the driving field is not periodic, but pure noise. It is an intriguing open question whether experimental setups like mixtures of quantum gases can effectively be described by an ohmic bath or if a more realistic description, e.g. in terms of coupling the system to Bogoliubov quasiparticles, is needed. Also studies with a finite coupling strength γ should be performed in order to map out how weak the coupling to the bath needs to be such that the hot-needle or the Floquet needle effect can be observed.

6. Weakly interacting Bose gases far from thermal equilibrium

We study weakly interacting Bose gases that are driven into nonequilibrium steady states due to the presence of multiple baths with different temperature. For the ideal gas a simple description of such open systems is given by the Born-Markov approximation. Within this framework, the bath induces quantum jumps between energy eigenstates. Taking into account temperature-dependent dissipation for the interacting gas is challenging. Already on the level of a simple mean-field approximation, it requires the diagonalization of the mean-field Hamiltonian in every step of the time integration. We propose and test a scheme to circumvent this problem by treating the system–bath coupling semi-classically. To this end, we decompose the system into overlapping bins and approximate that the bath may only drive transitions between wavelets that localize in such a bin. We thus find an approximate description of the action of the dissipative bath interaction that is independent of the interactions in the system. This provides a convenient tool to study far from equilibrium gases, whose steady state density profile in general is not known *ab-initio*.

The results in this chapter are unpublished.

6.1. Semiclassical description of bath action

In the previous chapters we have observed intriguing effects that occur in the nonequilibrium steady states of ideal Bose gases that are driven out of equilibrium by heterogeneous bath environments. Quite naturally, the question arises, whether effects like the high-temperature nonequilibrium condensation that we discuss in Chapter 5 may also be found in the presence of interactions. We would like to have a similar microscopic description of interacting quantum gases in terms of a Born-Markov rate equation.

However, as we shortly discuss already in Section 2.4, for a quantum many-body system the spectrum of the full many-body Hamiltonian is typically inaccessible. Thus, already writing down the exact Born-Markov rate equation, describing jumps between the many-particle eigenstates, is an extremely challenging task. An exception are many-body localized systems, where it is guaranteed that the Hamiltonian is diagonal in the Fock basis of quasi-localized integrals of motion (l-bits) [125] which for weak interactions might be computed perturbatively. Here, however, we are aiming at bosonic systems that are in an interaction regime where superfluidity is expected. To avoid the problem that the full spectrum is unknown, we develop a semiclassical description of the dissipative term that describes the action of the bath. It is based on the introduction of wavelet states that are localized both in space

6. Weakly interacting Bose gases far from thermal equilibrium

and with respect to momentum. Although we motivate and use this method only for systems where we describe interactions on a mean-field level, in principle this semiclassical form of the dissipator could also be combined with more sophisticated methods that deal with the interactions.

Let us consider in the following a model system of N interacting bosons. Here we are focusing on lattice systems that can be described by the Bose-Hubbard Hamiltonian,

$$H = -J \sum_{\langle i,j \rangle} [a_i^\dagger a_j + a_j^\dagger a_i] + \sum_{i=1}^M [V_i n_i + \frac{U}{2} n_i (n_i - 1)], \quad (6.1)$$

where $\langle \cdot, \cdot \rangle$ denotes the sum over nearest neighbors and J is the tunneling constant. Moreover, it enter trapping potential V_i , on-site interaction U , bosonic annihilation operator a_i for site i and number operator $n_i = a_i^\dagger a_i$. For the moment we also assume periodic boundary conditions. The system is allowed to exchange energy with multiple heat baths at different temperatures. The total Hamiltonian for such a setup reads

$$H_{\text{tot}} = H + \sum_{i=1}^M \gamma_i n_i \sum_{\alpha} c_{\alpha} (b_{\alpha,i} + b_{\alpha,i}^\dagger) + \sum_{\alpha,\ell} \hbar \omega_{\alpha} b_{\alpha,i}^\dagger b_{\alpha,i} \quad (6.2)$$

where the phonon baths are modeled by a collection of harmonic oscillators with annihilation operators $b_{\alpha,i}$ and frequencies ω_{α} . For each site i we couple a bath to the local density n_i of the gas. This coupling is mediated with strength γ_i and dimensionless coupling constants c_{α} .

For the noninteracting gas, $U = 0$, a microscopic description of the dynamics can be found using the Born-Markov approximation [108], as we discuss in Section 2.4. It assumes that the bath-correlation times are short when compared to the relaxation time scales and that the coupling is weak enough so that system and bath do not build up correlations. In this approximation, the equation of motion for the system density matrix ρ , Eq. (2.89), reads

$$\begin{aligned} \partial_t \rho &= -\frac{i}{\hbar} [H, \rho] + \mathcal{D}[\rho] \\ \mathcal{D}[\cdot] &= \sum_{klpq} \left[\frac{R_{ql,pk}}{2} (c_p^\dagger c_k \cdot c_l^\dagger c_q - c_l^\dagger c_q c_p^\dagger c_k \cdot) + \text{h.c.} \right] \end{aligned} \quad (6.3)$$

with the eigenstates $c_k^\dagger = \sum_{i=1}^M \langle i | \psi_k \rangle a_i^\dagger$ of the noninteracting Bose-Hubbard Hamiltonian $H = \sum_k \varepsilon_k c_k^\dagger c_k$. The evolution is given by the coherent evolution and the dissipative action of the bath that induces transitions between the energy eigenstates. This happens at single-particle rates which are the sum $R_{ql,pk} = \sum_{i=1}^M R_{ql,pk}^{(i)}$ of the rates corresponding to the coupling to the individual baths at site i ,

$$R_{ql,pk}^{(i)} = \frac{2\pi}{\hbar} \gamma_i^2 v_{ql}^{(i)*} v_{pk}^{(i)} g^{(i)}(\varepsilon_p - \varepsilon_k), \quad (6.4)$$

with the matrix elements of the coupling operator $v_{kq}^{(i)} = \langle \psi_k | n_i | \psi_q \rangle$, bath correlation function $g^{(i)}(\varepsilon) = J(\varepsilon) / [\exp(\varepsilon/k_B T_i) - 1]$ and spectral density of the bath $J(\varepsilon) = \sum_{\alpha} |c_{\alpha}|^2 [\delta(\varepsilon - \hbar \omega_{\alpha}) - \delta(\varepsilon + \hbar \omega_{\alpha})]$. Here we assume ohmic baths with a continuum of modes and $J(\varepsilon) = \varepsilon$ (remember that we absorb the

strength of the coupling into the constants γ_i). If all temperatures T_i of the baths are identical, the system will relax to a thermal state in the long time limit, while nonequilibrium steady states are found when the baths have different temperatures.

Note that without further approximations, the equation of motion Eq. (6.3) cannot be cast into Lindblad form. This Lindblad form only emerges after performing a rotating-wave (or secular) approximation which uses that for sufficiently weak system–bath coupling the density matrix ϱ will be diagonal in the energy eigenbasis in the long-time limit.

Let us now turn to the interacting problem, $U \neq 0$. While for large interaction U and integer filling N/M , the Bose-Hubbard system undergoes a phase transition into the Mott insulating phase [173], for weak interactions $U \ll Jn$, the system is superfluid. In the latter regime the interaction effects can be captured on a mean field level, which leads to a dynamics with an effective potential $V_i^{\text{eff}}(t) = V_i + 2U\langle n_i \rangle(t)$ that is “seen” by a single particle. This can be motivated by deriving equations of motion for the coherent part of the evolution of the single particle density matrix $\varrho_{ij} = \langle a_i^\dagger a_j \rangle = \text{Tr}(\varrho a_i^\dagger a_j)$,

$$\partial_t \varrho_{ij}|_{\text{coh}} \equiv -\frac{i}{\hbar} \langle [a_i^\dagger a_j, H] \rangle = -\frac{i}{\hbar} \sum_l \left(\varrho_{il} h_{lj} - h_{il} \varrho_{lj} + \frac{U}{2} \langle n_l [a_i^\dagger a_j, n_l] + [a_i^\dagger a_j, n_l] (n_l - 1) \rangle \right), \quad (6.5)$$

where in the second step we have defined the single-particle matrix elements of the Hamiltonian, $H|_{U=0} = \sum_{ij} h_{ij} a_i^\dagger a_j$. In the following we set $k_B = \hbar = 1$. Using $[a_i^\dagger a_j, n_l] = a_i^\dagger a_j (\delta_{jl} - \delta_{il})$, we find

$$\partial_t \varrho_{ij}|_{\text{coh}} = -i \sum_l \left[\varrho_{il} h_{lj} - h_{il} \varrho_{lj} + \frac{U}{2} (\sigma_{ij}^{jj} - \sigma_{ij}^{ii} + \sigma_{jj}^{ij} - \sigma_{ii}^{ij}) \right]. \quad (6.6)$$

Here we denote the two-particle correlations $\sigma_{kl}^{ij} = \langle a_i^\dagger a_j a_k^\dagger a_l \rangle$. For weak interactions and finite temperatures, we may neglect nontrivial particle-particle correlations, so it approximately holds the mean-field (Wick-)decomposition

$$\sigma_{kl}^{ij} \approx \varrho_{ij} \varrho_{kl} + \varrho_{il} (\varrho_{kj} + \delta_{kj}). \quad (6.7)$$

Note that for interacting systems mean-field methods are known to perform badly in one dimension, especially at $T = 0$. That is because they fail to predict the power-law decay of correlations in the ground state [174] which is due to interaction-induced phase fluctuations. At finite temperatures however, thermal fluctuations lead to an exponential decay of single-particle correlations which will dominate the behavior at large distances [175]. Such physics can be understood on a mean-field level. Nevertheless, in a finite system, if temperature is reduced, the coherence length of thermal fluctuations will become comparable to the system size, and one could imagine that interaction-induced fluctuations play a dominant role. For harmonically trapped one-dimensional gases a more detailed analysis shows that indeed there is an intermediate temperature regime where therefore only quasicondensation is found [176]. At low temperatures, however, a true condensate is found and a mean-field description is again valid. If the interaction strength is reduced to zero, the temperature regime of quasicondensation will also shrink to zero. As a result, for weak interactions this regime will be very small and we may

6. Weakly interacting Bose gases far from thermal equilibrium

ignore it.

Plugging Eq. (6.7) into Eq. (6.6), and using the notation $\bar{n}_i = \varrho_{ii} = \langle n_i \rangle$, we find

$$\partial_t \varrho_{ij}|_{\text{coh}} = -i \left[\sum_l (\varrho_{il} h_{lj} - h_{il} \varrho_{lj}) + \frac{U}{2} [(2\bar{n}_j + \delta_{ij}) \varrho_{ij} - (2\bar{n}_i + 1) \varrho_{ij} + \varrho_{ij} (2\bar{n}_j + 1) - \varrho_{ij} (2\bar{n}_i + \delta_{ij})] \right]. \quad (6.8)$$

This evolution can be recast into an effective equation of motion with mean-field Hamiltonian

$$H_{\text{MF}}(t) = \sum_{ij} (h_{ij} + 2U \bar{n}_i(t) \delta_{ij}) a_i^\dagger a_j, \quad (6.9)$$

which turns the problem into an effective single-particle problem. However the an effective potential $V_i^{\text{eff}}(t) = V_i + 2U \langle n_i \rangle(t)$ depends on the density profile of the gas $\langle n_i \rangle(t)$ itself, which is generally time dependent. Note that in contrast to the Gross-Pitaevskii Equation (GPE), here enters a factor of 2 in front of the effective potential $U \langle n_i \rangle(t)$. This is because the mean-field decomposition, Eq. (6.7), is exactly valid only for the grand canonical ensemble. For thermal bosons, occupations of the single-particle orbitals are small, and therefore number fluctuations in the canonical ensemble and the grand-canonical ensemble coincide in the thermodynamic limit. In a condensed phase, in turn, number fluctuations in the canonical ensemble are not correctly captured by the grand-canonical ensemble.

In the GPE, however, a canonical situation is assumed. For example, let us consider for the non-interacting gas a fully condensed state $\varrho = |\psi_F\rangle \langle \psi_F|$ with some Fock state $|\psi_F\rangle = (\psi_0^\dagger)^N |0\rangle / N!$, with $\psi_0^\dagger = \sum_i \phi(i) a_i^\dagger$. It is easy to see that in this state we may evaluate the expectation values of normal ordered products by the replacements $a_i \rightarrow \sqrt{N} \phi(i)$, $a_i^\dagger \rightarrow \sqrt{N} \phi(i)^*$, which is the essence behind the semiclassical theories like GPE, that treat the condensate as a complex order parameter $\sqrt{N} \phi$. Thus, in this fully condensed state the decomposition reads

$$\sigma_{kl}^{ij} = \varrho_{il} (\varrho_{kj} + \delta_{kj}), \quad (6.10)$$

and we would not find the factor 2 in the mean field potential.

Another viewpoint on the physical origin of this factor is bosonic bunching, which is best understood in the normalized second order-correlation function

$$g^{(2)}(\delta x) = \frac{\langle a_1^\dagger a_{1+\delta x}^\dagger a_{1+\delta x} a_1 \rangle}{\langle n_1 \rangle \langle n_{1+\delta x} \rangle}, \quad (6.11)$$

which is a standard quantity that for the ideal gas is well studied in the literature both theoretically [177, 178] but also experimentally [55, 179, 180]. Thermal bosons are known to show bunching when they are at the same position, $g^{(2)}(0) = 2$, i.e. if a boson is found at one position, the probability of finding a second boson at the same position is enhanced. This bunching only occurs on the correlation length ξ of the gas, at large distances $g^{(2)}(\delta x \gg \xi) = 1$ holds. This can be anticipated from a Wick decomposition of the numerator of Eq. (6.11). In a condensed phase in the grandcanonical ensemble, the Wick decomposition is still valid and since $\xi \rightarrow \infty$ one finds $g^{(2)}(\delta x) = 2$ everywhere. For a condensate

in the canonical ensemble, however, all particles occupy the same state and are indistinguishable, so these statistical fluctuations vanish such that $g^{(2)}(\delta x) = 1$.

As a result, we expect that our model gives a valid description only if we would allow additionally for particle exchange. For fixed particle number N , we expect correct results at high and intermediate temperatures only. In the presence of a large condensate fraction, the model might tend to overestimate interaction effects due to the presence of the factor 2 in the mean-field potential.

We aim to use the Born-Markov approximation, Eq. (6.3), for this mean-field Hamiltonian $H_{\text{MF}}(t)$, Eq. (6.9). The key to the Born-Markov approximation is a separation of time scales. It is assumed that the time scale τ_B of the bath correlations is much shorter than the time scale τ_R of relaxation. Since in Eq. (6.3) the rotating wave approximation is not performed, there is no assumption on the time scales of the system dynamics τ_S made. However, it is used that the system is autonomous, i.e. the Hamiltonian is time independent. This allows for the spectral decomposition of the coupling operator v that is done in order to obtain Eq. (6.3). The Hamiltonian $H_{\text{MF}}(t)$ is not autonomous and thus there is generally no notion of a spectrum. Nevertheless, if we assume that we can apply a separation of timescales, i.e. that the mean-field potential $V^{\text{eff}}(t)$ varies only slowly when compared to the typical time scale τ_S associated with the energies of the system, we may diagonalize the system at a fixed time t , iterate it with Eq. (6.3), obtain a new density profile $\langle n_i \rangle(t + \Delta t)$ and from this a new mean field $V^{\text{eff}}(t + \Delta t)$. This procedure is repeated until the dynamics is stationary. Since for this stationary state the two-time assumption is valid, we expect an exact description (in the framework of the Born-Markov approximation and mean-field interactions) of the stationary state and also of the late-time dynamics.

However, this idea is still challenging since it in principle requires to diagonalize the mean-field

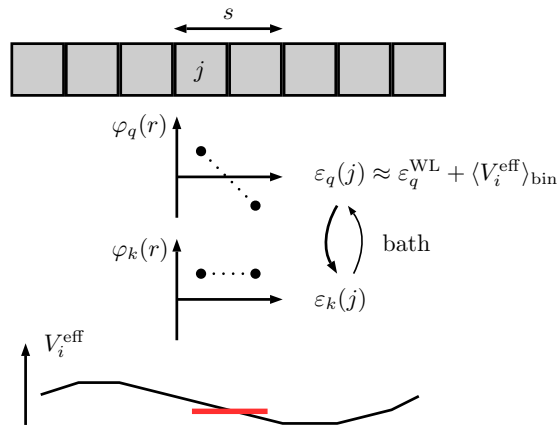


Figure 6.1.: Sketch of the method: We approximate that the action of the bath can be captured locally in transitions between wavelets. We define wavelets $\varphi_k(r)$ that form a local basis for the bin starting from site j with size s . Within such a bin the mean-field potential V_i^{eff} varies only weakly so that locally we may assume it is flat and replace it with the average value $\langle V_i^{\text{eff}} \rangle_{\text{bin}}$ in the bin (red line). Together with the kinetic energy of the wavelet $\varepsilon_k^{\text{WL}}$, we have the energy $\varepsilon_k(j)$ of the wavelets. From this we obtain rates for the transitions between the wavelets that are independent of the effective potential.

6. Weakly interacting Bose gases far from thermal equilibrium

potential $V_i^{\text{eff}}(t)$ at every timestep t from which one then deduces the instantaneous eigenstates and rates. Also, with such a scheme, casting Eq. (6.3) into Lindblad form through a rotating wave approximation (which reduces the numerical effort from computing the full single-particle density matrix to only occupations) is not feasible, because the steady state density profile $\langle n_i \rangle$ is not known ab-initio and therefore the basis in which the late-time dephasing occurs and the rotating wave approximation can be done is in principle unknown.

To circumvent the large numerical effort of diagonalizing the mean-field potential at every timestep, here we are presenting a semiclassical approximation of the action of the bath that, as we will see later, is valid for intermediate temperatures $T \gtrsim J$. In this approximation, that we visualize in Fig. 6.1, the bath drives transitions between wavelets

$$b_k^\dagger(j) = \sum_{r=0}^{s-1} \varphi_k(r) a_{j+r}^\dagger \quad (6.12)$$

that localize within overlapping bins that start from site j and have size s . Since the bins are overlapping, they form an overcomplete basis. Here the $\varphi_k(r)$ form an orthonormal basis within each bin, therefore there are s different wavelets. Such a wavelet treatment is inspired by microscopic derivations of the quantum Boltzmann equation [181]. There, ultimately, one is interested in the dynamics of the kinetic variable $f(j, k, t) = \langle b_k^\dagger(j) b_k(j) \rangle(t)$ which is a function of position j and momentum k (and time). In contrast to such quantum kinetic theories, however, here we aim for a semiclassical description on the level of the dissipator already. From this starting point, we will find a kinetic theory such that we can study the dynamics of the full single-particle density matrix, which allows for a coherence length ξ of the gas that is not limited by the bin size s as it would be in a Boltzmann equation.

Within the bins, we argue that the effective potential varies only weakly and therefore we may approximate it with its mean value $\langle V_i^{\text{eff}} \rangle_{\text{bin}}$. Thus, the wavelets are the same in every bin and the $\varphi_k(r)$ do not have an extra j -dependence. Also, this allows to identify energies $\varepsilon_k(j) = \varepsilon_k^{\text{WL}} + \langle V_i^{\text{eff}} \rangle_{\text{bin}}$ for the wavelet $b_k^\dagger(j)$, where $\varepsilon_k^{\text{WL}}$ is the kinetic energy of the wavelet that we will fix later. The bath may drive transitions between the different wavelets in the bin. Then we sum over all of these processes to find the corresponding dissipator for this semiclassical action of the bath

$$\mathcal{D}_{\text{WL}}[\cdot] = \frac{1}{s} \sum_{j=1}^M \sum_{klpq} \left[\frac{R_{ql,pk}(j)}{2} \left(b_p^\dagger(j) b_k(j) \cdot b_l^\dagger(j) b_q(j) - b_l^\dagger(j) b_q(j) b_p^\dagger(j) b_k(j) \right) + \text{h.c.} \right]. \quad (6.13)$$

The rates for the corresponding processes $R_{ql,pk}(j) = \sum_{r=0}^{s-1} R_{ql,pk}^{(r)}(j)$ are the sum over all rates of the transitions in the bin

$$R_{ql,pk}^{(r)}(j) = 2\pi\gamma_{j+r}^2 \varphi_q(r) \varphi_l(r)^* \varphi_p(r)^* \varphi_k(r) g^{(j+r)}(\varepsilon_p(j) - \varepsilon_k(j)). \quad (6.14)$$

There occur only energy differences $\varepsilon_p(j) - \varepsilon_k(j) = \varepsilon_p^{\text{WL}} - \varepsilon_k^{\text{WL}}$, therefore the dissipator and the rates are independent of the density profile of the gas which reduces the numerical effort dramatically. Note that the bin size s sets an upper limit for coherence length of the bath. Here, the baths couple to local

operators n_i in Eq. (6.2) only, therefore in our model the bath coherence length is zero. Hence, we may use any bin size s . Also this form of the dissipator does not rely on any approximations to the coherent evolution. Although we have used the picture of a mean-field interaction to motivate this form of the dissipator (and for all numerical results we will always use mean-field interactions), in principle this dissipator may be used also with more sophisticated methods to describe the interacting system.

Still, within this approximation, the steady states that we obtain in the equilibrium case are very close to thermal states. From Eq. (6.13), we find the steady-state single-particle density matrix ϱ_{ij} by deriving equations of motion for it

$$\partial_t \varrho_{ij}|_{\text{diss}} = \frac{1}{2s} \sum_{j'=1}^M \sum_{klpq} \left[R_{ql,pk}(j') \langle [b_l^\dagger(j') b_q(j'), a_i^\dagger a_j] b_p^\dagger(j') b_k(j') \rangle + \text{c.c.}, i \leftrightarrow j \right] \quad (6.15)$$

$$(6.16)$$

Here, we may evaluate the commutator

$$[b_l^\dagger(j') b_q(j'), a_i^\dagger a_j] = b_l^\dagger(j') \left(\sum_{a=0}^{s-1} \varphi_q(a)^* \delta_{j',i-a} \right) a_j - a_i^\dagger \left(\sum_{a=0}^{s-1} \varphi_l(a) \delta_{j',j-a} \right) b_q(j') \quad (6.17)$$

and by use of the definition of the wavelets, Eq. (6.12), we find

$$\partial_t \varrho_{ij}|_{\text{diss}} = \frac{1}{2s} \sum_{abcd=0}^{s-1} [\tilde{R}_{ab}^{cd}(x) \sigma_{x+c,x+d}^{x+b,j} - \tilde{R}_{ba}^{cd}(y) \sigma_{y+c,y+d}^{i,y+b} + \text{c.c.}, i \leftrightarrow j] \quad (6.18)$$

where in the sums one has to replace $x = i - a$ and $y = j - a$ and we define rates in position space

$$\tilde{R}_{ab}^{cd}(i) = \sum_{klpq} R_{ql,pk}(i) \varphi_q(a)^* \varphi_l(b) \varphi_p(c) \varphi_k(d)^*. \quad (6.19)$$

Note that, due to the locality of the wavelets, the sums in the dissipative part only runs over s terms. So already for the noninteracting system, this is a dramatic reduction from the extensive sum over M terms that one has to do without the approximation. To find a kinetic equation and treat Eq. (6.18) numerically, we again perform the mean-field approximation, Eq. (6.7), that neglects nontrivial particle-particle correlations

$$\begin{aligned} \partial_t \varrho_{ij}|_{\text{diss}} = \frac{1}{2s} \left(\sum_{abcd=0}^{s-1} [(\tilde{R}_{ab}^{cd}(x) + \tilde{R}_{ac}^{bd}(x)) \varrho_{x+b,j} \varrho_{x+c,x+d} - (\tilde{R}_{ba}^{cd}(y) + \tilde{R}_{da}^{cb}(y)) \varrho_{i,y+b} \varrho_{y+c,y+d}] \right. \\ \left. + \sum_{abcd=0}^{s-1} \tilde{R}_{ab}^{cd}(x) \varrho_{x+b,x+d} \delta_{j,x+c} - \sum_{abc=0}^{s-1} \tilde{R}_{bc}^{ba}(y) \varrho_{i,y+c} \right) + \text{c.c.}, i \leftrightarrow j, \end{aligned} \quad (6.20)$$

where again one has to replace $x = i - a$ and $y = j - a$. Again, the truncation on mean-field level is a practical choice and in general not necessary to apply the method. A more sophisticated treatment can for example be found by computing also the equation of motion for the four-point correlators σ_{kl}^{ij} and

6. Weakly interacting Bose gases far from thermal equilibrium

truncating the hierarchy by decomposing the six-point correlators that will occur in this evolution.

Finally, it is left to define the wavelets that we use. As we discuss in the following section, we observe that the optimal choice is given by $\varphi_k(r) = \sqrt{2/(s+1)} \sin[k(r+1)]$, with $k = \pi m/(s+1)$, $m = 1, 2, \dots, s$, i.e. standing waves of size s . Their energy $\varepsilon_k^{\text{WL}}$ is given also by the cosine dispersion $\varepsilon_k^{\text{WL}} = -2J_{\text{eff}} \cos(k)$, however with a renormalized hopping $J_{\text{eff}} = Js/(s-1)$. The reason why the hopping has to be renormalized can for example be seen for the $s = 2$ case where there is only the symmetric ($k = \pi/3$) and the antisymmetric ($k = 2\pi/3$) wavelet. Without the renormalization, the corresponding wavelet energies would be $-J$ and J , however when the ground state of the full system is probed by the wavelets it has maximum overlap with the symmetric wavelet and it should therefore rather give an energy of $-2J$.

6.2. Benchmark: Equilibrium states

We benchmark the method using the ideal gas, $U = 0$, in thermal equilibrium conditions i.e. identical temperature $T_\ell = T$, and coupling strength $\gamma_\ell = \gamma$ for all sites ℓ . In Fig. 6.2(a) and (b) we show the relative difference $\Delta_{\text{rel}} = \|\varrho_{ij} - \varrho_{ij}^{\text{TD}}\| / \|\varrho_{ij}^{\text{TD}}\|$ of the single-particle density matrix in the steady state, $\partial_t \varrho_{ij} = 0$, when compared to the thermal density matrix ϱ_{ij}^{TD} at the same parameters. Although we started out with a system with fixed particle number N , after performing the mean-field approximation $\langle N^2 \rangle = \langle N \rangle^2$ does not hold anymore, therefore there are particle number fluctuations. We thus compare to the grand canonical ensemble. We generally find errors that are on the order of a few percent only, including the case of the smallest possible choice of the bin size, $s = 2$. Without an external trapping potential $V_i = 0$, Fig. 6.2(a), the approximation that the potential does not vary within the bin is exact, therefore we observe the error that is due to the binning only. As expected, by increasing the bin size s the dynamics induced by the bath is reproduced better and better, so the error decreases. Note that depending on the choice of the wavelets $\varphi_k(r)$ and their kinetic energy $\varepsilon_k^{\text{WL}}$ this error can be very large (typically on the order of 1 for an uneducated guess). By numerical experiments, we find that the optimal choice are the standing waves that we define above.

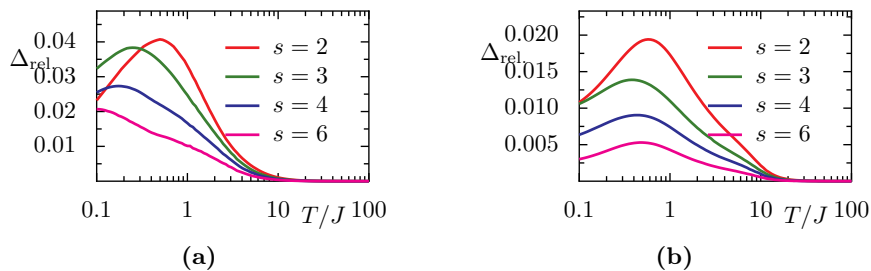


Figure 6.2.: Benchmark of the method (periodic boundary conditions): (a, b) Relative difference $\Delta_{\text{rel}} = \|\varrho_{ij} - \varrho_{ij}^{\text{TD}}\| / \|\varrho_{ij}^{\text{TD}}\|$ of the single-particle density matrix ϱ_{ij} obtained by the wavelet method with different bin sizes s for an ideal Bose gas, $U = 0$, system size $M = 12$, filling $n = N/M = 3$, in an equilibrium situation where $T_\ell = T$ and $\gamma_\ell = \gamma = 0.01J$ when compared to the equilibrium density matrix ϱ_{ij}^{TD} for (a) no trapping potential $V_i = 0$, (b) with trapping potential $V_i = 2J \cos(2\pi i/M)$.

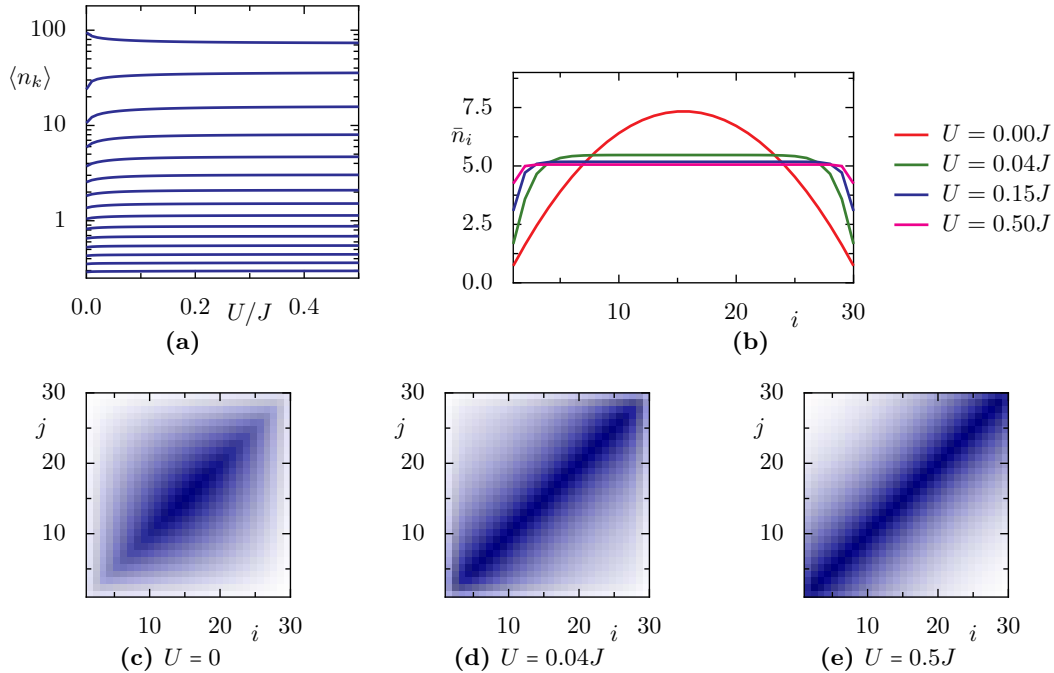


Figure 6.3.: (a) Eigenvalues $\langle n_k \rangle$ of the steady state single-particle density matrix as a function of interaction strength U for a gas of $n = N/M = 5$ particles per site, obtained by the wavelet method with $s = 2$, $T = J$, $\gamma = 0.05J$ for an open chain with $M = 30$ sites. (b) Corresponding real-space density profile \bar{n}_i and (c)-(e) full single-particle density matrix ρ_{ij} for some selected values of the interaction strength U .

Why the results without an external trapping potential $V_i = 0$, Fig. 6.2(a), are good, especially in the limit of high temperatures can be understood by calculating the resulting effective rates in the basis of the true eigenstates. In Appendix I, we show that for the case with bin size $s = 2$ and no trapping potential, these effective rates reproduce the first two orders of a high-temperature expansion (in powers of J/T) of the true rates in the true eigenbasis, i.e. the ones that appear in Eq. (6.3). We expect that similar correspondence is also found for increasing bin size s . On the other hand, we do not expect that the true rates are also reproduced by our wavelet method in higher orders of the high-temperature expansion, which is the reason why the error that we observe in Fig. 6.2(a) has its maximum around $T = J$. For temperatures in this regime, occupations of the depletion will have an error which stems from the contributions to the true rates that are on the order $(J/T)^2$ and that we do not reproduce with our wavelet method. At even lower temperatures, the occupations in the depletion get overall reduced and the resulting density matrix is again closer to the exact thermal density matrix. Also note that the calculation in Appendix I explicitly relies on the fact that the bath is ohmic. It seems that the semiclassical approximation as it is presented here only works for ohmic baths. We have experimented with other spectral densities (super-/subohmic, and constant) and generally we observe errors of the order of unity (not shown) when performing a similar comparison to thermal states as in Fig. 6.2. From our calculation in Appendix I, we observe the reason why the method only works for ohmic baths: in the resulting effective rates in the basis of the true eigenstates one can only

6. Weakly interacting Bose gases far from thermal equilibrium

recover a linear behavior in the spectral density $J(\varepsilon)$.

Remarkably, also in presence of a trapping potential $V_i = 2J \cos(2\pi i/M)$, Fig. 6.2(b), the result is very close to the thermal density matrix. Note that the steady state density matrix that we find is diagonal in the eigenstates of the potential and they are given the correct thermal weights even though in the evolution the dissipator is completely independent of these eigenstates. This is crucial for our aim to describe mean-field potentials, and we expect sensible results also in presence of finite mean-field interactions, $U \neq 0$.

In Figure 6.3, we present the resulting steady states of this method in the presence of mean-field interactions for the Bose-Hubbard system but with the slight modification of open boundary conditions, i.e. we break the periodicity in the sum over nearest neighbors in Eq. (6.1). In the semiclassical dissipator, Eq. (6.13), we therefore have to restrict the sum over j' such that it runs from 0 to $M - s$, because all other wavelets have contributions outside of the boundary. In contrast to the noninteracting system, we do not compare our results to exact thermal states, because exact diagonalization of the Bose-Hubbard Hamiltonian for $M = 30$ sites and $N = 150$ particles is numerically inaccessible. Figure 6.3(a) shows the eigenvalues $\langle n_k \rangle$ (note that the eigenstates k , or natural orbitals, depend on the interaction) of the single particle density matrix. In accordance with theoretical results [182–184] (for harmonic and box trapping potential) and experimental results [185] (for harmonic trapping potential) for interacting one-dimensional Bose gases, we observe that the condensate fraction decreases slightly with interaction strength U . In Figure 6.3(b) we show the steady-state density profile \bar{n}_i and in Fig. 6.3(c)-(f) the corresponding density matrices for some values of the interaction strength. Since the temperature T of the bath is fairly low, $T = J$, for the ideal gas, $U = 0$, about two third of the particles occupy the ground state and we observe its typical sinusoidal profile also in the thermal state density profile. For increasing interaction strength, we recover the typical behavior that is known from the Gross-Pitaevski equation (for $T = 0$; keep in mind that our theory might over-estimate interaction effects in this limit). Namely, in Thomas-Fermi approximation [7, 186] the density profile of the gas is given by the inverted profile of the trap, which means that for the box potential it is flat. This is true up to length scales of the healing length $\xi_h = \sqrt{J/Un}$ [187] on which the system reacts to variations of the potential, which leads to the behavior at the edges of the box. Note that a more detailed discussion of the validity of the states that we observe should be based on a comparison to extensions of the GPE to finite temperatures that have been developed in the literature [188–190]. Typically, Bogoliubov-de Gennes theories are used which divide the total gas into a condensed order-parameter field and a thermal cloud of Bogoliubov quasiparticles.

In conclusion, other than field-theoretic or hydrodynamic approaches to interacting Bose gases, our method is motivated by a microscopic description of the system and the action of the bath. The semiclassical treatment of the bath interaction provides efficient access to the full density matrix of thermal states with errors of a few percent only. This is true already for bin size $s = 2$, which we will use in the following. Note that our method is not limited to the decomposition ansatz, Eq. (6.7), of the four-point correlators σ_{kl}^{ij} . Similar as for the ideal Bose gas [83], we may also decompose only on the level of the six-point correlators into two- and four-point correlators and derive equations of

motion for those, both for the coherent and the dissipative evolution. We expect that such a treatment will describe fluctuations more precisely and thereby also resolve the problem of the occurrence of the factor 2 in the mean field potential for the canonical ensemble.

Our method is not limited to an equilibrium situation where the temperature of the individual baths are equal. Having gained confidence that the method is capable of producing plausible results for equilibrium states, we can now approach the nonequilibrium case. In the next section, we study nonequilibrium steady states in the ‘hot needle’ scenario that we introduced in Chapter 5, but in presence of weak interactions.

6.3. Nonequilibrium steady states: Hot-needle condensation in presence of weak interactions

While in equilibrium better approaches to study one-dimensional thermal Bose gases are available, this is not the case anymore when dealing with nonequilibrium systems in contact with more than one heat bath. Here we use the semiclassical wavelet method to shed some light on the question whether also in presence of weak interactions Bose condensation can be induced by a hot local bath, as we discussed in Chapter 5 for the ideal gas. Unfortunately, the hot-needle effect of a higher condensate fraction is more prominent at large system sizes M which are, despite the semiclassical approximation of the bath, still hard to reach numerically. Nevertheless, we show that also in presence of interactions, one can induce a condensate with a node at the ‘hot needle’ site.

Let us investigate the non-equilibrium situation, where in addition to the global bath environment, we couple a hot bath at temperature T_h at site ℓ , see sketch in Fig. 5.2(a), but with finite mean-field interaction U . In Figure 6.4 we show the same plots for the same parameters as in Figure 6.3 but in presence of a ‘hot needle’ at site $\ell = 10$. Note that different to Chapter 5, here we do not scale down the coupling to the environment $\gamma_i = \gamma$ with the root of the system size, but rather scale $\gamma_h \propto \sqrt{M}$. This leads to a slightly different notion of the coupling strength. This notion is reasonable, because here we do not perform the rotating wave approximation (in which γ is practically zero), so the strength of the coupling is relevant and can influence the steady state. It is unnatural to assume that the strength of the coupling to the global bath should depend on system size. But in order for the local drive to have the same magnitude as in Chapter 5, we scale up the coupling γ_h .

As we observe in Fig. 6.4 also for finite coupling strength $\gamma = 0.1J$, the noninteracting gas, $U = 0$, also shows the ‘hot needle’ effect. That is, the gas ‘avoids’ the strong inflow of heat by condensing in an excited state which has a node at the coupling site, which can clearly be observed in the density profile, Fig. 6.4(b), and in the amplitude of the condensed state, Fig. 6.4(f), which is the typical π/ℓ mode. Also the occupations in the condensate are slightly higher than in equilibrium, Fig. 6.3(a) for $U = 0$, which leads to an increase of coherence in the density matrix, Fig. 6.4(c). However, we observe that with increasing interaction the effect is reduced. This happens in three stages: There is a small regime $U \lesssim 0.05J$ where the hot-needle effect survives. Similar to thermal equilibrium, with mean-field interaction U the condensate fraction decreases. However, in the nonequilibrium steady

6. Weakly interacting Bose gases far from thermal equilibrium

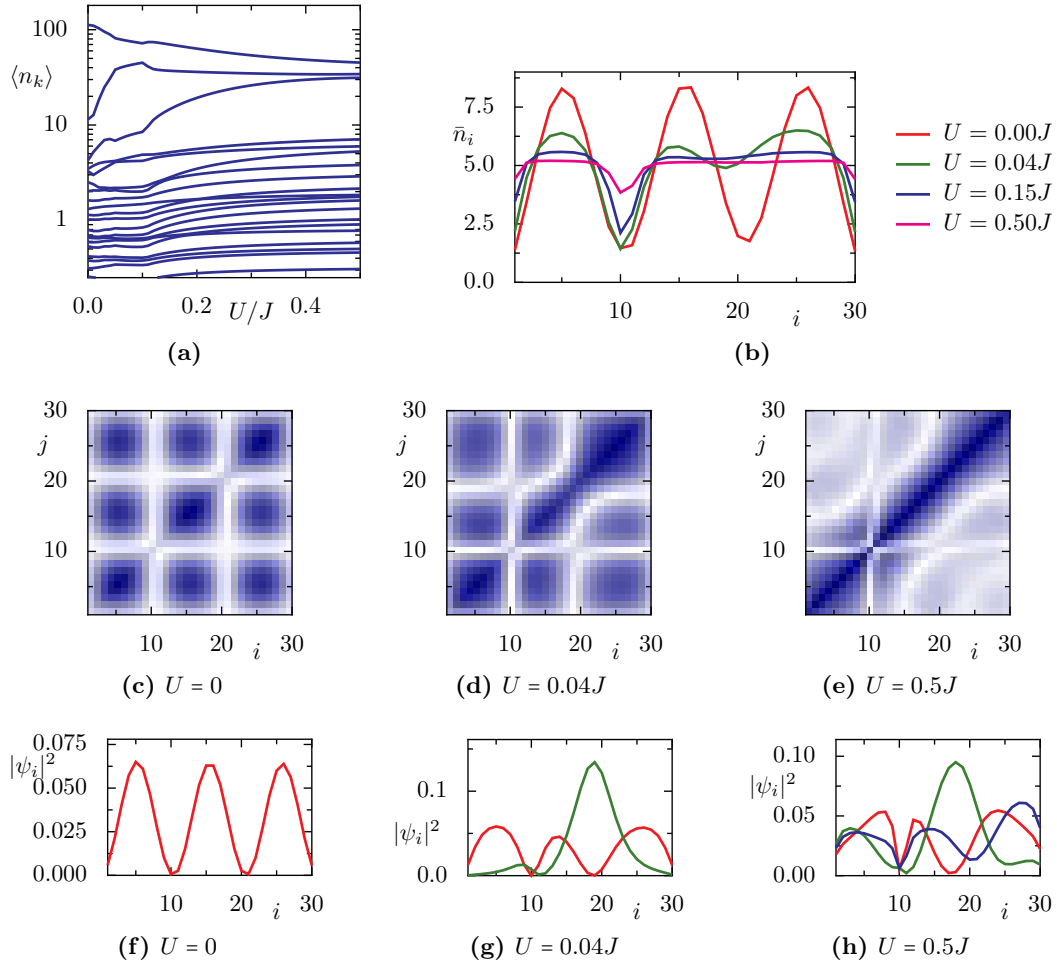


Figure 6.4.: (a)-(e) Same as in Fig. 6.3 but with a hot local bath with temperature $T_h = 25J$ at $\ell = 10$. Coupling strength is $\gamma_h = 0.2\gamma\sqrt{M}$. (f)-(h) Amplitude of the condensate(s) for the states in (c)-(e). Red is the condensate with largest occupation, green second largest, and blue third.

6.3. Nonequilibrium steady states: Hot-needle condensation in presence of weak interactions

state this drop is more severe since there is a second condensate emerging, which leads to the second regime $0.05J \lesssim U \lesssim 0.15J$.

Interestingly, in this second regime it seems that there are two condensates. Since for increasing repulsive interactions it becomes favorable that the density profile \bar{n}_i is flat, in equilibrium the shape of the condensate is flattened. In the driven system however, from Fig. 6.4(g) we observe that in this second phase the π/ℓ -like condensate (red line) has the highest occupation and differs only slightly from the noninteracting case. Instead of a flattening of this condensate, a second condensate emerges that localizes in the right well of the mean-field potential created by the first condensate, where there is no drive. This is surprising and means that in a nonequilibrium steady state, fragmented condensation can be switched on by varying the interaction strength. Also it is remarkable that fragmented condensation is found at all, because in the noninteracting case of the hot needle only phases with a single condensate (in the ground state or a decoupled state) are found.

Finally, in the third regime $U \gtrsim 0.15J$ there are three condensates. For increasing interaction strength, Fig. 6.4(h), the profile of the condensate with the highest occupation (red line) deviates more from the π/ℓ -shape and develops a relatively sharp node at the coupling site. The length scale on which the profile drops is on the order of the healing length ξ_h . Note that all three condensates have very little overlap with the coupling site also at relatively strong interactions, however coherence

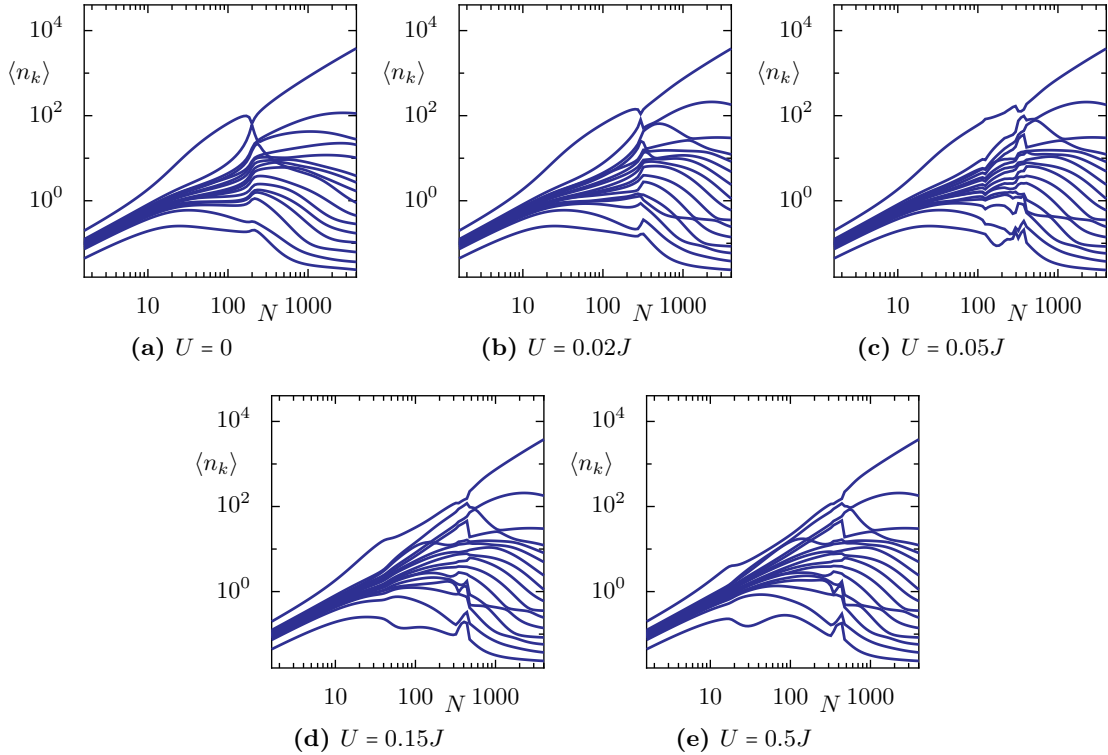


Figure 6.5.: Eigenvalues $\langle n_k \rangle$ of the single-particle density matrix as a function of total particle number N for the hot-needle setup with $M = 16$, $T = J$, $\ell = 4$, $T_h = 80J$, $\gamma = 0.02J$, $\gamma_h = 0.4\gamma\sqrt{M}$, calculated with the wavelet method and bin size $s = 2$ for different values of the mean-field interaction U .

6. Weakly interacting Bose gases far from thermal equilibrium

in the single-particle density matrix, Fig. 6.4(h), is reduced quite substantially when compared to the ideal gas, and also more dramatically than for the equilibrium system without the driving.

In Fig. 6.5 we plot the eigenvalues of the single-particle density matrix as a function of the total particle number N . Note that the parameters are different than in Fig. 6.4, because large particle numbers are very hard to reach numerically for system size $M = 30$. For the ideal gas, Fig. 6.5(a), also with our wavelet method, we observe the typical behavior as observed in Chapter 5, especially when comparing to Fig. 5.5(a). As discussed in Section 5.5, for intermediate particle numbers there is a condensate in the π/ℓ state that decouples from the needle, while there is a transition to ground-state condensation that is found in the limit $N \rightarrow \infty$. With increasing interaction U there are still two regimes found, where for intermediate numbers N the single-particle density matrices resemble the ones of the π/ℓ condensate and for large particle numbers similarity to a ground state condensate is found. The occupations $\langle n_k \rangle$ of the natural orbitals k however resemble the noninteracting case only

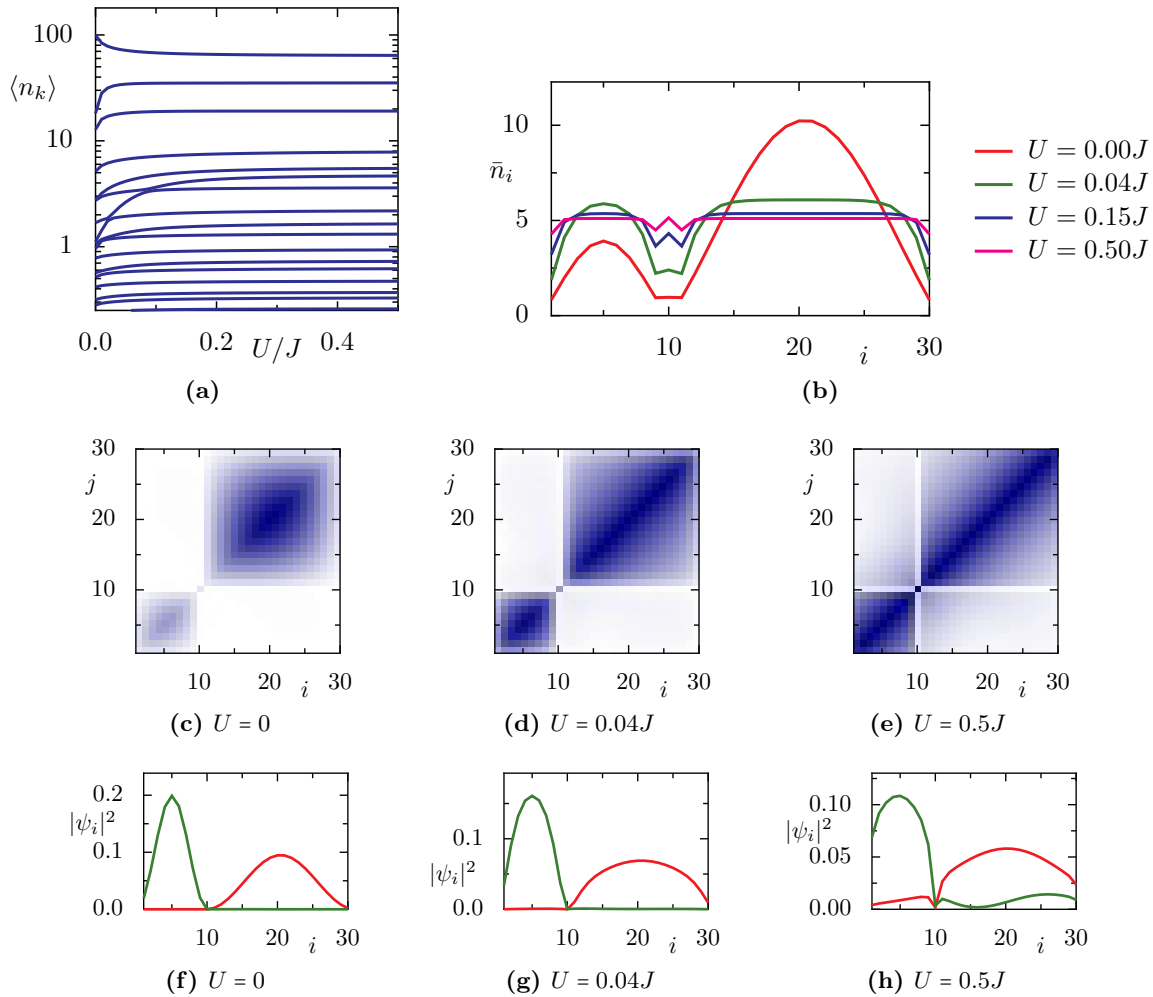


Figure 6.6.: Same as in Fig. 6.4 but with strong system-bath coupling $\gamma = 0.15J$ and a hot local bath with temperature $T_h = 40J$ at $\ell = 10$. Coupling strength is $\gamma_h = 0.6\gamma\sqrt{M}$. For such strong system-bath coupling the gas is essentially divided by the potential barrier due to the coupling at the driving site.

in the latter, ground-state like regime. The behavior in the intermediate regime is quite complicated and for larger U one might be able to identify more than a single condensate in this regime, but here the occupations of many of the states lie close.

A clear identification of condensates is expected for larger system size M . But larger system sizes are very hard to reach in the presence of interactions, since for large particle numbers a new timescale $\tau_{\text{int}} \propto 1/UN$ emerges in the coherent dynamics. Altogether, the dynamics happens on three time scales, since there are also the time scale of the noninteracting system $\tau_S \propto 1/J$ and the long time scale of relaxation $\tau_R \propto 1/\gamma^2$. For high particle numbers τ_{int} becomes very short which makes it difficult for the nonlinear solvers to find the steady state, which can easily take times that are on the order of 10^6 of τ_{int} (take for example $U = 0.1J$, $\gamma = 0.01J$, $N = 1000$) to emerge.

Allowing for larger γ however is not possible because then we would be far away from the weak coupling limit and already for the noninteracting system there is a back action of the coupling onto the system, which leads to the steady state density not being diagonal in the eigenstates of the system anymore. In Fig. 6.6 we show a typical example of the behavior in presence of a strong coupling to the environment. We observe that hot-needle-induced condensation is not found at strong coupling. Instead, the gas is divided by the hot local drive. Since the coupling strength γ_h is on the order of J , it provides a potential barrier that leads to the gas being expelled from the coupling site in the density profile, Fig. 6.6(b). Although the fact that the gas avoids the coupling site is reminiscent of the hot-needle effect, here, for the ideal gas, $U = 0$, coherence over the coupling site is almost destroyed and two separate condensates form that localize to the left and to the right of the coupling site, as can be observed from Fig. 6.6(c),(f). With increasing interaction U such a localization of particles becomes less favorable and some coherence between both sides is reestablished, cf. Fig. 6.6(e). Although the density profile, Fig. 6.6(b), shows that also the occupation at the driving site ℓ increases with the interaction strength, from Fig. 6.6(g),(f) we clearly see that both condensates retain a node at the coupling site, such that a strong inflow of heat from the hot bath is avoided. Hence, site ℓ is filled with particles from the depletion only.

6.4. Dynamics: Bistability in presence of local particle losses

In this section we are investigating a possible model for the bistability in a driven-dissipative superfluid that was observed in a recent experiment [91]. In this experiment, that is sketched in Fig. 6.7(a), a one-dimensional optical lattice is occupied with a weakly interacting Bose condensate with a few hundred atoms per site. Using a focused electron beam [192] the authors are able to engineer local single-particle loss in one of the wells. Then it is observed that there exists a regime of the loss rate γ_{loss} where the steady state depends on whether the driven site is full or empty in the initial state. While there are theoretical models using a discrete Gross-Pitaevski equation with local loss presented in Refs. [91, 191], the experimental behavior is reproduced only remotely. Neither the loss rate γ_{loss} where the bistable regime sets in, investigated in Ref. [91], nor the loss rate γ_{loss} where it ends, studied in Ref. [191], are correctly predicted by the GPE. Also, in the experiment a critical slowing down in

6. Weakly interacting Bose gases far from thermal equilibrium

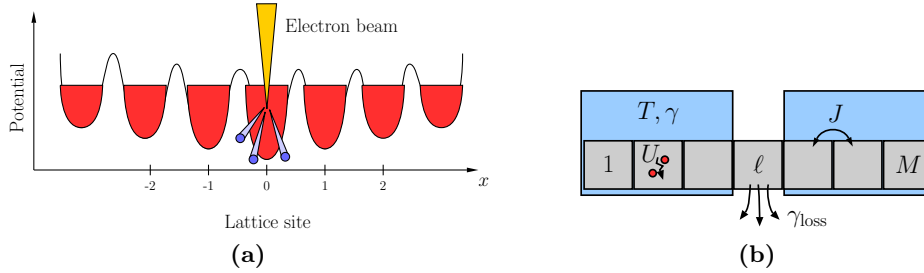


Figure 6.7.: (a) Sketch of the experiment by Labouvie et. al. [91] (following the sketch in Ref. [191]). A Bose condensate is loaded in a periodic potential with a wide trapping potential. The central site is irradiated with an electron beam which leads to single particle loss. (b) Sketch of the model: A one dimensional Bose-Hubbard chain with tunneling amplitude J and on-site interaction U undergoes single particle loss at site ℓ with a loss rate γ_{loss} . All sites but the central site are subject to a bath of temperature T which is coupled with strength γ to each individual site.

the bistable regime is observed which is not reproduced by the GPE [91].

We aim to investigate the setup with a simple microscopic model that also accounts for the incoherent processes leading to thermalization. As sketched in Fig. 6.7(b), we study the master equation

$$\partial_t \varrho = -i[H, \varrho] + \mathcal{D}_{\text{loss}}[\varrho] + \mathcal{D}_{\text{WL}}[\varrho] \quad (6.21)$$

with Bose-Hubbard Hamiltonian H , as in Eq. (6.1). We do not add a trapping potential, $V_i = 0$, and study the system with open boundary conditions. Additionally, there are two dissipative terms. The first term is a Lindblad term that corresponds to the particle loss with rate γ_{loss} at site ℓ

$$\mathcal{D}_{\text{loss}}[\varrho] = \gamma_{\text{loss}} \left(a_\ell \varrho a_\ell^\dagger - \frac{1}{2} \{a_\ell^\dagger a_\ell, \varrho\} \right). \quad (6.22)$$

Such a term has also been used in the GPE approaches [91, 191]. The second term \mathcal{D}_{WL} phenomenologically describes the thermalization (with the semiclassical wavelet method, Eq. (6.13)) that occurs due to incoherent scattering of the bosons in the individual wells. These incoherent processes are not captured by the mean-field interaction, which is why we add them by hand. From a one-boson perspective we may imagine that the particle in the well “sees” the coherent cloud and its thermal excitations that are described by Bogoliubov particles which for low energies are approximately phonons [193], and thus effectively provide a phononic bath to the particle. Similar ideas are also found in the literature [194], where it was found that the relaxation dynamics of an isolated (interacting) BEC can effectively be understood via a dynamical generation of heat baths of Bogoliubov quasiparticles. Also experimentally, thermalization has been observed in the refilling dynamics of the central site with temperatures T on the order of $3J$ [90]. Note that in our model, we do couple all sites to baths with equal strength, $\gamma_i = \gamma$, $i \neq \ell$, but not the driven site, $\gamma_\ell = 0$, because it is constantly emptied and cannot be expected to be described by local thermal equilibrium. A more refined theory might consider also the nonthermal distribution among the various levels on that site. In some cases, like in the limit of large γ_{loss} , as well as for initial states without atoms at site ℓ it will be unoccupied and thus there

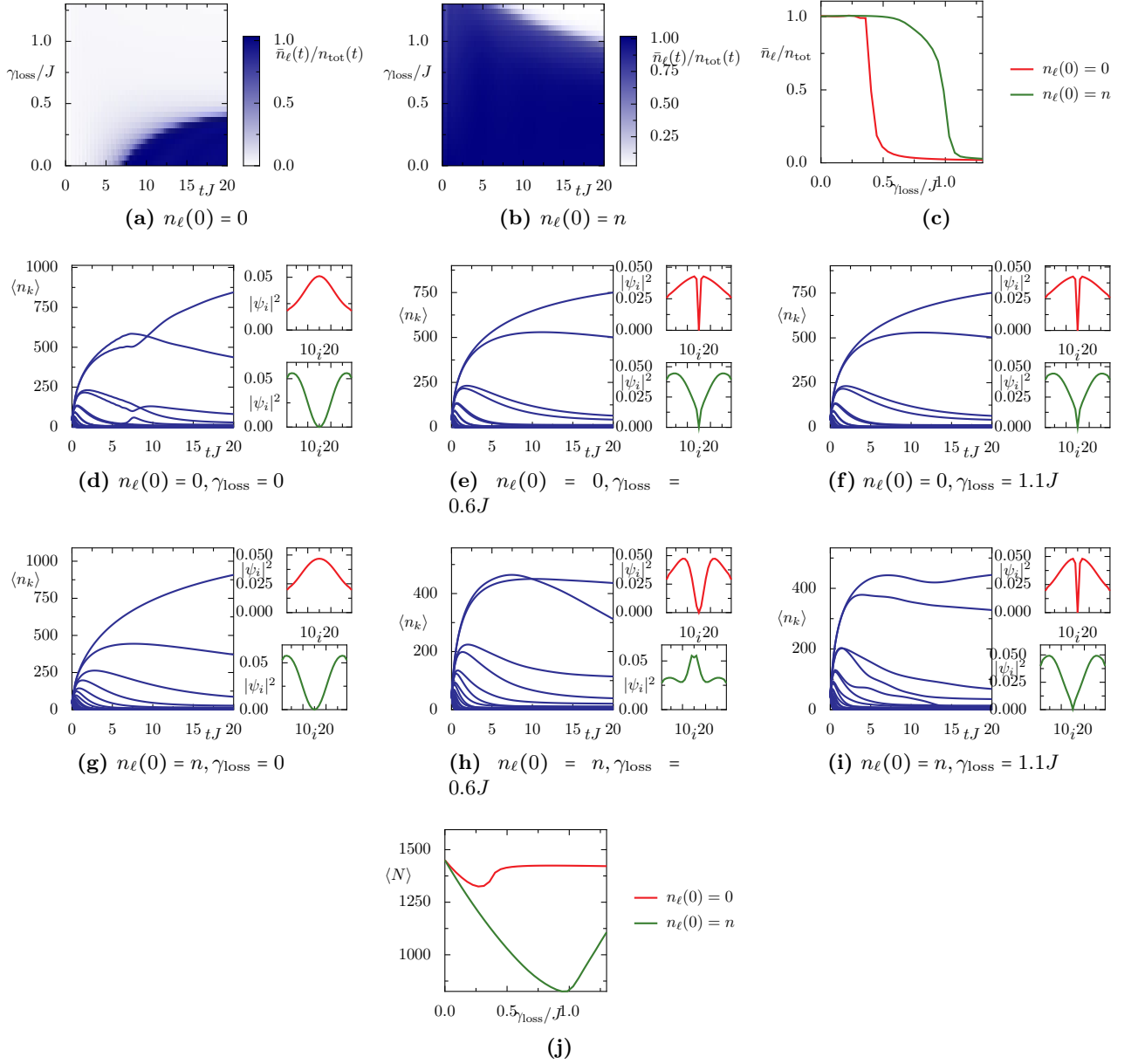


Figure 6.8.: Time evolution of the model, Fig. 6.7(b), with $M = 29$ sites, $\ell = 15$, $\gamma = 0.1J$, $U = 0.15J$ and $T = 3J$ and $n_{\text{init}} = 50$. (a), (b) Relative occupation (with respect to the time-dependent total density $n_{\text{tot}}(t)$ of bosons) of the driven site \bar{n}_ℓ as a function of time t for different values of the loss strength γ_{loss} for driving site that is initially (a) empty (b) full. (c) Occupation of the driven site at $t = 20/J$. Similar to Ref. [91] we observe a “bistable” regime where the system retains some memory of its initial state. (d)-(i) Instantaneous eigenvalues $\langle n_k \rangle$ of the single-particle density matrix ρ_{ij} as a function of t . We also show the amplitude $|\psi_i|^2$ of the orbital with the highest (red) and the second highest (green) occupation at $t = 20/J$. (j) Mean total number of particles $\langle N \rangle$ at $t = 20/J$.

6. Weakly interacting Bose gases far from thermal equilibrium

will be also no incoherent background present at this site.

In Fig. 6.8 we show a typical realization of the model for a system with $M = 29$ sites and bath temperature $T = 3J$, at relative strong coupling $\gamma = 0.1J$ which has also been observed experimentally [90]. Fig. 6.8(a) and (b) show the dynamics of the occupation number \bar{n}_ℓ of the driven site ℓ as a function of time and loss strength γ_{loss} for two kinds of initial state. Note that, in order to account for the overall particle losses, we show $\bar{n}_\ell(t)$ in relation to the overall density $n_{\text{tot}}(t) = \langle N \rangle(t)/M$ of the gas at that time t . The initial state in Fig. 6.8(b) is a uniformly filled classical state

$$\rho_{ij}(t=0) = n\delta_{ij}. \quad (6.23)$$

The initial state in Fig. 6.8(a) is an uniformly filled classical state with a vacancy in the driven site

$$\rho_{ij}(t=0) = n_i\delta_{ij} \text{ with } n_i = \begin{cases} 0, & i = \ell \\ n\frac{M}{M-1}, & \text{else} \end{cases}. \quad (6.24)$$

In Fig. 6.8(c) we show the relative filling $\bar{n}_\ell/n_{\text{tot}}$ of site ℓ in the long-time state at $t = 20/J$. The parameters are chosen such that there is some resemblance to the behavior that was reported in the experiment [91]. Namely, we observe that for intermediate values of γ_{loss} the filling \bar{n}_ℓ at $t = 20/J$ strongly depends on the initial state, i.e. if in the initial state the site was full (empty) it will have high (little) relative occupation in the long-time state.

This memory of the initial state is only found due to a finite interaction strength U as we observe in Fig. 6.9, where we repeat the plots from Fig. 6.8(a)-(c) with identical parameters, but $U = 0$. By comparing Fig. 6.9(a) and (b) we observe that the dynamics of the occupations is very similar and therefore memory of the initial state is lost after a short time of $t \approx 1/J$ already. An intuitive argument why the presence of interactions is required to see this bistability is the following: Let us consider the initial state with empty driving site first, Eq. (6.24). In the noninteracting case, a vacancy at the site ℓ will be filled by delocalizing the particles. In this process, energy of the order Jn is set free, which is first transformed to kinetic energy, and then at longer time scales damped into the bath. In presence of the interactions, however, when a particle is transferred from a neighboring site to the empty site ℓ an energy on the order Un^2 is set free, which cannot be absorbed as kinetic energy, so for large densities n the system is stuck and cannot fill site ℓ . It is of course only stuck up to the time

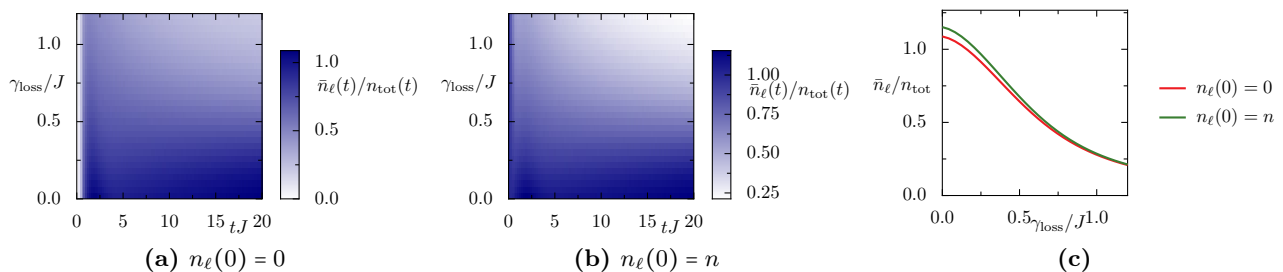


Figure 6.9.: Same as in Fig. 6.8(a)-(c) but for the noninteracting gas, $U = 0$.

scale of the bath relaxation, because the bath will eventually dissipate this energy. If some particles have entered the site already, this energetic discrepancy gets smaller and smaller, which leads then to a rapid filling up of the site as we observe nicely in Fig. 6.8(a) for $\gamma_{\text{loss}} = 0$. We have also varied the coupling strength γ to the bath and observe that the refilling time gets larger when γ is reduced (data not shown) which supports this hypothesis.

If now additionally the particle losses are ramped up, $\gamma_{\text{loss}} \neq 0$, particles that have entered site ℓ have an increasing probability of being removed again and a high energy mismatch persists. This leads to an increase in the time that is needed for the refilling to occur, as we observe in Fig. 6.8(a). Around $\gamma_{\text{loss}} \approx 0.5J$, for our parameters, it seems that this refilling time is shifted to infinity (which becomes more clear by looking at the dynamics at even later times, up to $t = 50/J$ in Fig. 6.10(a)) and the system is pinned to a steady state that has little occupation at the coupling site only. This can be observed Fig. 6.8(d)-(f) where we plot the eigenvalues of the single-particle density matrix as a function of time and the corresponding eigenstates at the latest time. As we see from Fig. 6.8(j), for states that have an initial vacancy, only around 10% of the total atoms are lost, which is also the case in the experiment [91].

If we turn to the dynamics with a site that is initially full, on the other hand, we see a particle loss that is much higher, up to about 50% Fig. 6.8(j). It seems that as soon as particles are lost, the driven site is refilled with particles rapidly which then are dissipated again. This is not observed in the experiment, where also for the state that is initially full only about 10% of the particles are lost. At later times, the total particle losses become even more severe, Fig. 6.10(d), and the true steady state of the system with an initially full site seems to have a vacancy at site ℓ above $\gamma_{\text{loss}} \approx 0.5J$ as well, Fig. 6.10(b) and (c), i.e. the region of bistability shrinks down until it vanishes. This can also be seen in the dynamics of the eigenvalues in Fig. 6.8(h). Even though the natural orbital with the

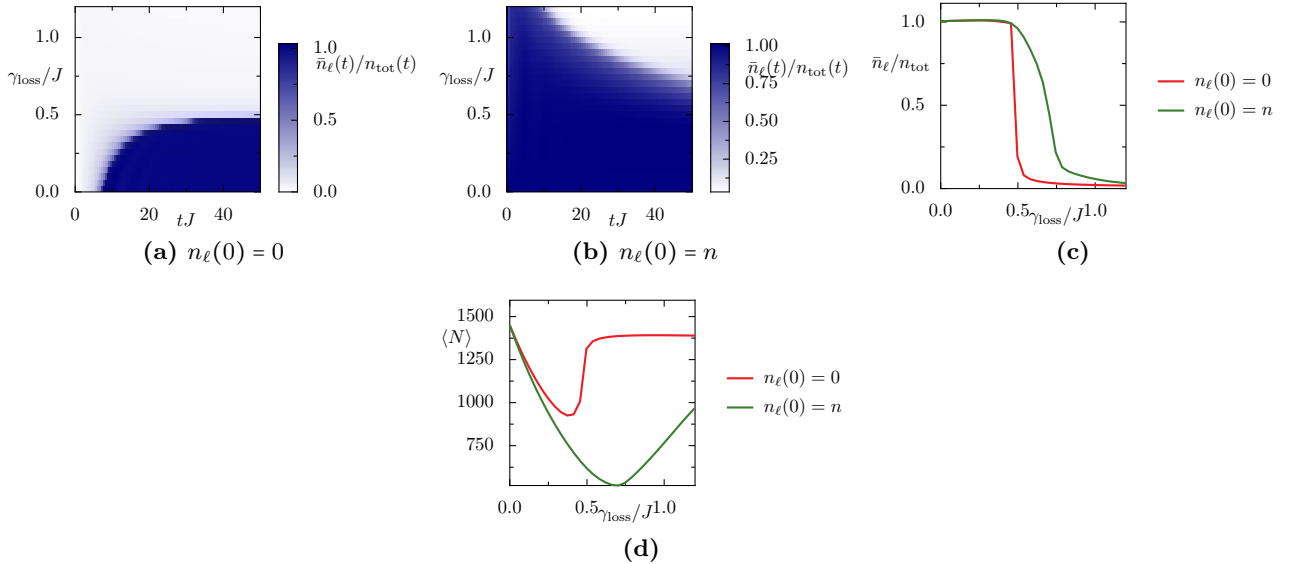


Figure 6.10.: Same as in Fig. 6.8(a)-(c), and (j) but for times up to $t = 50/J$.

6. Weakly interacting Bose gases far from thermal equilibrium

highest population has a node at the driven site, the relative occupation of the site is still close to unity because the natural orbital with the second largest occupation is such that it ‘fills’ the mean field potential of the first orbital and the resulting density profile is flat. This state however is subject to strong losses.

So while our model *could* provide an explanation for the behavior when the site is initially empty, the behavior when the site is initially full is such a true bistability in the steady state is not reproduced by the model. Nevertheless, there is some memory of the initial state for long times. One possible reason for the discrepancies could be that we have not taken into account that it was observed that the tunneling into the driven site depends on the filling of the driven site [90, 91], which could be implemented by using an occupation-dependent effective hopping rate $J(n_\ell)$ between site $\ell - 1$ and ℓ and site $\ell + 1$ and ℓ .

Similar to the data shown in Ref. [91], we may also show the phases as a function of the value of the tunneling J and the loss rate γ_{loss} . This is shown in Fig. 6.11 for parameters that give rise to a bistable regime that is quite similar to the observation in the experiment.

Let us make a final note that concerns our investigations on the interacting nonequilibrium steady states in Sec. 6.3. While for the rate equation equation describing the asymptotic dynamics of the noninteracting Bose gas, the uniqueness of the nonequilibrium steady state is guaranteed [82, 84], this is by no means clear for our interacting model. This could be another reason for the problems of convergence for the nonlinear solvers that we use to find the states in Sec. 6.3. Note that there we slowly ramp up the parameters (e.g. particle number or interaction strength), and use the ‘old’ steady state as an initial guess for the steady state at a new parameter. To find out whether the search for “the” steady state of the interacting hot needle setup is sensible at all, we should go back and study the dynamics of the model first (which unfortunately, due to a lack of time, we were not able to do in the scope of this thesis).

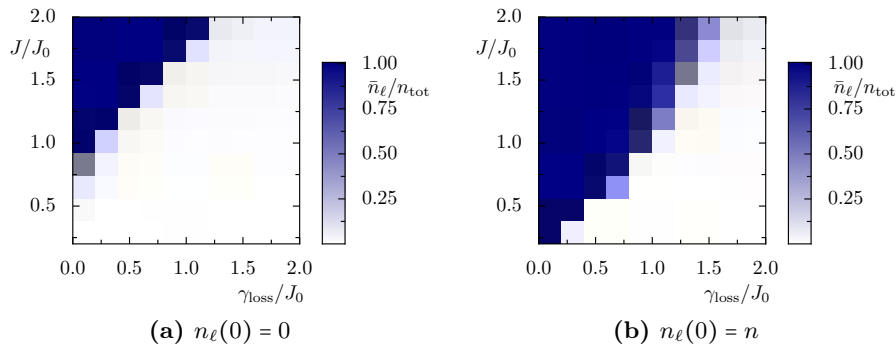


Figure 6.11.: Steady-state phase diagram of the relative filling of the driven site in the steady state (at $t = 20/J_0$) as a function of both hopping amplitude J and loss rate γ_{loss} for when the driven site is initially (a) empty and (b) full. Other parameters are $M = 29$, $l = 15$, $n = 50$, $\gamma = 0.1J_0$, $T = 3J_0$ as well as $U = 0.25J_0$.

7. Summary and outlook

In this thesis we have explored a whole variety of new possibilities for system- and state engineering that emerge due to the dissipative nature of driven open quantum systems.

First, we have investigated some of the challenges that occur when we want to generalize the concept of Floquet engineering to open quantum systems. Here we have focussed on the Markovian case, where the dynamics can be described with a time-periodic Lindblad operator. Similar to the Floquet Hamiltonian for the closed system, we ask whether there is an effective time-independent Lindblad generator, the Floquet Lindbladian, which gives rise to the stroboscopic dynamics. This generator basically follows from the logarithm of the dynamical map describing the one-cycle evolution. However, other than for the closed system, not all branches of the complex logarithm will give rise to a physical generator. For the qubit system that we use as a model, checking the branches is straightforward because they are labeled by a single integer. But for more complex models, the number of branches will scale with the dimensionality of the Hilbert space squared. It has even been proven that extracting the corresponding Lindbladian (if it exists) from a given CPTP map is a problem which is generally NP-hard [137, 195]. This problem is sometimes referred to as the *Markovianity problem*. Time-periodically driven open quantum systems with many degrees of freedom have already been studied e.g. in Ref. [135]. It is a very appealing question, if there are ways to avoid the Markovianity problem when trying to extract the Floquet Lindbladian in this situation. For example, in the high-frequency limit all candidate branches but the principle branch will scale linearly with frequency. If this limit is perturbative, the asymptotic Floquet Lindbladian can only be finite if it connects to the principle branch at high frequencies. An idea to find the right branch for the Floquet Lindbladian also at intermediate frequencies would be sweeping from high frequencies and keeping track of possible changes of branch. Also, recently it was shown that for classical fields that are described by a Langevin equation that is time-periodic [196], an effective time-independent Langevin equation can be found. As a result, in the classical limit the existence of the Floquet Lindbladian should always be guaranteed.

For the model system we show that (for all driving phases) the Floquet Lindbladian exists in extended regions around the adiabatic- (or low-frequency-), the diabatic (high-frequency-) limit, as well as in the limit of strong driving. A striking question is whether this also holds for more complex models (or even for all time-periodic Lindbladians). Finding answers seems especially hard since, e.g., we observe that the conventional high-frequency expansions are tools that must be used carefully. They produce a series expansion of the generator that, when cut-off at some order, can give rise to a non-physical generator even though the Floquet Lindbladian is guaranteed to exist. The reason is that the rates, i.e. the eigenvalues of the coefficient matrix of the dissipative term in the Lindblad

7. Summary and outlook

equation, can pick up terms that are higher than the order in which we perform the high-frequency expansion [100]. We show that this problem can be reduced, and a valid approximation to the Floquet Lindbladian may be found, by performing the high-frequency expansion in the rotating frame. Still, also in the rotating frame cutting off the expansion is in principle uncontrolled. Therefore, the hope is that in the future an alternative expansion can be developed which overcomes this problem by giving rise to a generator with rates that only have contributions on the order of the expansion.

The model system shows that the region where no Floquet Lindbladian exists can strongly depend on the driving phase. Even more, we have seen indications that there *could* be a phase-independent effective Lindbladian which exists for all parameters. The effective nonmarkovian phase could thus be due to the fact that for the open system the micromotion is a nonunitary rotation that rotates the effective Lindbladian into a generator that is not physical anymore. Future works should investigate the nontrivial role that is played by the micromotion in dissipative Floquet systems in more detail.

In the regime where no Floquet Lindbladian exists, we are able to find an effective evolution with a time-homogeneous exponential memory kernel for our model system. This opens up a completely new pathway for Floquet engineering: It suggests that effective nonmarkovian dynamics can be engineered in a setup where we only have Markovian channels at hand. However, as was noted in the literature [105], the so-achievable quantum channels are only a subset in the space of all nonmarkovian channels. It is thus by no means guaranteed that any given memory kernel can be “Floquet engineered”. Further investigation to classify the “engineerable” memory kernels is needed. Also the contrary question is completely open: Can any time-periodic Markovian channel effectively be mapped into an evolution with a time-homogeneous memory kernel? If so, is it always possible to use an exponential kernel?

The huge number of fundamental open questions confirms that the field of dissipative Floquet engineering has just started to evolve.

Furthermore, we have studied nonequilibrium steady states of ideal Bose gases that may exchange heat with their environment. First, we have turned to general considerations about the number M_S of Bose-selected states that are expected for driven ideal Bose gases in a system with a total of M states. The Bose-selected states are defined as those states whose occupations will not saturate in the limit of infinite particle number (while keeping all other parameters fixed). These selected states can be inferred from the (Pauli) rates for the quantum jumps between different single-particle states. We find that in some cases, like for rates that emerge from a discretization of some continuous function or in cases where the system is coupled to a few single-particle operators only (and the rates obey a product structure), indeed it is guaranteed that the number M_S of selected states is independent of the total number M of single-particle states. In these cases, (fragmented) condensation can be found in the nonequilibrium steady state, since each selected state may acquire a macroscopic occupation in the thermodynamic limit $M \rightarrow \infty$ at fixed particle density $n = N/M$. However, it will additionally depend on the specific model if (fragmented) Bose condensation is really found in the thermodynamic limit. To this end, the characteristic density n_c for when the system reaches the ultra-degenerate regime and condensation sets in must also saturate in the thermodynamic limit (which is not even the case for the hot needle, where for large M eventually the one-dimensional nature of the system is resolved and

n_c will grow linearly with M). Then, there are cases where we show that the number of selected states will scale with the total number of single-particle states, like for random rates or for time-periodically driven chaotic systems. Here the steady state will never feature an ordered phase, because also for large particle numbers the state looks essentially classical (from the viewpoint of quantum statistics), apart from the fact that a whole fraction of the states remains almost unpopulated. For the chaotic Floquet systems, we observe about three quarter of the states are Bose selected. This number is significantly higher number than half of the states, which is what is found for uncorrelated random rates. It means that there must be additional correlations in the rates. We present a naive model that gives rise to more than half of the states being selected, nevertheless future research should trace the origin of these correlations back to the kinetics of the model.

Our results provide one of the few examples where a relatively complete classification of nonequilibrium steady states in a given setup has been achieved. Based on these results a systematic study of the factors determining the number of Bose-selected states in suitable photonic systems should be possible. Bose selection is expected in systems where the dynamics is governed by the interplay of pumping, particle loss, and thermalization [62, 84]. As a result, Bose selection connects in some limits to Bose condensation while in other limits to lasing.

Then, we have shown that indeed the nonthermal statistics of nonequilibrium steady states can be used to engineer quantum many-body states with properties that are absent in the corresponding equilibrium state (i.e. if we would take away the driving): By using two heat reservoirs that both have a temperature that is well above the equilibrium condensation temperature, we find that in a (finite) one-dimensional ideal Bose gas high-temperature nonequilibrium condensation can be induced. Condensation occurs not only in the ground state, but for sufficiently strong driving also in excited single-particle states. We find that this effect is always found if one of the baths is very hot and there exists at least one single-particle state that couples only weakly to this bath. The basic intuition for why the effect occurs is that by condensing in a mode that couples only weakly to the hot bath, the system can avoid a strong inflow of heat. It should thus be applicable as a general strategy for the robust preparation of quantum degenerate nonequilibrium states. The fact that the system runs into a state that decouples from the drive has some similarity to the quantum Zeno effect [197]. Interestingly, even though the system is one dimensional, for intermediate system sizes the environmental temperature at which the system condenses is independent of the system size, much like in equilibrium in three dimensions. Only at large system sizes the true one-dimensional nature of the model is revealed. However, the corresponding length scale is a function of the driving parameters and thus in principle tunable.

This is in accordance with the findings for two-dimensional driven condensates, where on intermediate length scales algebraic correlations may be found, but on long scales correlations will always decay exponentially on a length scale that is set by the relation of pump- and loss rate [56]. Note that also in driven-dissipative Rydberg atoms, anomalously long-range correlations between Rydberg excitations have been observed in one dimension [198, 199], but later works have traced the physics back to the Hohenberg-Halperin Model A [99, 200–202], which rules out true long-range order in one dimension.

7. Summary and outlook

Also here the correlation length is governed by the relation between pump- and de-excitation rate. This asymptotic scaling of the correlation length with the ratio of pump- and loss rate (in our case of heat, not particles) holds also for our model of the hot needle, as we observe by solving the relevant equation not for the critical temperature T_c^{ne1} but for the critical system size M_c where Bose condensation breaks down. More detailed investigations should be made to clarify if and how the hot-needle effect relates to such similar observations of long-range order in nonequilibrium steady states, and whether common concepts for all of these systems can be developed.

Another intriguing question is whether the hot needle scenario can be implemented in an experimental setup. We have shown that the hot bath can also be replaced by a noisy Floquet drive, which might be easier to implement than a local bath for a cold atom experiment. We even expect that the physics is similar for noise that is not time-periodic. A hope is that the environmental bath could be realized by a cloud of atoms of another species [170]. To this end, bath models that provide a more realistic description for such situations should be considered. Also, we may think of an implementation in photonic systems, possibly in an array of pumped microcavities with one site being coupled to an additional reservoir. That steady states in a pumped polariton gas can in principle be described by a similar rate equation with thermal rates has been shown in Ref. [62].

Also the question of how finite system–bath coupling and weak interactions modify the hot-needle effect is crucial for any possible experiment. It has only been answered partially by our semiclassical theory and requires further investigations (even though we indeed have seen signatures of the effect for small system sizes). This semiclassical theory is necessary to overcome the problem that for interacting quantum many-body systems the spectrum and eigenstates of the full Hamiltonian are in most cases inaccessible. This is a problem if we want to find a microscopic description of the system in terms of a Born-Markov rate equation, where the bath induces jumps between the eigenstates at rates that depend on their energy difference. We develop a semiclassical way around this problem by defining localized wavelets with defined position and momentum for a Bose-Hubbard Hamiltonian. A thermal bath will drive transitions between all of these wavelets. We argue that the energy difference in these transitions is only due to their change in kinetic energy, because the wavelets are localized. We benchmark this method with thermal states and observe excellent agreement for high- and intermediate temperatures. Our method only applies to ohmic baths, whether a similar description can also be found for other spectral densities is a question that remains open.

The semiclassical method is a promising tool to describe steady states of interacting systems within a mean-field approximation both in the hot needle setup as well as in setups where we observe Bose selection for the ideal gas. Still, also within this method, mean-field interacting nonequilibrium steady states are extremely hard to compute numerically. This is a consequence of the fact that the dynamics happens on three time scales, which may differ in several orders of magnitude: because the system–bath coupling should be weak, relaxation happens on extremely long time scales, while the time scale of the mean-field interaction gets shorter as we add more particles to the system. New ideas (at least from a numerical perspective) are required to overcome this problem.

Finally, we have used this method to study the dynamics of a Bose Hubbard system that is both

coupled to a thermal bath and also subject to local single-particle losses. This model is motivated by a recent quantum gas experiment [91], where a focused electron beam was used to engineer local particle losses, and interesting nonequilibrium steady states in weakly interacting Bose gases were observed. For intermediate times, in the presence of mean-field interactions, we observe a bistability that shares some similarities with the behavior that was observed in the experiment. Nevertheless, the long-time behavior is not truly bistable and there are no signatures of a critical slowing down as was observed in the experiment. Thus, the hope is that the model can be refined in order to account for example for the internal structure of the lattice sites. Still, the idea of describing isolated interacting Bose gases with the help of an artificial bath environment in order to model for the incoherent thermalization processes (that are in our case due to a suspected formation of a reservoir of Bogoliubov quasiparticles) seems quite promising. To find a rigid description of the thermalization dynamics, it might however be necessary to consider also a time-dependence of the temperature and the coupling strength of the artificial bath.

Appendix

A. Extracting Hamiltonian and Lindblad operators from a Lindbladian generator matrix

In the region where the Floquet Lindbladian \mathcal{L}_F exists, we can extract its components, that are a time-independent effective Hamiltonian H_F and a set of effective jump operators $\{L_i\}$. Here we describe a general procedure to extract these quantities.

To this end, we use the fact that any Lindbladian may be represented in the form [112]

$$\mathcal{L}(\varrho) = \varphi(\varrho) - \kappa\varrho - \varrho\kappa^\dagger, \quad (\text{A.1})$$

where $\kappa \in \mathbb{C}^{n \times n}$ and φ is a completely positive map with $\varphi^*(\mathbb{1}) = \kappa + \kappa^\dagger$. Then, iH_F is given by the antihermitian part of κ , $iH_F = \frac{1}{2}(\kappa - \kappa^\dagger)$, and the Lindblad operators are the Kraus operators of φ , $\varphi(\cdot) = \sum_i L_i \cdot L_i^\dagger$.

Now we may use that in the Basis $B = (|\Omega\rangle, \dots)$, where $|\Omega\rangle \in \mathbb{C}^n \otimes \mathbb{C}^n$ is a maximally entangled state, the Choi matrix of \mathcal{L} has the structure

$$\mathcal{L}^\Gamma = (\mathcal{L} \otimes \text{id})(|\Omega\rangle\langle\Omega|) = \underbrace{\begin{pmatrix} 0 & 0 & 0 & 0 & \dots \\ 0 & \bullet & \bullet & \bullet & \\ 0 & \bullet & \bullet & \bullet & \\ 0 & \bullet & \bullet & \bullet & \\ \dots & & & & \end{pmatrix}}_{\varphi^\Gamma} + \underbrace{\begin{pmatrix} a & b^* & c^* & d^* & \dots \\ b & 0 & 0 & 0 & \\ c & 0 & 0 & 0 & \\ d & 0 & 0 & 0 & \\ \dots & & & & \end{pmatrix}}_{-(\kappa + \kappa^\dagger)^\Gamma}. \quad (\text{A.2})$$

This allows for the direct identification of κ and thus the Hamiltonian (up to a global shift of the energies).

For a two-level system, the above representation can be rewritten in the Bell basis $B = (|\Omega\rangle, |\Sigma\rangle, |\Gamma\rangle, |\Lambda\rangle)$, with $|\Omega/\Sigma\rangle = \frac{1}{\sqrt{2}}(|00\rangle \pm |11\rangle)$, $|\Gamma/\Lambda\rangle = \frac{1}{\sqrt{2}}(|01\rangle \pm |10\rangle)$. This yields

$$H_F = \frac{1}{2} \begin{pmatrix} -\text{Im}(b) & -\text{Im}(c) + i \text{Re}(d) \\ -\text{Im}(c) - i \text{Re}(d) & \text{Im}(b) \end{pmatrix}. \quad (\text{A.3})$$

Since \mathcal{L}_F exists, we know that φ^Γ is positive semi-definite and we can bring it to the form $\varphi^\Gamma = \sum_i v_i v_i^\dagger$

with vectors $v_i = (0, v_{i2}, v_{i3}, \dots)$. Note that these vectors are already the representation of the Lindblad operators L_i in the sense that $|v_i\rangle = (L_i \otimes \text{id})|\Omega\rangle$. For a two-level system we therefore find

$$L_i = \frac{1}{\sqrt{2}} \begin{pmatrix} v_{i2} & v_{i3} + v_{i4} \\ v_{i3} - v_{i4} & -v_{i2} \end{pmatrix}. \quad (\text{A.4})$$

B. Construction of an effective memory kernel

Here, we discuss technical details of the construction of the memory kernel in Section 3.3.

B.1. Characteristic decay function of exponential kernel

In Section 3.3, we show that with a special choice of the spectral decomposition of the Kernel Lindbladian \mathcal{L}_K the problem of engineering an effective evolution with a time-homogeneous memory kernel can be reduced to solving a scalar integro-differential equation for the characteristic decay functions $h_a(t)$. Here we solve this equation.

The equation (3.29)

$$\partial_t h_a(t) = \int_0^t d\tau e^{\Gamma(\tau-t)} \lambda_a^K h_a(\tau) \quad (\text{B.1})$$

(we set $\Gamma = 1/\tau_{\text{mem}}$ for convenience) can be transformed into a second order differential equation, by taking its derivative,

$$\partial_t^2 h_a(t) = -\Gamma \int_0^t d\tau e^{-\Gamma(t-\tau)} \lambda_a^K h_a(\tau) + e^{-\Gamma t} e^{+\Gamma t} \lambda_a^K h_a(t) \quad (\text{B.2})$$

$$= -\Gamma \partial_t h_a(t) + \lambda_a^K h_a(t), \quad (\text{B.3})$$

where additionally we have to satisfy the boundary conditions $h_a(0) = 1$, $\partial h_a(t)|_{t=0} = 0$ [by setting $t = 0$ in Eq. (B.1)].

This homogeneous second order differential equation can be solved by exponential ansatz

$$h_a(t) = e^{\mu_a t} \quad (\text{B.4})$$

which leads to the characteristic polynomial

$$(\mu_a^2 + \Gamma \mu_a - \lambda_a^K) h_a(t) = 0 \quad (\text{B.5})$$

which is solved by

$$\mu_a^\pm = -\Gamma/2 \pm \Gamma_a \quad (\text{B.6})$$

with the complex root $\Gamma_a = \sqrt{\Gamma^2/4 + \lambda_a^K}$. So the general solution takes the form

$$h_a(t) = e^{-\Gamma t/2} (\alpha e^{\Gamma_a t} + \beta e^{-\Gamma_a t}) \quad (\text{B.7})$$

By imposing $h_a(0) = 1$, $\partial h_a(t)|_{t=0} = 0$ we find

$$\alpha + \beta = 1, \quad \text{and} \quad -\frac{\Gamma}{2}(\alpha + \beta) + \Gamma_a(\alpha - \beta) = 0. \quad (\text{B.8})$$

This we can solve for

$$2\alpha = 1 + \frac{\Gamma}{2\Gamma_a} \quad (\text{B.9})$$

and finally get

$$h_a(t) = e^{-\Gamma t/2} \left[\frac{1}{2} (e^{\Gamma_a t} + e^{-\Gamma_a t}) + \frac{\Gamma}{4\Gamma_a} (e^{\Gamma_a t} - e^{-\Gamma_a t}) \right]. \quad (\text{B.10})$$

B.2. Numerically stable procedure to find eigenvalues of \mathcal{L}_K

By setting $\mathcal{P}(T) = \sum_a \lambda_a P_a \equiv \tilde{\mathcal{P}}(T) = \sum_a h_a(T) P_a$ we require that the kernel evolution coincides stroboscopically with the dynamical map. Nevertheless, solving the nonlinear equation $h_a(T) = \lambda_a$ for λ_a^K can in general not be performed analytically. Here we present a numerically stable to obtain these eigenvalues λ_a^K .

For the steady state subspace, $\lambda_a = 1$, we directly infer that $\lambda_a^K = 0$ is a solution. Note that one eigenvalue 0 is required, since $\mathcal{L}_K(\Gamma)$ has to be a valid generator and thus obey the form

$$\mathcal{L}_K[\cdot] = 0 \cdot P_{SS}[\cdot] + \sum_r \lambda_r^K P_r[\cdot] + \sum_c (\lambda_c^K P_c[\cdot] + \bar{\lambda}_c^K P_{\bar{c}}[\cdot]) \quad (\text{B.11})$$

with real eigenvalues λ_r^K and pairs of complex conjugated eigenvalues $\lambda_c^K, \bar{\lambda}_c^K$. One way to determine the remaining λ_a^K would be to use a numerical root finding algorithm. However, the stroboscopic identity $h_a(T) = \lambda_a$ has generally infinitely many solutions in the complex plane, and a root finding algorithm can converge into solutions with large imaginary part (which generally yields a \mathcal{L}_K that is not a valid generator; similar to the Markovian case we suspect that high branches do not give a valid generator anymore).

A numerical way around this is expanding the equation in a power series, then cutting it off at some index, so we have a polynomial equation, where all roots of the polynomial can be evaluated from the numerics. Rewriting $h_a(T) = \lambda_a$ in a power series gives

$$\sum_{n=0}^{\infty} \left(\frac{(\Gamma_a T)^{2n}}{(2n)!} + \frac{\Gamma}{4\Gamma_a} \frac{(\Gamma_a T)^{2n+1}}{(2n+1)!} \right) = \lambda_a e^{\Gamma T/2}, \quad (\text{B.12})$$

and using the definition of Γ_a we find

$$\sum_{n=0}^{\infty} (\Gamma^2/4 + \lambda_a^K)^n T^{2n} \left(\frac{1}{(2n)!} + \frac{\Gamma}{4} \frac{T}{(2n+1)!} \right) = \lambda_a e^{\Gamma T/2}, \quad (\text{B.13})$$

where numerically, we cut off the power series at some index n_0 , solve for all solutions $z = \Gamma^2/4 + \lambda_a^K$, and then regain all possible $\lambda_a^K = z - \Gamma^2/4$. By this we again find infinitely many candidates for \mathcal{L}_K . For the case where λ_a is real of course we only may take the one root z where λ_a^K is real, but for the complex pair λ_c^K there is no restriction apart from them occurring in a pair, so we can choose any complex solution λ_c^K . However only for solutions with a small absolute value, we may cut off the sum at index n_0 . In order to avoid inaccuracies, we thus restrict ourselves to a few solutions λ_c^K with small imaginary part. Still, for the two-level system one can always find a parameter Γ such that a valid kernel evolution exists and we observe that in most cases it suffices to consider the solution λ_c^K with the smallest imaginary part.

C. Discrepancy to the Magnus expansions presented in the literature

We discuss a discrepancy in the general expressions of the second order of the Magnus expansion (in terms of the Fourier components of the generator) that are presented in Refs. [100, 136]. One should therefore be cautious when using these expressions .

As it was shown in the literature [100, 136], by plugging the Fourier expansion, Eq. (3.32), into the conventional Magnus expansion [131] one finds on the lowest orders

$$\mathcal{K}^{(0)} = \mathcal{L}_0, \quad (\text{C.1})$$

$$\mathcal{K}^{(1)} = \sum_{n=1}^{\infty} \frac{[\mathcal{L}_n, \mathcal{L}_{-n}] + [\mathcal{L}_0, \mathcal{L}_n - \mathcal{L}_{-n}]}{n}. \quad (\text{C.2})$$

However on the order $1/\omega^2$ there is a discrepancy between the results in the different works. In Ref. [100] it is presented

$$\begin{aligned} \mathcal{K}_{\text{FCM}}^{(2)} = & \sum_{n \neq 0} \sum_{m \neq 0} \left(\frac{[[\mathcal{L}_n, \mathcal{L}_{-n}], \mathcal{L}_m]}{2nm} - \frac{[\mathcal{L}_n, [\mathcal{L}_m, \mathcal{L}_{-n-m}]]}{3nm} \right) - \sum_{n \neq 0} \sum_{m \neq 0, m \neq n} \frac{[\mathcal{L}_n, [\mathcal{L}_0, \mathcal{L}_m]]}{2nm} \\ & + \sum_{n=1}^{\infty} \sum_{m \neq 0, m \neq -n} \frac{[[\mathcal{L}_n, \mathcal{L}_m] + [\mathcal{L}_{-n}, \mathcal{L}_{-m}], \mathcal{L}_0]}{2n(n+m)}, \end{aligned} \quad (\text{C.3})$$

while in Ref. [136] it was found

$$\begin{aligned} \mathcal{K}_{\text{LMV}}^{(2)} = & - \sum_{n \neq 0} \sum_{m \neq 0} \left(\frac{[\mathcal{L}_m, [\mathcal{L}_{-m}, \mathcal{L}_n]]}{nm} + \frac{[\mathcal{L}_m, [\mathcal{L}_n, \mathcal{L}_0]]}{2nm} \right) - \sum_{n \neq 0} \sum_{m \neq 0, m \neq n} \frac{[\mathcal{L}_m, [\mathcal{L}_{n-m}, \mathcal{L}_{-n}]]}{3nm} \\ & + \sum_{n \neq 0} \left(\frac{[\mathcal{L}_0, [\mathcal{L}_0, \mathcal{L}_n]]}{2n^2} - \frac{[\mathcal{L}_n, [\mathcal{L}_0, \mathcal{L}_{-n}]]}{2n^2} \right), \end{aligned} \quad (\text{C.4})$$

where we have adapted the expression to our notation for the dissipative Floquet system. Here, by $n \neq 0$ we denote the sum over $n \in \mathbb{Z} \setminus \{0\}$.

Note that with these expressions for our qubit model with $\varphi = 0$ we find

$$\mathcal{K}_{\text{FCM}}^{(2)} = [\mathcal{L}_0, [\mathcal{L}_0, \mathcal{L}_1]] + \frac{1}{3} [\mathcal{L}_1, [\mathcal{L}_0, \mathcal{L}_1]], \quad (\text{C.5})$$

$$\mathcal{K}_{\text{LMV}}^{(2)} = [\mathcal{L}_0, [\mathcal{L}_0, \mathcal{L}_1]] - [\mathcal{L}_1, [\mathcal{L}_0, \mathcal{L}_1]], \quad (\text{C.6})$$

which differ by the prefactors of both terms from the direct calculation

$$\mathcal{K}^{(2)} = 2[\mathcal{L}_0, [\mathcal{L}_0, \mathcal{L}_1]] - [\mathcal{L}_1, [\mathcal{L}_0, \mathcal{L}_1]]. \quad (\text{C.7})$$

This is worrisome because the result of the direct calculation was obtained in the same way, but for a special choice of the driving, so in principle all expressions should coincide.

However, in Ref. [136] another expression for the second order term is presented. This expression was obtained by performing the van-Vleck-type Floquet-Magnus expansion, yielding an effective Hamiltonian/generator in the rotated basis (the basis rotation D_F is unitary, if the dynamics is coherent)

$$\Lambda(t) = D_F e^{\bar{\mathcal{L}}_F t} D_F^{-1} \equiv e^{\mathcal{L}_F t}. \quad (\text{C.8})$$

The Floquet Lindbladian \mathcal{L}_F can then be obtained in second order in $1/\omega$ by finding $\bar{\mathcal{L}}_F$ up to second order combined with the second order of the expansion of the rotation matrix

$$D_F = \exp \left[i(S^{(1)}/\omega + S^{(2)}/\omega^2) \right]. \quad (\text{C.9})$$

With this identification it is found

$$\mathcal{K}^{(0)'} = \mathcal{K}^{(0)}, \quad \mathcal{K}^{(1)'} = \mathcal{K}^{(1)}, \quad \mathcal{K}_{\text{LMV}}^{(2)'} = \mathcal{K}_{\text{LMV}}^{(2)} - \sum_{n \neq 0} \sum_{m \neq 0} \frac{[\mathcal{L}_0, [\mathcal{L}_m, \mathcal{L}_{n-m}]]}{nm} \quad (\text{C.10})$$

and argued that the difference between the both expressions is due to approximations in the derivation of the van-Vleck expansion [136].

Interestingly, in our case of the driven qubit, by calculating

$$\mathcal{K}_{\text{LMV}}^{(2)'} = 2[\mathcal{L}_0, [\mathcal{L}_0, \mathcal{L}_1]] - [\mathcal{L}_1, [\mathcal{L}_0, \mathcal{L}_1]] \quad (\text{C.11})$$

we recover the expression in Eq. (C.7) that we found by directly performing the conventional Magnus expansion. We therefore expect that there could be a small error in the direct derivation of $\mathcal{K}_{\text{LMV}}^{(2)}$ via the Magnus expansion and that it maybe also holds that $\mathcal{K}_{\text{LMV}}^{(2)} = \mathcal{K}_{\text{LMV}}^{(2)'}$.

As a result, the only expression that could be correct is $\mathcal{K}_{\text{LMV}}^{(2)'}$.

D. Commutator of two general qubit Lindblad superoperators

Given are two arbitrary Lindbladians $\mathcal{L}^{(1)}$ and $\mathcal{L}^{(2)}$ for a qubit system. We find a general expression for their commutator.

The Lindbladians $\mathcal{L}^{(1)}$ and $\mathcal{L}^{(2)}$ can be represented as

$$\mathcal{L}^{(i)} = -i[H^{(i)}, \cdot] + \sum_{nm} d_{nm}^{(i)} \left(\sigma_n \cdot \sigma_m - \frac{1}{2} \{ \sigma_m \sigma_n, \cdot \} \right), \quad (\text{D.1})$$

where the indices n, m in the following run over 1, 2, 3. Their commutator therefore reads

$$\begin{aligned} [\mathcal{L}^{(1)}, \mathcal{L}^{(2)}] &= -[H^{(1)}, [H^{(2)}, \cdot]] + [H^{(2)}, [H^{(1)}, \cdot]] \\ &\quad - i \sum_{nm} d_{nm}^{(1)} \left(\sigma_n [H^{(2)}, \cdot] \sigma_m - \frac{1}{2} \{ \sigma_m \sigma_n, [H^{(2)}, \cdot] \} - [H^{(2)}, \sigma_n \cdot \sigma_m] + \frac{1}{2} [H^{(2)}, \{ \sigma_m \sigma_n, \cdot \}] \right) \\ &\quad + i \sum_{nm} d_{nm}^{(2)} \left(\sigma_n [H^{(1)}, \cdot] \sigma_m - \frac{1}{2} \{ \sigma_m \sigma_n, [H^{(1)}, \cdot] \} - [H^{(1)}, \sigma_n \cdot \sigma_m] + \frac{1}{2} [H^{(1)}, \{ \sigma_m \sigma_n, \cdot \}] \right) \\ &\quad + \sum_{nm,kl} (d_{nm}^{(1)} d_{kl}^{(2)} - d_{kl}^{(1)} d_{nm}^{(2)}) \left[\sigma_n \left(\sigma_k \cdot \sigma_l - \frac{1}{2} \{ \sigma_l \sigma_k, \cdot \} \right) \sigma_m - \frac{1}{2} \left\{ \sigma_m \sigma_n, \sigma_k \cdot \sigma_l - \frac{1}{2} \{ \sigma_l \sigma_k, \cdot \} \right\} \right]. \end{aligned} \quad (\text{D.2})$$

This can be simplified to read

$$\begin{aligned} [\mathcal{L}^{(1)}, \mathcal{L}^{(2)}] &= -i[H^{\text{coh}}, \cdot] + i \sum_{nm} d_{nm}^{(1)} \left([H^{(2)}, \sigma_n] \cdot \sigma_m + \sigma_n \cdot [H^{(2)}, \sigma_m] - \frac{1}{2} \{ [H^{(2)}, \sigma_m \sigma_n], \cdot \} \right) \\ &\quad - i \sum_{nm} d_{nm}^{(2)} \left([H^{(1)}, \sigma_n] \cdot \sigma_m + \sigma_n \cdot [H^{(1)}, \sigma_m] - \frac{1}{2} \{ [H^{(1)}, \sigma_m \sigma_n], \cdot \} \right) \\ &\quad + \sum_{nm,kl} (d_{nm}^{(1)} d_{kl}^{(2)} - d_{kl}^{(1)} d_{nm}^{(2)}) \left[\sigma_n \left(\sigma_k \cdot \sigma_l - \frac{1}{2} \{ \sigma_l \sigma_k, \cdot \} \right) \sigma_m - \frac{1}{2} \left\{ \sigma_m \sigma_n, \sigma_k \cdot \sigma_l - \frac{1}{2} \{ \sigma_l \sigma_k, \cdot \} \right\} \right]. \end{aligned} \quad (\text{D.3})$$

with resulting Hamiltonian due to the coherent parts

$$H^{\text{coh}} = -i[H^{(1)}, H^{(2)}] = 2 \sum_{kql} \varepsilon_{kql} h_k^{(1)} h_q^{(2)} \sigma_l. \quad (\text{D.4})$$

In the last step we have represented the Hamiltonians in the Pauli basis,

$$H^{(i)} = h_0^{(i)} \mathbb{1} + \sum_k h_k^{(i)} \sigma_k. \quad (\text{D.5})$$

Note that the first and second line of Eq. (D.3) are already in Lindblad form. The third line, however,

needs more work, but one can show that it can be brought to Lindblad form

$$\sum_{nm,kl} (d_{nm}^{(1)}d_{kl}^{(2)} - d_{kl}^{(1)}d_{nm}^{(2)}) \left[\sigma_n \left(\sigma_k \cdot \sigma_l - \frac{1}{2} \{ \sigma_l \sigma_k, \cdot \} \right) \sigma_m - \frac{1}{2} \left\{ \sigma_m \sigma_n, \sigma_k \cdot \sigma_l - \frac{1}{2} \{ \sigma_l \sigma_k, \cdot \} \right\} \right] \quad (\text{D.6})$$

$$= -i \left[H^{\text{diss}}, \cdot \right] + \sum_{mn} d_{mn}^{\text{diss}} \left(\sigma_m \cdot \sigma_n - \frac{1}{2} \{ \sigma_m \sigma_n, \cdot \} \right) \quad (\text{D.7})$$

with resulting hamiltonian due to the dissipative parts,

$$H^{\text{diss}} = -2 \sum_{nmkq} \varepsilon_{nmq} \text{Re}(d_{nk}^{(1)}) \text{Re}(d_{mk}^{(2)}) \sigma_q, \quad (\text{D.8})$$

as well as

$$d_{nm}^{\text{diss}} = 2i \sum_k \text{Im}(d_{nk}^{(1)}d_{mk}^{(2)} - d_{mk}^{(1)}d_{nk}^{(2)}). \quad (\text{D.9})$$

Therefore, in total the commutator reads

$$\left[\mathcal{L}^{(1)}, \mathcal{L}^{(2)} \right] = -i \left[H^{\text{coh}} + H^{\text{diss}}, \cdot \right] + \sum_{nm} (d_{nm}^{\text{c-d}} + d_{nm}^{\text{diss}}) \left[\sigma_n \cdot \sigma_m - \frac{1}{2} \{ \sigma_m \sigma_n, \cdot \} \right] \quad (\text{D.10})$$

where we have also evaluated the terms coming from the mixed coherent and dissipative terms

$$d_{nm}^{\text{c-d}} = 2 \sum_{kl} \left[\left(d_{lm}^{(1)} h_k^{(2)} - d_{lm}^{(2)} h_k^{(1)} \right) \varepsilon_{knl} + \left(d_{nl}^{(1)} h_k^{(2)} - d_{nl}^{(2)} h_k^{(1)} \right) \varepsilon_{kml} \right]. \quad (\text{D.11})$$

E. Matrix representation of the most general qubit Lindbladian

For the qubit the Hilbert space is $\mathcal{H} = \mathbb{C}^2$. Under the identification

$$\varrho = \begin{pmatrix} a & b \\ c & d \end{pmatrix} \quad \rightarrow \quad |\varrho\rangle = \begin{pmatrix} a \\ b \\ c \\ d \end{pmatrix} \quad (\text{E.1})$$

we may represent density matrices as vectors and superoperators as matrices. Here we provide an explicit translation table of the superoperator into matrix notation for the most general static qubit Lindbladian.

The most general Lindbladian has the form

$$\mathcal{L} = -i \left[\sum_k h_k \sigma_k, \cdot \right] + \sum_{mn} d_{mn} \left(\sigma_m \cdot \sigma_n - \frac{1}{2} \{ \sigma_n \sigma_m, \cdot \} \right) \quad (\text{E.2})$$

with coefficient matrix

$$d = \begin{pmatrix} a & d + ie & f + ig \\ d - ie & b & s + it \\ f - ig & s + it & c \end{pmatrix}. \quad (\text{E.3})$$

After some algebra one finds its matrix form as

$$\mathcal{L} = \begin{pmatrix} -a - b - 2e & ih_1 - h_2 + f + is & -ih_1 - h_2 + f - is & a + b - 2e \\ ih_1 + h_2 + f - is - 2ig - 2t & -2ih_3 - a - b - 2c & a - b - 2id & -ih_1 - h_2 - f + is - 2ig - 2t \\ -ih_1 + h_2 + f + is + 2ig - 2t & a - b + 2id & 2ih_3 - a - b - 2c & ih_1 - h_2 - f - is + 2ig - 2t \\ a + b + 2e & -ih_1 + h_2 - f - is & ih_1 + h_2 - f + is & -a - b + 2e \end{pmatrix}. \quad (\text{E.4})$$

F. Degenerate perturbation theory in extended space for the dissipative system

For the coherent system, it was shown [39] that a high-frequency expansion can be derived from a canonical van-Vleck degenerate perturbation theory in the extended Hilbert space. Here we list the steps that are necessary to generalize this ansatz to the open system.

To this end, let us suppose that we may divide the quasienergy superoperator in the following fashion

$$\bar{\mathcal{Q}} = \bar{\mathcal{Q}}_0 + \lambda \bar{\mathcal{V}} \quad (\text{F.1})$$

where the spectrum of the operator $\bar{\mathcal{Q}}_0$ is known. Note that since the system is dissipative, we need to consider the right eigenvectors

$$\bar{\mathcal{Q}}_0 |a, m\rangle\rangle = \Omega_{a,m}^{(0)} |a, m\rangle\rangle \quad (\text{F.2})$$

as well as the left eigenvectors

$$\langle\langle \tilde{a}, m | \bar{\mathcal{Q}}_0 = \langle\langle \tilde{a}, m | \Omega_{a,m}^{(0)} \quad (\text{F.3})$$

since for non-hermitian operators these will differ in general. Here we split the photon index m from the eigenindex, since the spectrum will obey

$$\Omega_{a,m+n}^{(0)} = \Omega_{a,m}^{(0)} + n\omega. \quad (\text{F.4})$$

It holds the orthogonality relation

$$\langle\langle \tilde{a}, m | b, n \rangle\rangle = \delta_{ab} \delta_{mn}. \quad (\text{F.5})$$

Note that even though we denote the eigenvectors as ket- and bra-vectors, they are actually density matrices, so e.g. in Eq. (F.5) the inner product that is occurring is actually relying on the Frobenius inner product

$$(A, B)_F = \text{tr}(A^\dagger B). \quad (\text{F.6})$$

Let us elaborate a bit on this point. The eigenvectors have the form

$$|a, m\rangle\rangle \equiv \begin{pmatrix} \dots \\ \Phi_{a,m,-1} \\ \Phi_{a,m,0} \\ \Phi_{a,m,1} \\ \dots \end{pmatrix}, \quad \langle\langle \tilde{a}, m| \equiv \left(\dots \quad \tilde{\Phi}_{a,m,-1} \quad \tilde{\Phi}_{a,m,0} \quad \tilde{\Phi}_{a,m,1} \quad \dots \right), \quad (\text{F.7})$$

As we show in Appendix E as an example for the qubit, it is possible to map density matrices Φ_{ij} (here, i, j are the matrix indices) in the N -dimensional Hilbert space \mathcal{H} onto N^2 -dimensional vectors $|\Phi\rangle = |\Phi_{11}, \dots, \Phi_{1N}, \Phi_{21}, \dots, \Phi_{NN}\rangle$. Then, superoperators are just (non-hermitian) matrices of shape $N^2 \times N^2$. We can then use standard linear algebra to diagonalize the matrix representation of the superoperator. For this matrix we find eigenvectors $|\Phi_b\rangle, \langle\tilde{\Phi}_a|$ fulfilling $\langle\tilde{\Phi}_a|\Phi_b\rangle = \delta_{ab}$. Translating it back to density matrices we find

$$\delta_{ab} = \langle\tilde{\Phi}_a|\Phi_b\rangle = \sum_{i,j} (\tilde{\Phi}_a)_{ij}^* (\Phi_b)_{ij} = \text{tr}(\tilde{\Phi}_a^\dagger \Phi_b) = (\tilde{\Phi}_a, \Phi_b)_F. \quad (\text{F.8})$$

Therefore, the inner product in the extended Hilbert space, Eq. (F.5), reads

$$\langle\langle \tilde{a}, m|b, n\rangle\rangle = \sum_k (\tilde{\Phi}_{a,m,k}, \Phi_{b,n,k})_F. \quad (\text{F.9})$$

Remarkably, using this language, one is able to generalize the perturbative procedure that was found in Ref. [39]. The aim is to find a transformation to the new basis states of the perturbed problem,

$$|a, m\rangle\rangle_B = \bar{\mathcal{D}}|a, m\rangle\rangle, \quad {}_B\langle\langle \tilde{a}, m| = \langle\langle \tilde{a}, m|\bar{\mathcal{D}}^{-1}, \quad (\text{F.10})$$

such that in the transformed basis the quasi-energy operator is block diagonal,

$${}_B\langle\langle \tilde{b}, m|\bar{\mathcal{Q}}|a, n\rangle\rangle_B = 0, \quad \forall m \neq n. \quad (\text{F.11})$$

It is clear that the left eigenvectors have to transform with $\bar{\mathcal{D}}^{-1}$, because also in the transformed basis, it has to hold ${}_B\langle\langle \tilde{a}, m|b, n\rangle\rangle_B = \delta_{ab}\delta_{mn}$.

Now, like in the coherent case [39], we can separate the block-diagonal part of this equation

$$\left[\bar{\mathcal{D}}^{-1}(\bar{\mathcal{Q}}_0 + \lambda\bar{\mathcal{V}}_D + \lambda\bar{\mathcal{V}}_X)\bar{\mathcal{D}} \right]_D = \bar{\mathcal{Q}}_0 + \bar{\mathcal{W}}_D, \quad (\text{F.12})$$

Appendix

from the block-off-diagonal part

$$[\bar{\mathcal{D}}^{-1}(\bar{\mathcal{Q}}_0 + \lambda\bar{\mathcal{V}}_D + \lambda\bar{\mathcal{V}}_X)\bar{\mathcal{D}}]_X = 0. \quad (\text{F.13})$$

with some block diagonal operator $\bar{\mathcal{W}} = \bar{\mathcal{W}}_D$. Here, we use the convention

$$\bar{\mathcal{A}}_D = \sum_m \bar{\mathcal{P}}_m \bar{\mathcal{A}} \bar{\mathcal{P}}_m, \quad \bar{\mathcal{A}}_X = \sum_{m \neq n} \bar{\mathcal{P}}_m \bar{\mathcal{A}} \bar{\mathcal{P}}_n \quad (\text{F.14})$$

with projector $\bar{\mathcal{P}}_m = \sum_a |a, m\rangle\langle\tilde{a}, m|$. By representing the rotation as

$$\bar{\mathcal{D}} = \exp(\bar{\mathcal{G}}_X) \quad \text{it directly follows} \quad \bar{\mathcal{D}}^{-1} = \exp(-\bar{\mathcal{G}}_X). \quad (\text{F.15})$$

Here the rotation $\bar{\mathcal{G}} = \bar{\mathcal{G}}_X$ is chosen such that it does not affect the blocks with the same photon number m . We then can expand the operators

$$\bar{\mathcal{G}}_X = \sum_{n=1}^{\infty} \lambda^n \bar{\mathcal{G}}_X^{(n)}, \quad \bar{\mathcal{W}}_D = \sum_{n=1}^{\infty} \lambda^n \bar{\mathcal{W}}_D^{(n)}, \quad (\text{F.16})$$

plug this into Eq. (F.12) and Eq. (F.13), sort it by orders of λ and find exactly the same expressions as in Appendix C of Ref. [39]. Let us just present the first nontrivial order $\propto \lambda^1$, where it has to hold

$$\bar{\mathcal{W}}_D^{(1)} = \bar{\mathcal{V}}_D, \quad \text{as well as} \quad [\bar{\mathcal{G}}_X^{(1)}, \bar{\mathcal{Q}}_0] = \bar{\mathcal{V}}_X. \quad (\text{F.17})$$

Very similar to the coherent case, the occurring commutators $[\bar{\mathcal{G}}_X^{(n)}, \bar{\mathcal{Q}}_0]$ may be unraveled by taking matrix elements of the form

$$\langle\tilde{a}, m| [\bar{\mathcal{G}}_X^{(1)}, \bar{\mathcal{Q}}_0] |b, n\rangle = (\Omega_{a,m} - \Omega_{b,n}) \langle\tilde{a}, m| \bar{\mathcal{G}}_X^{(1)} |b, n\rangle = \langle\tilde{a}, m| \bar{\mathcal{V}}_X |b, n\rangle, \quad (\text{F.18})$$

with $m \neq n$. Therefore, we see that the argumentation for the closed system can be directly translated to the open system by replacing the real quasienergies $\varepsilon_{a,m}^{(0)}$ with the complex eigenvalues $\Omega_{a,m}^{(0)}$, the bra-vectors $\langle a, m|$ with left eigenvectors $\langle\tilde{a}, m|$ and the rotation $\bar{\mathcal{U}}$ with $\bar{\mathcal{D}}$ as well as $\bar{\mathcal{U}}^\dagger$ with $\bar{\mathcal{D}}^{-1}$.

Thus, like in the coherent case, we may find a high-frequency expansion of the superoperator by taking

$$\mathcal{Q}_0 = -i\partial_t, \quad \text{such that} \quad \mathcal{Q}_0 |a, m\rangle = m\omega |a, m\rangle \quad (\text{F.19})$$

and with the natural basis $|a, m\rangle$. Note that \mathcal{Q}_0 is hermitian, therefore the left eigenvectors are just $\langle a, m|$.

G. Fourier components of the superoperator generating the rotating frame transformation

Here we prove Eq. (3.119) which provides an explicit expression of the extended-space superoperator $\bar{\Lambda}$ generating the (generalized) rotating frame transformation for an operator of the form of Eq. (3.118).

By definition

$$\Lambda_n = \frac{1}{T} \int_0^T dt e^{-in\omega t} \exp\left(\int_0^t dt' \mathcal{L}_d(t')\right). \quad (\text{G.1})$$

We can further evaluate this expression if we assume that, like for our model system, it holds that

$$\mathcal{L}_d(t) = \phi(t) \mathcal{L}'_d \quad (\text{G.2})$$

with some periodic scalar function $\phi(t) = \sum_{m \neq 0} e^{im\omega t} \phi_m$. Then we may evaluate

$$\int_0^t dt' \mathcal{L}_d(t') = \chi(t) \mathcal{L}'_d \quad \text{with} \quad \chi(t) = \int_0^t dt' \phi(t') = \sum_{m \neq 0} \frac{e^{im\omega t} - 1}{im\omega} \phi_m. \quad (\text{G.3})$$

We may rewrite $e^{im\omega t} - 1 = \cos(m\omega t) - 1 + i \sin(m\omega t)$. This gives

$$\Lambda_n = \frac{1}{T} \int_0^T dt e^{-in\omega t} \exp\left(\sum_{m \neq 0} \frac{\sin(m\omega t)}{m\omega} \phi_m \mathcal{L}'_d + \sum_{m \neq 0} \frac{\cos(m\omega t) - 1}{im\omega} \phi_m \mathcal{L}'_d\right) \quad (\text{G.4})$$

$$= \frac{1}{T} \int_0^T dt e^{-in\omega t} \prod_{m \neq 0} \exp\left(\frac{\sin(m\omega t)}{m\omega} \phi_m \mathcal{L}'_d\right) \exp\left(\frac{\cos(m\omega t) - 1}{im\omega} \phi_m \mathcal{L}'_d\right) \quad (\text{G.5})$$

We may now represent \mathcal{L}'_d using its spectral decomposition

$$\mathcal{L}'_d = \sum_a \lambda_a \left| \Phi_a^{(d)} \right\rangle \left\langle \tilde{\Phi}_a^{(d)} \right| \quad (\text{G.6})$$

and may use the Bessel functions of first kind J_n to evaluate

$$f_n^{(m)}(x) = \frac{1}{T} \int_0^T dt e^{-in\omega t + ix \sin(m\omega t)} = \frac{1}{T} \int_0^T dt e^{-in\omega t} \sum_{k \in \mathbb{Z}} J_k(x) e^{ikm\omega t} \quad (\text{G.7})$$

$$= \begin{cases} J_{n/m}(x) & \text{if } n = km, k \in \mathbb{Z} \\ 0 & \text{else.} \end{cases} \quad (\text{G.8})$$

Similarly, with the modified Bessel functions of first kind I_n we find

$$g_n^{(m)}(x) = \frac{1}{T} e^{-x} \int_0^T dt e^{-in\omega t + x \cos(m\omega t)} = \begin{cases} e^{-x} I_{n/m}(x) & \text{if } n = km, k \in \mathbb{Z} \\ 0 & \text{else.} \end{cases} \quad (\text{G.9})$$

Note that in Eq. (G.5) occurs the Fourier transform of a product of the functions that we transformed above, which gives rise to a relatively involved structure. A compact form can be obtained in extended

Hilbert space where it holds

$$\bar{\Lambda} = \sum_a \prod_{m \neq 0} \bar{f}^{(m)} \left(\frac{\phi_m \lambda_a}{im\omega} \right) \bar{g}^{(m)} \left(\frac{\phi_m \lambda_a}{im\omega} \right) |\Phi_a^{(d)}\rangle\rangle \langle\langle \tilde{\Phi}_a^{(d)} | \quad (\text{G.10})$$

$$= \prod_{m \neq 0} \bar{f}^{(m)} \left(\frac{\phi_m \mathcal{L}'_d}{im\omega} \right) \bar{g}^{(m)} \left(\frac{\phi_m \mathcal{L}'_d}{im\omega} \right). \quad (\text{G.11})$$

H. Explicit calculation of the perturbative expansion in extended space for the driven-dissipative qubit

Instead of the explicit rotating-frame transformation on the level of the superoperator, as presented in Sec. (3.4.4) for the driven-dissipative qubit, here we calculate the components $\tilde{\mathcal{L}}_n$ in matrix representation by using Eq. (3.123). This matrix representation can be used to evaluate the Floquet-Magnus expansion numerically.

For our model system, by using Eq. (E.4) we find the matrix representations

$$A = i\mathcal{L}_1 = i\mathcal{L}_{-1} = \frac{E}{2} \begin{pmatrix} 0 & -1 & 1 & 0 \\ -1 & 0 & 0 & 1 \\ 1 & 0 & 0 & -1 \\ 0 & 1 & -1 & 0 \end{pmatrix} \quad \text{and} \quad \mathcal{L}_0 = \begin{pmatrix} -4\gamma & 0 & 0 & 0 \\ 0 & -i - 2\gamma & 0 & 0 \\ 0 & 0 & i - 2\gamma & 0 \\ 4\gamma & 0 & 0 & 0 \end{pmatrix}. \quad (\text{H.1})$$

We start by diagonalizing the Hermitian matrix A . One can show that $A = UDU^\dagger$ with

$$U = \frac{1}{2} \begin{pmatrix} -1 & 0 & \sqrt{2} & -1 \\ -1 & \sqrt{2} & 0 & 1 \\ 1 & \sqrt{2} & 0 & -1 \\ 1 & 0 & \sqrt{2} & 1 \end{pmatrix} \quad \text{and} \quad D = \begin{pmatrix} -E & 0 & 0 & 0 \\ 0 & 0 & 0 & 0 \\ 0 & 0 & 0 & 0 \\ 0 & 0 & 0 & E \end{pmatrix}. \quad (\text{H.2})$$

As can be seen from the power series of J_k it holds that $J_k(-2A/\omega) = UJ_k(-2D/\omega)U^\dagger$ yielding

$$J_k \left(-\frac{2A}{\omega} \right) = \frac{1}{2} \begin{pmatrix} a_k & c_k & -c_k & b_k \\ c_k & a_k & b_k & -c_k \\ -c_k & b_k & a_k & c_k \\ b_k & -c_k & c_k & a_k \end{pmatrix} (z). \quad (\text{H.3})$$

where we set $z = 2E/\omega$ and define the functions

$$a_k(z) = e_k J_k(z) + \delta_{k0}, \quad (\text{H.4})$$

$$b_k(z) = -e_k J_k(z) + \delta_{k0}, \quad (\text{H.5})$$

$$c_k(z) = o_k J_k(z) \quad (\text{H.6})$$

H. Explicit calculation of the perturbative expansion in extended space for the driven-dissipative qubit

Here we have used that $J_k(0) = \delta_{k0}$, $J_k(-z) = (-1)^k J_k(z)$ and the definitions

$$e_k = \begin{cases} 1, & k \text{ even,} \\ 0, & k \text{ odd,} \end{cases} \quad \text{and } o_k = \begin{cases} 0, & k \text{ even,} \\ 1, & k \text{ odd.} \end{cases} \quad (\text{H.7})$$

With this, we evaluate

$$\mathcal{L}_0 J_k \left(-\frac{2A}{\omega} \right) = \begin{pmatrix} -4\gamma a_k & -4\gamma c_k & -4\gamma c_k & 4\gamma b_k \\ (-i-2\gamma)c_k & (-i-2\gamma)a_k & (-i-2\gamma)b_k & (i+2\gamma)c_k \\ (-i+2\gamma)c_k & (i-2\gamma)b_k & (i-2\gamma)a_k & (i-2\gamma)c_k \\ 4\gamma a_k & 4\gamma c_k & -4\gamma c_k & 4\gamma b_k \end{pmatrix} (z), \quad (\text{H.8})$$

and

$$\begin{aligned} \tilde{\mathcal{L}}_n &= \sum_{k \in \mathbb{Z}} J_{k-n} \left(-\frac{2A}{\omega} \right) \mathcal{L}_0 J_k \left(-\frac{2A}{\omega} \right) \\ &= -\gamma \sum_{k \in \mathbb{Z}} J_{k-n}(z) J_k(z) \begin{pmatrix} e_n p_k & o_n q_k & -o_n q_k & -e_n p_k \\ o_n p_k & e_n q_k & -e_n q_k & -o_n p_k \\ -o_n p_k & -e_n q_k & e_n q_k & o_n p_k \\ -e_n p_k & -o_n q_k & o_n q_k & e_n p_k \end{pmatrix} - \gamma \delta_{n0} \begin{pmatrix} 0 & 0 & 0 & 0 \\ 0 & 1 & 1 & 0 \\ 0 & 1 & 1 & 0 \\ 0 & 0 & 0 & 0 \end{pmatrix} \\ &\quad + \frac{1}{2} \begin{pmatrix} -4\gamma e_n J_0 & -i o_n J_0 & -i o_n J_0 & -4\gamma e_n J_0 \\ o_n(-4\gamma J_0 - i J_n) & -i e_n(J_0 + J_n) & -i e_n(J_0 - J_n) & o_n(-4\gamma J_0 + i J_n) \\ o_n(4\gamma J_0 + J_n) & -i e_n(-J_0 + J_n) & -i e_n(-J_0 - J_n) & o_n(4\gamma J_0 + i J_n) \\ 4\gamma e_n J_0 & i o_n J_0 & i o_n J_0 & 4\gamma e_n J_0 \end{pmatrix} (z), \end{aligned} \quad (\text{H.9})$$

with $p_k = 2e_k + o_k$, as well as $q_k = 2o_k + e_k$. Therefore, we finally find the representation of the zeroth order expansion

$$\mathcal{K}^{(0)} = \tilde{\mathcal{L}}_0 = \begin{pmatrix} -\gamma[2J_0 + 2f + g] & 0 & 0 & -\gamma[2J_0 - 2f - g] \\ 0 & -iJ_0 - \gamma[1 + f + 2g] & -\gamma[1 - f - 2g] & 0 \\ 0 & -\gamma[1 - f - 2g] & iJ_0 - \gamma[1 + f + 2g] & 0 \\ \gamma[2J_0 + 2f + g] & 0 & 0 & \gamma[2J_0 - 2f - g] \end{pmatrix} (z) \quad (\text{H.10})$$

where we define $f(z) = \sum_{k \in \mathbb{Z}} e_k J_k(z)^2$ as well as $g(z) = \sum_{k \in \mathbb{Z}} o_k J_k(z)^2$. Note that it holds,

$$f(z) + g(z) = \sum_{k \in \mathbb{Z}} J_k(z)^2 = 1, \quad (\text{H.11})$$

which allows to express $\mathcal{K}^{(0)}$ in terms of $J_0(z)$ and $g(z)$ only

$$\mathcal{K}^{(0)} = \begin{pmatrix} -\gamma[2J_0 + 2 - g] & 0 & 0 & -\gamma[2J_0 - 2 + g] \\ 0 & -iJ_0 - \gamma[2 + g] & \gamma g & 0 \\ 0 & \gamma g & iJ_0 - \gamma[2 + g] & 0 \\ \gamma[2J_0 + 2 - g] & 0 & 0 & \gamma[2J_0 - 2 + g] \end{pmatrix} (z). \quad (\text{H.12})$$

By comparing the matrix representation $\mathcal{K}^{(0)}$ to the most general form of the qubit Lindbladian, Eq. (E.4), we find the Hamiltonian and the dissipator matrix,

$$\mathcal{K}^{(0)} = \mathcal{L}(H, d) \text{ with } H = \frac{J_0(z)}{2} \sigma_z, \text{ and } d = \gamma \begin{pmatrix} 1 & iJ_0(z) & 0 \\ -iJ_0(z) & 1 - g(z) & 0 \\ 0 & 0 & g(z) \end{pmatrix}. \quad (\text{H.13})$$

Note that this is exactly the same result that we obtained in Eq. (3.102). To see this, we use the Bessel function identity $J_n(y+z) = \sum_{k \in \mathbb{Z}} J_k(y) J_{n-k}(z)$ to rewrite

$$J_0(2z) = \sum_{k \in \mathbb{Z}} J_k(z) J_{-k}(z) = \sum_{k \in \mathbb{Z}} (-1)^k J_k(z)^2 = \sum_{k \in \mathbb{Z}} e_k J_k(z)^2 - \sum_{k \in \mathbb{Z}} o_k J_k(z)^2 = f(z) - g(z). \quad (\text{H.14})$$

Together with $f(z) + g(z) = 1$ we find that

$$g(z) = \frac{1}{2} [1 - J_0(2z)]. \quad (\text{H.15})$$

I. Effective rates for the wavelet method

Remarkably, the semiclassical wavelet method reproduces thermal states up to a few percents for an equilibrium situation where $\gamma_\ell = \gamma$ and $T_\ell = T$. Why the method performs so good can be seen for the noninteracting gas, $U = 0$, without a trapping potential, $V_i = 0$. Then one finds that within the semiclassical method the effective rates between the eigenstates k are identical up to order T to the exact thermal rates in the limit of high temperatures $T \gg J$.

Similar to the kinetic Eq. (6.18) in real space, one may find equations of motion for the single particle density matrix $\langle c_k^\dagger c_q \rangle$ in k -space, $c_k^\dagger = \sum_{j=0}^{M-1} e^{ikj} a_j^\dagger / \sqrt{M}$. Therefore we express the wavelet operators in terms of k -space operators $b_q^\dagger(j) = \sum_k e^{-ikj} \phi_q(k) c_k^\dagger / \sqrt{M}$ where $\phi_q(k) = \sum_{r=0}^{s-1} e^{-ikr} \varphi_q(r)$. Plugging this into the semiclassical Eq. (6.13) we find for the dissipative evolution

$$\partial_t \langle c_k^\dagger c_q \rangle_{\text{diss}} = \frac{1}{2} \sum_{lpm} \left(R_{kl,pm}^{\text{eff}} \langle c_l^\dagger c_q c_p^\dagger c_m \rangle - R_{lq,pm}^{\text{eff}} \langle c_k^\dagger c_l c_p^\dagger c_m \rangle + \text{c.c.}, k \leftrightarrow q \right) \quad (\text{I.1})$$

which obeys the same form as the equation of motion that one finds for the exact Born-Markov

evolution, Eq. (6.3), but with effective rates

$$R_{kl,pq}^{\text{eff}} = \frac{1}{sM^2} \sum_{j=0}^{M-1} \sum_{\alpha\beta\gamma\delta} [R_{\alpha\beta,\gamma\delta}(j) e^{i(k-l-p+q)j} \phi_{\alpha}^*(k) \phi_{\beta}(l) \phi_{\gamma}(p) \phi_{\delta}^*(q)]. \quad (\text{I.2})$$

As discussed in the Sec. 2.3.3, the evolution leads to the density matrix being diagonal in the eigenbasis of the Hamiltonian, $\langle c_k^\dagger c_q \rangle = \bar{n}_k \delta_{kq}$. Given the mean-field decompositions, in the first term in Eq. (I.1) only rates of the type $R_{kl,kl}^{\text{eff}}$ and $R_{kk,ll}^{\text{eff}}$ are dominating the asymptotic dynamics. Note that due to the second term the rates $R_{kk,ll}^{\text{eff}}$ drop out and only rates of type $R_{kl,kl}^{\text{eff}}$ are left. Here we show for the case of the bin with two sites, $s = 2$, for an ohmic bath, these rates coincide with the thermal rates $R_{kl,kl}$ in the first two orders of a high- T expansion.

Using the definition of $R_{\alpha\beta,\gamma\delta}(j)$ for the equilibrium case where $\gamma_\ell = \gamma$ and $T_\ell = T$, and $\phi_\alpha(k) = \sum_{r=0}^{s-1} e^{-ikr} \varphi_\alpha(r)$, we may perform the sum over α and β in Eq. (I.2) and use the orthonormality of the wavelets, $\sum_\alpha \varphi_\alpha^*(r) \varphi_\alpha(r') = \delta_{rr'}$, to find

$$R_{kl,kl}^{\text{eff}} = \frac{2\pi\gamma^2}{\hbar s M} \sum_{\gamma\delta} \phi_\gamma(k) \phi_\delta^*(l) f_\delta^\gamma(k-l) g(\varepsilon_\gamma^{\text{WL}} - \varepsilon_\delta^{\text{WL}}). \quad (\text{I.3})$$

Here we have defined $f_\delta^\gamma(k) = \sum_{r=0}^{s-1} \varphi_\gamma^*(r) \varphi_\delta(r) e^{ikr}$. From now on let us restrict to the $s = 2$ case. In this case, the wavelet basis reads $\varphi_\gamma(r) = (-1)^{\gamma r} / \sqrt{2}$ (let us, for simplicity label the wavelet basis $\gamma = 0, 1$). Then we have $\phi_\gamma(k) \propto 1 + (-1)^\gamma e^{-ik}$ and $f_\delta^\gamma(k) \propto 1 + (-1)^{\gamma+\delta} e^{ik}$. Putting this together gives

$$R_{kl,kl}^{\text{eff}} = \frac{2\pi\gamma^2}{\hbar 4M} \sum_{\gamma\delta} [1 + (-1)^\gamma \cos(k) + (-1)^\delta \cos(l) + (-1)^{\gamma+\delta} \cos(k-l)] g(\varepsilon_\gamma^{\text{WL}} - \varepsilon_\delta^{\text{WL}}). \quad (\text{I.4})$$

Note that up to now this is an exact expression for the effective rates in the case of bin size $s = 2$. We find that the effective rates are up the first order reproducing the exact rates in the limit where k and l are close, such that $|k-l| \ll 1$ and we may approximate $\cos(k-l) \approx 1$. Under this approximation, it holds

$$R_{kl,kl}^{\text{eff}} = \frac{2\pi\gamma^2}{\hbar M} \left[g(0) + \frac{1}{4} (\cos(k) - \cos(l)) (g(-4J) - g(4J)) \right]. \quad (\text{I.5})$$

Now if we perform a high-temperature expansion, $T \gg \varepsilon$, of the bath correlation function

$$g(\varepsilon) = \frac{\varepsilon}{e^{\varepsilon/T} - 1} \approx T - \frac{1}{2}\varepsilon + T \mathcal{O}\left(\frac{\varepsilon^2}{T^2}\right) \quad (\text{I.6})$$

we recover exactly the high-temperature expansion of the exact rates

$$R_{kl,kl} = \frac{2\pi\gamma^2}{\hbar M} g(\varepsilon_k - \varepsilon_l) \approx \frac{2\pi\gamma^2}{\hbar M} \left[T - \frac{1}{2} (-2J \cos(k) + 2J \cos(l)) \right]. \quad (\text{I.7})$$

Note that within this calculation we explicitly use that the spectral density is ohmic, $J(E) \propto E$. A

Appendix

generalization to other spectral densities is not obvious.

List of Figures

2.1.	Sketch of system, environment and interaction between both of them	7
2.2.	Sketch of the occupation dynamics in an ideal Bose gas	25
3.1.	Distance to Markovianity for the exact generator \mathcal{K} of the stroboscopic dynamics for the qubit model	34
3.2.	Distance to Markovianity along cuts through the phase diagram and behavior of the model in the weak-dissipation limit	35
3.3.	Shortest memory time of the effective non-Markovian generator	37
3.4.	Eigenvalues of the Choi matrix of the dynamical maps for parameters with and without Floquet Lindbladian	39
3.5.	Distance of the leading order Magnus expansion \mathcal{K}_{Mag} to the exact generator and sketch of the characteristic polynomial of coefficient matrix	41
3.6.	Distance of the zeroth order $\tilde{\mathcal{K}}_{\text{Mag},0}$ and first order $\tilde{\mathcal{K}}_{\text{Mag},1}$ of the Magnus expansion in the rotating frame to the exact generator	52
3.7.	Distance to Markovianity for the first order $\tilde{\mathcal{K}}_{\text{Mag},1}$ of the Magnus expansion in the rotating frame	53
3.8.	Distance to Markovianity and distance to the exact generator for the first order $\tilde{\mathcal{K}}_{\text{vV},1}$ of the van-Vleck high-frequency expansion in the rotating frame	56
3.9.	Distance to Markovianity μ_{min} of the exact effective generator \mathcal{K} as in Fig. 3.1 for some intermediate values of the driving phase φ	57
3.10.	Distance to Markovianity for the effective Lindbladian $\tilde{\mathcal{K}}_{\text{eff},2}$ obtained from second order van-Vleck high-frequency expansion	59
4.1.	Mean occupations of the single-particle states in an ideal Bose gas for a system in contact with one, two heat baths and for a Floquet system in contact with a heat bath	64
4.2.	Sketch of the typical behavior of the function $a(k)$ that determines the selected states for continuous rates	67
4.3.	Gallery of selected states in the random wave model	69
4.4.	Typical example for Bose selection in a more complex rate matrix	70
4.5.	Mean number of selected states as a function of wavenumber and number of wave components in the random wave model	71
4.6.	Number of selected states for exponentially distributed random rates and for chaotic quantum kicked rotor	74

List of Figures

4.7.	Number of selected states in random wave model with large wavenumber, and in modified random wave model	78
4.8.	Maximum- and mean number of selected states for a random chaotic system as a function of the number of positive- and negative-temperature baths that are coupled to it	80
5.1.	Sketch of the tight-binding chain in the equilibrium situation and condensate fraction as a function of temperature and system size in equilibrium	86
5.2.	Sketch of the tight-binding chain with “hot needle” and condensate fraction in the nonequilibrium steady state as function of the two temperatures and of system size	87
5.3.	Comparison of mode occupations as well as heat capacity per particle and heat current in the nonequilibrium- and in the equilibrium steady state as function of temperature of the global bath	88
5.4.	Mode occupations as well as inner energy and heat current in the nonequilibrium steady state as function of needle temperature	90
5.5.	Mode occupations in the nonequilibrium- and in the equilibrium steady state as a function of total particle number	96
5.6.	Comparison of mode occupations obtained from the mean field (or kinetic equation) to quasixact Monte-Carlo calculations	98
5.7.	Sketch of the hot-needle setup for particles in a box and condensate fraction in the nonequilibrium steady state as function of both temperatures	99
5.8.	Mode occupations for the hot-needle setup for particles in a box	100
5.9.	Occupations of the Floquet modes and snapshots of the condensate wave functions for the Floquet needle	104
5.10.	Same as in Fig. 5.9, but for different parameters	106
6.1.	Sketch of the wavelet method	111
6.2.	Benchmark of the wavelet method for an ideal gas in equilibrium with and without trapping potential	114
6.3.	Steady-state density matrices obtained from the wavelet method for a weakly interacting Bose-Hubbard chain with open boundaries coupled to a global heat bath	115
6.4.	Same as in Fig. 6.3 but in the hot-needle setup	118
6.5.	Mean occupations of the natural orbitals as a function of total particle number for the hot-needle setup with weak interactions	119
6.6.	Same as in Fig. 6.4 but with strong system-bath coupling	120
6.7.	Sketch of the experiment by Labouvie et. al. [91] and sketch of the minimal model that is used	122
6.8.	Time evolution of the single-particle density-matrix for the interacting model for both a driving site that is initially empty or full	123
6.9.	Same as in Fig. 6.8(a)-(c) but for the noninteracting gas, $U = 0$	124

6.10. Same as in Fig. 6.8(a)-(c), and (j) but for times up to $t = 50/J$ 125

6.11. Steady-state phase diagram of the relative filling of the driven site in the steady state
as a function of hopping amplitude and loss rate 126

Bibliography

- [1] R. B. Griffiths: *Dependence of critical indices on a parameter*, Phys. Rev. Lett. **24** (1970), 1479. Cited on page 1.
- [2] L. P. Kadanoff: *Scaling and universality in statistical physics*, Physica A: Statistical Mechanics and its Applications **163** (1990), 1–14. Cited on page 1.
- [3] H. E. Stanley: *Scaling, universality, and renormalization: Three pillars of modern critical phenomena*, Reviews of modern physics **71** (1999), S358. Cited on page 1.
- [4] N. D. Mermin and H. Wagner: *Absence of Ferromagnetism or Antiferromagnetism in One- or Two-Dimensional Isotropic Heisenberg Models*, Phys. Rev. Lett. **17** (1966), 1133. Cited on page 1.
- [5] P. C. Hohenberg: *Existence of Long-Range Order in One and Two Dimensions*, Phys. Rev. **158** (1967), 383. Cited on page 1.
- [6] A. Gelfert and W. Nolting: *The absence of finite-temperature phase transitions in low-dimensional many-body models: a survey and new results*, Journal of Physics: Condensed Matter **13** (2001), R505–R524. Cited on page 1.
- [7] M. Ueda: *Fundamentals and New Frontiers of Bose-Einstein Condensation*, (WORLD SCIENTIFIC), (2010). Cited on pages 1 and 116.
- [8] A. Eckardt: *Colloquium: Atomic quantum gases in periodically driven optical lattices*, Rev. Mod. Phys. **89** (2017), 011004. Cited on pages 1, 27, and 103.
- [9] M. Bukov, L. D’Alessio, and A. Polkovnikov: *Universal High-Frequency Behavior of Periodically Driven Systems: from Dynamical Stabilization to Floquet Engineering*, Adv. in Phys. **64** (2015), 139. Cited on pages 1 and 28.
- [10] H. Lignier, C. Sias, D. Ciampini, Y. Singh, A. Zenesini, O. Morsch, and E. Arimondo: *Dynamical Control of Matter-Wave Tunneling in Periodic Potentials*, Phys. Rev. Lett. **99** (2007), 220403. Cited on page 1.
- [11] C. E. Creffield, F. Sols, D. Ciampini, O. Morsch, and E. Arimondo: *Expansion of matter waves in static and driven periodic potentials*, Phys. Rev. A **82** (2010), 035601. Cited on page 1.

Bibliography

- [12] A. Eckardt, C. Weiss, and M. Holthaus: *Superfluid-Insulator Transition in a Periodically Driven Optical Lattice*, Phys. Rev. Lett. **95** (2005), 260404. Cited on page 1.
- [13] A. Zenesini, H. Lignier, D. Ciampini, O. Morsch, and E. Arimondo: *Coherent control of dressed matter waves*, Phys. Rev. Lett. **102** (2009), 100403. Cited on page 1.
- [14] M. Aidelsburger, M. Atala, S. Nascimbène, S. Trotzky, Y.-A. Chen, and I. Bloch: *Experimental Realization of Strong Effective Magnetic Fields in an Optical Lattice*, Phys. Rev. Lett. **107** (2011), 255301. Cited on pages 1 and 28.
- [15] M. Aidelsburger, M. Atala, M. Lohse, J. T. Barreiro, B. Paredes, and I. Bloch: *Realization of the Hofstadter Hamiltonian with ultracold atoms in optical lattices*, Phys. Rev. Lett. **111** (2013), 185301. Cited on page 1.
- [16] J. Struck, C. Ölschläger, M. Weinberg, P. Hauke, J. Simonet, A. Eckardt, M. Lewenstein, K. Sengstock, and P. Windpassinger: *Tunable Gauge Potential for Neutral and Spinless Particles in Driven Optical Lattices*, Phys. Rev. Lett. **108** (2012), 225304. Cited on page 1.
- [17] H. Miyake, G. A. Siviloglou, J. Kennedy, W. C. Burton, and W. Ketterle: *Realizing the Harper Hamiltonian with Laser-Assisted Tunneling in Optical Lattices*, Phys. Rev. Lett. **111** (2013), 185302. Cited on page 1.
- [18] M. Aidelsburger, M. Lohse, C. Schweizer, M. Atala, J. T. Barreiro, S. Nascimbène, N. R. Cooper, I. Bloch, and N. Goldman: *Measuring the Chern number of Hofstadter bands with ultracold bosonic atoms*, Nat. Phys. **1** (2015), 162. Cited on pages 1 and 28.
- [19] G. Jotzu, M. Messer, T. U. Rémi Desbuquois, Martin Lebrat, D. Greif, and T. Esslinger: *Experimental realization of the topological Haldane model with ultracold fermions*, Nature **515** (2014), 237. Cited on pages 1 and 28.
- [20] N. Fläschner, B. S. Rem, M. Tarnowski, D. Vogel, D.-S. Lühmann, K. Sengstock, and C. Weitenberg: *Experimental reconstruction of the Berry curvature in a Floquet Bloch band*, Science **352** (2016), 1091–1094. Cited on pages 1 and 28.
- [21] N. Y. Yao and C. Nayak: *Time crystals in periodically driven systems*, Physics Today **71** (2018), 40–47. Cited on page 1.
- [22] D. V. Else, B. Bauer, and C. Nayak: *Floquet Time Crystals*, Phys. Rev. Lett. **117** (2016), 090402. Cited on page 1.
- [23] D. V. Else, B. Bauer, and C. Nayak: *Prethermal Phases of Matter Protected by Time-Translation Symmetry*, Phys. Rev. X **7** (2017), 011026. Cited on page 1.
- [24] V. Khemani, A. Lazarides, R. Moessner, and S. L. Sondhi: *Phase Structure of Driven Quantum Systems*, Phys. Rev. Lett. **116** (2016), 250401. Cited on page 1.

- [25] C. W. von Keyserlingk, V. Khemani, and S. L. Sondhi: *Absolute stability and spatiotemporal long-range order in Floquet systems*, Phys. Rev. B **94** (2016), 085112. Cited on page 1.
- [26] J. Zhang, P. W. Hess, A. Kyprianidis, P. Becker, A. Lee, J. Smith, G. Pagano, I.-D. Potirniche, A. C. Potter, A. Vishwanath, N. Y. Yao, and C. Monroe: *Observation of a discrete time crystal*, Nature **543** (2017), 217. Cited on page 1.
- [27] S. Choi, J. Choi, R. Landig, G. Kucsko, H. Zhou, J. Isoya, F. Jelezko, S. Onoda, H. Sumiya, V. Khemani, C. von Keyserlingk, N. Y. Yao, E. Demler, and M. D. Lukin: *Observation of discrete time-crystalline order in a disordered dipolar many-body system*, Nature **543** (2017), 221. Cited on page 1.
- [28] A. Lazarides, A. Das, and R. Moessner: *Fate of Many-Body Localization Under Periodic Driving*, Phys. Rev. Lett. **115** (2015), 030402. Cited on page 1.
- [29] P. Ponte, Z. Papić, F. m. c. Huveneers, and D. A. Abanin: *Many-Body Localization in Periodically Driven Systems*, Phys. Rev. Lett. **114** (2015), 140401. Cited on page 1.
- [30] T. Oka and H. Aoki: *Photovoltaic Hall effect in graphene*, Phys. Rev. B **79** (2009), 081406. Cited on page 1.
- [31] T. Kitagawa, T. Oka, A. Brataas, L. Fu, and E. Demler: *Transport properties of nonequilibrium systems under the application of light: Photoinduced quantum Hall insulators without Landau levels*, Phys. Rev. B **84** (2011), 235108. Cited on page 1.
- [32] L. E. F. Foa Torres, P. M. Perez-Piskunow, C. A. Balseiro, and G. Usaj: *Multiterminal Conductance of a Floquet Topological Insulator*, Phys. Rev. Lett. **113** (2014), 266801. Cited on page 1.
- [33] J. W. McIver, B. Schulte, F. U. Stein, T. Matsuyama, G. Jotzu, G. Meier, and A. Cavalleri: *Light-induced anomalous Hall effect in graphene*, arXiv e-prints (2018), arXiv:1811.03522. Cited on page 1.
- [34] M. Mitrano, A. Cantaluppi, D. Nicoletti, S. Kaiser, A. Perucchi, S. Lupi, P. D. Pietro, D. Pontiroli, M. Ricco, S. R. Clark, D. Jaksch, and A. Cavalleri: *Possible light-induced superconductivity in K_3C_{60} at high temperature*, Nature **530** (2016), 461. Cited on page 1.
- [35] D. Fausti, R. I. Tobey, N. Dean, S. Kaiser, A. Dienst, M. C. Hoffmann, S. Pyon, T. Takayama, H. Takagi, and A. Cavalleri: *Light-Induced Superconductivity in a Stripe-Ordered Cuprate*, Science **331** (2011), 189–191. Cited on page 1.
- [36] A. Cavalleri: *Photo-induced superconductivity*, Contemporary Physics **59** (2018), 31–46. Cited on page 1.
- [37] L. D’Alessio and M. Rigol: *Long-time Behavior of Isolated Periodically Driven Interacting Lattice Systems*, Phys. Rev. X **4** (2014), 041048. Cited on page 2.

Bibliography

- [38] A. Lazarides, A. Das, and R. Moessner: *Equilibrium states of generic quantum systems subject to periodic driving*, Phys. Rev. E **90** (2014), 012110. Cited on page 2.
- [39] A. Eckardt and E. Anisimovas: *High-frequency approximation for periodically driven quantum systems from a Floquet-space perspective*, New J. Phys. **17** (2015), 093039. Cited on pages 2, 28, 35, 39, 44, 45, 46, 47, 57, 140, 141, and 142.
- [40] M. Weinberg, C. Ölschläger, C. Sträter, S. Prella, A. Eckardt, K. Sengstock, and J. Simonet: *Multiphoton interband excitations of quantum gases in driven optical lattices*, Phys. Rev. A **92** (2015), 043621. Cited on page 2.
- [41] M. Reitter, J. Näger, K. Wintersperger, C. Sträter, I. Bloch, A. Eckardt, and U. Schneider: *Interaction Dependent Heating and Atom Loss in a Periodically Driven Optical Lattice*, Phys. Rev. Lett. **119** (2017), 200402. Cited on page 2.
- [42] C. Sträter and A. Eckardt: *Interband heating processes in a periodically driven optical lattice*, Zeitschrift für Naturforschung A **71** (2016), 909–920. Cited on page 2.
- [43] T. Bilitewski and N. R. Cooper: *Scattering theory for Floquet-Bloch states*, Phys. Rev. A **91** (2015), 033601. Cited on page 2.
- [44] M. Messer, K. Sandholzer, F. Görg, J. Minguzzi, R. Desbuquois, and T. Esslinger: *Floquet Dynamics in Driven Fermi-Hubbard Systems*, Phys. Rev. Lett. **121** (2018), 233603. Cited on page 2.
- [45] T. Bilitewski and N. R. Cooper: *Population dynamics in a Floquet realization of the Harper-Hofstadter Hamiltonian*, Phys. Rev. A **91** (2015), 063611. Cited on page 2.
- [46] T. Qin and W. Hofstetter: *Spectral functions of a time-periodically driven Falicov-Kimball model: Real-space Floquet dynamical mean-field theory study*, Phys. Rev. B **96** (2017), 075134. Cited on page 2.
- [47] I. Carusotto and C. Ciuti: *Quantum fluids of light*, Rev. Mod. Phys. **85** (2013), 299. Cited on page 2.
- [48] R. M. Stevenson, V. N. Astratov, M. S. Skolnick, D. M. Whittaker, M. Emam-Ismael, A. I. Tartakovskii, P. G. Savvidis, J. J. Baumberg, and J. S. Roberts: *Continuous Wave Observation of Massive Polariton Redistribution by Stimulated Scattering in Semiconductor Microcavities*, Phys. Rev. Lett. **85** (2000), 3680–3683. Cited on page 2.
- [49] H. Deng, G. Weihs, C. Santori, J. Bloch, and Y. Yamamoto: *Condensation of Semiconductor Microcavity Exciton Polaritons*, Science **298** (2002), 199–202. Cited on page 2.
- [50] J. Kasprzak, M. Richard, S. Kundermann, A. Baas, P. Jeambrun, J. M. J. Keeling, M. H. FM Marchetti et al.: *Bose–Einstein condensation of exciton polaritons*, Nature **443** (2006), 409–414. Cited on page 2.

- [51] T. Byrnes, N. Y. Kim, and Y. Yamamoto: *Exciton-polariton condensates*, Nature Phys. **10** (2014), 803–813. Cited on page 2.
- [52] H. Deng, H. Haug, and Y. Yamamoto: *Exciton-polariton Bose-Einstein condensation*, Rev. Mod. Phys. **82** (2010), 1489–1537. Cited on page 2.
- [53] J. Klaers, J. Schmitt, F. Vewinger, and M. Weitz: *Bose-Einstein condensation of photons in an optical microcavity*, Nature **468** (2010), 545–548. Cited on page 2.
- [54] J. Schmitt, T. Damm, D. Dung, F. Vewinger, J. Klaers, and M. Weitz: *Observation of Grand-Canonical Number Statistics in a Photon Bose-Einstein Condensate*, Phys. Rev. Lett. **112** (2014), 030401. Cited on page 2.
- [55] J. Schmitt: *Dynamics and correlations of a Bose-Einstein condensate of photons*, Journal of Physics B: Atomic, Molecular and Optical Physics **51** (2018), 173001. Cited on pages 2 and 110.
- [56] E. Altman, L. M. Sieberer, L. Chen, S. Diehl, and J. Toner: *Two-Dimensional Superfluidity of Exciton Polaritons Requires Strong Anisotropy*, Phys. Rev. X **5** (2015), 011017. Cited on pages 2 and 129.
- [57] L. M. Sieberer, S. D. Huber, E. Altman, and S. Diehl: *Dynamical Critical Phenomena in Driven-Dissipative Systems*, Phys. Rev. Lett. **110** (2013), 195301. Cited on page 2.
- [58] M. H. Szymańska, J. Keeling, and P. B. Littlewood: *Nonequilibrium Quantum Condensation in an Incoherently Pumped Dissipative System*, Phys. Rev. Lett. **96** (2006), 230602. Cited on page 2.
- [59] P. Kirton and J. Keeling: *Nonequilibrium Model of Photon Condensation*, Phys. Rev. Lett. **111** (2013), 100404. Cited on page 2.
- [60] A. Chiocchetta and I. Carusotto: *Quantum Langevin model for nonequilibrium condensation*, Phys. Rev. A **90** (2014), 023633. Cited on page 2.
- [61] H. A. M. Leymann, D. Vorberg, T. Lettau, C. Hopfmann, C. Schneider, M. Kamp, S. Höfling, R. Ketzmerick, J. Wiersig, S. Reitzenstein, and A. Eckardt: *Pump-Power-Driven Mode Switching in a Microcavity Device and Its Relation to Bose-Einstein Condensation*, Phys. Rev. X **7** (2017), 021045. Cited on page 2.
- [62] D. Vorberg, R. Ketzmerick, and A. Eckardt: *Unified theory for excited-state, fragmented, and equilibriumlike Bose condensation in pumped photonic many-body systems*, Phys. Rev. A **97** (2018), 063621. Cited on pages 2, 4, 129, and 130.
- [63] H. E. Türeci, A. D. Stone, and B. Collier: *Self-consistent multimode lasing theory for complex or random lasing media*, Phys. Rev. A **74** (2006), 043822. Cited on page 2.

Bibliography

- [64] H. Cao: *Lasing in random media*, Waves in Random Media **13** (2003), R1–R39. Cited on page 2.
- [65] M. Sondermann, M. Weinkath, T. Ackemann, J. Mulet, and S. Balle: *Two-frequency emission and polarization dynamics at lasing threshold in vertical-cavity surface-emitting lasers*, Phys. Rev. A **68** (2003), 033822. Cited on page 2.
- [66] M. Marconi, J. Javaloyes, F. Raineri, J. A. Levenson, and A. M. Yacomotti: *Asymmetric mode scattering in strongly coupled photonic crystal nanolasers*, Opt. Lett. **41** (2016), 5628–5631. Cited on page 2.
- [67] L. Ge, D. Liu, A. Cerjan, S. Rotter, H. Cao, S. G. Johnson, H. E. Türeci, and A. D. Stone: *Interaction-induced mode switching in steady-state microlasers*, Opt. Express **24** (2016), 41–54. Cited on page 2.
- [68] S. Rahimzadeh Kalaleh Rodriguez, A. Amo, I. Carusotto, I. Sagnes, L. Le Gratiet, E. Galopin, A. Lemaître, and J. Bloch: *Nonlinear Polariton Localization in Strongly Coupled Driven-Dissipative Microcavities*, ACS Photonics **5** (2018), 95–99. Cited on page 2.
- [69] P. St-Jean, V. Goblot, E. Galopin, A. Lemaître, T. Ozawa, L. Le Gratiet, I. Sagnes, J. Bloch, and A. Amo: *Lasing in topological edge states of a one-dimensional lattice*, Nature Photonics **11** (2017), 651. Cited on page 2.
- [70] H. Zhao, P. Miao, M. H. Teimourpour, S. Malzard, R. El-Ganainy, H. Schomerus, and L. Feng: *Topological hybrid silicon microlasers*, Nature communications **9** (2018), 981. Cited on page 2.
- [71] H.-P. Breuer, W. Huber, and F. Petruccione: *Quasistationary distributions of dissipative nonlinear quantum oscillators in strong periodic driving fields*, Phys. Rev. E **61** (2000), 4883. Cited on pages 2 and 28.
- [72] R. Ketzmerick and W. Wustmann: *Statistical mechanics of Floquet systems with regular and chaotic states*, Phys. Rev. E **82** (2010), 021114. Cited on pages 2 and 28.
- [73] W. Wustmann: *Statistical mechanics of time-periodic quantum systems*, PhD thesis, TU Dresden, Fakultät für Mathematik und Naturwissenschaften (2010). Cited on pages 2, 4, 7, 21, 63, 72, 77, and 103.
- [74] T. Shirai, T. Mori, and S. Miyashita: *Condition for emergence of the Floquet-Gibbs state in periodically driven open systems*, Phys. Rev. E **91** (2015), 030101. Cited on pages 2 and 28.
- [75] T. Shirai, J. Thingna, T. Mori, S. Denisov, P. Hänggi, and S. Miyashita: *Effective Floquet-Gibbs states for dissipative quantum systems*, New J. Phys. **18** (2016), 053008. Cited on pages 2 and 28.

- [76] T. Iadecola and C. Chamon: *Floquet systems coupled to particle reservoirs*, Phys. Rev. B **91** (2015), 184301. Cited on page 2.
- [77] K. I. Seetharam, C.-E. Bardyn, N. H. Lindner, M. S. Rudner, and G. Refael: *Controlled Population of Floquet-Bloch States via Coupling to Bose and Fermi Baths*, Phys. Rev. X **5** (2015), 041050. Cited on pages 2 and 28.
- [78] H. Dehghani, T. Oka, and A. Mitra: *Out-of-equilibrium electrons and the Hall conductance of a Floquet topological insulator*, Phys. Rev. B **91** (2015), 155422. Cited on pages 2 and 28.
- [79] T. Qin, A. Schnell, K. Sengstock, C. Weitenberg, A. Eckardt, and W. Hofstetter: *Charge density wave and charge pump of interacting fermions in circularly shaken hexagonal optical lattices*, Phys. Rev. A **98** (2018), 033601. Cited on pages 2 and 28.
- [80] T. Iadecola, T. Neupert, and C. Chamon: *Occupation of topological Floquet bands in open systems*, Phys. Rev. B **91** (2015), 235133. Cited on pages 2 and 28.
- [81] S. Mathey and S. Diehl: *Absence of Criticality in the Phase Transitions of Open Floquet Systems*, Phys. Rev. Lett. **122** (2019), 110602. Cited on page 2.
- [82] D. Vorberg, W. Wustmann, R. Ketzmerick, and A. Eckardt: *Generalized Bose-Einstein Condensation into Multiple States in Driven-Dissipative Systems*, Phys. Rev. Lett. **111** (2013), 240405. Cited on pages 2, 3, 5, 26, 28, 61, 62, 64, 65, 72, 74, 97, and 126.
- [83] D. Vorberg, W. Wustmann, H. Schomerus, R. Ketzmerick, and A. Eckardt: *Nonequilibrium steady states of ideal bosonic and fermionic quantum gases*, Phys. Rev. E **92** (2015), 062119. Cited on pages 2, 3, 5, 23, 24, 26, 28, 62, 63, 65, 68, 74, 85, 97, 98, 103, and 116.
- [84] D. Vorberg: *Generalized Bose-Einstein Condensation in Driven-dissipative Quantum Gases*, Ph.D. thesis, Technische Universität Dresden, Fakultät Physik, (2017). Cited on pages 2, 26, 126, and 129.
- [85] A. Schnell, R. Ketzmerick, and A. Eckardt: *On the number of Bose-selected modes in driven-dissipative ideal Bose gases*, Phys. Rev. E **97** (2018), 032136. Cited on pages 2, 28, and 61.
- [86] P. M. Geiger, J. Knebel, and E. Frey: *Topologically robust zero-sum games and Pfaffian orientation: How network topology determines the long-time dynamics of the antisymmetric Lotka-Volterra equation*, Phys. Rev. E **98** (2018), 062316. Cited on page 3.
- [87] J. Knebel, M. F. Weber, T. Krüger, and E. Frey: *Evolutionary games of condensates in coupled birth-death processes*, Nature Communications **6** (2015), 6977. Cited on page 3.
- [88] S. Diehl: *Non-equilibrium condensation: State of the game*, Nature Physics **11** (2015), 446. Cited on page 3.

Bibliography

- [89] K. O. Chong, J.-R. Kim, J. Kim, S. Yoon, S. Kang, and K. An: *Observation of a non-equilibrium steady state of cold atoms in a moving optical lattice*, Nature Communications Physics **1** (2018), 25. Cited on pages 3 and 28.
- [90] R. Labouvie, B. Santra, S. Heun, S. Wimberger, and H. Ott: *Negative Differential Conductivity in an Interacting Quantum Gas*, Phys. Rev. Lett. **115** (2015), 050601. Cited on pages 3, 122, 124, and 126.
- [91] R. Labouvie, B. Santra, S. Heun, and H. Ott: *Bistability in a Driven-Dissipative Superfluid*, Phys. Rev. Lett. **116** (2016), 235302. Cited on pages 3, 5, 121, 122, 123, 124, 125, 126, 131, and 150.
- [92] T. Tomita, S. Nakajima, I. Danshita, Y. Takasu, and Y. Takahashi: *Observation of the Mott insulator to superfluid crossover of a driven-dissipative Bose-Hubbard system*, Science Advances **3** (2017). Cited on page 3.
- [93] S. Krinner, T. Esslinger, and J.-P. Brantut: *Two-terminal transport measurements with cold atoms*, Journal of Physics: Condensed Matter **29** (2017), 343003. Cited on page 3.
- [94] D. Husmann, M. Lebrat, S. Häusler, J.-P. Brantut, L. Corman, and T. Esslinger: *Breakdown of the Wiedemann–Franz law in a unitary Fermi gas*, Proceedings of the National Academy of Sciences **115** (2018), 8563–8568. Cited on page 3.
- [95] T. E. Lee, H. Häffner, and M. C. Cross: *Collective Quantum Jumps of Rydberg Atoms*, Phys. Rev. Lett. **108** (2012), 023602. Cited on page 3.
- [96] I. Lesanovsky and J. P. Garrahan: *Kinetic Constraints, Hierarchical Relaxation, and Onset of Glassiness in Strongly Interacting and Dissipative Rydberg Gases*, Phys. Rev. Lett. **111** (2013), 215305. Cited on page 3.
- [97] N. Šibalić, C. G. Wade, C. S. Adams, K. J. Weatherill, and T. Pohl: *Driven-dissipative many-body systems with mixed power-law interactions: Bistabilities and temperature-driven nonequilibrium phase transitions*, Phys. Rev. A **94** (2016), 011401. Cited on page 3.
- [98] F. Letscher, O. Thomas, T. Niederprüm, M. Fleischhauer, and H. Ott: *Bistability Versus Metastability in Driven Dissipative Rydberg Gases*, Phys. Rev. X **7** (2017), 021020. Cited on pages 3 and 28.
- [99] M. Hoening, W. Abdussalam, M. Fleischhauer, and T. Pohl: *Antiferromagnetic long-range order in dissipative Rydberg lattices*, Phys. Rev. A **90** (2014), 021603. Cited on pages 3 and 129.
- [100] F. Haddadfarshi, J. Cui, and F. Mintert: *Completely Positive Approximate Solutions of Driven Open Quantum Systems*, Phys. Rev. Lett. **114** (2015), 130402. Cited on pages 3, 28, 34, 36, 40, 41, 42, 60, 128, and 136.

- [101] S. Restrepo, J. Cerrillo, V. M. Bastidas, D. G. Angelakis, and T. Brandes: *Driven Open Quantum Systems and Floquet Stroboscopic Dynamics*, Phys. Rev. Lett. **117** (2016), 250401. Cited on pages 3, 28, and 34.
- [102] C. M. Dai, Z. C. Shi, and X. X. Yi: *Floquet theorem with open systems and its applications*, Phys. Rev. A **93** (2016), 032121. Cited on pages 3, 28, and 34.
- [103] C. Dai, H. Li, W. Wang, and X. Yi: *Generalized Floquet theory for open quantum systems*, arXiv preprint arXiv:1707.05030 (2017). Cited on pages 3, 46, and 47.
- [104] V. Reimer, K. G. L. Pedersen, N. Tanger, M. Pletyukhov, and V. Gritsev: *Nonadiabatic effects in periodically driven dissipative open quantum systems*, Phys. Rev. A **97** (2018), 043851. Cited on pages 3, 36, 40, and 60.
- [105] M. M. Wolf, J. Eisert, T. S. Cubitt, and J. I. Cirac: *Assessing Non-Markovian Quantum Dynamics*, Phys. Rev. Lett. **101** (2008), 150402. Cited on pages 5, 28, 31, 32, 33, and 128.
- [106] R. Alicki: *Invitation to quantum dynamical semigroups*, in: *Dynamics of Dissipation*, 239–264, (Springer), (2002). Cited on pages 7 and 10.
- [107] R. Alicki and K. Lendi: *Quantum Dynamical Semigroups and Applications*, Lecture Notes in Physics, (Springer Berlin Heidelberg), (2007). Cited on page 7.
- [108] H. Breuer and F. Petruccione: *The Theory of Open Quantum Systems*, (Oxford University Press, Oxford & New York), (2002). Cited on pages 7, 62, 84, and 108.
- [109] H. Carmichael: *An open systems approach to quantum optics: lectures presented at the Université Libre de Bruxelles, October 28 to November 4, 1991*, vol. 18, (Springer Science & Business Media), (2009). Cited on pages 7 and 14.
- [110] M. M. Wilde: *Quantum information theory*, (Cambridge University Press), (2013). Cited on pages 7 and 10.
- [111] J. Thingna: *Steady-state transport properties of anharmonic systems*, Ph.D. thesis, National University Singapore, (2013). Cited on pages 7 and 21.
- [112] G. Lindblad: *On the generators of quantum dynamical semigroups*, Communications in Mathematical Physics **48** (1976), 119–130. Cited on pages 9, 29, and 133.
- [113] V. Gorini, A. Kossakowski, and E. C. G. Sudarshan: *Completely positive dynamical semigroups of N-level systems*, Journal of Mathematical Physics **17** (1976), 821–825. Cited on page 9.
- [114] R. Alicki and M. Fannes: *Quantum dynamical systems*, (Oxford university press), (2001). Cited on page 10.
- [115] M.-D. Choi: *Completely positive linear maps on complex matrices*, Linear Algebra and its Applications **10** (1975), 285 – 290. Cited on pages 10 and 33.

Bibliography

- [116] M. Jiang, S. Luo, and S. Fu: *Channel-state duality*, Phys. Rev. A **87** (2013), 022310. Cited on page 11.
- [117] P. Cappellaro: *MIT OpenCourseWare: Open Quantum Systems*, https://ocw.mit.edu/courses/nuclear-engineering/22-51-quantum-theory-of-radiation-interactions-fall-2012/lecture-notes/MIT22_51F12_Ch8.pdf, (last visited 2019-01-11). Cited on page 11.
- [118] M. Nakatani and T. Ogawa: *Quantum Master Equations for Composite Systems: Is Born–Markov Approximation Really Valid?*, Journal of the Physical Society of Japan **79** (2010), 084401. Cited on page 17.
- [119] L. Diósi: *Ohmic vs Markovian heat bath — two-page-tutorial*, <http://www.rmki.kfki.hu/~diosi/tutorial/ohmmarkovtutor.pdf>, (last visited 2019-01-22). Cited on page 21.
- [120] D. M. Basko, I. L. Aleiner, and B. L. Altshuler: *Metal insulator transition in a weakly interacting many-electron system with localized single-particle states*, Annals of Physics **321** (2006), 1126–1205. Cited on page 23.
- [121] I. V. Gornyi, A. D. Mirlin, and D. G. Polyakov: *Interacting Electrons in Disordered Wires: Anderson Localization and Low-T Transport*, Phys. Rev. Lett. **95** (2005), 206603. Cited on page 23.
- [122] E. Altman and R. Vosk: *Universal Dynamics and Renormalization in Many-Body-Localized Systems*, Annual Review of Condensed Matter Physics **6** (2015), 383–409. Cited on page 23.
- [123] R. Nandkishore and D. A. Huse: *Many-Body Localization and Thermalization in Quantum Statistical Mechanics*, Annual Review of Condensed Matter Physics **6** (2015), 15–38. Cited on page 23.
- [124] F. Alet and N. Laflorencie: *Many-body localization: An introduction and selected topics*, Comptes Rendus Physique (2018). Cited on page 23.
- [125] L.-N. Wu, A. Schnell, G. D. Tomasi, M. Heyl, and A. Eckardt: *Describing many-body localized systems in thermal environments*, New Journal of Physics **21** (2019), 063026. Cited on pages 23, 24, and 107.
- [126] A. Schnell, A. Eckardt, and S. Denisov: *Is there a Floquet Lindbladian?*, arXiv preprint arXiv:1809.11121 (2018). Cited on pages 27 and 31.
- [127] J. H. Shirley: *Solution of the Schrödinger Equation with a Hamiltonian Periodic in Time*, Phys. Rev. **138** (1965), B979. Cited on page 27.
- [128] H. Sambe: *Steady States and Quasienergies of a Quantum-Mechanical System in an Oscillating Field*, Phys. Rev. A **7** (1973), 6. Cited on page 27.

- [129] M. C. Rechtsman, J. M. Zeuner, Y. Plotnik, Y. Lumer, D. Podolsky, F. Dreisow, S. Nolte, M. Segev, , and A. Szameit: *Photonic Floquet topological insulators*, Nature **496** (2013), 196. Cited on page 28.
- [130] J. Struck, M. Weinberg, C. Ölschläger, P. Windpassinger, J. Simonet, K. Sengstock, R. Höppner, P. Hauke, A. Eckardt, M. Lewenstein, and L. Mathey: *Engineering Ising-XY spin models in a triangular lattice via tunable artificial gauge fields*, Nat. Phys. **9** (2013), 738. Cited on page 28.
- [131] S. Blanes, F. Casas, J. A. Oteo, and J. Ros: *The Magnus expansion and some of its applications*, Physics Reports **470** (2009), 151. Cited on pages 28, 39, 40, 59, and 136.
- [132] N. Goldman and J. Dalibard: *Periodically Driven Quantum Systems: Effective Hamiltonians and Engineered Gauge Fields*, Phys. Rev. X **4** (2014), 031027. Cited on page 28.
- [133] H.-P. Breuer, E.-M. Laine, and J. Piilo: *Measure for the Degree of Non-Markovian Behavior of Quantum Processes in Open Systems*, Phys. Rev. Lett. **103** (2009), 210401. Cited on pages 28 and 29.
- [134] K. Szczygielski: *On the application of Floquet theorem in development of time-dependent Lindbladians*, Journal of Mathematical Physics **55** (2014), 083506. Cited on page 29.
- [135] M. Hartmann, D. Poletti, M. Ivanchenko, S. Denisov, and P. Hänggi: *Asymptotic Floquet states of open quantum systems: the role of interaction*, New J. Phys. **19** (2017), 083011. Cited on pages 29 and 127.
- [136] M. Leskes, P. Madhu, and S. Vega: *Floquet theory in solid-state nuclear magnetic resonance*, Progress in Nuclear Magnetic Resonance Spectroscopy **57** (2010), 345 – 380. Cited on pages 30, 41, 136, and 137.
- [137] T. S. Cubitt, J. Eisert, and M. M. Wolf: *The Complexity of Relating Quantum Channels to Master Equations*, Comm. Math. Phys. **310** (2012), 383. Cited on pages 31, 32, and 127.
- [138] M. Ramana and A. J. Goldman: *Some geometric results in semidefinite programming*, Journal of Global Optimization **7** (1995), 33–50. Cited on pages 32 and 163.
- [139] L. Khachiyan and L. Porkolab: *Integer optimization on convex semialgebraic sets*, Discrete & Computational Geometry **23** (2000), 207–224. Cited on page 32.
- [140] (), The definition of the spectrahedron was given in Ref. [138] for symmetric matrices. In the same work it was shown that this definition can be easily extended to include Hermitian matrices, by splitting them into symmetric and skew-symmetric parts. Cited on page 32.
- [141] A. Rivas, S. F. Huelga, and M. B. Plenio: *Entanglement and Non-Markovianity of Quantum Evolutions*, Phys. Rev. Lett. **105** (2010), 050403. Cited on page 33.

Bibliography

- [142] A. Jamiołkowski: *Linear transformations which preserve trace and positive semidefiniteness of operators*, Reports on Mathematical Physics **3** (1972), 275 – 278. Cited on page 33.
- [143] A. S. Holevo: *Quantum systems, channels, information: a mathematical introduction*, vol. 16, (Walter de Gruyter), (2012). Cited on page 33.
- [144] A. A. Budini: *Stochastic representation of a class of non-Markovian completely positive evolutions*, Phys. Rev. A **69** (2004), 042107. Cited on pages 36, 37, and 38.
- [145] H.-P. Breuer, E.-M. Laine, J. Piilo, and B. Vacchini: *Colloquium: Non-Markovian dynamics in open quantum systems*, Rev. Mod. Phys. **88** (2016), 021002. Cited on page 36.
- [146] D. Chruściński and P. Należyty: *Non-Markovian Quantum Evolution: Time-Local Generators and Memory Kernels*, Reports on Mathematical Physics **77** (2016), 399 – 414. Cited on page 36.
- [147] E. Anisimovas, G. Žlabys, B. M. Anderson, G. Juzeliūnas, and A. Eckardt: *Role of real-space micromotion for bosonic and fermionic Floquet fractional Chern insulators*, Phys. Rev. B **91** (2015), 245135. Cited on page 43.
- [148] P. C. Moan and J. Niesen: *Convergence of the Magnus series*, Foundations of Computational Mathematics **8** (2008), 291–301. Cited on page 59.
- [149] A. Schnell: *Anomalously long-range order in non-equilibrium steady states of one-dimensional ideal Bose gases*, Master’s thesis, Technische Universität Dresden, Fakultät Mathematik und Naturwissenschaften, (2014). Cited on page 61.
- [150] S. Kohler, T. Dittrich, and P. Hänggi: *Floquet-Markovian description of the parametrically driven, dissipative harmonic quantum oscillator*, Phys. Rev. E **55** (1997), 300. Cited on page 62.
- [151] D. W. Hone, R. Ketzmerick, and W. Kohn: *Statistical mechanics of Floquet systems: The pervasive problem of near degeneracies*, Phys. Rev. E **79** (2009), 051129. Cited on page 63.
- [152] T. Langen, S. Erne, R. Geiger, B. Rauer, T. Schweigler, M. Kuhnert, W. Rohringer, I. E. Mazets, T. Gasenzer, and J. Schmiedmayer: *Experimental observation of a generalized Gibbs ensemble*, Science **348** (2015), 207–211. Cited on page 63.
- [153] F. Lange, Z. Lenarčič, and A. Rosch: *Pumping approximately integrable systems*, Nature Communications **8** (2017), 15767. Cited on page 63.
- [154] S. Braun, J. P. Ronzheimer, M. Schreiber, S. S. Hodgman, T. Rom, I. Bloch, and U. Schneider: *Negative Absolute Temperature for Motional Degrees of Freedom*, Science **339** (2013), 52–55. Cited on page 63.

- [155] B. V. Chirikov: *A universal instability of many-dimensional oscillator systems*, Physics Reports **52** (1979), 263 – 379. Cited on page 63.
- [156] A. Schnell, D. Vorberg, R. Ketzmerick, and A. Eckardt: *High-Temperature Nonequilibrium Bose Condensation Induced by a Hot Needle*, Phys. Rev. Lett. **119** (2017), 140602. Cited on pages 66 and 83.
- [157] M. V. Berry: *Regular and irregular semiclassical wavefunctions*, Journal of Physics A: Mathematical and General **10** (1977), 2083. Cited on pages 70 and 78.
- [158] D. C. Fisher and R. B. Reeves: *Optimal strategies for random tournament games*, Linear Algebra and its Applications **217** (1995), 83 – 85, Proceedings of a Conference on Graphs and Matrices in Honor of John Maybee. Cited on page 72.
- [159] T. Chawanya and K. Tokita: *Large-Dimensional Replicator Equations with Antisymmetric Random Interactions*, Journal of the Physical Society of Japan **71** (2002), 429–431. Cited on page 72.
- [160] S. Allesina and J. M. Levine: *A competitive network theory of species diversity*, Proceedings of the National Academy of Sciences **108** (2011), 5638–5642. Cited on page 72.
- [161] J. Knebel, M. F. Weber, T. Krüger, and E. Frey: *Evolutionary games of condensates in coupled birth–death processes*, Nature Communications **6** (2015), 6977. Cited on page 72.
- [162] A. Bäcker, R. Ketzmerick, and S. Löck: *Direct regular-to-chaotic tunneling rates using the fictitious-integrable-system approach*, Phys. Rev. E **82** (2010), 056208. Cited on page 78.
- [163] M. V. Berry: *Statistics of nodal lines and points in chaotic quantum billiards: perimeter corrections, fluctuations, curvature*, Journal of Physics A: Mathematical and General **35** (2002), 3025. Cited on page 78.
- [164] M. B. Plenio and P. L. Knight: *The quantum-jump approach to dissipative dynamics in quantum optics*, Rev. Mod. Phys. **70** (1998), 101–144. Cited on page 98.
- [165] C. Chin, R. Grimm, P. Julienne, and E. Tiesinga: *Feshbach resonances in ultracold gases*, Rev. Mod. Phys. **82** (2010), 1225–1286. Cited on page 103.
- [166] C. J. Myatt, E. A. Burt, R. W. Ghrist, E. A. Cornell, and C. E. Wieman: *Production of Two Overlapping Bose-Einstein Condensates by Sympathetic Cooling*, Phys. Rev. Lett. **78** (1997), 586–589. Cited on page 103.
- [167] K. Günter, T. Stöferle, H. Moritz, M. Köhl, and T. Esslinger: *Bose-Fermi Mixtures in a Three-Dimensional Optical Lattice*, Phys. Rev. Lett. **96** (2006), 180402. Cited on page 103.

Bibliography

- [168] N. Spethmann, F. Kindermann, S. John, C. Weber, D. Meschede, and A. Widera: *Dynamics of Single Neutral Impurity Atoms Immersed in an Ultracold Gas*, Phys. Rev. Lett. **109** (2012), 235301. Cited on page 103.
- [169] T. Lausch, A. Widera, and M. Fleischhauer: *Prethermalization in the cooling dynamics of an impurity in a Bose-Einstein condensate*, Phys. Rev. A **97** (2018), 023621. Cited on page 103.
- [170] F. Schmidt, D. Mayer, Q. Bouton, D. Adam, T. Lausch, N. Spethmann, and A. Widera: *Quantum Spin Dynamics of Individual Neutral Impurities Coupled to a Bose-Einstein Condensate*, Phys. Rev. Lett. **121** (2018), 130403. Cited on pages 103 and 130.
- [171] A. Rubio-Abadal, J.-y. Choi, J. Zeiher, S. Hollerith, J. Rui, I. Bloch, and C. Gross: *Probing many-body localization in the presence of a quantum bath*, arXiv preprint arXiv:1805.00056 (2018). Cited on page 103.
- [172] C. Gross and I. Bloch: *Quantum simulations with ultracold atoms in optical lattices*, Science **357** (2017), 995–1001. Cited on page 103.
- [173] M. P. A. Fisher, P. B. Weichman, G. Grinstein, and D. S. Fisher: *Boson localization and the superfluid-insulator transition*, Phys. Rev. B **40** (1989), 546. Cited on page 109.
- [174] F. D. M. Haldane: *Effective Harmonic-Fluid Approach to Low-Energy Properties of One-Dimensional Quantum Fluids*, Phys. Rev. Lett. **47** (1981), 1840–1843. Cited on page 109.
- [175] D. S. Petrov: *Bose-Einstein condensation in low-dimensional trapped gases*, Ph.D. thesis, University of Amsterdam, (2003). Cited on page 109.
- [176] D. S. Petrov, G. V. Shlyapnikov, and J. T. M. Walraven: *Regimes of Quantum Degeneracy in Trapped 1D Gases*, Phys. Rev. Lett. **85** (2000), 3745. Cited on page 109.
- [177] C. Cohen-Tannoudji and C. Robilliard: *Wave functions, relative phase and interference for atomic Bose-Einstein condensates*, Comptes Rendus de l'Académie des Sciences - Series IV - Physics **2** (2001), 445 – 477. Cited on page 110.
- [178] C. Miniatura, L. Kwek, M. Ducloy, B. Grémaud, B. Englert, L. Cugliandolo, and A. Ekert: *Ultracold Gases and Quantum Information: Lecture Notes of the Les Houches Summer School in Singapore: Volume 91, July 2009*, Lecture Notes of the Les Houches Summer School, (OUP Oxford), (2011). Cited on page 110.
- [179] W. Ketterle and H.-J. Miesner: *Coherence properties of Bose-Einstein condensates and atom lasers*, Phys. Rev. A **56** (1997), 3291–3293. Cited on page 110.
- [180] T. Jelte, J. M. McNamara, W. Hogervorst, W. Vassen, V. Krachmalnicoff, M. Schellekens, A. Perrin, H. Chang, D. Boiron, A. Aspect et al.: *Comparison of the Hanbury Brown–Twiss effect for bosons and fermions*, Nature **445** (2007), 402. Cited on page 110.

- [181] C. W. Gardiner and P. Zoller: *Quantum kinetic theory: A quantum kinetic master equation for condensation of a weakly interacting Bose gas without a trapping potential*, Phys. Rev. A **55** (1997), 2902–2921. Cited on page 112.
- [182] M. Krämer, C. Menotti, L. Pitaevskii, and S. Stringari: *Bose-Einstein condensates in 1D optical lattices*, The European Physical Journal D - Atomic, Molecular, Optical and Plasma Physics **27** (2003), 247–261. Cited on page 116.
- [183] J. L. DuBois and H. R. Glyde: *Natural orbitals and bose-einstein condensates in traps: A diffusion monte carlo analysis*, Physical Review A **68** (2003), 033602. Cited on page 116.
- [184] J. Sato, E. Kaminishi, and T. Deguchi: *Finite-size scaling behavior of Bose-Einstein condensation in the 1D Bose gas*, arXiv preprint arXiv:1303.2775 (2013). Cited on page 116.
- [185] M. Köhl, T. Stöferle, H. Moritz, C. Schori, and T. Esslinger: *1D Bose gases in an optical lattice*, Applied Physics B **79** (2004), 1009–1012. Cited on page 116.
- [186] C. J. Pethick and H. Smith: *Bose-Einstein Condensation in Dilute Gases*, (Cambridge University Press, Cambridge UK), 2nd edn., (2008). Cited on page 116.
- [187] S. D. Huber and N. H. Lindner: *Topological transitions for lattice bosons in a magnetic field*, Proceedings of the National Academy of Sciences **108** (2011), 19925–19930. Cited on page 116.
- [188] S. Giorgini, L. P. Pitaevskii, and S. Stringari: *Thermodynamics of a Trapped Bose-Condensed Gas*, Journal of Low Temperature Physics **109** (1997), 309–355. Cited on page 116.
- [189] A. Griffin, T. Nikuni, and E. Zaremba: *Bose-condensed gases at finite temperatures*, (Cambridge University Press), (2009). Cited on page 116.
- [190] N. P. Proukakis and B. Jackson: *Finite-temperature models of Bose-Einstein condensation*, Journal of Physics B: Atomic, Molecular and Optical Physics **41** (2008), 203002. Cited on page 116.
- [191] A. Müllers, B. Santra, C. Baals, J. Jiang, J. Benary, R. Labouvie, D. A. Zezyulin, V. V. Konotop, and H. Ott: *Coherent perfect absorption of nonlinear matter waves*, Science Advances **4** (2018). Cited on pages 121 and 122.
- [192] G. Barontini, R. Labouvie, F. Stubenrauch, A. Vogler, V. Guarrera, and H. Ott: *Controlling the Dynamics of an Open Many-Body Quantum System with Localized Dissipation*, Phys. Rev. Lett. **110** (2013), 035302. Cited on page 121.
- [193] R. Ozeri, N. Katz, J. Steinhauer, and N. Davidson: *Colloquium: Bulk Bogoliubov excitations in a Bose-Einstein condensate*, Rev. Mod. Phys. **77** (2005), 187–205. Cited on page 122.

Bibliography

- [194] A. Posazhennikova, M. Trujillo-Martinez, and J. Kroha: *Thermalization of Isolated Bose-Einstein Condensates by Dynamical Heat Bath Generation*, *Annalen der Physik* **530** (), 1700124. Cited on page 122.
- [195] T. S. Cubitt, J. Eisert, and M. M. Wolf: *Extracting Dynamical Equations from Experimental Data is NP Hard*, *Phys. Rev. Lett.* **108** (2012), 120503. Cited on page 127.
- [196] S. Higashikawa, H. Fujita, and M. Sato: *Floquet engineering of classical systems*, arXiv preprint arXiv:1810.01103 (2018). Cited on page 127.
- [197] B. Misra and E. C. G. Sudarshan: *The Zeno's paradox in quantum theory*, *J. Math. Phys.* **18** (1977), 756. Cited on page 129.
- [198] A. Hu, T. E. Lee, and C. W. Clark: *Spatial correlations of one-dimensional driven-dissipative systems of Rydberg atoms*, *Phys. Rev. A* **88** (2013), 053627. Cited on page 129.
- [199] T. E. Lee, H. Häffner, and M. C. Cross: *Antiferromagnetic phase transition in a nonequilibrium lattice of Rydberg atoms*, *Phys. Rev. A* **84** (2011), 031402. Cited on page 129.
- [200] D. Petrosyan, M. Hönig, and M. Fleischhauer: *Spatial correlations of Rydberg excitations in optically driven atomic ensembles*, *Phys. Rev. A* **87** (2013), 053414. Cited on page 129.
- [201] M. Hönig, D. Muth, D. Petrosyan, and M. Fleischhauer: *Steady-state crystallization of Rydberg excitations in an optically driven lattice gas*, *Phys. Rev. A* **87** (2013), 023401. Cited on page 129.
- [202] M. Marcuzzi, E. Levi, S. Diehl, J. P. Garrahan, and I. Lesanovsky: *Universal Nonequilibrium Properties of Dissipative Rydberg Gases*, *Phys. Rev. Lett.* **113** (2014), 210401. Cited on page 129.

Danksagung / Acknowledgements

Ich danke in erster Linie André Eckardt für seine absolut hervorragende Betreuung im Rahmen meiner Doktorarbeit. Seine Kreativität und sein unglaublich breites Wissen über die aktuell relevante Forschung haben mich immer wieder inspiriert und motiviert. André ist ein außergewöhnlicher Wissenschaftler mit der Gabe Ideen von Studenten aufzunehmen, einzuordnen, zu schärfen, und ihre Forschung für ein halbes Jahr weiterzudenken. Sein Weg ist auch deshalb von solchem Erfolg gekrönt weil er freundlich, fair, humorvoll und zugänglich ist, was die Zusammenarbeit mit ihm extrem angenehm macht.

Weiterhin danke ich Prof. Ketzmerick für die großartige finanzielle und wissenschaftliche Unterstützung. Ich glaube alle seiner Studenten werden bestätigen, dass Prof. Ketzmerick ein besonderes Talent besitzt die richtigen Fragen zu stellen, wissenschaftliche Sachverhalte auf die Essenz zu reduzieren und diese dann ansprechend zu präsentieren. Dabei legt er einen beeindruckenden Perfektionismus an den Tag, den man während der Arbeit mit ihm immer wieder als herausfordernd erlebt. Jedoch wird man stets mit einem außergewöhnlich guten Resultat belohnt.

Während meiner Arbeit habe ich von vielen Diskussionen mit großartigen Wissenschaftlern profitiert. Herausstellen möchte ich hier vor allem Sergey Denisov und Daniel Vorberg. Außerdem erwähnen möchte ich Tao Qin, Ling-Na Wu, Giuseppe de Tomasi, Markus Heyl, Juzar Thingna, Sebastian Diehl, Herwig Ott, Artur Widera, Dariusz Chruscinski, Karol Zyczkowski, Mikhail Fistul, Johannes Knebel, Konstantin Clauss, Botao Wang, Alexander Leymann, Kieran Bull, Tobias Becker, Toni Ehmke, Martin Körber und Normann Mertig.

Für Korrekturen am Text dieser Arbeit danke ich Konstantin Clauss, Botao Wang und insbesondere André Eckardt. Für die technische Unterstützung mit den Programmpaketen PyxGraph und QMaps gilt Dank allen Autoren des Programmcodes und vor allem Prof. Arnd Bäcker.

Außerdem danke ich dem Max-Planck-Institut für Physik komplexer Systeme und der International Max Planck Research School “Many-Particle Systems in Structured Environments” für kontinuierliche finanzielle Unterstützung. Mein großer Dank geht auch an das IBS Center for Theoretical Physics of Complex Systems in Daejeon, Korea für die Finanzierung von zwei prägenden Forschungsaufenthalten in Daejeon.

Schlussendlich danke ich meiner Familie und meinen Freunden für unendliche Unterstützung und Liebe. Der eigentliche Sinn des Lebens kommt am Ende nie aus dem eigenen Handeln, sondern immer nur aus der Liebe die man erfährt.

List of publications

- A. Schnell, D. Vorberg, R. Ketzmerick, A. Eckardt, *High-temperature nonequilibrium Bose condensation induced by a hot needle*, Physical Review Letters **119** (14), 140602 (2017).
- A. Schnell, R. Ketzmerick, A. Eckardt, *On the number of Bose-selected modes in driven-dissipative ideal Bose gases*, Physical Review E **97** (3), 032136 (2018).
- T. Qin, A. Schnell, K. Sengstock, C. Weitenberg, A. Eckardt, W. Hofstetter, *Charge density wave and charge pump of interacting fermions in circularly shaken hexagonal optical lattices*, Physical Review A **98** (3), 033601 (2018).
- A. Schnell, A. Eckardt, S. Denisov, *Is there a Floquet Lindbladian?*, arXiv preprint, arXiv:1809.11121 (2018).
- L.N. Wu, A. Schnell, G. De Tomasi, M. Heyl, A. Eckardt, *Describing many-body localized systems in thermal environments*, New Journal of Physics **21**, 063026 (2019).

Versicherung

Diese Arbeit wurde am Max-Planck-Institut für Physik komplexer Systeme in Dresden und am Institut für Theoretische Physik der Technischen Universität Dresden unter der wissenschaftlichen Betreuung von Dr. André Eckardt und Prof. Dr. Roland Ketzmerick durchgeführt.

Hiermit versichere ich, dass ich die vorliegende Arbeit ohne unzulässige Hilfe Dritter und ohne Benutzung anderer als der angegebenen Hilfsmittel angefertigt habe; die aus fremden Quellen direkt oder indirekt übernommenen Gedanken sind als solche kenntlich gemacht. Die Arbeit wurde bisher weder im Inland noch im Ausland in gleicher oder ähnlicher Form einer anderen Prüfungsbehörde vorgelegt.

Darüber hinaus erkenne ich die Promotionsordnung des Bereichs Mathematik und Naturwissenschaften der Technischen Universität Dresden vom 23. Februar 2011 an.

Alexander Schnell

Dresden, den 19. März 2019